THE DIRECT IMPLICATIONS OF WARMING ON THE PHENOTYPE AND UNDERLYING FUNCTIONAL TRAITS OF MARINE PHYTOPLANKTON

KIRRALEE G BAKER

MAY 2016

A Thesis Submitted In Fulfillment Of The Requirements For The Degree Of Doctor Of Philosophy In Science

Plant Functional Biology And Climate Change Cluster, School Of Life Sciences, University Of Technology Sydney

CERTIFICATE OF AUTHORSHIP/ORIGINALITY

This thesis is the result of a research candidature conducted jointly with another University as part of a collaborative Doctoral degree. I certify that the work in this thesis has not previously been submitted for a degree nor has it been submitted as part of requirements for a degree except as part of the collaborative doctoral degree and/or fully acknowledged within the text.

I also certify that the thesis has been written by me. Any help that I have received in my research work and the preparation of the thesis itself has been acknowledged. In addition, I certify that all information sources and literature used are indicated in the thesis.

Kirralee G. Baker

This thesis is dedicated to my everlasting satellites RB and PB, who always guide me and initially inspired me to discover the natural world, and DR who since joining my path, has filled my life with overwhelming happiness, love and adventure.

ACKNOWLEDGEMENTS

In preparation of this thesis and the work it presents, I would like to thank my thesis committee members– Martina Doblin and Peter Ralph for your counsel. And thank you also to all the current and past members of the Aquatic Processes Group and the Coastal oceanography and algal research team. In particular, warmest thanks to Drs Katherina Petrou, Daniel Nielson, Louiza Norman, Christian Evenhuis, Milan Szabo and Joey Croswell for your patience but particularly your wisdom and expertise, and to Charlotte Robinson, Michaela Larsson, Lauren Messer and Dale Radford, for your many insightful and understanding discussions.

Thank you to Assoc. Prof. Justin Seymour, Drs Allison McInnes and Christian Evenhuis, and Dale Radford, Charlotte Robinson, Lauren Messer and Marco Alvarez Rodriguez who have provided support in the form of thoughtful discussions, data collection, analysis and methodologies that have allowed this thesis to come to fruition. Your individual contributions are acknowledged within this thesis.

Throughout this research I have been in receipt of financial support from a number of sources and would like to thank the Australian Government for their provision of an APA scholarship, and the School of Life Sciences and C3 Cluster for providing research funding.

TABLE OF CONTENTS

LIST OF FIGURES

LIST OF TABLES

LIST OF SUPPLEMENTARY FIGURES

LIST OF SUPPLEMENTARY TABLES

SUMMARY

Marine phytoplankton mediate oceanic biogeochemical cycling by linking cellular metabolism with many elemental fluxes including C, N, P and Si. These elemental transformations are physiologically regulated processes that are influenced by phytoplankton phenotypes that change over different spatial and temporal scales. It is expected ocean warming (increasing sea surface temperatures; SST) will alter these patterns because temperature is the primary environmental control governing metabolism and growth in many phytoplankton groups. Whilst research on the effects of warming SST on biogeographical range shifts is advancing, it remains unknown how phytoplankton mediated biogeochemical transformations may be altered.

Focusing on patterns in species functional traits (FTs), this thesis applied trait-based approaches in laboratory and field studies to explore how biogeochemically-related FTs vary over environmental gradients. I quantified the thermal performance curves (TPCs) of FTs in representative species from two laboratory-cultured phytoplankton functional types to understand trade-offs associated with thermal acclimation and adaptation. To assess whether these laboratory-based patterns of FT trade-offs and expression were consistent in the field; I replicated a similar TPC experiment with a natural phytoplankton community. Finally, to understand how multiple environmental gradients interact to influence phytoplankton FT expression, I tracked a diatom-specific FT over northern Australia to spatially map the diatom phenotypes present to deduce the likely biogeochemical roles of the species in the region.

This thesis demonstrates the importance of understanding the relationship between the duration of thermal exposure, FT expression and trade-offs in regulating the phytoplankton phenotype, as all of these factors differentially affect species' growth rates (and therefore fitness and biogeography) but also the acquisition of C, N, P and Si, and therefore the marine cycling of these elements. Furthermore, ocean mapping of FTs proves insightful for understanding variability of biogeochemical transformations between different ocean regions by providing a link between cellular and community level processes.

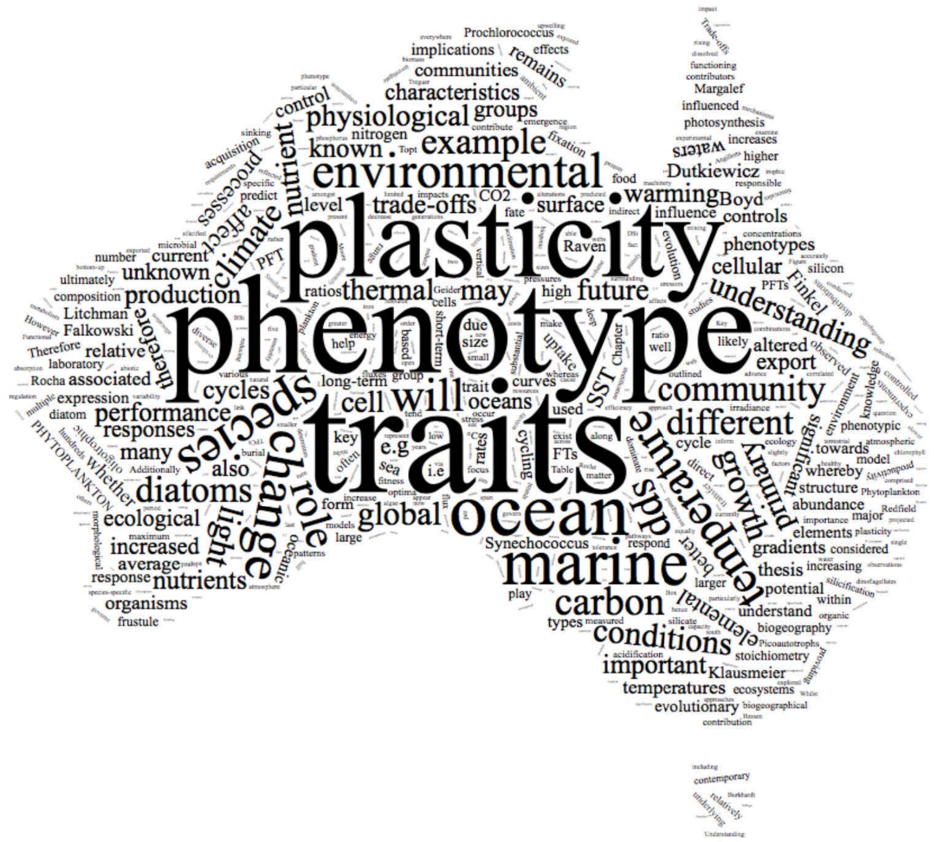
phenotype
traits
plasticity
ocean
marine
environmental
species
change
temperature
carbon
conditions
community
different
diatoms
spp
growth
primary
understanding
elemental
role
light
will
climate
example
physiological
production
warming
future
thermal
may
cell
global
nutrients
important
performance
cycles
ecological
increased
unknown
trade-offs
oceans
Synechococcus
Prochlorococcus
Dutkiewicz
Boyd
Finkel
Litchman
Falkowski
Rocha
Klausmeier
Margalef
Raven
cellular
phenotypes
export
altered
characteristics
communities
implications
known
groups
surface
nutrient
control
remains
processes
affect
therefore
associated
relative
responses
many
also
average
organisms
frustule
response
expression
temperatures
evolutionary
ecosystems
stoichiometry
biogeography
thesis
potential
gradients
abundance
structure
elements
whereby
towards
controls
influence
evolution
significant
waters
higher
increases
photosynthesis
influenced
contributors
functioning

DECLARATION OF THE CONTRIBUTION TO EACH CHAPTER

Chapter 2

This chapter has been published in Frontiers in Marine Science. The publication is titled "Thermal performance curves of functional traits aid understanding of thermally induced changes in diatom-mediated biogeochemical fluxes", and the authors are; Kirralee G. Baker, Charlotte, M. Robinson, Dale T. Radford, Allison S. McInnes, Christian Evenhuis, and Martina A. Doblin. I was responsible for conception of the experiment, methodological development, data interpretation and write-up of the manuscript. I was responsible for 2-(4-pyridyl)-5-((4-(2-dimethylaminoethylaminocarbamoyl)methoxy)phenyl)oxazole (PDMPO) assays, growth and cell size data. Dr. Allison McInnes (UTS) and myself conducted flow cytometry analyses. Assoc. Prof. Martina Doblin (UTS) conducted the primary productivity assays and Charlotte Robinson (UTS) collected photophysiology data. I was mostly responsible for post-processing of samples, with assistance in nutrient analysis from Dale Radford (UTS). I was mainly responsible for data analysis, with assistance in bootstrapping of data from Dr. Christian Evenhuis (UTS).

Chapter 3

The data presented in this chapter was a joint laboratory effort. I was responsible for conception of the experiment, methodological development, data analysis and interpretation, and write-up of the manuscript. Biogenic silicon production and PDMPO assays were conducted by myself. Source water collection and characterisation (primary productivity and pigment analyses) were conducted by Marco Alvarez-Rodrigues (UTS). Dr. Allison McInnes (UTS) and myself conducted flow cytometry analyses. Assoc. Prof. Martina Doblin (UTS) conducted the primary productivity assays and Charlotte Robinson (UTS) collected photophysiology data.

Chapter 4

The majority of the data presented in this chapter was collected by myself during the SS2013-t03 voyage in northern Australia (RV Southern Surveyor, July-August 2013). Assoc. Prof. Martina Doblin (UTS), Assoc. Prof. Justin Seymour (UTS), Lauren Messer (UTS) and Charlotte Robinson (UTS) were key contributors securing ship time for this voyage. I was responsible for conception of the experimental design, methodology development, data analysis and interpretation, and write-up of the manuscript. Biogenic silicon production, PDMPO and nitrate addition assays were conducted by myself. I also collected the particulate organic matter and phytoplankton pigment samples, these samples were processed by Lauren Messer (UTS) and Charlotte Robinson (UTS). Dr. Daniel Nielson (UTS) and Dale Radford (UTS) assisted with image analysis and Dr. Penelope Ajani assisted with phytoplankton identification.

Chapter 5

The data presented in this chapter was a joint laboratory effort. I was responsible for conception of the experimental design, methodological development, data interpretation, and write-up of the manuscript. I was responsible for the collection of the growth, cell size, photophysiological data. Dale Radford (UTS) assisted with nutrient analyses and I assisted Dr. Unnikrishnan Kuzhiumparambil (UTS) with fatty-acid methyl esters (FAME) analysis. I was mostly responsible for data analysis, with assistance in bootstrapping of data from Dr. Christian Evenhuis (UTS). Assoc. Prof. Martina Doblin (UTS) conducted the primary productivity assays and Lisa Hou (UTS) initially established the laboratory cultures used for this experiment.

CHAPTER 1:
GENERAL INTRODUCTION

1.1 Phytoplankton

The term “phytoplankton” refers to a ubiquitous, diverse and polyphyletic group of photosynthetic microbes that drift in sunlit surface waters (Falkowski and Raven 1997). They span a diverse range of sizes (Finkel et al. 2009), morphologies, behaviour (Tomas 1997) and biochemistry (Geider and La Roche 2002). Together, marine phytoplankton account for almost half of global primary production annually (Field et al. 1998) and, therefore, the ecological role of these organisms underpins healthy marine functioning. This is because they are the base of the food web and hence the entire oceanic food web, either directly or indirectly, relies on the transfer of energy from these microscopic algae. Ultimately the processes of carbon fixation and trophic transfer provide significant ecosystem ‘services’ upon which humans rely, including; fisheries and aquaculture production, water purification, nutrient transformation, and recreation (Costanza et al. 2014).

The role of phytoplankton in marine ecosystems, biogeochemical cycling and climate feedbacks are not only reliant on their stocks and rates, but also phytoplankton species composition. Traditionally this species diversity would be based on taxonomic identification (e.g. Shannon's index; Shannon and Weaver 1949), but has since been represented by pooling species into a few functional groups based on similar ecological characteristics (Reynolds et al. 2002), or more recently, biogeochemical characteristics (Le Quere et al. 2005). Different functional groups have different modes of acquisition and utilisation of elements such as, carbon (C), nitrogen (N), phosphorus (P) and silicon (Si) (Falkowski 2004). Therefore, as phytoplankton community composition varies over spatial and temporal scales they are able to influence biogeochemical cycles and characteristics of their surrounding environment (Hood et al. 2006, Moline and Prezelin 1996, Smith and Asper 2001). Hence, a better understanding of the community ecology of marine phytoplankton will ultimately lead to advancing knowledge about large-scale marine elemental fluxes and how these marine functions are likely to be altered by global change (see Box 1 for overview of projected climate impacts).

Box 1 Key impacts of climate change on the marine environment.

The life-filled oceans of Earth make this planet unique, with marine (and terrestrial) organisms playing an important role in climate regulation. Earth has been subjected to significant climatic variations over geological timescales during which life has flourished, diminished and/or become extinct. We are now in another period of significant change, occurring at unprecedented rates and there is overriding evidence that human activities are the cause of this epoch known as the Anthropocene (Steffen et al. 2007).

The further enrichment of carbon dioxide (CO_2) and other greenhouse gases in our atmosphere has increased global average temperatures by ~0.2 °C per decade over the last 30 years, and through photosynthesis and abiotic absorption, our oceans capture a proportion of this anthropogenic C (Hoegh-Guldberg and Bruno 2010). These increasing ocean temperatures are responsible for rising sea levels, increased ocean stratification, decreased sea-ice extent, and altered patterns of ocean circulation, precipitation, and freshwater input (Doney et al. 2012). Over the next century, warming SST have the potential to reduce upwelling and decrease primary production by phytoplankton in low latitudes by reducing the flux of C from the atmosphere to the ocean (Beardall and Raven 2004). Observed changes in phytoplankton abundance, community structure and phenology driven by natural climate variability and anthropogenic climate change are already apparent, and given their huge socioeconomic value, last estimated ~$US125-trillion yr^{-1} globally, it is crucial to understand the implications of future changes on stocks and productivity of phytoplankton (Barton et al. 2015, Costanza et al. 2014, Hays et al. 2005).

1.2 The ecological and biogeochemical roles of phytoplankton

Phytoplankton mediate biogeochemical cycles by providing a link between metabolic processes and the flux of C, N, P, Si, sulphur (S), iron (Fe) and other trace elements (Barsanti and Gualtieri 2006). The cycling of some elements is restricted to a specific phytoplankton functional group (PFG) (**Table 1.1**). For example, diazotrophs are solely responsible for fixation of atmospheric N_2, whereas, phytoplankton regulation of the Si cycle is controlled by diatoms and silicoflagellates– although there is now increasing evidence Si is taken up by the marine picocyanobacterium *Synechococcus* (Baines et al. 2012, Ohnemus et al. 2016). As outlined by the modified version of the Richards (1965) equation, the major elements are incorporated into the "average marine plankton" biomass as outlined by Anderson (1995):

$$106CO_2 + 16HNO_3 + H_3PO_4 + 78H_2O + light \rightarrow C_{106}H_{175}O_{42}N_{16}P + 150O_2$$

whereby a phytoplankton cell incorporates inorganic forms of carbon (CO_2), nitrogen (HNO_3) and phosphate (H_3PO_4) as well as other micronutrients (e.g. Fe and Si) in the presence of light (i.e., through photosynthesis) into organic matter ($C_{106}H_{263}O_{106}N_{16}P$) and evolves oxygen ($O_2$) (Anderson 1995). The rate and ratios of uptake determines cellular composition, and the availability of these nutrients and light combined with growth requirements of taxa therefore underpin the biogeography of these organisms.

The physiological characteristics of phytoplankton species within the community determine the quantity and elemental composition of organic matter that is transferred to higher trophic levels and/or exported to the deep sea for burial (Finkel et al. 2009). To protect themselves from predators, phytoplankton have evolved to escape by swimming (enabled by flagellum, e.g. dinoflagellates) or by mechanical protection; mineral (e.g. Si:C in the cell walls of diatoms) or tough organic cell walls to deter piercers or crushers (Smetacek 2001) and in turn, significantly influence phytoplankton elemental stoichiometry. The elemental composition, in part, also governs the fate of C in organisms, food webs and ecosystems by determining C-use efficiency (Hessen et al. 2004). For example, high C:elemental ratios of phytoplankton can lead to reduced consumer (herbivores and detritivores) growth at the organismal level due to lower nutritional value, and more C will be diverted for sediment burial; changing the fate of C (Hessen et al. 2004, Hessen and Elser 2005).

The atomic C/N/P ratio of 106:16:1 was used to represent the "average marine plankton" by Redfield et al. (1963) to help identify which dissolved nutrients may be limiting for growth (based on changes in the relative uptake of C). Since its establishment, the 'Redfield' ratio is well reflected by natural communities of marine plankton but shows some variability because it can be altered by changes in cell size and species present (Finkel et al. 2009). For example, smaller cells tend to have greater cellular C and N per unit volume than larger cells (Verity et al. 1992). Additionally, group/class specific ratios are known to exist, whereby the C:P and C:N ratios of green algae are much higher than those of diatoms which is thought to be due to phylogenetic inheritance, i.e., genetically-based differences (Ho et al. 2003, Quigg et al. 2003). Additionally, phytoplankton can exhibit substantial plasticity in their elemental stoichiometry as a physiological response to their ambient physicochemical conditions. For example, threefold and sixfold changes in N:P have been observed under N- an P-limitation, respectively (Geider and La Roche 2002), and can also change in response to alterations in irradiance (Finkel et al. 2006), temperature and CO_2 (Burkhardt et al. 1999, Fu et al. 2007, Fu et al. 2008, Hutchins et al. 2007). Therefore, it is likely, that phytoplankton elemental stoichiometry is influenced by *in situ* conditions that are encountered by cells on timescales equivalent to intra-generational turnover and in turn, governs the fate of C in marine ecosystems.

Table 1.1 Key phytoplankton functional groups (PFG) and their role in various marine biogeochemical cycles. Note that some illustrative species appear more than once and exemplifies that clustering of PFGs are based on similarities in ecological and/or biogeochemical role, rather than phylogeny.

Functional	Species	Role in marine biogeochemical cycle	Reference
Silicifiers	Diatom spp. and silicoflagellate spp.	Exert major influence on the ocean biogeochemical cycles of C, Si, N, and Fe in open ocean. They are reported to contribute up to 40% of oceanic primary productivity. Some species are known to form chains and in conjunction with their silica ballast have been shown to contribute significantly to downward export, particularly after bloom events.	(Sarthou et al. 2005, Smetacek 1999, Tréguer and De La Rocha 2013)
Calcifiers	Coccolithophore spp.	Responsible for more than half of marine carbonate export. They influence the air-sea CO_2 equilibrium, alkalinity, surface carbonate chemistry. They are significant contributors to carbon export as their dense ballasts are observed in sinking particles.	(Klaas and Archer 2002, Schiebel 2002)
Phytoplankton N_2-fixers	*Trichodesmium* spp., diatom-diazotroph interactions, and N_2-	Use atmospheric N_2 and therefore help to control the balance of total oceanic N. By providing a new bioavailable source of nitrogen to the ocean (and their symbiotic hosts), they fuel new and export production.	(Falkowski et al. 1998, Montoya et al. 2004, Tyrrell 1999, Zehr et al.
DMS-producers	Diatoms spp., dinoflagellate spp. *Phaeocystis* spp.	They affect the atmospheric sulphur cycle through their conversion of dimethyl-sulfoniopropionate (DSMP) to DMS	(Simó 2001, Stefels et al. 1995)
Picoautotrophs	*Synechococcus* spp. *Prochlorococcus* spp.	Found everywhere, mainly in oligotrophic gyres and hence play an important role in microbial food webs and ocean N cycle. They contribute a substantial proportion towards primary production but an insignificant contribution to export and, therefore, also play an important role in global C biogeochemistry.	(Boyd et al. 2010, Partensky et al. 1999, Raven 1998)
Generic small phytoplankton	*Synechococcus* spp. *Prochlorococcus* spp.	Characterised by slower growth rates, different cellular machinery and more efficient at lower nutrient concentrations so play an important role in oligotrophic conditions.	(Arrigo 2005, Dutkiewicz et al. 2013)
Generic large phytoplankton	Diatom spp. and dinoflagellate spp.	Higher maximum growth rates and due to their larger relative sizes, are responsible for greater export.	(Arrigo 2005, Dutkiewicz et al. 2013)

1.3 The biogeographical distribution of phytoplankton functional groups

Based on the concept that phytoplankton community dynamics are governed by bottom-up physical forcing (Margalef 1978), Longhurst (2010) partitioned the ocean into 54 biogeographical provinces, each province with a unique cluster of underlying physicochemical properties. These provinces have different external pressures (e.g. light, nutrients, temperature) that govern the emergence of different PFGs that are each characterised by a set of FTs that offer alternative strategies of survival. As a result, PFGs can have specific ecological or biogeochemical roles (Follows and Dutkiewicz 2011, Hood et al. 2006, Iglesias‐Rodríguez et al. 2002, Le Quere et al. 2005, Nair et al. 2008). In this way, physical controls such as light and vertical mixing, ultimately structure phytoplankton community assembly and dynamics along environmental gradients (Litchman et al. 2007, Longhurst 2010), and ultimately affect the biogeochemical cycling of many elements (C, N, P, Si) due to changes in relative abundances of different PFGs (Falkowski 2004). Modeller's have used these principles to project the current and future distributions of such ecotypes (Dutkiewicz et al. 2013).

In ocean biogeochemical models, it is invaluable to explicitly represent key PFGs (**Table 1.1**) because of their intrinsic link to biogeochemical pathways (Falkowski 2004). How PFGs are classified depends on the scientific question of interest (e.g. Gregg and Casey 2007, Le Quere et al. 2005, Moore et al. 2004). The PFG classifications can range from more simplistic descriptions including a two cell-size model (i.e., smaller phytoplankton that are slower growing, with low nutrient requirements, and a larger phytoplankton class (faster growing, high nutrient requiring) such as the ocean biogeochemical model of Aumont & Bopp (2006), to the more complex ten-classification system of Le Quere et al. (2005). In most models, diatoms are considered as a separate PFG based on their importance in determining the sinking and sedimentation of organic matter and role in the Si cycle (for examples see Aumont and Bopp 2006, Dutkiewicz et al. 2013, Litchman 2006, Moore et al. 2002). A few dominant functional groups are the focus of this thesis, notably the diatoms, dinoflagellates and picoautotrophs (**Table 1.1**).

Diatoms are typically considered relatively large phytoplankton but span a wide size range from approximately 2 μm to 2000 μm (maximum linear dimension) and mostly dominate turbulent, nutrient-rich waters such as coastal and upwelling zones (Tréguer

and De La Rocha 2013). This functional group is intrinsically linked to the marine C and Si cycles because diatoms are the largest contributors to biosilicification and are the dominant contributors to global C fixation and export (Behrenfeld et al. 2015, Martin-Jezequel et al. 2000, Nelson et al. 1995). All oceanic inputs of Si in the form of dissolved Si (DSi) originate from terrestrial weathering and enter the ocean via river and groundwater discharges (Tréguer and De La Rocha 2013). Here, Si is taken up by diatoms and used for growth, a process whereby the DSi, in the form of silicic acid $Si(OH)_4$, is biomineralised into the cell wall to form the frustule and produces what is known as biogenic Si, (BSi) (Martin-Jézéquel and Lopez 2003). This BSi is partly recycled in surface waters where it dissolves and forms $Si(OH)_4$ (where it is reused by future generations of cells) and the remainder sinks and is exported to the deep sea floor for burial, as biogenic opal (Tréguer and De La Rocha 2013).

Dinoflagellates, like diatoms, are relatively large phytoplankton (4-2000 μm) but in contrast, tend to dominate in stratified, nutrient-deplete conditions such as oligotrophic seas or following a spring bloom event (Margalef 1978). Additionally, dinoflagellates have two flagella that enable motility and vertical migration behavior and can be found as free-living organisms or in symbiosis with animals such as corals (Murray et al. 2016). Dinoflagellate habitats are diverse and form important components of both water column and benthic phytoplankton communities.

Picoautotrophs, such as *Prochlorococcus* spp. and *Synechococcus* spp. are small (~0.5-3 μm) and dominate the oligotrophic open oceans but have slightly different distributions and ecology (Johnson et al. 2006). For example, *Synechococcus* spp. tend to favor slightly higher nutrient concentrations and the upper well-lit layer, whereas, *Prochlorococcus* spp. tend to be less ubiquitous and their abundance decreases at latitudes higher than 45 °N (Partensky et al. 1999). Picoautotrophs make a substantial contribution to primary production, but unlike diatoms, have a negligible contribution to carbon export (Le Quere et al. 2005), but see Richardson and Jackson (2007).

There are many other PFGs (**Table 1.1**) that are not considered in this thesis, but I mainly focus on those outlined above. However, whilst some traits are specific to certain PFG, other traits measured in this thesis are universal across all phytoplankton (e.g. growth rate, cell size, photosynthesis) and therefore, many of the mechanisms and patterns discussed may extend to groups outside those measured here.

1.4 Functional traits, trade-offs and phenotypic plasticity

The application of trait-based approaches to phytoplankton communities offers the potential to investigate and advance understanding of the ecological community organisation in our current oceans, but also their reorganisation in future oceans under climate change and other global stressors (Litchman and Klausmeier 2008) Traits are key physiological characteristics that determine the ecological and biogeochemical role of phytoplankton and their performance along environmental gradients (Litchman and Klausmeier 2008). **Figure 1.1** summarises FTs that have been measured in phytoplankton. Together, multiple phytoplankton FTs such as growth or nutrient uptake and tolerance curves for numerous abiotic factors can be used to estimate ecological niches and predict how they may be altered under environmental change (Litchman et al. 2012).

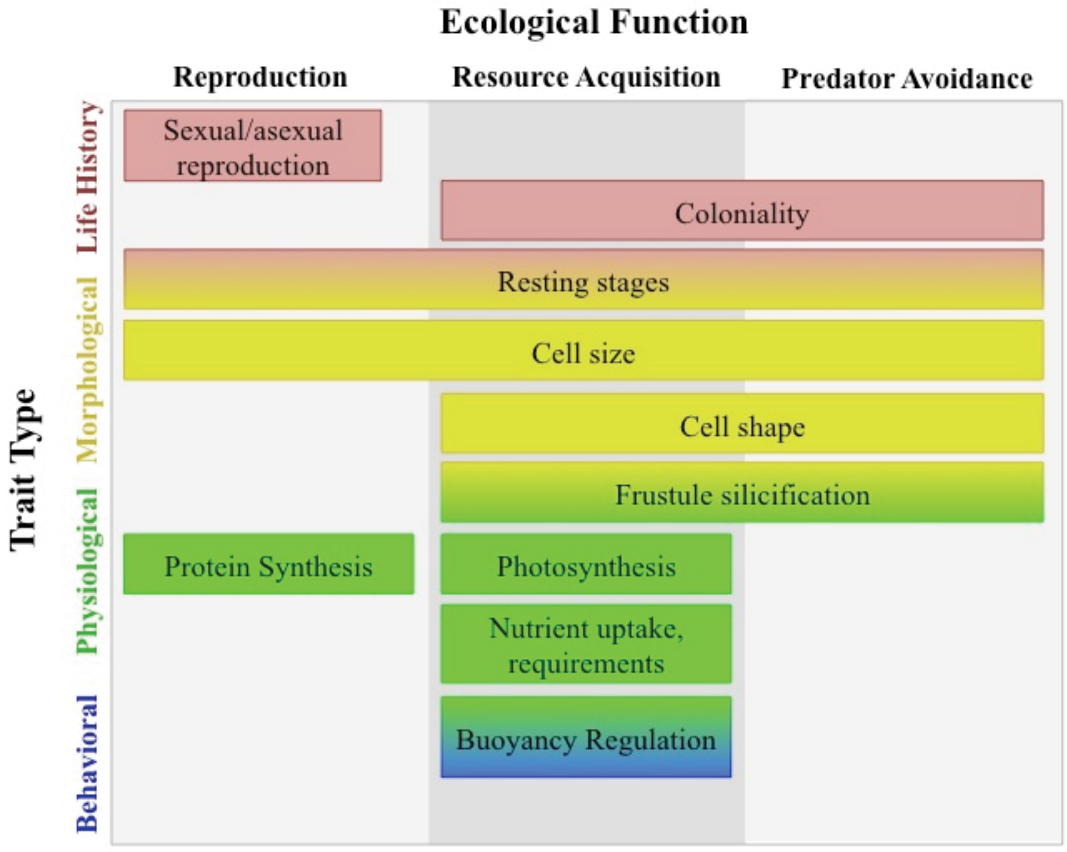

Figure 1.1 Typology of functional traits (FTs) redrawn from Litchman and Klausmeier (2008). Trade-offs between many FTs have significant implications for the functional ecology of marine systems, as many of these traits are involved in resource acquisition and have direct control over biogeochemical fluxes. Physiological traits such as nutrient uptake directly affect the elemental cycles of C, N, P and Si; whereas, morphological traits such as cell size and frustule silicification regulate these biogeochemical cycles by influencing cell aggregation, cell sinking rates and vulnerability to grazing.

Given that the overall phenotype of an individual can be comprised of hundreds if not thousands of traits (Johnston and Bennett 1996), we must make decisions surrounding how many and what traits should be considered. For example, restricting our laboratory efforts into understanding FTs only, i.e., traits that infer fitness, will help predict how these traits respond to climate change induced conditions. Similarly, as has been done for environmental controls on PFGs (Boyd et al. 2010), it is important to quantify and parameterise key FTs. This will assist in the ranking of the relative importance of traits to increase confidence in model predictions of climate-induced changes in phytoplankton primary production and community structure. For example, some traits such as cell size and elemental stoichiometry respond predictably to environmental conditions and therefore are not only promising traits for modelling, but also for monitoring changes within communities (Finkel et al. 2009).

Predicting how environmental gradients control individual FT expression is further complicated by the direct and indirect effects they have on overall fitness and are often correlated with a number of other FTs that are also under selective pressures (Geber and Griffen 2003). Therefore, while the number of combinations between FTs are infinite in theory, in nature, this is impossible, bound by the laws of conservation of resources and morphological considerations at the cellular level, traits are often not independent but positively or negatively correlated (Follows and Dutkiewicz 2011, Litchman et al. 2012). These trait relationships are reflected by the emergence of trade-offs; the costs and benefits of particular trait combinations (Litchman and Klausmeier 2008). Trade-offs on inter-generational timescales give rise to the dominance of different functional groups in contrasting environments, whereby species sorting occurs as individuals better adapted to ambient conditions will increase in abundance, replacing poorly adapted species (Litchman et al. 2012, Litchman et al. 2007, Margalef 1978). For example, the emergence of lightly silicified diatoms in conditions where silicate concentrations are low (Ajani et al. 2014) or heavily silicified diatoms when nutrients are abundant (Shimada et al. 2006).

FTs at the cellular level, as described above, can equally exist at the sub-cellular level (Angilletta Jr 2006, Angilletta Jr et al. 2003, Litchman and Klausmeier 2008). Being physiological (phenotypic) characteristics, further trait diversity arises through phenotypic plasticity, that is, changes in an organism's phenotype (comprised of

hundreds of underlying traits) as a response to changes in the environment. For example, nutrient acquisition can be controlled by temperature (Nedwell 1999, Reay et al. 1999), cellular chlorophyll (Chl) to C and N (Chl:C, Chl:N) is influenced by irradiance (Geider et al. 1998), Si:C content of diatoms (i.e. the degree of frustule silicification) is strongly affected by external silicate concentrations (Finkel and Kotrc 2010). Therefore the phenotypic plasticity of key FTs have important ecological and biogeochemical consequences, in this case, alterations in chlorophyll content can affect maximum rates of photosynthesis and changes in C:elemental molar ratios can govern the fate of C in the oceans.

Similarly, trade-offs between FTs can also occur at the cellular level, for example, allocation trade-offs can occur, whereby the allocation of energy and resources towards growth assembly machinery, such as ribosomes may limit investment towards resource-acquisition machinery, such as nutrient-uptake proteins and chloroplasts (Arrigo 2005, Klausmeier et al. 2004). These trade-offs are seldom static but instead respond dynamically to their ambient surroundings. Trade-offs amongst characteristics of light absorption versus photoprotection are known to occur when cells are exposed to different irradiance intensities, resulting in high-light and low-light phenotypes (McKew et al. 2013). Heterotrophs are known to adjust the composition of their lipid membranes as a response to temperature; enabling them to reduce respiration costs at high temperature but this reduces the efficiency of resource acquisition at lower temperatures (Hall et al. 2010). Mapping the biogeography of particular traits will help to reveal the mechanisms that underpin the phytoplankton community structure, however, our understanding is currently limited by the scarcity of observations (Barton et al. 2013).

1.5 Predicting responses of phytoplankton to anthropogenic climate change

There is an ever increasing number of short-term experimental studies demonstrating the significant effects of projected ocean warming (Boyd et al. 2013) and acidification (Burkhardt et al. 1999, Fu et al. 2007, Fu et al. 2008, Hutchins et al. 2007) on marine phytoplankton. However, it remains unknown whether these short-term manipulative approaches are reliable for predicting the impacts of long-term (decadal) climate change because we do not currently understand the adaptive capacity of phytoplankton over these timescales. One such experimental approach to investigate their evolutionary

potential and better understand and predict phytoplankton responses to climate change is known as 'contemporary evolution' or 'evolutionary rescue' experiments (Reusch and Boyd 2013). Whilst numerically fewer than those conducted over shorter exposures (i.e., weeks), contemporary evolution studies (i.e., years) have effectively demonstrated that short-term perturbation experiments can underestimate microbial performance in a future ocean as they do not consider adaptation processes (Collins and Bell 2004, Lohbeck et al. 2012, Schaum et al. 2012, Schluter et al. 2014). It is therefore imperative to experiment on these longer time-scales of months to years.

The focus of current work exploring the evolutionary potential of phytoplankton has been directed towards understanding the long-term effects of ocean acidification, with species-specific evolutionary responses (Collins et al. 2014). These conflicting reports may be taxon or species-specific responses as various environmental controls are likely to affect phytoplankton groups differently (Boyd et al. 2010). Alternatively, it is possible that true performance is not being accurately assessed because physiological stress is relative to the magnitude and direction of environmental change and the organism in question. For example, the thermal optimum ($T_{opt.}$) can vary between and within populations of the same species (Zhang et al. 2014); meaning a 2 °C increase in temperature will cause varying degrees of stress amongst species due to differences the relative change to the $T_{opt.}$ As a result, it is difficult to accurately define thermal stress and predict the response of phytoplankton to ocean warming if the T_{opt} is unknown. This logic extends to any other environmental control. To move forward, we can examine traits over multiple points along these environmental gradients (e.g. temperature) — these are known as performance curves (Angilletta 2009). Understanding how performance curves change under long term selection pressures (e.g. increased temperature) can better inform evolutionary models (e.g. Chevin et al. 2010) to help better our understanding of how phytoplankton will respond to global change.

1.6 The implications of warming on phytoplankton

Of all the environmental factors undergoing alteration under climate change (light, nutrients, CO_2), temperature has been ranked as the dominating control for a number of phytoplankton groups and its importance remains unknown for many others (Boyd et al. 2010). Temperature underpins phytoplankton metabolism and activity (Eppley 1972, Raven and Geider 1988) and ultimately determines their species' abundance and

biogeography based on underlying characteristics such as $T_{opt.}$ and niche width (Thomas et al. 2012). Because each species has a different range of tolerance and physiological responses, the predicted 2-3 °C rise in average SST can cause increased metabolic activity and growth in some species but push others beyond their temperature optima/optimum (Beardall and Raven 2004). Whilst the implications of increased SST on phytoplankton biogeography has been broadened by examining the affects of high temperatures on species fitness and community composition (Feng et al. 2009, Tatters et al. 2013), it remains unknown how the reorganisation of phytoplankton communities will affect primary productivity and other biogeochemical transformations (Dutkiewicz et al. 2013).

It is predicted that increases in average SST will affect phytoplankton through both 'direct' and 'indirect' pathways. Expected changes in light and nutrient regimes are attributed to a (projected) shoaling of the mixed layer depth, decreasing the upwards transfer of nutrients from deep waters to the surface and thus reducing phytoplankton exposure to nutrients and increasing average daily incident irradiances (Beardall and Raven 2004, Cubasch et al. 2001, Doney et al. 2012, Hobday et al. 2006). The direct effects of warming on phytoplankton are associated with the biological responses to increased temperature and may in fact counteract indirect effects (Taucher and Oschlies 2011). However, the extent to which increased metabolism may offset reduced growth (due to reduced nutrient concentrations) remains relatively unknown, particularly when different physiological responses to temperature appear to be species-specific (Bopp et al. 2013).

Not all ocean regions will be equally affected by rising SST (Bopp et al. 2013, Steinacher et al. 2010). The ocean waters in south eastern Australia are expected to be a hot spot for ocean warming (up to five times the global average) due to the strengthening of the flow of the East Australian Current (EAC), one of the five major boundary currents, carrying tropical waters further south (Hobday et al. 2006, Ridgway and Hill 2009). For example, recent observations suggest a decrease in microplankton abundance in this region associated with long-term increases in SST (Ajani et al. 2014), but it remains unknown what the associated implications for primary productivity and other biogeochemical cycles in this region may be.

1.7 Research objectives and thesis outline

Marine phytoplankton play an integral role in the healthy functioning of our marine ecosystems through their role in the foodweb and biogeochemical processes that they control. Substantial knowledge gaps exist in regard to how the current and future warming of the surface oceans that these photoautotrophs inhabit will impact the biogeochemical fluxes that these organisms mediate. Understanding the capacity for short-term acclimation (i.e. weeks) and long-term adaptation (i.e. years) to increases in temperature will further our understanding of how phytoplankton performance and elemental cycling may be altered by warming average SSTs associated with climate change.

The goal of this thesis is to examine how the phenotypes of phytoplankton are determined by trade-offs between underlying FTs; how environmental controls influence these trade-offs and in turn, shape the biogeographical distribution of these phenotypes; and how these physiological changes at the cellular level can influence marine functioning via the ecological and biogeochemical role of phytoplankton.

Our current state of knowledge regarding the variability in thermal optima between and within phytoplankton functional types is expanding, providing insight into the differential responses that are often observed between species to ocean warming (Boyd et al. 2013). Yet, knowledge about different thermal optima for various biogeochemical processes and functional traits remains unknown. In Chapter 2, I explored how the phenotypic expression of a major phytoplankton functional group and ubiquitously distributed species, namely diatoms, can be influenced over a gradient of temperature, a single environmental stressor. Specifically, I conducted controlled laboratory experiments to quantify the TPCs of FTs in the cosmopolitan diatom, *Thalassiosira pseudonana* to advance understanding of trade-offs between physiological (photoacclimation, carbon fixation, nitrate, phosphate and silicate uptake) and morphological traits (cell volume and frustule silicification) associated with thermal acclimation in order to better understand how the future warmed ocean will affect phytoplankton-mediated biogeochemical processes. I expand TPCs from a single species to a mixed phytoplankton community in Chapter 3 to assess whether these patterns in functional trait expression are observed when other additional stressors such as competition, grazing and parasites are present.

Knowing whether laboratory studies are able to inform changes in large, ecosystem-scale biogeochemical processes, is impeded by our limited understanding of how FT expression is regulated by the interaction between multiple environmental controls. In Chapter 4, I investigated natural diatom communities, recognising that they are exposed to multi-faceted environmental seascapes of nutrients, light, salinity and temperature, rather than simple unilateral gradients. I created a spatial map of diatom phenotypes by recording the expression of a diatom-specific functional traits across a subtropical to temperate oceanic gradient in order to understand whether some environmental gradients act as primary bottom-up controls and can be used as a predictor of local biogeochemical fluxes.

In Chapter 5, I returned to the laboratory to explore whether the current biogeographical distributions of phytoplankton phenotypes are likely to be altered by longer-term changes in ocean conditions. Adopting a contemporary evolution approach in conjunction with TPCs, I investigated whether increases in average SSTs influenced the thermal characteristics (e.g. T_{opt}) and the evolution of phytoplankton phenotypes over hundreds of generations. Using the data collected, I explored the trade-offs associated with long-term exposure to supra-optimal temperatures and discuss the potential implications for biogeochemical cycling as well as changes in ecological niche occupancy.

The final chapter of this thesis provides a synthesis of the key findings that have arisen from the research conducted and discusses the research contributions towards the larger discipline of ocean change biology, concluding with suggestions for future directions in this field.

1.8 Literature cited

Ajani, P. A., Allen, A. P., Ingleton, T. and Armand, L. (2014) A decadal decline in relative abundance and a shift in microphytoplankton composition at a long‐term coastal station off southeast Australia. *Limnology and Oceanography,* 59(2), pp. 519-531.

Anderson, L. A. (1995) On the hydrogen and oxygen content of marine phytoplankton. *Deep Sea Research Part I: Oceanographic Research Papers,* 42(9), pp. 1675-1680.

Angilletta Jr, M. J. (2006) Estimating and comparing thermal performance curves. *Journal of Thermal Biology,* 31(7), pp. 541-545.

Angilletta Jr, M. J., Wilson, R. S., Navas, C. A. and James, R. S. (2003) Tradeoffs and the evolution of thermal reaction norms. *Trends in Ecology & Evolution,* 18(5), pp. 234-240.

Angilletta, M. J. (2009) *Thermal adaptation: a theoretical and empirical synthesis,* Oxford University Press.

Arrigo, K. R. (2005) Marine microorganisms and global nutrient cycles. *Nature,* 437(7057), pp. 349-355.

Aumont, O. and Bopp, L. (2006) Globalizing results from ocean in situ iron fertilization studies. *Global Biogeochemical Cycles,* 20(2). doi:10.1029/2005GB002591.

Baines, S. B., Twining, B. S., Brzezinski, M. A., Krause, J. W., Vogt, S., Assael, D. and McDaniel, H. (2012) Significant silicon accumulation by marine picocyanobacteria. *Nature Geoscience,* 5(12), pp. 886-891.

Barsanti, L. and Gualtieri, P. (2006) *Algae : anatomy, biochemistry, and biotechnology,* Boca Raton, Fla.: CRC Taylor & Francis.

Barton, A. D., Lozier, M. S. and Williams, R. G. (2015) Physical controls of variability in North Atlantic phytoplankton communities. *Limnology and Oceanography,* 60(1), pp. 181-197.

Barton, A. D., Pershing, A. J., Litchman, E., Record, N. R., Edwards, K. F., Finkel, Z. V., Kiørboe, T. and Ward, B. A. (2013) The biogeography of marine plankton traits. *Ecology letters,* 16(4), pp. 522-534.

Beardall, J. and Raven, J. A. (2004) The potential effects of global climate change on microalgal photosynthesis, growth and ecology. *Phycologia,* 43(1), pp. 26-40.

Behrenfeld, M. J., O'Malley, R. T., Boss, E. S., Westberry, T. K., Graff, J. R., Halsey, K. H., Milligan, A. J., Siegel, D. A. and Brown, M. B. (2015) Revaluating ocean warming impacts on global phytoplankton. *Nature Climate Change*, pp. 1-8. doi:10.1038/NCLIMATE2838.

Bopp, L., Resplandy, L., Orr, J. C., Doney, S. C., Dunne, J. P., Gehlen, M., Halloran, P., Heinze, C., Ilyina, T. and Séférian, R. (2013) Multiple stressors of ocean ecosystems in the 21st century: projections with CMIP5 models. *Biogeosciences,* 10(10), pp. 6225-6245.

Boyd, P. W., Rynearson, T. A., Armstrong, E. A., Fu, F., Hayashi, K., Hu, Z., Hutchins, D. A., Kudela, R. M., Litchman, E., Mulholland, M. R., Passow, U., Strzepek, R. F., Whittaker, K. A., Yu, E. and Thomas, M. K. (2013) Marine Phytoplankton Temperature versus Growth Responses from Polar to Tropical Waters – Outcome of a Scientific Community-Wide Study. *PLoS One,* 8(5), pp. e63091. doi:10.1371/journal.pone.0063091.

Boyd, P. W., Strzepek, R., Fu, F. and Hutchins, D. A. (2010) Environmental control of open-ocean phytoplankton groups: Now and in the future. *Limnology and Oceanography,* 55(3), pp. 1353-1376. doi:10.4319/lo.2010.55.3.1353.

Burkhardt, S., Zondervan, I. and Riebesell, U. (1999) Effect of CO_2 concentration on C: N: P ratio in marine phytoplankton: A species comparison. *Limnology and Oceanography,* 44(3), pp. 683-690.

Chevin, L. M., Lande, R. and Mace, G. M. (2010) Adaptation, plasticity, and extinction in a changing environment: towards a predictive theory. *PLoS biology,* 8(4). doi:p.e1000357.

Collins, S. and Bell, G. (2004) Phenotypic consequences of 1,000 generations of selection at elevated CO2 in a green alga. *Nature,* 431(7008), pp. 566-569.

Collins, S., Rost, B. and Rynearson, T. A. (2014) Evolutionary potential of marine phytoplankton under ocean acidification. *Evolutionary Applications,* 7(1), pp. 140-155. doi:10.1111/eva.12120.

Costanza, R., de Groot, R., Sutton, P., van der Ploeg, S., Anderson, S. J., Kubiszewski, I., Farber, S. and Turner, R. K. (2014) Changes in the global value of ecosystem services. *Global Environmental Change,* 26, pp. 152-158.

Cubasch, U., Meehl, G. A., Boer, G. J., Stouffer, R. J., Dix, M., Noda, A., Senior, C. A., Raper, S. and Yap, K. S. (2001) *Projections of future climate change. In Climate Change 2001: The Scientific Basis,* New York: Cambridge University Press: 525–582.

Doney, S. C., Ruckelshaus, M., Duffy, J. E., Barry, J. P., Chan, F., English, C. A., Galindo, H. M., Grebmeier, J. M., Hollowed, A. B. and Knowlton, N. (2012) Climate change impacts on marine ecosystems. *Marine Science,* 4. doi:10.1146/annurev-marine-041911-111611.

Dutkiewicz, S., Scott, J. R. and Follows, M. J. (2013) Winners and losers: ecological and biogeochemical changes in a warming ocean. *Global Biogeochemical Cycles,* 27(2), pp. 463-477.

Eppley, R. W. (1972) Temperature and phytoplankton growth in the sea. *Fisheries Bulletin,* 70(4), pp. 1063-1085.

Falkowski, P. G. (2004) Biogeochemistry of Primary Production in the Sea. in Schlesinger, W. H., (ed.) *Treatise on Geochemistry*: Gulf Professional Publishing. pp. 185–213.

Falkowski, P. G., Barber, R. T. and Smetacek, V. (1998) Biogeochemical controls and feedbacks on ocean primary production. *Science,* 281(5374), pp. 200-206.

Falkowski, P. G. and Raven, J. A. (1997) *Aquatic Photosynthesis,* Oxford, Englad: Blackwell Scientific.

Feng, Y., Hare, C. E., Leblanc, K., Rose, J. M., Zhang, Y., DiTullio, G. R., Lee, P. A., Wilhelm, S. W., Rowe, J. M., Sun, J., Nemcek, N., Gueguen, C., Passow, U., Benner, I., Brown, C. and Hutchins, D. A. (2009) Effects of increased pCO_2 and temperature on the North Atlantic spring bloom. I. The phytoplankton community and biogeochemical response. *Marine Ecology Progress Series,* 388, pp. 13-25. doi:10.3354/meps08133.

Field, C., Behrenfeld, M., Randerson, J. and Falkowski, P. (1998) Primary production of the biosphere: integrating terrestrial and oceanic components. *Science,* 281(5374), pp. 237-240.

Finkel, Z. V., Beardall, J., Flynn, K. J., Quigg, A., Rees, T. A. V. and Raven, J. A. (2009) Phytoplankton in a changing world: cell size and elemental stoichiometry. *Journal of Plankton Research*. doi:fbp098.

Finkel, Z. V. and Kotrc, B. (2010) Silica Use Through Time: Macroevolutionary Change in the Morphology of the Diatom Frustule. *Geomicrobiology Journal,* 27(6-7), pp. 596-608. doi:10.1080/01490451003702941.

Finkel, Z. V., Quigg, A., Raven, J. A., Reinfelder, J. R., Schofield, O. E. and Falkowski, P. G. (2006) Irradiance and the elemental stoichiometry of marine phytoplankton. *Limnology and Oceanography,* 51(6), pp. 2690-2701.

Follows, M. J. and Dutkiewicz, S. (2011) Modelling diverse communities of marine microbes. *Annual Review of Marine Science,* 3, pp. 427-451.

Fu, F. X., Warner, M. E., Yaohong, Z., Yuanyuan, F. and Hutchins, D. A. (2007) Effects of increased temperature and CO_2 on photosynthesis, growth, and elemental ratios in marine *Synechococcus* and *Prochlorococcus* (cyanobacteria). *Journal of Phycology,* 43, pp. 485-496.

Fu, F. X., Zhang, Y., Warner, M. E., Feng, Y., Sun, J. and Hutchins, D. A. (2008) A comparison of future increased CO_2 and temperature effects on sympatric *Heterosigma akashiwo* and *Prorocentrum minimum*. *Harmful Algae,* 7(1), pp. 76-90.

Geber, M. A. and Griffen, L. R. (2003) Inheritance and natural selection on functional traits. *International Journal of Plant Sciences,* 164(S3), pp. S21-S42.

Geider, R. and La Roche, J. (2002) Redfield revisited: variability of C: N: P in marine microalgae and its biochemical basis. *European Journal of Phycology,* 37(1), pp. 1-17.

Geider, R. J., MacIntyre, H. L. and Kana, T. M. (1998) A dynamic regulatory model of phytoplanktonic acclimation to light, nutrients, and temperature. *Limnology and Oceanography,* 43(4), pp. 679-694.

Gregg, W. W. and Casey, N. W. (2007) Modeling coccolithophores in the global oceans. *Deep Sea Research Part II: Topical Studies in Oceanography,* 54(5), pp. 447-477.

Hall, E. K., Singer, G. A., Kainz, M. J. and Lennon, J. T. (2010) Evidence for a temperature acclimation mechanism in bacteria: an empirical test of a membrane‐mediated trade‐off. *Functional Ecology,* 24(4), pp. 898-908.

Hays, G. C., Richardson, A. J. and Robinson, C. (2005) Climate change and marine plankton. *Trends in Ecology & Evolution,* 20(6), pp. 337-344.

Hessen, D. O., Ågren, G. I., Anderson, T. R., Elser, J. J. and de Ruiter, P. C. (2004) Carbon sequestration in ecosystems: the role of stoichiometry. *Ecology,* 85(5), pp. 1179-1192.

Hessen, D. O. and Elser, J. J. (2005) Elements of ecology and evolution. *Oikos,* 109(1), pp. 3-5.

Ho, T. Y., Quigg, A., Finkel, Z. V., Milligan, A. J., Wyman, K., Falkowski, P. G. and Morel, F. M. (2003) The elemental composition of some marine phytoplankton. *Journal of Phycology,* 39(6), pp. 1145-1159.

Hobday, A. J., Okey, T. A., Poloczanska, E. S., Kunz, T. J. and Richardson, A. J. (2006) Part C. Literature Review. in *Impacts of climate change on Australian marine life: Report to the Australian Greenhouse Office, Canberra, Australia*,Canberra: CSIRO.

Hoegh-Guldberg, O. and Bruno, J. F. (2010) The Impact of Climate Change on the World's Marine Ecosystems. *Science,* 328(5985), pp. 1523-1528. doi:10.1126/science.1189930.

Hood, R. R., Laws, E. A., Armstrong, R. A., Bates, N. R., Brown, C. W., Carlson, C. A., Chai, F., Doney, S. C., Falkowski, P. G. and Feely, R. A. (2006) Pelagic functional group modeling: Progress, challenges and prospects. *Deep Sea Research Part II: Topical Studies in Oceanography,* 53(5), pp. 459-512.

Hutchins, D. A., Fu, F. X., Zhang, Y., Warner, M. E., Feng, Y., Portune, K., Bernhardt, P. W. and Mulholland, M. R. (2007) CO_2 control of *Trichodesmium* N_2 fixation, photosynthesis, growth rates, and elemental ratios: Implications for past, present, and future ocean biogeochemistry. *Limnology and Oceanography,* 52(4), pp. 1293-1304.

Iglesias‐Rodríguez, M. D., Brown, C. W., Doney, S. C., Kleypas, J., Kolber, D., Kolber, Z., Hayes, P. K. and Falkowski, P. G. (2002) Representing key phytoplankton functional groups in ocean carbon cycle models: Coccolithophorids. *Global Biogeochemical Cycles,* 16(4). doi:10.1029/2001GB001454.

Johnson, Z. I., Zinser, E. R., Coe, A., McNulty, N. P., Woodward, E. M. S. and Chisholm, S. W. (2006) Niche partitioning among Prochlorococcus ecotypes along ocean-scale environmental gradients. *Science,* 311(5768), pp. 1737-1740.

Johnston, I. A. and Bennett, A. F. (1996) *Animals and Temperature: Phenotypic and Evolutionary Adaptation, Society for Experimental Biology seminar series,* Cambridge, UK: Cambridge University Press.

Klaas, C. and Archer, D. E. (2002) Association of sinking organic matter with various types of mineral ballast in the deep sea: Implications for the rain ratio. *Global Biogeochemical Cycles,* 16(4). doi:10.1029/2001GB001765.

Klausmeier, C. A., Litchman, E., Daufresne, T. and Levin, S. A. (2004) Optimal nitrogen-to-phosphorus stoichiometry of phytoplankton. *Nature,* 429(6988), pp. 171-174. doi:10.1038/nature02454.

Le Quere, C. L., Harrison, S. P., Colin Prentice, I., Buitenhuis, E. T., Aumont, O., Bopp, L., Claustre, H., Cotrim Da Cunha, L., Geider, R., Giraud, X. and Klaas, C. (2005) Ecosystem dynamics based on plankton functional types for global ocean biogeochemistry models. *Global Change Biology,* 11(11), pp. 2016-2040.

Litchman, E., Edwards, K. F., Klausmeier, C. A. and Thomas, M. K. (2012) Phytoplankton niches, traits and eco-evolutionary responses to global environmental change. *Marine Ecology Progress Series,* 470, pp. 235-248. doi:10.3354/meps09912.

Litchman, E. and Klausmeier, C. A. (2008) Trait-based community ecology of phytoplankton. *Annual Review of Ecology, Evolution, and Systematics,* 39, pp. 615-639.

Litchman, E., Klausmeier, C. A., Schofield, O. and Falkowski, P. G. (2007) The role of functional traits and trade‐offs in structuring phytoplankton communities: scaling from cellular to ecosystem level. *Ecology letters,* 10(12), pp. 1170-1181.

Litchman, E., Klausmeier, C.A., Miller, J.R., Schofield, O.M. and Falkowski, P.G., 2006. (2006) Multi-nutrient, multi-group model of present and future oceanic phytoplankton communities. *Biogeosciences Discussions,* 3(3), pp. 607-663.

Lohbeck, K. T., Riebesell, U. and Reusch, T. B. (2012) Adaptive evolution of a key phytoplankton species to ocean acidification. *Nature Geoscience,* 5(5), pp. 346-351.

Longhurst, A. R. (2010) *Ecological geography of the sea,* 2nd ed., San Diego, California, USA: Academic Press.

Margalef, R. (1978) Life-forms of phytoplankton as survival alternatives in an unstable environment. *Oceanologica acta,* 1(4), pp. 493-509.

Martin-Jezequel, V., Hildebrand, M. and Brzezinski, M. A. (2000) Silicon metabolism in diatoms: Implications for growth. *Journal of Phycology,* 36(5), pp. 821-840. doi:10.1046/j.1529-8817.2000.00019.x.

Martin-Jézéquel, V. and Lopez, P. J. (2003) Silicon—a central metabolite for diatom growth and morphogenesis. in *Silicon Biomineralization*,Berlin Heidelberg: Springer 2003. pp. 99-124.

McKew, B. A., Davey, P., Finch, S. J., Hopkins, J., Lefebvre, S. C., Metodiev, M. V., Oxborough, K., Raines, C. A., Lawson, T. and Geider, R. J. (2013) The trade‐off between the light‐harvesting and photoprotective functions of fucoxanthin‐chlorophyll proteins dominates light acclimation in *Emiliania huxleyi* (clone CCMP 1516). *New Phytologist.,* 200(1), pp. 74-85.

Moline, M. A. and Prezelin, B. B. (1996) Long-term monitoring and analyses of physical factors regulating variability in coastal Antarctic phytoplankton biomass, in situ productivity and taxonomic composition over subseasonal, seasonal and interannual time scales. *Marine Ecology Progress Series,* 145, pp. 143-160.

Montoya, J. P., Holl, C. M., Zehr, J. P., Hansen, A., Villareal, T. A. and Capone, D. G. (2004) High rates of N_2 fixation by unicellular diazotrophs in the oligotrophic Pacific Ocean. *Nature,* 430(7003), pp. 1027-1032.

Moore, J. K., Doney, S. C., Kleypas, J. A., Glover, D. M. and Fung, I. Y. (2002) An intermediate complexity marine ecosystem model for the global domain. . *Deep Sea Research Part II: Topical Studies in Oceanography,* 49(1), pp. 403-462.

Moore, J. K., Doney, S. C. and Lindsay, K. (2004) Upper ocean ecosystem dynamics and iron cycling in a global three‐dimensional model. *Global Biogeochemical Cycles,* 18(4), pp. 1-21. doi:doi:10.1029/2004GB002220.

Nair, A., Sathyendranath, S., Platt, T., Morales, J., Stuart, V., Forget, M. H. and Bouman, H. (2008) Remote sensing of phytoplankton functional types. *Remote Sensing of Environment,* 112(8), pp. 3366-3375.

Nedwell, D. B. (1999) Effect of low temperature on microbial growth: lowered affinity for substrates limits growth at low temperature. *FEMS Microbiology Ecology,* 30(2), pp. 101-111. doi:10.1111/j.1574-6941.1999.tb00639.x.

Nelson, D. M., Treguer, P., Brzezinski, M. A., Leynaert, A. and Queguiner, B. (1995) Production and dissolution of biogenic silica in the ocean - revised global estimates, comparison with regional data and relationship to biogenic sedimentation. *Global Biogeochemical Cycles,* 9(3), pp. 359-372. doi:10.1029/95gb01070.

Ohnemus, D. C., Rauschenberg, S., Krause, J. W., Brzezinski, M. A., Collier, J. L., Geraci-Yee, S., Baines, S. B. and Twining, B. S. (2016) Silicon content of individual cells of Synechococcus from the North Atlantic Ocean. *Marine Chemistry,* 187, pp. 16-24.

Partensky, F., Blanchot, J. and Vaulot, D. (1999) Differential distribution and ecology of *Prochlorococcus* and *Synechococcus* in oceanic waters: a review. *Bulletin-Institut oceanographique monaco-numero special*, pp. 457-476.

Quigg, A., Finkel, Z. V., Irwin, A. J., Rosenthal, Y., Ho, T. Y., Reinfelder, J. R., Schofield, O., Morel, F. M. and Falkowski, P. G. (2003) The evolutionary inheritance of elemental stoichiometry in marine phytoplankton. *Nature,* 425(6955), pp. 291-294.

Raven, J. A. (1998) The twelfth Tansley Lecture. Small is beautiful: the picophytoplankton. *Functional Ecology,* 12(4), pp. 503-513.

Raven, J. A. and Geider, R. J. (1988) Temperature and algal growth. *New Phytologist*, pp. 441-461.

Reay, D. S., Nedwell, D. B., Priddle, J. and Ellis-Evans, J. C. (1999) Temperature dependence of inorganic nitrogen uptake: reduced affinity for nitrate at suboptimal temperatures in both algae and bacteria. *Applied and environmental microbiology,* 65(6), pp. 2577-2584.

Redfield, A. C., Ketchum, B. H. and Richards, F. A. (1963) *The influence of organisms on the composition of seawater, The sea,* New York: Interscience.

Reusch, T. B. and Boyd, P. W. (2013) Experimental evolution meets marine phytoplankton. *Evolution,* 67(7), pp. 1849-59. doi:10.1111/evo.12035.

Reynolds, C. S., Huszar, V., Kruk, C., Naselli-Flores, L. and Melo, S. (2002) Towards a functional classification of the freshwater phytoplankton. *Journal of Plankton Research,* 24(5), pp. 417-428.

Richards, F. A. (1965) *Anoxic basins and fjords, Chemical Oceanography* New York: Academic Presspp. 611-645.

Richardson, T. L. and Jackson, G. A. (2007) Small phytoplankton and carbon export from the surface ocean. *Science,* 315(5813), pp. 838-840.

Ridgway, K. and Hill, K. (2009) The East Australian Current. in Poloczanska, E. S., Hobday, A. J. and Richardson, A. J., (eds.) *A Marine Climate Change Impacts and Adaptation Report for Australia 2009*: NCCARF Publication.

Sarthou, G., Timmermans, K. R., Blain, S. and Tréguer, P. (2005) Growth physiology and fate of diatoms in the ocean: a review. *Journal of Sea Research,* 53(1), pp. 25-42.

Schaum, E., Rost, B., Millar, A. J. and Sinéad, C. (2012) Variation in plastic responses to ocean acidification in a globally distributed picoplankton species. *Nature Climate Change*, pp. 1-5.

Schiebel, R. (2002) Planktic foraminiferal sedimentation and the marine calcite budget. *Global Biogeochemical Cycles,* 16(4). doi:10.1029/2001GB001459.

Schluter, L., Lohbeck, K. T., Gutowska, M. A., Groger, J. P., Riebesell, U. and Reusch, T. B. H. (2014) Adaptation of a globally important coccolithophore to ocean warming and acidification. *Nature Climate Change,* 4(11), pp. 1024-1030. doi:10.1038/nclimate2379.

Shannon, C. E. and Weaver, W. (1949) *The mathematical theory of communication,* Urbana, USA: The University of Illinois Press117.

Shimada, C., Tanaka, Y. and Tanimura, Y. (2006) Seasonal variation in skeletal silicification of *Neodenticula seminae*, a marine planktonic diatom: sediment trap experiments in the NW Pacific Ocean (1997–2001). *Marine Micropaleontology,* 60(2), pp. 130-144.

Simó, R. (2001) Production of atmospheric sulfur by oceanic plankton: biogeochemical, ecological and evolutionary links. *Trends in Ecology & Evolution,* 16(6), pp. 287-294.

Smetacek, V. (1999) Diatoms and the ocean carbon cycle. *Protist,* 150(1), pp. 25-32.

Smetacek, V. (2001) A watery arms race. *Nature,* 411(6839), pp. 745-745.

Smith, W. O. and Asper, V. L. (2001) The influence of phytoplankton assemblage composition on biogeochemical characteristics and cycles in the southern Ross Sea, Antarctica. *Deep Sea Research Part I: Oceanographic Research Papers,* 48(1), pp. 137-161.

Stefels, J., Dijkhuizen, L. and Gieskes, W. W. C. (1995) The marine sulfur-cycle: Importance of *Phaeocystis* sp. in DMS-production during a nearshore springbloom. *Studies in Environmental Science,* 65, pp. 241-243.

Steffen, W., Crutzen, P. J. and McNeill, J. R. (2007) The Anthropocene: are humans now overwhelming the great forces of nature. *AMBIO: A Journal of the Human Environment,,* 36(8), pp. 614-621.

Steinacher, M., Joos, F., Frolicher, T. L., Bopp, L., Cadule, P., Cocco, V., Doney, S. C., Gehlen, M., Lindsay, K. and Moore, J. K. (2010) Projected 21st century decrease in marine productivity: a multi-model analysis. *Biogeosciences,* 7(3). doi:10.5194/bg-7-979-2010.

Tatters, A. O., Roleda, M. Y., Schnetzer, A., Fu, F., Hurd, C. L., Boyd, P. W., Caron, D. A., Lie, A. A. Y., Hoffmann, L. J. and Hutchins, D. A. (2013) Short- and long-term conditioning of a temperate marine diatom community to acidification and warming. *Philosophical Transactions of Royal Society B: Biological Sciences,* 368. doi:10.1098/rstb.2012.0437.

Taucher, J. and Oschlies, A. (2011) Can we predict the direction of marine primary production change under global warming? *Geophysical Research Letters,* 38(2), pp. L02603. doi:10.1029/2010GL045934.

Tomas, C. R. (1997) *Identifying marine phytoplankton.,* San Diego, California, USA: Academic press.

Tréguer, P. J. and De La Rocha, C. L. (2013) The world ocean silica cycle. *Annual Review of Marine Science,* 5, pp. 477-501.

Tyrrell, T. (1999) The relative influences of nitrogen and phosphorus on oceanic primary production. *Nature,* 400(6744), pp. 525-531.

Verity, P. G., Robertson, C. Y., Tronzo, C. R., Andrews, M. G., Nelson, J. R. and Sieracki, M. E. (1992) Relationships between cell volume and the carbon and nitrogen content of marine photosynthetic nanoplankton. *Limnology and Oceanography,* 37(7), pp. 1434-1446.

Zehr, J. P., Waterbury, J. B., Turner, P. J., Montoya, J. P., Omoregie, E., Steward, G. F., Hansen, A. and Karl, D. M. (2001) Unicellular cyanobacteria fix N_2 in the subtropical North Pacific Ocean. *Nature,* 412(6847), pp. 635-638.

CHAPTER 2:
THERMAL PERFORMANCE CURVES OF FUNCTIONAL TRAITS AID UNDERSTANDING OF THERMALLY-INDUCED CHANGES IN DIATOM-MEDIATED BIOGEOCHEMICAL FLUXES

K. G. Baker*, C. M. Robinson, D.T. Radford, A. S. McInnes, C. Evenhuis, M. A. Doblin.

Plant Functional Biology and Climate Change Cluster, School of Life Sciences, University of Technology Sydney, Sydney, New South Wales, Australia.

*** Correspondence:** Kirralee G Baker, Plant Functional Biology and Climate Change Cluster, University of Technology Sydney, Broadway, Ultimo, New South Wales, 2007, Australia

Kirralee.G.Baker@student.uts.edu.au

Keywords: temperature, warming, thermal performance curves, phytoplankton, biogeochemistry, functional traits, plasticity, photoacclimation.

2.1 Introduction

Marine phytoplankton are a ubiquitous and diverse group of photosynthetic microbes found in the sunlit layers of our global ocean. Their metabolic processes and, therefore, distribution and abundance, are mainly controlled by ocean temperature (Thomas et al. 2012), which is shifting as a result of contemporary climate change, and creating novel environments not yet encountered by phytoplankton (Boyd et al. 2010). Ocean temperature will act selectively on phytoplankton physiology, impacting fitness and modifying distributions by favouring populations with 'fit phenotypes' for their respective habitats (Chevin et al. 2013). From the whole cell perspective, the 'fit phenotype' is a culmination of trade-offs between many FTs, the underlying elements of the phenotype that dictate fitness and ecological function (Litchman and Klausmeier 2008). Trade-offs are likely to have significant implications for marine biogeochemical processes, because many FTs are either directly or indirectly related to elemental transformations (**Figure 1.1**) (Falkowski et al. 1998, Litchman and Klausmeier 2008).

Diatoms, a group of silicifying phytoplankton, are major drivers of both the C and Si cycles through their large contribution to total oceanic primary production (20-25%; Nelson et al. 1995), C export from surface oceans, and obligate requirement for Si to build cell walls. When diatoms encounter environmentally stressful conditions, they become more silicified because C assimilation relative to Si uptake slows, leading to an uncoupling between C and Si cycling (Finkel and Kotrc 2010). To advance our understanding of how diatom-mediated biogeochemical fluxes are impacted by anthropogenic climate change, more detailed experimentation, observations and modelling are necessary to quantify changes in specific phenotypic traits and physiological trade-offs under different environmental conditions.

Investigation of individual traits of an organism is known as *phenomics* and the relationship between these traits and the environmental parameter of interest is usually achieved through measurement of *performance curves*, typically determined under constant conditions along a gradient of one environmental variable (Gilchrist 1995). Performance curves are powerful for modelling purposes as they describe the shape of the trait-environment relationship. TPCs are the distinct case where temperature is chosen as the environmental variable of interest and typically have a bell-curve shape (Huey and Stevenson 1979). This contrasts with performance curves for increasing

light, inorganic carbon or dissolved nutrients, which are often hyperbolic (Geider et al. 1993). TPCs show significant within (and between) taxon variability, as a community wide study demonstrated when several strains of the same species grown under identical culture conditions had different T_{opt} and critical minimum (CT_{min}) and maximum (CT_{max}) temperatures (Boyd et al. 2013). Furthermore, FTs may not have the same shaped response as growth, due to differences in their plasticity or underlying mechanistic controls e.g., cell size often changes linearly (Atkinson et al. 2003), and some traits remain relatively constant (Davison 1991). The significant diversity underlying species and trait-specific TPCs explains why, for most studies to date, traits have only been measured at a limited number of points across the range of an environmental parameter (Lohbeck et al. 2012) or in numerous species but for a limited number of traits (Boyd et al. 2013).

To our knowledge, no study to date has provided a comprehensive analysis of multiple trait responses across a full range of temperatures. Additionally, by detailing how physiological traits and rate processes are controlled by temperature, trade-offs between FTs can be examined. Trait-based approaches such as these have been invaluable for demonstrating that trade-offs largely determine species niches and biogeochemical/ecological function, but so far have only been modelled along nutrient gradients (Litchman et al. 2007); trade-offs between FTs along temperature gradients remain relatively unknown.

To advance understanding of how ocean warming will affect diatom-mediated biogeochemical fluxes, we conducted an in-depth characterisation of TPCs in FTs of the cosmopolitan, model diatom species *T. pseudonana*. We focused specifically on morphological traits: cell size and frustule silicification, as well as physiological traits: photosynthesis, and the assimilation of carbon and other nutrients (nitrogen, phosphorus, silicon). Whilst the shapes of these TPCs have not yet been elucidated in this species, we hypothesised that the thermal optimum and shape of these individual functional traits would differ from the whole organism growth response.

2.2 Methods and materials

2.2.1 Experimental setup

The coastal centric diatom, *T. pseudonana* CS-173 was obtained from the Australian National Algae Culture Collection (CSIRO, Hobart, Australia). This marine strain originates from Moriches Bay of the Forge River (Long Island, New York, USA) in the North Atlantic Ocean (NAO) and is identical to the National Centre of Marine Algae and Microbiota (NCMA) strain CCMP1335. *T. pseudonana* was maintained in glass Erlenmeyer flasks at 20 °C in seawater medium (0.2 µm filtered coastal seawater obtained from Port Hacking National Reference Station, PH100, New South Wales, Australia) with f/2 enrichment (Guillard and Ryther (1962); 8.82 x 10^{-4} M $NaNO_3$; 3.62 x 10^{-5} M, NaH_2PO_4 H_2O; 1.06 10^{-4} M, Na_2SiO_3 H_2O, trace metal solution and vitamin solution). Before experimental measurements were made, cultures of 30 mL were grown in triplicate glass vessels for 3-4 generations over a temperature gradient spanning 11 to 35 ˚C. This temperature range was selected as to capture the minimum and maximum temperatures for growth (CT_{min} and CT_{max}, respectively) in order to constrain estimates of these parameters in later analysis (discussed below). The temperature gradient was established using a thermal gradient block; where hot and cold water was generated using separate immersion heater chillers (Julabo GmbH, Germany) and was then circulated through milled channels at opposite ends of the block (for experimental set-up see **Supplementary Figure 2.1**). Temperature was monitored using a calibrated thermocouple (Comark, United Kingdom). Light (cool white) was supplied (50 µmol photons m^{-2} s^{-1}) by an array of light emitting diodes (LEDs; Schenzen Cidly Group, China) set to a 12 h: 12 h light: dark cycle. This irradiance was consistent with previous light conditions of inoculum cultures and was verified with a microspherical quantum sensor (Walz, Germany). Morphological and physiological trait measurements (described below) were made during the exponential growth phase following 3-4 generations of acclimation.

2.2.2 Phenotype fitness

The exponential growth of cells was used to estimate fitness of the phenotype expressed at each temperature (twelve temperatures across the 11 to 35 °C gradient). Cell counts were performed daily using a flow cytometer (BD Influx, Becton Dickinson, Brussels, Belgium) equipped with a 50 mW laser emitting at a fixed wavelength of 488 nm. To

assess mortality and estimate growth of live cells, a nucleic acid stain (SYTOX green, Molecular Probes, Leden, Nederland) was used following the protocol of Peperzak and Brussaard (2011). Briefly, samples of 100 µL were incubated with the stain (final concentration 0.5 µM) in the dark at room temperature for 10 minutes prior to flow cytometric analysis. Live cells were selected as negative for SYTOX stain (gated on side scatter and green fluorescence (585/40 nm) (for more information see gating logic in **Supplementary Figure 2.2**). Population statistics were calculated using particle counts in gates that were consistent across the experiment, acquired with the same instrument settings.

2.2.3 Morphological traits

2.1.1.1 Cellular volume

Cells were harvested in exponential growth phase when volumes of 1 mL were sampled and stored in glutaraldehyde (final concentration 1% v/v Sigma-Aldrich, Australia) until later analysis was carried out using a Coulter Counter equipped with a 20 µm aperture (Multisizer 4, Beckman Coulter GmbH, Germany). Sample volumes of 1 mL were diluted in 4 mL freshly filtered seawater (0.2 µm) to meet instrument operational requirements (minimum analytical volume of 5 mL). Population statistics were then calculated from ≥500 cells, ranging from 2–9 µm in length. These cell sizes were then calibrated against external standards with beads of known size (2.0 µm, 4.1 µm and 5.7 µm; ThermoFisher Scientific, Australia) and produced a linear regression of R^2 >0.99.

2.1.1.2 Frustule silicification

To measure newly deposited silicon into diatom frustules, samples of 10 mL were harvested in exponential phase and incubated in the presence of the fluorescent label Lysosensor Yellow/Blue DND-160 (otherwise known as PDMPO, ThermoFisher Scientific, Australia) following the labeling protocol of Leblanc and Hutchins (2005). Briefly, cells were incubated in the presence of the dye (final concentration 0.125 µM) along with a control sample that did not contain PDMPO (to quantify background fluorescence) at experimental conditions for 24 h. Following incubation, a 500 µL aliquot of each sample was enumerated flow cytometrically (BD Influx, Becton Dickinson, Brussels, Belgium) where the mean relative fluorescence of incorporated PDMPO for each diatom population was quantified against the mean fluorescence of

the fluorescent bead population (1 µm, ThermoFisher Scientific, Australia) at UV excitation of 355 nm and blue fluorescence at 469/29 nm (for more information see gating logic in). Fluorescence per cell was then normalised to cellular volume (quantified by the Coulter Counter method as described above) to correct for any differences in fluorescence due to cell size.

2.2.4 Physiological traits

2.2.4.1 Photophysiology

Fast repetition rate fluorometry (FRRf) was applied to assess the electron transport kinetics of photosystem II (PSII) at each temperature. Samples (2 mL) were harvested during exponential growth and measurements were made on each sample immediately after being removed from the temperature block (2 h after onset of light phase). The first measurement was performed in the dark (to allow down-regulation of very fast relaxing non-photochemical quenching) and actinic white light at the growth irradiance intensity (47 µmol photons m^{-2} s^{-1}) was supplied by a white LED for 1 min and measurements performed at 20 s intervals during the actinic light exposure. The last measurement of each set was used in further calculations of photochemical efficiency. A Chelsea Technologies FASTocean fluorometer supplied single-turnover excitation flashlets (of 1.1 µs duration) at 450 nm at a rate of 2 µs to achieve full saturation of PSII reaction centers followed by longer intervals of 100 µs to allow relaxation and reoxidation of Q_A. Profiles of the fluorescence emission were fitted within the FastPro8 software (v. 1.0.55; Chelsea Technologies) to the Kolber-Prasil-Falkowski model (Kolber et al. 1998) to yield the minimum (F_O or F'; ' indicates light adapted samples) and maximum fluorescence (F_M or F_M'), effective absorption cross section of PSII (σ or σ'; nm^2) and reoxidation kinetic of Q_A (τ; µs). Values for the photochemical efficiency (Φ_{PSII} or Φ_{PSII}'; both dimensionless) were calculated from these parameters as (F_M-F_O/F_M) or (F_M'-F'/F_M') for light adapted samples. Sample filtrate (after filtration through 0.2 µm Millipore syringe filters) was also measured in the FRRf to account for background fluorescence. The data was visually inspected to ensure no fluorescence induction in the filtrate (indicating an absence of phytoplankton) and the mean F_O and F_M of the filtrate were averaged into a single value to be subtracted from all F_O (or F') and F_M (or F_M') values.

A second series of measurements was performed to parameterise the light-dependent response of electron transport kinetics and identify shifts in the light-saturated rates of electron transport and the light utilisation efficiency. In the interest of minimising diurnal impacts (Schuback et al. 2015), we conducted rapid light curves (RLC) on a single replicate for each temperature to reduce the time period of measurements. Measurements of the light dependent electron transport rate (ETR) were achieved with a RLC protocol where samples were illuminated by the FASTAct instrument chamber that supplied actinic white light at increasing light intensities of 0, 10, 28, 47, 66, 85, 104, 123, 160, 251, 330, 402, 550, 756, 905, 1208 μmol photons m^{-2} s^{-1}. Each sample was dark adapted for 10 minutes prior to measurement at ambient temperature, and each actinic light intensity was applied for 20 s and measurements collected every 10 s, with the last measurement at each light step recorded as the fluorescence yield for that light step. The ambient temperature of each temperature treatment was maintained during RLC measurements using a flow-through water bath attached to the FASTAct sample chamber set at the required temperature. The ETR was calculated using an in-built 'Sigma algorithm' within FASTPro8 (see Oxborough et al. 2012, Robinson et al. 2014). The light dependency of the electron transport rate was modeled by fitting ETR to a Jassby-Platt model (Jassby and Platt 1976) to derive the light utilisation efficiency (α) and light saturation irradiance (E_k).

2.2.4.2 Chlorophyll *a* content

Sample volumes of 2 mL were harvested in exponential growth phase and centrifuged at 5000 *g* for 5 min at 20 ˚C. The supernatant was discarded and cell pellets stored frozen at -80 °C until analysis (carried out within 3 months). Pigments were extracted for 15 min in the dark at 4 °C in a 3 mL volume of 3:2 90% acetone: 100% dimethyl sulfoxide extraction reagent (Shoaf and Lium 1976). Chlorophyll *a* was determined in a fluorometer (TD-700, Turner Designs, USA) using the non-acidification method of (Welschmeyer 1994). The fluorometer was calibrated with pure chlorophyll *a* (Sigma-Aldrich, USA), whose concentration was calculated from absorbance via using the coefficients in (Jeffrey et al. 1997).

2.2.4.3 Primary productivity (^{14}C uptake)

To estimate primary productivity across the temperature gradient, C fixation rates were measured using ^{14}C-labelled bicarbonate in small volume incubations as described in (Doblin et al. 2011). Specifically, radiolabeled $NaH^{14}CO_3$ (stock solution 1.85 x 10^7 Bq) was added to 5 mL of culture in clear glass tubes (1.5 µCi per tube) and incubated in the thermal gradient block for 60–80 min under the growth irradiance. Activity in the samples was determined by removing a 100 µL aliquot from three randomly selected tubes and placing it into 5 mL of refrigerated 0.1 M NaOH, adding 10 mL scintillation fluid (Ultima Gold^{TM}, Perkin Elmer) and shaking before counting using a liquid scintillation counter (Packard TriCarb 2900 TR). Each temperature contained a dark sample wrapped in aluminum foil to quantify carbon fixation in the dark. Following incubation, tube contents were transferred to scintillation jars, acidified with 100 µL 6 M HCl and shaken on an orbital shaker for 12 h to remove inorganic ^{14}C. Scintillation fluid (10 mL Ultima Gold^{TM}; Perkin Elmer) was then added to each sample, vigorously shaken and left for 3 h before counting. Counting time was set to 5 min so that counts were within a 5% counting error.

2.2.4.4 Uptake of nitrogen, phosphate and silicate

To estimate the net cellular uptake of N, P and Si (added to cultures as nitrate, phosphate and silicate) the difference between nutrient concentrations at the start and end of the experiment was calculated and normalised to the difference in cell abundance to account for differences in growth. Subsamples at each time point were removed from all experimental vessels and centrifuged at 5000 *g* for 5 min at 20 ˚C. The supernatant (500 µL) was then removed and stored frozen at -20 °C until colorimetric analysis to determine concentrations of nitrate (NO_3^-), nitrite (NO_2^{2-}), phosphate (PO_4^{3-}) and reactive silicate (SiO_4^{4-}). NO_3^- contents were determined indirectly as described in Schnetger and Lehners (2014). Briefly, NO_2^- concentrations were analysed by the Griess-Ilosvay method and subtracted from total N (NO_x) obtained though the vanadium (III) chloride reduction reaction. The NO_3^- values were linear between 1 and 100 µM and the detection limit was 0.15 µM. Inorganic P was determined by the sensitive detection method of Hoenig et al. (1989) where values were linear between 1 and 15 µM and the detection limit was 0.95 µM. Reactive SiO_4^{4-} was determined by a

miniaturised modification of Strickland and Parsons (1968) where values were linear between 1 and 150 μM and the detection limit was 9.5 μM. We note that freezing samples for reactive silicate analyses may have produced Si polymerisation resulting in underestimates of absolute rates of Si uptake. Where necessary, samples were diluted in order to obtain concentrations within the linear detection range of each colorimetric method.

2.2.5 Data analysis

Prior to this study, the TPCs for many FTs had not been described, so trait responses were visually inspected before analysis. Traits that showed positive, negative or no relationships with temperature were described using simple linear regression where statistical significance was accepted at p <0.01. Traits that exhibited a bell-shaped curve were described by the following equation:

$$f(T) = ae^{bT}\,(CT_{max} - T)(T - CT_{min}) \quad \textbf{(Equation 2.1)}$$

This is a transformation of the equation described by Boyd et al. (2013) and Thomas et al. (2012) so that it is parameterised by the CT_{min} and CT_{max} temperatures. The shape of the TPC is controlled by three important temperature traits: CT_{min} and CT_{max} (which determine the thermal niche width), and b, a coefficient from the Eppley curve (Eppley 1972), an exponential relationship thought to provide the upper bound constraint on community-level phytoplankton growth as a function of temperature.

The $T_{opt,}$ is where the slope of the curve is zero. This can be found by taking the derivative of **Equation 2.1** with respect to T and finding where it is 0 by solving a quadratic equation. This yields the following equation:

$$T_{opt} = \frac{-B-\sqrt{B^2-4AC}}{2A} \qquad \textbf{(Equation 2.2)}$$

where:

$$A = -b \qquad \textbf{(Equation 2.2.1)}$$

$$B = +b\ \frac{CT_{max}+CT_{min}}{2} - 2 \qquad \textbf{(Equation 2.2.2)}$$

$$C = CT_{max} + CT_{min} - bCT_{max}CT_{min} \qquad \textbf{(Equation 2.2.3)}$$

When fitting curves to data for individual traits, it was found that estimates of CT_{min} produced unrealistic results and therefore it was necessary to constrain b and CT_{min} to positive values.

The parameter values in **Equation 2.1** were found by Maximum Likelihood Estimation (MLE) (assuming normally distributed errors). Confidence intervals (CI) were found by parametric bootstrapping. Using the MLE of the parameters: (i) synthetic data with the same temperature sampling as the experimental data was generated using **Equation 2.1**, (ii) **Equation 2.1** was then fitted to a synthetic data set by MLE, (iii) new parameter values, as well as the T_{opt} and maximum values were stored. This process was repeated a total of 5,000 times. From these distributions the 95% CI were calculated as the range between the 2.5th and 97.5th quantiles. These estimates of uncertainty were vital for subsequent analyses, as they allowed us to appropriately account for the inherent differences in uncertainty of multiple traits. Confidence bands were calculated in a similar fashion. For each synthetic dataset the function values were stored from 0 to 40 °C in 0.5 °C increments. At each stored temperature the confidence intervals were calculated as above.

2.3 Results

Consistent with our hypothesis, the TPCs of some FTs could be well described by bell-shaped curves, including growth rate, primary productivity and chlorophyll content. These FTs had better goodness-of-fit, with relatively low values of root mean squared error; RMSE (i.e., close to zero) and hence better predictability with temperature (**Table 2.1**). In contrast, cellular uptake of nitrite, phosphate, and silicate was less predictable, with higher values of RMSE (i.e., wider confidence intervals) (**Table 2.1**). Other traits were better described by linear functions (**Table 2.2**), showing significant positive or negative linearity with temperature (p <0.01) including cell volume, frustule silicification, effective quantum yield, reoxidation of Q_A and chlorophyll normalised productivity (P^b) (**Table 2.2**). Other traits, such as cross-sectional area servicing PSII, ETR and nitrate uptake showed no relationship with temperature - i.e., remained relatively constant from 11 to 35 ˚C (p >0.01). Some of these traits were more strongly correlated with temperature than others (i.e., higher R^2) such as re-oxidation of Q_A (**Table 2.2**).

T. pseudonana showed considerable thermal plasticity, demonstrating relatively high fitness (growth >0.2 d^{-1}) over a large temperature range (**Figure 2.1**). Temperature was found to be a good predictor of growth (RMSE =0.1) and the MLE of the T_{opt} for growth was 18.6 °C, with 95% CI being 17.0 to 20.1 °C (T_{opt} range). The maximum growth rate attained within the T_{opt} range (hereafter referred to T_{opt} for simplicity) was estimated as 0.8±0.07 d^{-1}. Growth rates were lowest at 33 °C (0.18±0.1 d^{-1}) and ceased at 35 °C (CT_{max}) where loss of cells indicated mortality. Samples from 35 °C were therefore excluded from further trait analyses. Unlike the CT_{max}, the CT_{min} for growth was not observed in the experimental data. As a result, we lack critical values at the lower temperature threshold to fully characterise CT_{min} and consequently, our estimates of both CT_{min} and niche widths have high uncertainty (i.e., lie between 0 and 6 °C for CT_{min}). Note this is also the case for all remaining FTs (**Table 2.1**).

Table 2.1 Estimated thermal performance curve (TPC) parameters and associated uncertainty calculated from parametric bootstrapping for each functional trait (FT) fitted using **Equation 2.1**; thermal optimum T_{opt}, trait value at thermal optimum and thermal niche width.

Functional trait	**Units**	**Temperature optimum (T_{opt})**			**Trait value at T_{opt}**			**Thermal niche width (° C)**			**RMSE**
		lower CI	**MLE**	**upper CI**	**lower CI**	**MLE**	**upper CI**	**lower CI**	**MLE**	**upper CI**	
Growth rate	d^{-1}	17	18.6	20.1	0.7	0.8	0.9	24.9	29.9	34.8	0.1
Primary productivity	pgC $cell^{-1}$ h^{-1}	19.5	20.8	22.2	4.2	4.5	4.7	29	34.2	38.3	0.5
Chlorophyll content	pgChl $cell^{-1}$	22.9	23.9	25.3	2.2	2.4	2.6	28.4	32.1	38.1	0.4
Nitrite uptake	pmol cell d^{-1}	22.8	24.1	25.3	131.3	138.2	145.4	37.7	40.5	46.9	13.7
Phosphate uptake	pmol cell d^{-1}	20.7	21.5	22.5	67.9	70.5	73.5	36.2	40.8	44.2	5.2
Silicate uptake	pmol cell d^{-1}	20.6	21.4	22.5	717.8	741.4	765.9	39.5	42.4	44.3	54.4

Table 2.2 Estimated thermal performance curve (TPC) parameters for functional traits (FT) fitted using linear regression and associated uncertainty calculated by parametric bootstrapping, including: the proportional change in trait value per degree Celsius relative to the thermal optimum (T_{opt}) for growth (Δ °C) and trait value at thermal optimum.

Functional trait	**Units**	***p*-value**	**Adjusted-R^2**	**Δ °C**			**Trait value at T_{opt}**		
				lower CI	**MLE**	**upper CI**	**lower CI**	**MLE**	**upper CI**
Cell volume	μm^3	0.00022	0.340	0.0033	0.0064	0.0100	23.4	23.9	24.4
Frustule silicification	RFUs per μm^3	0.00007	0.407	-0.0183	-0.0147	-0.0099	0.240	0.256	0.271
Effective quantum yield	arbitrary units	0.00034	0.323	-0.0064	-0.0059	-0.0054	0.551	0.554	0.557
Reoxidation of Q_A	μs	0.00000	0.841	-0.0081	-0.0072	-0.0063	668	674	681
Chlorophyll normalised productivity	pgC $pgChl^{-1}$ h^{-1}	0.00004	0.439	-0.0225	-0.0186	-0.0134	11.86	13.01	14.12

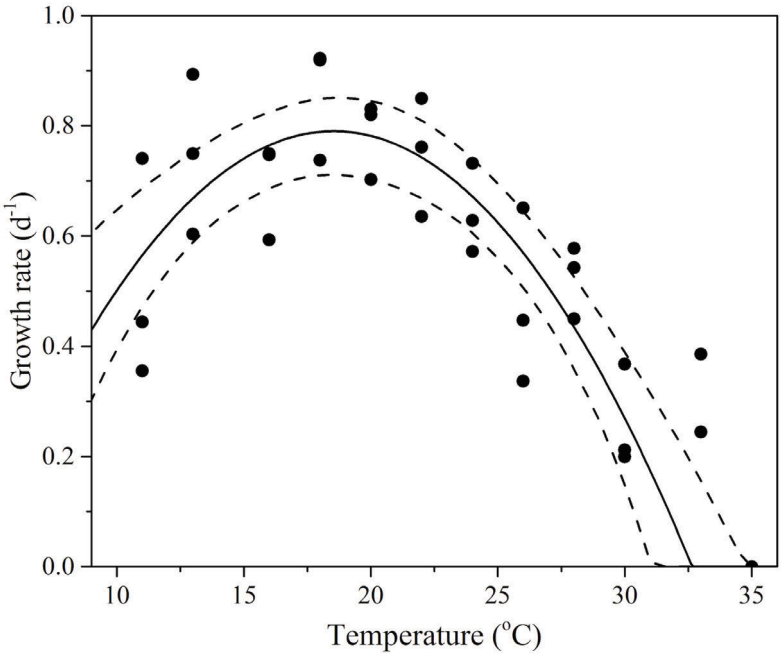

Figure 2.1 Thermal performance curves (TPC) of fitness in the cosmopolitan model diatom *T. pseudonana* showing growth rate as a function of temperature (n = 33, RSME =0.1). Each symbol represents a distinct biological replicate. The solid line corresponds to maximum likelihood estimate (MLE) with broken lines corresponding to the 95 % confidence intervals (CI) of the bell-shape function (**Equation 2.1**) estimated by parametric bootstrapping.

Temperature also affected *T. pseudonana* morphology, as cell volume and frustule silicification exhibited significant linear relationships (p <0.001) with increasing temperature but with opposite signs (**Figure 2.2**). Cell volume ranged between 22±0.4 μm^3 at the lowest (11 °C) and 26±0.4 μm^3 at the highest (33 °C) temperatures assayed (15% rise overall), with a median cell volume of 23.9±0.2 μm^3 observed at the growth T_{opt} (**Figure 2.2a**). In contrast, silicification of *T. pseudonana* decreased with increasing temperature, from 0.3 relative fluorescence units (RFUs) per μm^3 at 11 °C to 0.1 RFUs per μm^3 at 33 °C, equivalent to a 66% reduction in frustule thickness (**Figure 2.2b**).

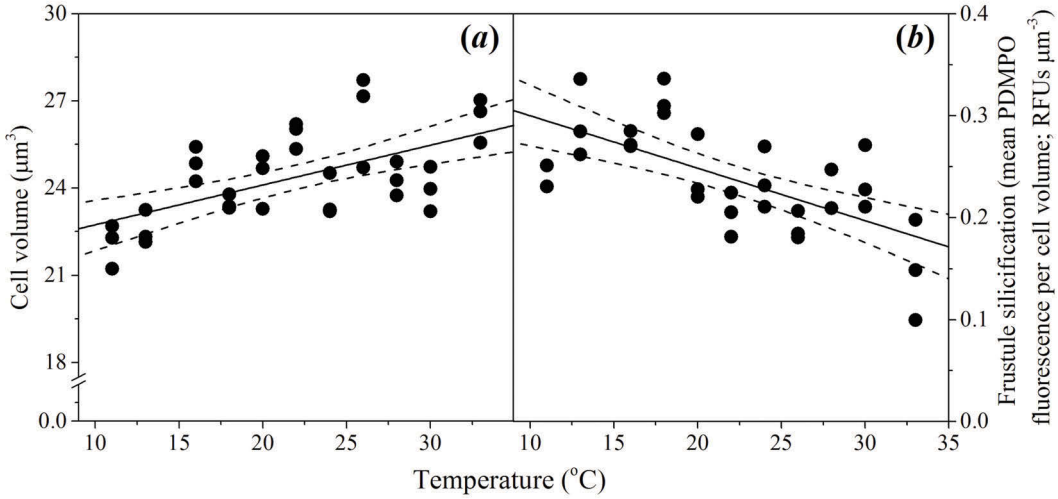

Figure 2.2 Thermal performance curves (TPC) of morphological traits in the diatom *T. pseudonana* portraying (a) cell volume (n = 33, p <0.01, R^2 =0.34); and (b) frustule silicification (n = 31, p <0.01, R^2 =0.41), as a function of temperature. Each symbol represents a distinct biological replicate. The solid line corresponds to maximum likelihood estimate (MLE) with broken lines corresponding to the 95 % confidence intervals (CI) of a linear regression both estimated by parametric bootstrapping.

Photophysiological trait analysis of *T. pseudonana* revealed assay temperature significantly affected a number of biophysical properties such as light harvesting and utilisation. The functional absorption cross-section servicing functional PSII reaction centres (σPSII) was similar (3 nm^2 $PSII^{-1}$; p =0.03) across all temperatures assayed, varying by as little as 0.5 nm^2 over the ~20 °C gradient. Greater variability in σ_{PSII} was observed at temperature extremes (i.e., wider confidence band; **Figure 2.3a**). While cells retained the ability to harvest light over the entire temperature range, the ability to utilise light declined at warming temperatures, demonstrated by a significant decrease (p <0.001; R^2 =0.32) in the photochemical efficiency of PSII (effective quantum yield; Φ_{PSII}) (**Figure 2.3b**). Despite the decline in light energy being directed towards photochemistry with increasing temperatures, electron flux through PSII was relatively similar across all temperatures assayed, as there was no significant relationship between ETRs and temperature (p =0.23; R^2 =0.2) (**Figure 2.3c**). There was, however, an acceleration of downstream electron transport processes (acceptor side of PSII, donor side of PSI), accounting for the reduced operational efficiency at PSII. This was indicated by the decrease in the re-oxidation time of Q_A (τ) with increasing temperature (p <0.01; R^2 =0.84), from 800 µs at 11 °C to 600 µs at 33 °C (**Figure 2.3d**). RLC measurements indicated that there is a trend of increasing irradiance needed to saturate

photosynthesis with warming temperatures, as the saturation irradiance (E_k) increased from 100 to 500 μmol photons m^{-2} s^{-1} for samples incubated at 11 °C and 33 °C, respectively (**Figure 2.3e**). Finally, the TPCs of light harvesting efficiency (α) followed a similar trend to ETRs, showing a small decrease at intermediate temperatures. Cells at lower and higher temperatures than the T_{opt} had highest light utilisation efficiency (**Figure 2.3f**).

Temperature had a direct and predictable affect on key metrics of C cycling traits of primary productivity (RSME =0.5), cellular chlorophyll content (RSME =0.4) and chlorophyll normalised productivity rates (p <0.001; R^2 =0.44) (**Figure 2.4**). Primary productivity (PP) gradually increased from 3.4±0.8 pgC $cell^{-1}$ h^{-1} at 11 °C, to a maximum rate of 4.5±0.2 pgC $cell^{-1}$ h^{-1} at T_{opt} (between 19.5 and 22.2 °C) and then decreased more sharply with warming temperatures, where PP was lowest at 33 °C with values of 1.9±0.1 pgC $cell^{-1}$ h^{-1} (**Figure 2.4a**). Minimum cellular chlorophyll *a* content was observed at the cold end of the temperature spectrum (0.75±0.3 pgChl $cell^{-1}$), rising rapidly with increasing temperature to a maximum cell quota of 2.4±0.2 pgChl $cell^{-1}$ between 22.9 and 25.3 °C and then gradually declined to 1.5±0.25 pgChl $cell^{-1}$ at 33 °C (**Figure 2.4b**). Chlorophyll normalised productivity was greatest at colder temperatures, decreasing linearly with temperature from ~2.4 pgC $pgChl^{-1}$ h^{-1} at 11 °C to ~1.3 pgC $pgChl^{-1}$ h^{-1} at 33 °C (**Figure 2.4c**), at a rate of 0.37 pgC $pgChl^{-1}$ h^{-1} per °C (**Table 2.2**).

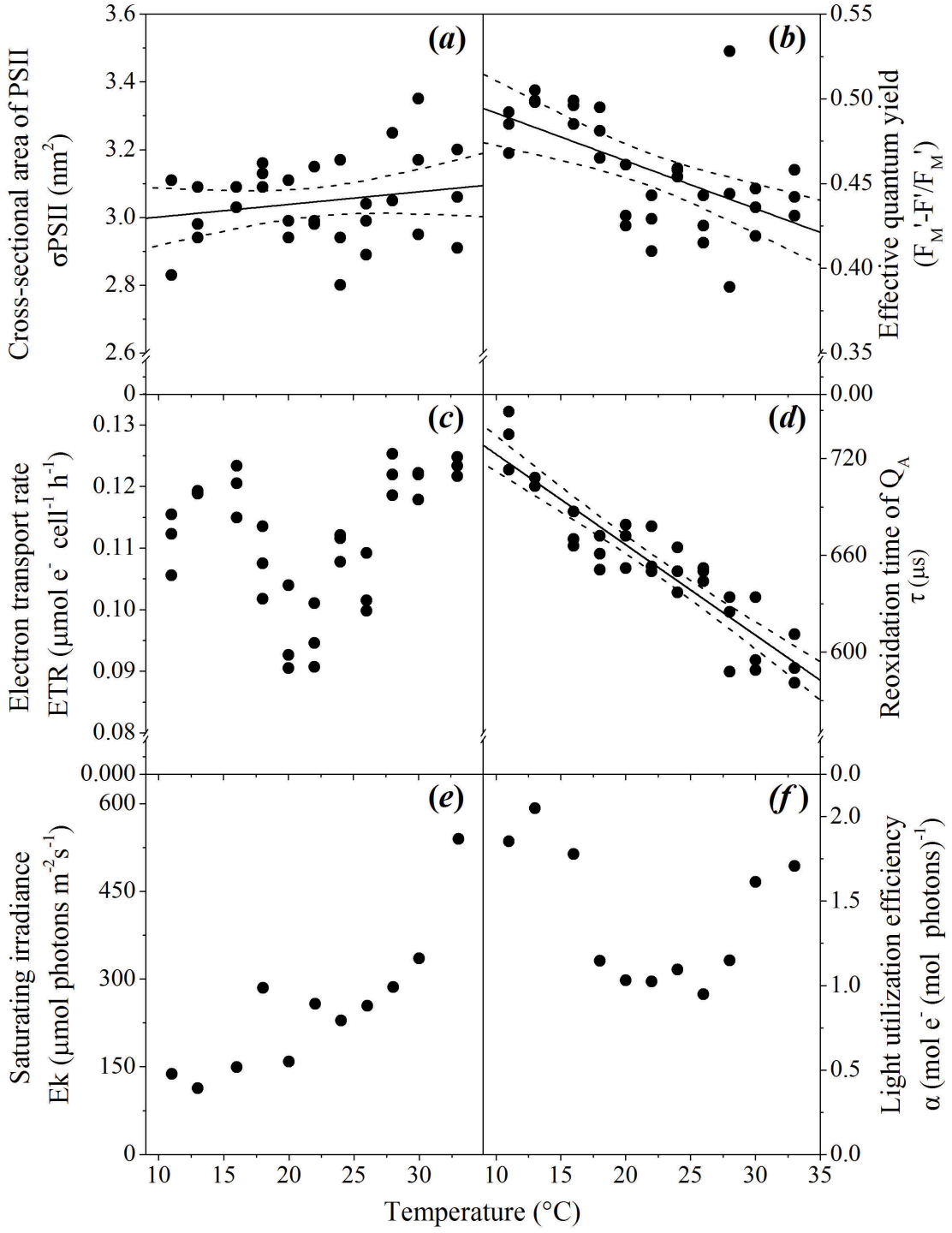

Figure 2.3 Thermal performance curves (TPC) of *T. pseudonana* photophysiological traits relating to light acquisition and harvesting showing (a) Functional cross-sectional area of PSII (n = 32, p =0.03, R^2 =0.59); (b) Effective quantum yield (n = 33, p <0.01, R^2 =0.32); (c) Electron transport rate (n = 33, p =0.23, R^2 =0.01); (d) Reoxidation time of Q_A (n = 33, p <0.01, R^2 =0.59); (e) Saturating irradiance (n =12); and (f) Light harvesting efficiency (n =12), as a function of temperature. Cells were harvested from cultures grown at 50 µmol photons m^{-2} s^{-1}, with each symbol representing a distinct biological replicate. Solid line corresponds to maximum likelihood estimate (MLE) with broken lines corresponding to the 95 % confidence intervals (CI) of a linear regression, all estimated by parametric bootstrapping. (e - f) Data shown are parameters derived from rapid light curves with a single biological replicate, hence no maximum likelihood estimates or confidence intervals.

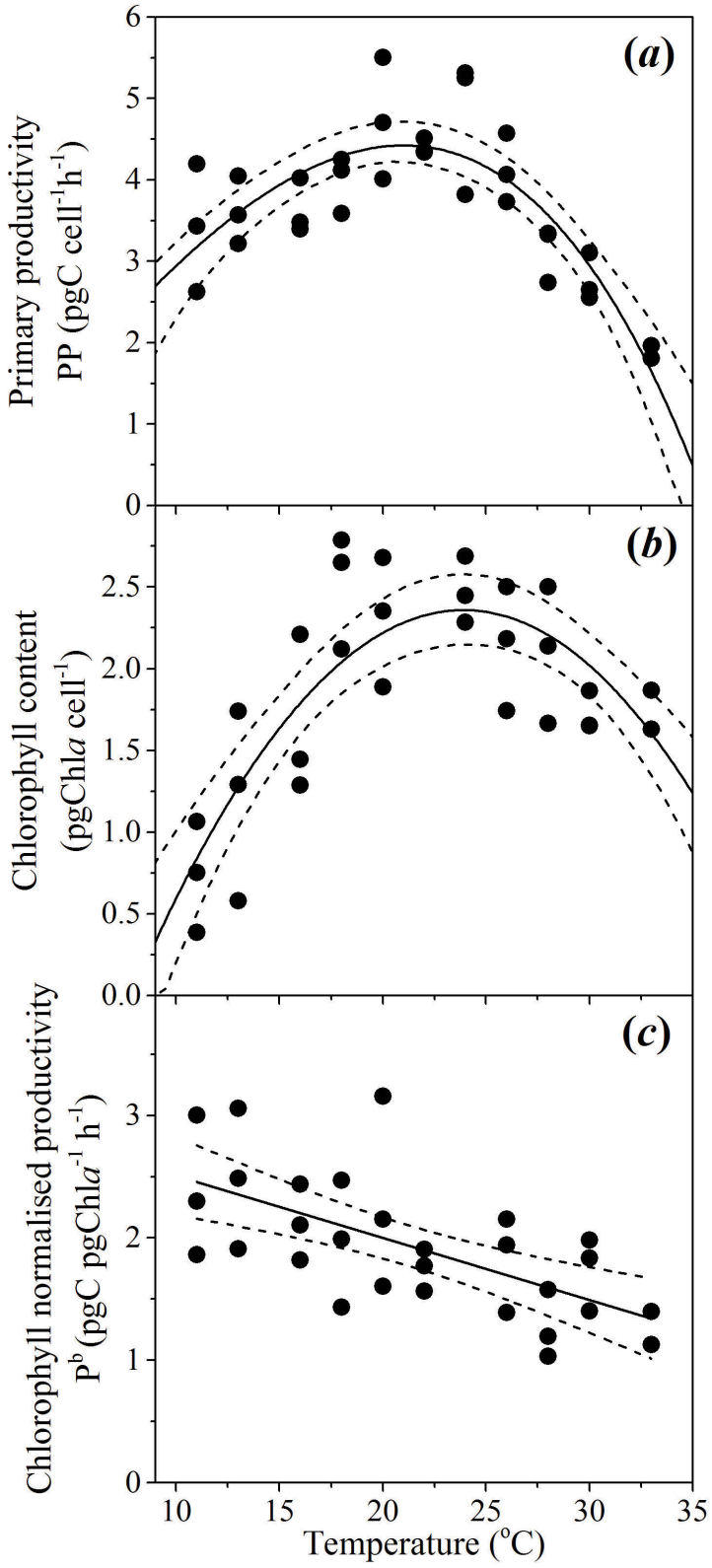

Figure 2.4 Thermal performance curves (TPC) of physiological traits in the diatom *T. pseudonana* describing (a) primary productivity (n = 32, RSME =0.5); (b) chlorophyll content (n = 29, RSME =0.4); and (c) chlorophyll normalised productivity (n = 29, p <0.01, R^2 =0.44), as a function of temperature. Each symbol represents a distinct biological replicate. Solid lines correspond to maximum likelihood estimate (MLE) with broken lines corresponding to the 95 % confidence intervals (CI) of the (a, b) bell-shape function (**Equation 2.1**), and (c) linear regression, all estimated by parametric bootstrapping.

Resource acquisition of dissolved N, P and Si by *T. pseudonana* differed across the experimental temperature gradient (**Figure 2.5**), but responded less predictably with temperature in comparison to primary productivity and chlorophyll content (i.e., greater RSME; **Table 2.1**). Unlike the other dissolved nutrients measured in this study, NO_3^- uptake was not affected by temperature (p =0.04; R^2 =0.01) (**Table 2.2**). In contrast to NO_3^-, uptake of NO_2^-, P and Si exhibited bell-shaped curves as a function of temperature (**Figure 2.5b-d**). The MLE of the thermal optimum for NO_2^- uptake was 24.1 °C, with 95% CI being 22.8 to 25.3 °C (T_{opt} range; **Table 2.1**). Dissolved NO_2^- uptake increased gradually from ~80 pmol cell d^{-1} at 11 °C to a maximum uptake rate of 138±7 pmol cell d^{-1} at T_{opt} and then decreased gradually with further increases in temperature to ~95 pmol cell d^{-1} at 33 °C (**Figure 2.5b**). This T_{opt} range significantly differed from that of P and Si, where very similar MLE of T_{opt} were obtained for both nutrients, with maximum net uptake occurring at 21.5 and 21.4 °C, respectively (**Table 2.1**). Temperatures exceeding the T_{opt} range of P and Si, resulted in a gradual decline of P and Si uptake, to a minimum of ~50 pmol cell d^{-1} and ~450 pmol cell d^{-1}, respectively at 33 °C (**Figure 2.5c,d**). This decrease of apparent Si uptake at supra-optimal temperatures may also explain the reduced frustule silicification observed with warming temperatures (**Figure 2.5b**).

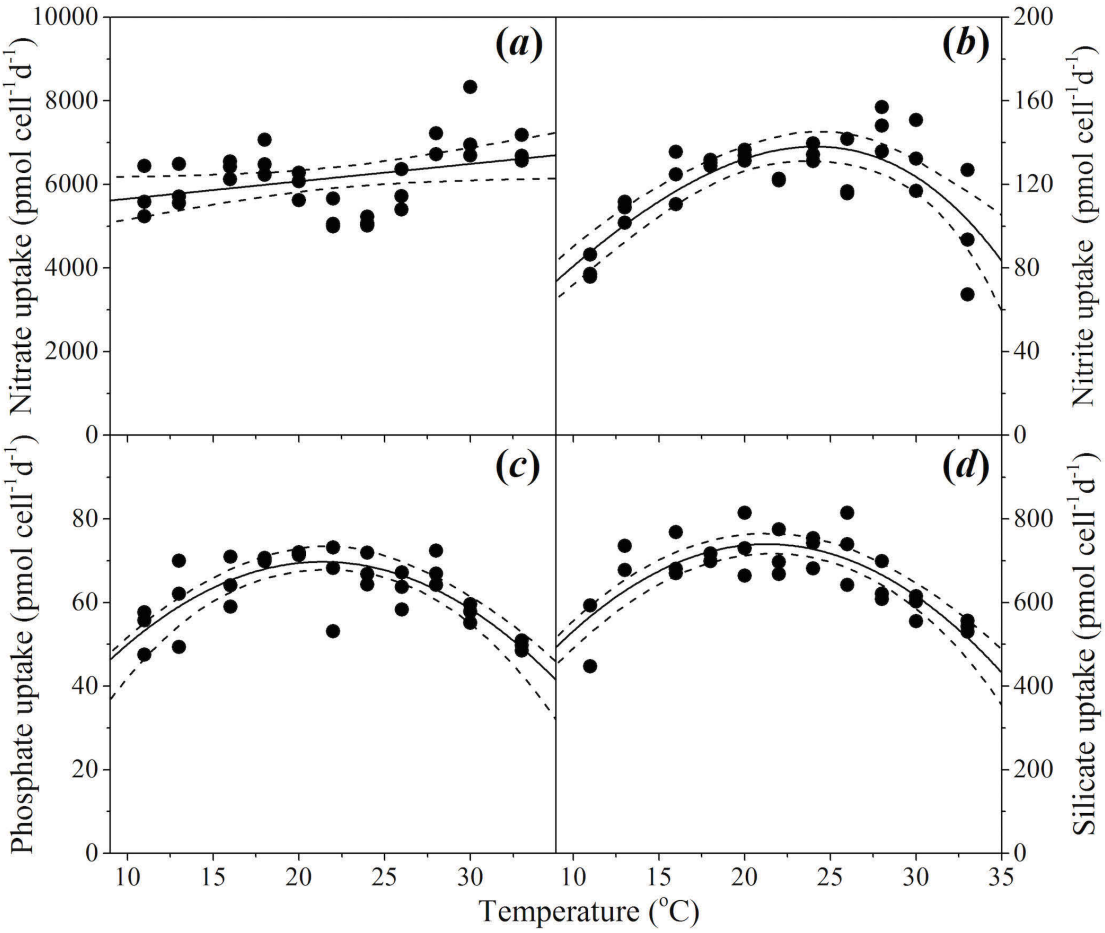

Figure 2.5 Thermal performance curves (TPC) of physiological traits in the diatom *T. pseudonana* depicting uptake of dissolved nutrients (a) nitrate (n = 33, p =0.039, R^2 =0.10); (b) nitrite (n = 33, RSME =13.7); (c) phosphate (n = 33, RSME =5.2); and (d) silicate (n = 33, RSME =54.4), as a function of temperature. Each symbol represents a distinct biological replicate. Solid lines corresponds to maximum likelihood estimate (MLE) with broken lines corresponding to the 95 % confidence intervals (CI) of (a) linear regression, and (b - d) the bell-shape function (**Equation 2.1**), all estimated by parametric bootstrapping.

A comparison of the thermal optima and niche widths of different traits was made with overall fitness (**Figure 2.6**). Functional traits were observed to separate into three distinct groups: similar T_{opt} and niche width to growth (Group I), greater T_{opt} but similar niche width to growth (Group II), and greater T_{opt} and greater niche width than growth (Group III). Some FTs appeared to overlap between different groups (e.g. primary productivity between Group I, II and II), whereas others were clearly distinguishable (e.g. Si uptake in Group III only). Physiological traits related to photosynthesis operated over similar niche widths but showed greater T_{opt} than growth – e.g., chlorophyll content. In comparison, FTs related to resource acquisition (NO_2^-, P and Si uptake) were characterised by their ability to function over wider niche widths and higher T_{opt} in comparison to growth (**Figure 2.6**).

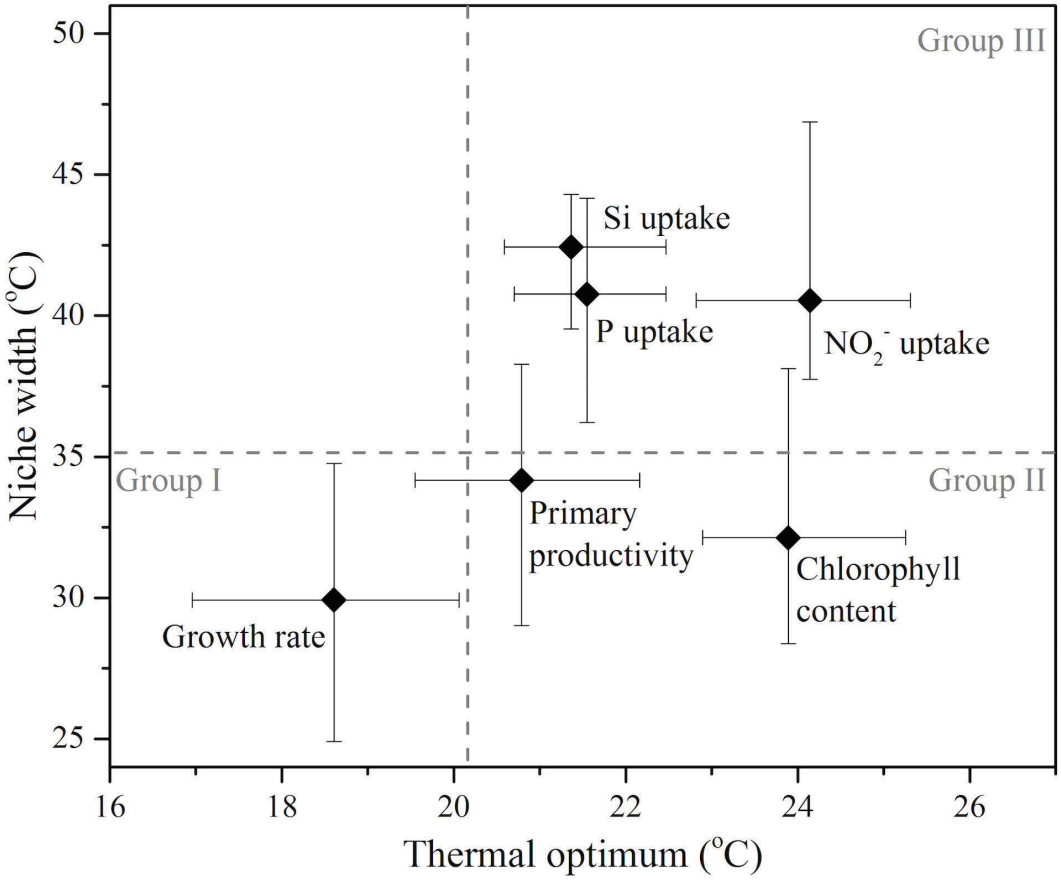

Figure 2.6 A comparison of the thermal optimum (temperature range over which the maximum trait value is obtained), and niche width (temperature range over which trait value is positive) of various functional traits measured in the diatom *T. pseudonana,* which were parameterised by fitting the bell-shaped function (**Equation 2.1**). Symbols represent maximum likelihood estimate (MLE) and error bars correspond to the 95 % confidence intervals (CI), both estimated by parametric bootstrapping. Functional traits (FT) are sub-categorised into three groups (Group I, II and II) separated by the upper 95% CI for the thermal optimum and niche width for growth (broken grey lines).

FTs that exhibited a significant and relatively strong linear relationship with temperature (p <0.05; R^2 >0.30) are summarised in **Table 2.2**, including important thermal characteristics such as: the trait value at T_{opt}, and the proportional change in trait value per °C relative to the optimal for growth (Δ °C). Comparing Δ °C between FTs provided insight into differences in thermal sensitivities. For example, Δ °C was relatively consistent between traits, changing between 0.0064 (e.g. cell volume) and 0.0186 (e.g. P^b) relative units, equivalent to 0.6 and 1.8% per degree Celsius (**Table 2.2**). However, these traits varied in their direction of change (positive or negative) (**Table 2.2**). One trait was an exception: chlorophyll normalised productivity (P^b) that changed by 0.02 Δ °C T_{opt} (i.e., gradient more vertical) indicating increased flexibility and perhaps greater thermal sensitivity of this trait per unit increase in temperature.

2.4 Discussion

2.4.1 Thermal performance curves reveal phenotypic plasticity

The shape and/or T_{opt} of TPCs were unique for each FT assessed in this study. These have yielded insight into the biological controls underlying the trait response and also provide a measure of thermal sensitivity. The most thermally resilient traits measured were the σPSII and ETRs, which had a flat thermal response (**Figure 2.3a,c**). Regulation of σPSII under thermal stress has also been found in heat tolerant phylotypes of the symbiotic dinoflagellate *Symbiodinium* (McGinley et al. 2012) and may suggest that the photosynthetic apparatus of the broadly distributed diatom *T. pseudonana* is also thermally stable. Large temperature deviations from the growth T_{opt} had significant implications on growth (reduced by 80%). In comparison, small changes were observed for cell volume and effective quantum yield (Δ °C; **Table 2.2**); both of these traits showed linear TPCs. Nutrient fluxes (NO_2, PO_4, SiO_4) decreased by ~10% across the temperature gradient compared to optimal conditions, with a large proportion of the TPC being flat. The greatest magnitude of temperature-induced change was observed for traits with bell-shaped TPCs, specifically C fixation, which was ~50% lower at temperature extremes compared to the T_{opt}. The shape of the curves suggest that the thermal sensitivity of traits increased in the following order: flat (light harvesting; σPSII) > linear (light utilisation; Φ_{PSII}, cell morphology; volume) > concave (NO_2, PO_4, SiO_4 flux) > bell-shaped (growth, primary productivity, chlorophyll content). Linear performance curves have the least amount of thermal sensitivity because for a given amount of change in temperature always produces the same amount of change in the trait response. In contrast, for a trait with a bell-shaped performance curve, the specific temperature dictates the degree of response; a given amount of temperature change will induce a small change for temperature close to the T_{opt} but a large response towards the tails. If we use the derivative of the performance curve to define trait plasticity, we observe greater thermal sensitivity in traits that express more plasticity (for further discussions see; Angilletta 2009). On the other hand, traits must have considerable plasticity to express a flat response curve because in order to maintain performance, cells must be able to adjust their physiology at the same rate of the environmental change (Schulte et al. 2011). Whichever way it is defined, it is clear that phenotype plasticity plays a significant role in thermal acclimation.

2.4.2 Temperature driven changes in fitness and other functional traits

In keeping with our hypothesis, we observed the T_{opt} of growth was different to the T_{opt} for each underlying FT, being the lowest amongst all traits measured (**Figure 2.6**). The mechanisms behind these trait responses are likely due to the thermal specificity of the underlying enzymes responsible for these processes. Furthermore, some FT TPCs do not have a definitive T_{opt} because they were constant (i.e., electron transport rate) or linear (i.e., photosynthetic efficiency of PSII, cell volume). Despite these traits not exhibiting a typical TPC shape, it does not mean that they are not thermally regulated. In the following sections we discuss the likely candidates of the biological processes that underlie the shapes and T_{opt} of TPCs obtained for the morphological and physiological traits measured in this study.

The cosmopolitan model diatom, *T. pseudonana*, demonstrated relatively high fitness over a large thermal range (**Figure 2.1**), consistent with the global distribution of this genus (Leblanc et al. 2012). Furthermore, maximum growth rates were comparable to previously reported values for this strain; ~0.9 d^{-1} at 18 °C and 80 μmol photons m^{-2} sec^{-1} (Li and Campbell 2013). In contrast to other studies, we found that the T_{opt} range (17.0 and 20.1 °C, centered on 18.6 °C) was slightly colder than previously reported values (Boyd et al. 2015, Thompson et al. 1992) and may be due to the lower growth irradiance used in our study (Sandnes et al. 2005). In terms of morphological traits, absolute cell volumes were within range of previously reported values (Li and Campbell 2013) and consistent with Thompson et al.(1992), with cells becoming larger with increasing temperature (**Figure 2.2a**). These changes in cell volume, although small (i.e., ~10%), may have significant implications for vertical export of carbon, as has been demonstrated in other small, spherical phytoplankton taxa (coccolithophores; Pantorno et al. 2013). However, the degree of frustule silicification (**Figure 2.2b**) must also be taken into consideration, because the specific gravity of BSi exceeds that of any other polymer and has significant effects on the density of the cell as a whole (Raven and Waite 2004). For example, colder temperatures (11 °C) result in smaller, thicker diatoms (**Figure 2.2**) and may be more likely to reach the deep sea floor for burial because of their proportionally greater cell specific gravity. In contrast, warmer temperatures (33 °C) result in larger but thinner diatoms (**Figure 2.2**) that may sink more rapidly because of their larger cell size (as explained above). Alternatively,

thinner frustules also reduce physical defenses and provide grazers with food of a different biochemical composition, i.e. greater C content (Raven and Waite 2004) and as a result may reduce the likelihood of the whole cell reaching the cell floor. Therefore, interaction between these two morphological traits (i.e., cell volume and frustule silicification) along a temperature gradient may create different phenotypes with different functional and biogeochemical roles.

The temperature driven changes in cell volume observed in this study have significant impacts for photophysiological responses to irradiance as cells may increase light-harvesting pigment content to processes associated with C fixation (Finkel et al. 2009). We see evidence of temperature-driven changes in photophysiological responses through changes in chlorophyll normalised primary productivity (P^b), light harvesting efficiency (α), and saturation irradiance (E_k). Despite the cross-sectional area of the pigment antennae funneling light to PSII remaining relatively unchanged with temperature (**Figure 2.3a**), RLC reveal different functional light responses by cells at cold and warm temperatures. At cold temperatures (between 11 and 16 °C) lower E_k and higher α values suggest the presence of a "bottle-neck" in downstream electron-transport processing from harvested photons, e.g., in the Calvin Cycle. To a phytoplankton cell, these biomolecular triggers mimic those encountered when PSII is under pressure from excess light, and signals cold-acclimated cells to down-regulate chlorophyll synthesis (Behrenfeld et al. 2015) and cell volume declines to compensate for pigment packaging effects (Kirk 1994, Raven 1984). As temperature rises, cells appear to require more light to saturate photosynthesis despite light conditions remaining constant. This is evidenced by the increases in saturation irradiance (**Figure 2.3e**), coupled by corresponding declines in P^b (**Figure 2.3c**) and reoxidation time of Q_A (**Figure 2.3d**) and because $E_k = 1 / \sigma * \tau$ (Sakshaug et al. 1997). Together these results suggest that with increasing temperature, photosynthesis becomes rate-limited by the light reactions. As a result, cells attempt to increase light-harvesting capacity by synthesising nitrogen-rich chlorophyll (**Figure 2.4b**). However, cells become increasingly larger and pigment-packaging effects seem to counteract any benefits associated with increased pigmentation and absolute rates of primary productivity decline (**Figure 2.4c**). As the efficiency of the Calvin Cycle decreases, alternative electron sinks e.g. cyclic electron transport around PSII, Mehler reaction, terminal

oxidase activity, nitrate reduction also become progressively more important with increasing temperature (Hancke et al. 2008, Kulk et al. 2012).

Resource acquisition of NO_2-, P and Si appeared to conform to a conventional TPC shape but was less predictable than growth (**Figure 2.5**). Additionally, the curvature of these TPCs appeared less pronounced in comparison to the TPCs of growth and primary productivity and as a result exhibited wider thermal niches. As has been demonstrated previously, temperatures below the T_{opt} of growth appeared to lower the affinity for all inorganic substrates and is believed to be due to more inflexible membranes leading to decreased efficiency of embedded transporter proteins (Nedwell 1999). Comparatively, at higher temperatures, membranes become more fluid and may become more susceptible to attack by reactive oxygen species and, as a result, membrane transporter proteins become targeted by oxidative protein damage (Lesser 2006). The TPCs of nitrite, phosphate and silicate suggest a high degree of thermal stability in these physiological processes as the net uptake rates at the hot (33 °C) and cold (11 °C) end of the gradient were only reduced by ~10% in comparison to rates observed at the T_{opt}. This might mean that elemental fluxes may be relatively resilient to temperature variation at least in comparison to other processes such as growth and carbon fixation. In stark contrast, NO_3^- uptake remained relatively unaffected by temperature (weakly significant; p =0.04). However, this does not necessarily mean that temperature does not mediate nitrate utilisation. For example, the assimilation of NO_3^- involves a number of mechanisms: NO_3^- reductase, NO_2^- reductase, associated active transport systems, cellular ATP and NADPH (Mulholland and Lomas 2008). In *T. pseudonana*, these linked cellular processes may not necessarily result in an overall TPC, even though each underlying step may be affected by temperature. Furthermore, it is known that NO_3^- can be released shortly after it is assimilated, on timescales as short as hours (Mulholland and Lomas 2008). As such, it is possible that measuring the drawdown of dissolved NO_3^- from the culture medium, is not a sensitive enough method to detect temperature effects on nitrate acquisition, due to the timescale over which the nutrient can be exported from the cell.

2.4.3 Phenotype-dependent functional roles

Defining the relationship between the TPCs of various FTs provides insight into how functional roles of different phytoplankton types can be altered under seasonal cycles in

temperature overlaid with climate variability. The oceanic province from which this strain originates (NAO) encounters substantial fluctuations in temperature. On an annual timescale, sea surface temperatures (SST) reach a maximum of ~25 °C and minimum of ~10 °C in boreal summer and winter, respectively (NOAA 2015, Reynolds and Smith 1995). Overlaying this annual temperature window (solid lines; **Figure 2.7**) on the TPCs of the various FTs obtained in this study, demonstrates why such a large degree of phenotypic plasticity is advantageous, enabling the survival of a single genotype over large temperature fluctuations. Under future ocean change, modelling suggests departures of up to +2 °C from present mean SST are expected by 2100 for the NAO province (Boyd et al. 2015). Under these new conditions, the annual temperature window becomes warm-shifted (broken lines; **Figure 2.7**) and a further separation between cell volume and frustule silicification occurs, along with a sharp decrease in primary productivity and overall fitness.

The interaction between the two morphological traits measured along the temperature gradient, i.e., cell volume and frustule silicification, results in different diatom phenotypes (**Figure 2.7**) with potentially distinct functional roles. For example, at cold temperatures, where diatom frustules are thicker, the increased specific gravity and resistance to grazers (Raven and Waite 2004) may increase vertical export of C. In contrast, larger but thinner cells, that are more readily penetrated by grazers (Raven and Waite 2004) may increase the elemental residence times of C and Si in the euphotic zone through assimilation into grazer biomass (Hutchins et al. 1995). This may result in two alternative pathways: either the subsequent transfer of C and Si to higher trophic levels, or, its incorporation into fecal pellets, resulting in more rapid transfer to the ocean's interior (Honjo et al. 2008, Hutchins et al. 1995). Together, these results demonstrate that temperature amongst other environmental factors can directly affect the biogeochemical fate of C and Si, through alterations in diatom morphology.

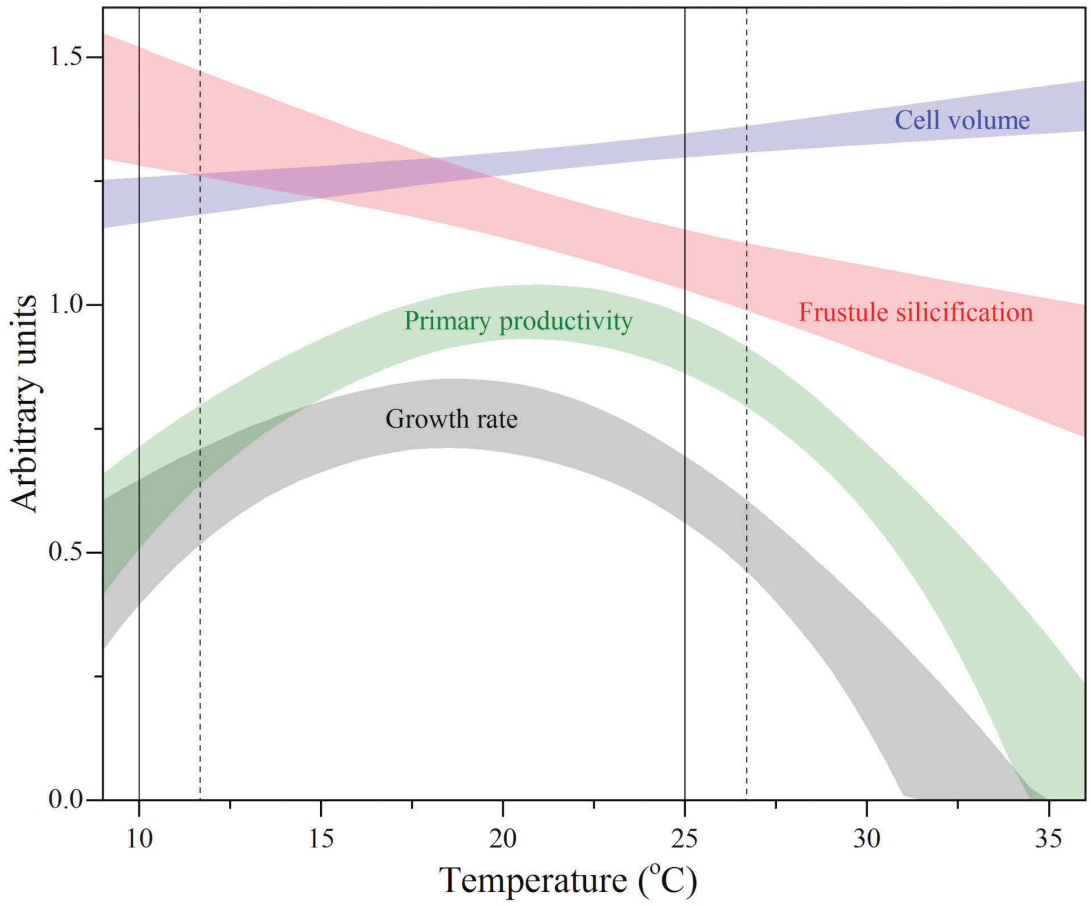

Figure 2.7 Thermal performance curves (TPC) of fitness (*grey band*) and other functional traits (FT) including primary productivity (*green band*), cell volume (*blue band*) and frustule silicification (*red band*) in the marine diatom *T. pseudonana* (CCMP 1335) originally isolated from the North Atlantic Ocean. Each confidence band represents the maximum likelihood estimate (MLE) with 95 % confidence intervals (CI), both estimated by parametric bootstrapping for each functional trait. Solid vertical lines correspond to the thermal window currently encountered in the North Atlantic Ocean (NAO) ranging from the minimum boreal winter temperature (~ 10 °C) and maximum boreal summer temperature (~ 25 °C), both estimated from monthly sea surface temperatures for December 2014 and July 2015 obtained from NOAA. Broken line depicts predicted estimates of future mean sea surface temperature (SST) warming of the NAO (Boyd et al. 2015).

2.4.4 Implications and future research directions

Quantitatively, the most biogeochemically important phytoplankton belong to the centric diatoms, including genera such as *Chaetoceros* and *Thalassiosira* because together, they contribute almost a third of total biomass of marine diatoms, globally (Leblanc et al. 2012). Due to their high species diversity, phytoplankton blooms dominated by *Thalassiosira* spp. can occur worldwide, including in such locations as Antarctica, upwelling regions off the African coastline, and recurrent blooms in temperate and boreal regions (Leblanc et al. 2012, Schmidt and Schaechter 2012, Sorokin 1999). As evidenced by sediment trap records, these episodic, seasonal blooms

that often coincide with high nutrient concentrations, typically result in high vertical export (Honjo et al. 2008, Sarthou et al. 2005). If the TPCs of FTs in *T. pseudonana* (this study) are representative of the thermal response of the genus or centric diatoms as a whole, we anticipate that temperature-driven distributions of diatom phenotypes may differentially contribute to the regulation of C and Si, and subsequently, the marine food web and biological carbon pump.

Firstly, our findings exemplify the need to better quantify the performance curves of specific functional traits so that we can make comparisons between their plasticity. This will increase our understanding of the capacity of specific taxa to physiologically adjust to changing ocean conditions and examine the implications of these phenotypic responses in current and future scenarios. Secondly, whilst diatoms play a significant role in marine biogeochemical functioning, they are not the only contributors to global elemental cycles and as a result, we suggest that similar studies should be conducted for model species of other functional types of phytoplankton (e.g. diazotrophs, calcifiers). This information is required in order to advance the understanding of the diversity of taxon-specific responses to temperature change and what implications this has on the biogeochemical fluxes that they regulate. Thirdly, current and future ocean global change is multifaceted and includes not only warming but also changes in CO_2 concentrations, nutrient and light availability, as well as the interactions between these environmental variables (Boyd et al. 2010). Taxon- and trait-specific performance curves are not restricted to temperature and can therefore be extended to all of the stressors mentioned above. Equally, it is not only the mean trajectory of these stressors that is changing in a future ocean but also increased variability. Multi-trait analyses over more resolved environmental gradients (e.g. twelve temperature treatments) replication provides a useful framework to advance understanding of how taxon-specific FTs will respond to complex ocean change. Finally, we have seen evidence that the distribution of phenotypes has changed over macro-evolutionary timescales (Finkel and Kotrc 2010), suggesting that to predict the future functioning of the biological carbon pump and other biogeochemical processes we must consider adaptive constraints or trade-offs between these functional traits (Litchman et al. 2015). To explore this, evolutionary experiments (Huertas et al. 2011) could be combined with studies such as ours by incorporating longer timescales of exposure.

2.5 Acknowledgements

The authors would like to thank Associate Professor David Suggett, Professor Douglas Campbell and Dr. Katherina Petrou for their insightful discussions and Professor Maria Byrne for access to the thermal gradient blocks. The authors would also like to thank two anonymous reviewers for their invaluable improvements to this manuscript.

This research was funded by a student scholarship awarded through the School of Life Sciences and Plant Functional Biology and Climate Change Cluster- (C3), University of Technology Sydney to KB and an Australian Research Council Discovery Grant Scheme (DP14010134) to MD.

2.6 Literature cited

Angilletta, M. J. (2009) *Thermal adaptation: a theoretical and empirical synthesis,* Oxford University Press.

Atkinson, D., Ciotti, B. J. and Montagnes, D. J. (2003) Protists decrease in size linearly with temperature: ca. 2.5% C− 1. *Proceedings of the Royal Society of London. Series B: Biological Sciences,* 270(1533), pp. 2605-2611.

Behrenfeld, M. J., O'Malley, R. T., Boss, E. S., Westberry, T. K., Graff, J. R., Halsey, K. H., Milligan, A. J., Siegel, D. A. and Brown, M. B. (2015) Revaluating ocean warming impacts on global phytoplankton. *Nature Climate Change*, pp. 1-8. doi:10.1038/NCLIMATE2838.

Boyd, P. W., Lennartz, S. T., Glover, D. M. and Doney, S. C. (2015) Biological ramifications of climate-change-mediated oceanic multi-stressors. *Nature Climate Change,* 5(1), pp. 71-79.

Boyd, P. W., Rynearson, T. A., Armstrong, E. A., Fu, F., Hayashi, K., Hu, Z., Hutchins, D. A., Kudela, R. M., Litchman, E., Mulholland, M. R., Passow, U., Strzepek, R. F., Whittaker, K. A., Yu, E. and Thomas, M. K. (2013) Marine Phytoplankton Temperature versus Growth Responses from Polar to Tropical Waters – Outcome of a Scientific Community-Wide Study. *PLoS One,* 8(5), pp. e63091. doi:10.1371/journal.pone.0063091.

Boyd, P. W., Strzepek, R., Fu, F. and Hutchins, D. A. (2010) Environmental control of open-ocean phytoplankton groups: Now and in the future. *Limnology and Oceanography,* 55(3), pp. 1353-1376. doi:10.4319/lo.2010.55.3.1353.

Chevin, L. M., Collins, S. and Lefèvre, F. (2013) Phenotypic plasticity and evolutionary demographic responses to climate change: taking theory out to the field. *Functional Ecology,* 27(4), pp. 967-979.

Davison, I. R. (1991) Environmental effects on algal photosynthesis: temperature. *Journal of Phycology,* 27(1), pp. 2-8.

Doblin, M. A., Petrou, K. L., Shelly, K., Westwood, K., Van den Enden, R., Wright, S., Griffiths, B. and Ralph, P. J. (2011) Diel variation of chlorophyll-a fluorescence, phytoplankton pigments and productivity in the Sub-Antarctic and Polar Front Zones south of Tasmania. *Australia Deep Sea Research Part II: Topical Studies in Oceanography,* 58(21), pp. 2189-2199.

Eppley, R. W. (1972) Temperature and phytoplankton growth in the sea. *Fisheries Bulletin,* 70(4), pp. 1063-1085.

Falkowski, P. G., Barber, R. T. and Smetacek, V. (1998) Biogeochemical controls and feedbacks on ocean primary production. *Science,* 281(5374), pp. 200-206.

Finkel, Z. V., Beardall, J., Flynn, K. J., Quigg, A., Rees, T. A. V. and Raven, J. A. (2009) Phytoplankton in a changing world: cell size and elemental stoichiometry. *Journal of Plankton Research*. doi:fbp098.

Finkel, Z. V. and Kotrc, B. (2010) Silica Use Through Time: Macroevolutionary Change in the Morphology of the Diatom Fustule. *Geomicrobiology Journal,* 27(6-7), pp. 596-608. doi:10.1080/01490451003702941.

Geider, R., Ishizaka, J., Kiefer, D., Marra, J., Sakshaug, E., Raven, J. and Cullen, J. J. (1993) Towards a general description of phytoplankton growth for biogeochemical models. in *Towards a model of ocean biogeochemical processes*: Springer. pp. 153-176.

Gilchrist, G. W. (1995) Specialists and generalists in changing environments. I. Fitness landscapes of thermal sensitivity. *American Naturalist*, pp. 252-270.

Guillard, R. R. and Ryther, J. H. (1962) Studies of marine planktonic diatoms. I. *Cyclothella nana* Hustedt and *Detonula confervacea* Gran. . *Canadian journal of microbiology,* 8(2), pp. 229-239.

Hancke, K., Hancke, T., Olsen, L. M., Johnsen , G. and Glud, R. N. (2008) Temperature effects on Microalgal Photosynthesis-Light responses measured by O2 production, Pulse-Amplitude-Modulated Fluorescence, and 14C assimilation. *Journal of Phycology,* 44, pp. 501-14.

Hoenig, M., Lee, R. J. and Ferguson, D. C. (1989) A microtiter plate assay for inorganic phosphate. *Journal of biochemical and biophysical methods,* 19(2), pp. 249-251.

Honjo, S., Manganini, S. J., Krishfield, R. A. and Francois, R. (2008) Particulate organic carbon fluxes to the ocean interior and factors controlling the biological pump: A synthesis of global sediment trap programs since 1983. *Progress in Oceanography,* 76(3), pp. 217-285.

Huertas, I. E., Rouco, M., López-Rodas, V. and Costas, E. (2011) Warming will affect phytoplankton differently: evidence through a mechanistic approach. *Proceedings of the Royal Society B: Biological Sciences,* 278(1724), pp. 3534-3543.

Huey, R. B. and Stevenson, R. (1979) Integrating thermal physiology and ecology of ectotherms: a discussion of approaches. *American Zoologist,* 19(1), pp. 357-366.

Hutchins, D. A., Wang, W. X. and Fisher, N. S. (1995) Copepod grazing and the biogeochemical fate of diatom iron. . *Limnology and Oceanography,* 40(5), pp. 989-994.

Jassby, A. D. and Platt, T. (1976) Mathematical formulation of the relationship between photosynthesis and light for phytoplankton. *Limnology and Oceanography,* 21(4), pp. 540-547.

Jeffrey, S. W., Mantoura, R. F. C. and Bjørnland, T. (1997) *Data for the identification of 47 key phytoplankton pigments. Phytoplankton pigments in oceanography: guidelines to modern methods,* Paris, France: UNESCO.

Kirk, J. T. (1994) *Light and photosynthesis in aquatic ecosystems,* Cambridge University Press.

Kolber, Z. S., Prášil, O. and Falkowski, P. G. (1998) Measurements of variable chlorophyll fluorescence using fast repetition rate techniques: defining methodology and experimental protocols. *Biochimica et Biophysica Acta (BBA)-Bioenergetics,* 1367(1), pp. 88-106.

Kulk, G., de Vries, P., van de Poll, W. H., Visser, R. J. W. and Buma, A. G. J. (2012) Temperature-dependent growth and photophysiology of prokaryotic and eukaryotic oceanic picophytoplankton. . *Mar. Ecol. Prog. Ser.,* 466, pp. 43–55.

Leblanc, K., Arístegui, J., Armand, L., Assmy, P., Beker, B., Bode, A., Breton, E., Cornet, V., Gibson, J., Gosselin, M. P., Kopczynska, E., Marshall, H., Peloquin, J., Piontkovski, S., Poulton, A. J., Quéguiner, B., Schiebel, R., Shipe, R., Stefels, J., van Leeuwe, M. A., Varela, M., Widdicombe, C. and Yallop, M. (2012) A global diatom database – abundance, biovolume and biomass in the world ocean. *Earth Syst. Sci. Data,* 4(1), pp. 149-165. doi:10.5194/essd-4-149-2012.

Leblanc, K. and Hutchins, D. A. (2005) New applications of a biogenic silica deposition fluorophore in the study of oceanic diatoms. *Limnology and Oceanography: Methods,* 3, pp. 462-476.

Lesser, M. P. (2006) Oxidative stress in marine environments: biochemistry and physiological ecology. *Annu. Rev. Physiol.,,* 68, pp. 253-278.

Li, G. and Campbell, D. A. (2013) Rising CO2 interacts with growth light and growth rate to alter photosystem II photoinactivation of the coastal diatom Thalassiosira pseudonana. *PLoS One,* 8(1), pp. e55562.

Litchman, E. and Klausmeier, C. A. (2008) Trait-based community ecology of phytoplankton. *Annual Review of Ecology, Evolution, and Systematics,* 39, pp. 615-639.

Litchman, E., Klausmeier, C. A., Schofield, O. and Falkowski, P. G. (2007) The role of functional traits and trade‐offs in structuring phytoplankton communities: scaling from cellular to ecosystem level. *Ecology letters,* 10(12), pp. 1170-1181.

Litchman, E., Tezanos Pinto, P., Edwards, K. F., Klausmeier, C. A., Kremer, C. T. and Thomas, M. K. (2015) Global biogeochemical impacts of phytoplankton: a trait‐based perspective. *Journal of Ecology,* 103(6), pp. 1384-1396.

Lohbeck, K. T., Riebesell, U. and Reusch, T. B. (2012) Adaptive evolution of a key phytoplankton species to ocean acidification. *Nature Geoscience,* 5(5), pp. 346-351.

McGinley, M. P., Aschaffenburg, M. D., Pettay, D. T., Smith, R. T., LaJeunesse, T. C. and Warner, M. E. (2012) Transcriptional response of two core photosystem genes in Symbiodinium spp. exposed to thermal stress. *PLoS One*. doi:10.1371/journal.pone.0050439.

Mulholland, M. R. and Lomas, M. W. (2008) Nitrogen uptake and assimilation. in Capone, D. G., (ed.) *Nitrogen in the Marine Environment. 2nd ed.*,New York: Elsevier. pp. 303-384.

Nedwell, D. B. (1999) Effect of low temperature on microbial growth: lowered affinity for substrates limits growth at low temperature. *FEMS Microbiology Ecology,* 30(2), pp. 101-111. doi:10.1111/j.1574-6941.1999.tb00639.x.

Nelson, D. M., Treguer, P., Brzezinski, M. A., Leynaert, A. and Queguiner, B. (1995) Production and dissolution of biogenic silica in the ocean - revised global estimates, comparison with regional data and relationship to biogenic sedimentation. *Global Biogeochemical Cycles,* 9(3), pp. 359-372. doi:10.1029/95gb01070.

NOAA (2015) *NOAA Optimum Interpolation Sea Surface Temperature Analysis*, Available: http://www.emc.ncep.noaa.gov/research/cmb/sst_analysis/images/archive/monthly_sst/ [Accessed 20th November 2015].

Oxborough, K., Moore, C. M., Suggett, D. J., Lawson, T., Chan, H. G. and Geider, R. J. (2012) Direct estimation of functional PSII reaction center concentration and PSII electron flux on a volume basis: a new approach to the analysis of Fast Repetition Rate fluorometry (FRRf) data. *Limnology and Oceanography: Methods,* 10(3), pp. 142-154.

Pantorno, A., Holland, D. P., Stojkovic, S. and Beardall, J. (2013) Impacts of nitrogen limitation on the sinking rate of the coccolithophorid Emiliania huxleyi (Prymnesiophyceae). *Phycologia,* 52(3).

Peperzak, L. and Brussaard, C. P. (2011) Flow cytometry applicability of fluorescent vitality probes on phytolankton. *Journal of Phycology,* 47(3), pp. 692-702.

Raven, J. and Waite, A. (2004) The evolution of silicification in diatoms: inescapable sinking and sinking as escape? *New Phytologist,* 162(1), pp. 45-61.

Raven, J. A. (1984) A cost-benefit analysis of photon absorption by photosynthetic unicells. *New Phytologist,* 98(4), pp. 593-625.

Reynolds, R. W. and Smith, T. M. (1995) A high-resolution global sea surface temperature climatology. *Journal of Climate,* 8(6), pp. 1571-1583.

Robinson, C., Suggett, D. J., Cherukuru, N., Ralph, P. J. and Doblin, M. A. (2014) Performance of Fast Repetition Rate fluorometry based estimates of primary productivity in coastal waters. *Journal of Marine Systems,* 139, pp. 299-310.

Sakshaug, E., Bricaud, A., Dandonneau, Y., Falkowski, P. G., Kiefer, D. A., Legendre, L. and Takahashi, M. (1997) Parameters of photosynthesis: definitions, theory and interpretation of results. *Journal of Plankton Research,* 19(11), pp. 1637-1670.

Sandnes, J. M., Källqvist, T., Wenner, D. and Gislerød, H. R. (2005) Combined influence of light and temperature on growth rates of Nannochloropsis oceanica: linking cellular responses to large-scale biomass production. *Journal of applied phycology,* 17(6), pp. 515-525.

Sarthou, G., Timmermans, K. R., Blain, S. and Tréguer, P. (2005) Growth physiology and fate of diatoms in the ocean: a review. *Journal of Sea Research,* 53(1), pp. 25-42.

Schmidt, T. M. and Schaechter, M. (2012) *Topics in ecological and environmental microbiology.,* San Diego, California, USA: Academic Press.

Schnetger, B. and Lehners, C. (2014) Determination of nitrate plus nitrite in small volume marine water samples using vanadium (III) chloride as a reduction agent. *Marine Chemistry,* 160, pp. 91-98.

Schuback, N., Flecken, M., Maldonado, M. T. and Tortell, P. D. (2015) Diurnal variation in the coupling of photosynthetic electron transport and carbon fixation in iron-limited phytoplankton in the NE subarctic Pacific. *Biogeosciences Discussions,* 12(20).

Schulte, P. M., Healy, T. M. and Fangue, N. A. (2011) Thermal performance curves, phenotypic plasticity, and the time scales of temperature exposure. *Integr Comp Biol,* 51(5), pp. 691-702. doi:10.1093/icb/icr097.

Shoaf, W. T. and Lium, B. W. (1976) Improved extraction of chlorophyll a and b from algae using dimethyl sulfoxide. . *Limnology and Oceanography,* 21(6), pp. 926-928.

Sorokin, Y. I. (1999) Data on primary production in the Bering Sea and adjacent Northern Pacific. . *Journal of Plankton Research,* 21(4), pp. 615-636.

Strickland, J. D. H. and Parsons, T. R. (1968) *A practical handbook of seawater analysis,* Ottawa, Canada: Fisheries Research Board of Canada.

Thomas, M. K., Kremer, C. T., Klausmeier, C. A. and Litchman, E. (2012) A Global Pattern of Thermal Adaptation in Marine Phytoplankton. *Science,* 338(6110), pp. 1085-1088. doi:10.1126/science.1224836.

Thompson, P. A., Guo, M. X. and Harrison, P. J. (1992) Effects of variation in temperature. I. On the biochemical composition of eight species of marine phytoplankton. *Journal of Phycology,* 28(4), pp. 481-488.

Welschmeyer, N. A. (1994) Fluorometric analysis of chlorophyll a in the presence of chlorophyll b and pheopigments. *Limnology and Oceanography,* 39(8), pp. 1985-1992.

2.7 Supplementary Figures

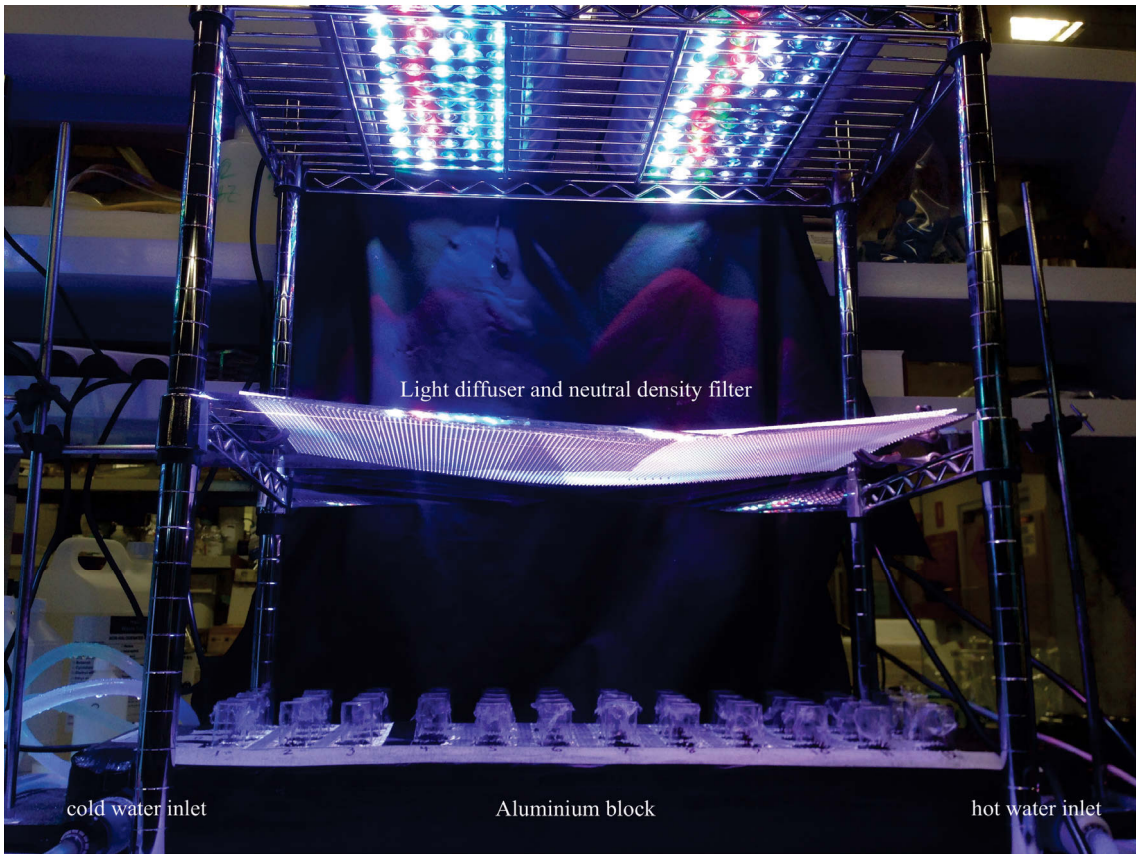

Supplementary Figure 2.1 Experimental setup of thermal gradient block. A temperature gradient was established across the aluminium block by circulating hot and cold water through milled channels at opposite ends of the block.

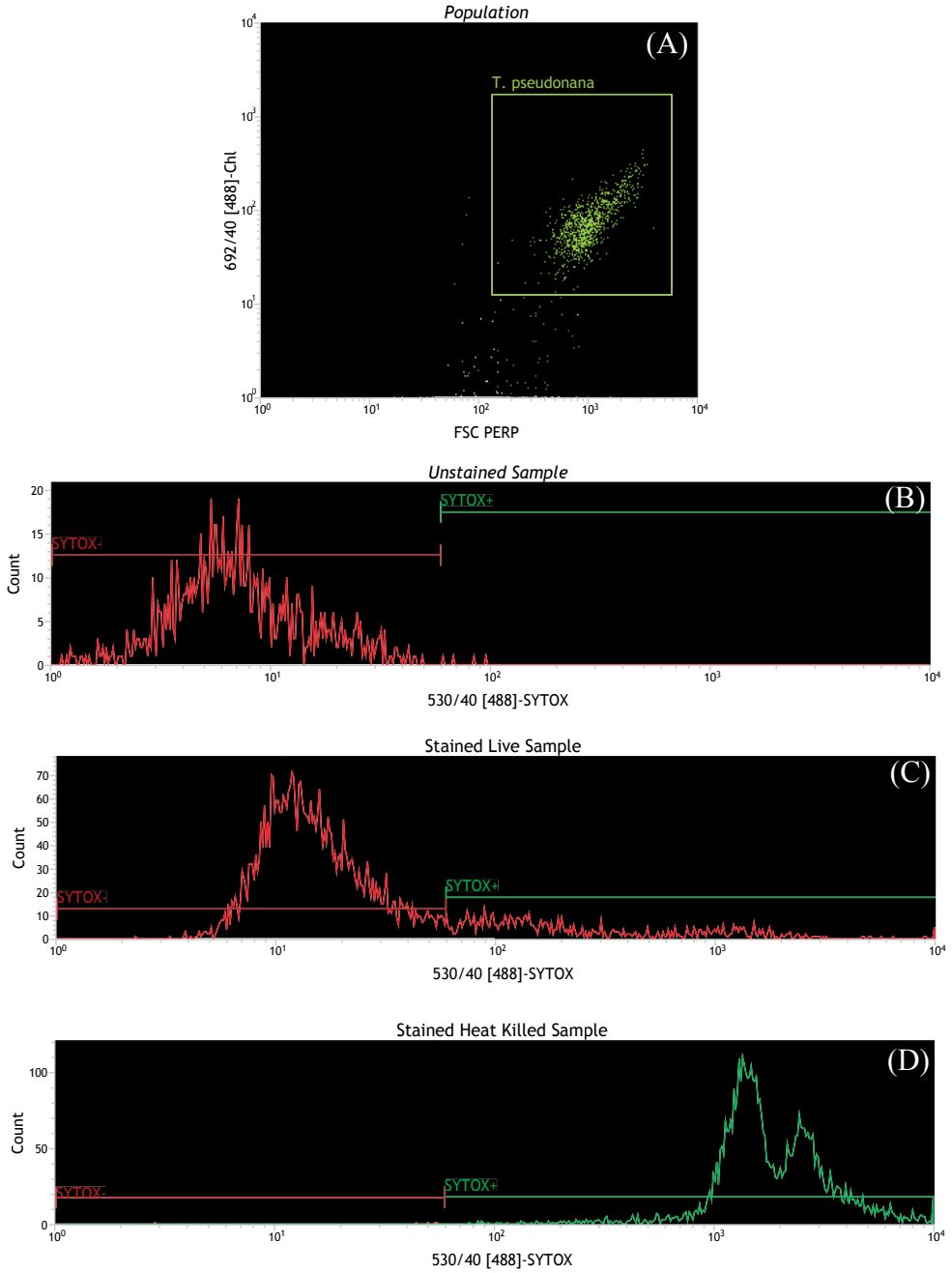

Supplementary Figure 2.2 Gating logic for flow cytometric analysis of SYTOX incorporation in the diatom *T. pseudonana*. Cells were discriminated based upon chlorophyll fluorescence (692/40 nm) and forward scatter (FSC) (A). Gates were set on these populations to account for any auto fluorescence in these channels using cells not incubated in the presence of the stain (B). Gates were then set on populations with cells incubated in the presence of the stain (C). Heat-killed cells incubated in the presence of the stain were used as a positive control (D).

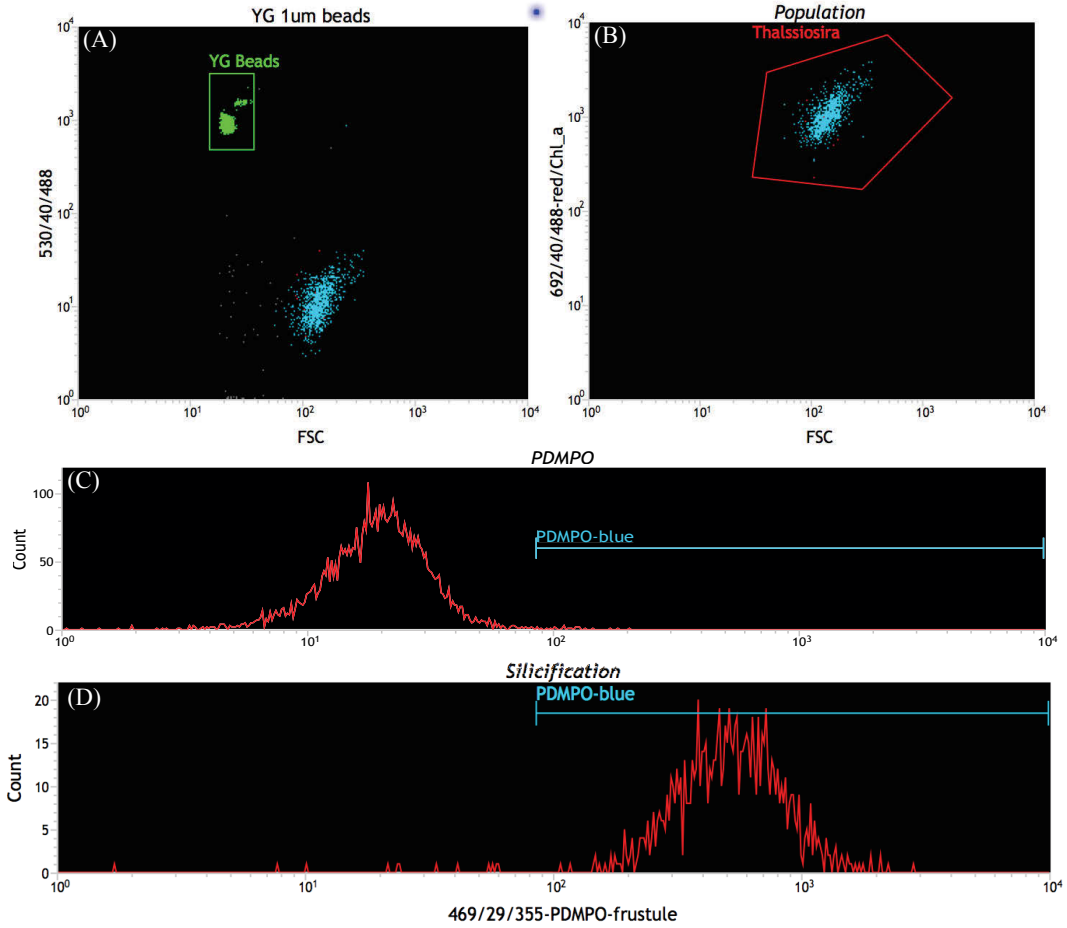

Supplementary Figure 2.3 Gating logic for flow cytometric analysis of PDMPO incorporation in the diatom *T. pseudonana*. Standard fluorescent yellow-green beads (1 µm) were discriminated on fluorescence (530/40 nm) and forward scatter (FSC) (A). Cells were discriminated based upon chlorophyll fluorescence (692/40 nm) and forward scatter (FSC) (B). Gates were set on these populations to account for any auto fluorescence in the detection channel (469/29) with cells not incubated in the presence of PDMPO stain (C). Cells stained in the presence of PDMPO for 24 h (C).

CHAPTER 3:
FUNCTIONAL TRAIT PLASTICITY ENABLES THERMAL TOLERANCE IN A NATURAL PHYTOPLANKTON COMMUNITY FROM SOUTH EAST AUSTRALIA

K. G. Baker*, A. S. McInnes, C. M. Robinson, M. Rodriguez Alvarez, M. A. Doblin.

Plant Functional Biology and Climate Change Cluster, School of Life Sciences, University of Technology Sydney, Sydney, New South Wales, Australia.

*** Correspondence:** Kirralee G Baker, Plant Functional Biology and Climate Change Cluster, University of Technology Sydney, Broadway, Ultimo, New South Wales, 2007, Australia
Kirralee.G.Baker@student.uts.edu.au

Key words: climate change, diatom, phytoplankton community, PDMPO, flow cytometry, physiology, phenotype, temperature, warming

3.1 Introduction

Substantial changes in the present-day ocean are creating significant challenges for marine inhabitants such as phytoplankton (Boyce and Worm 2015, Boyd et al. 2010). Phytoplankton are microscopic primary producers that drift in sunlit surface oceans and play an integral role in many marine biogeochemical cycles including C, N and Si (Falkowski 2004). Being ectotherms, their underlying metabolism and therefore biogeography is largely determined by ocean temperature (Thomas et al. 2012), but see (Marañón et al. 2014). Warming oceans associated with increases in SST will *indirectly* affect phytoplankton communities by changing the physical ocean characteristics and mixing which, in turn, alter light and nutrient regimes in the upper ocean (Beardall and Raven 2004, Cubasch et al. 2001, Hobday et al. 2006). There is some evidence to suggest that *direct* effects of ocean warming may counteract these effects (Taucher and Oschlies 2011), as increases in SST may be associated with enhanced metabolic activity (Eppley 1972, Raven and Geider 1988, Toseland et al. 2013). However, the extent to which warming will prove beneficial to phytoplankton remains unknown, particularly when different species exhibit different physiological responses to temperature (Boyd et al. 2013)– increasing metabolism and growth in some species, whilst pushing others past their thermal limits. In this way, the direct effects of temperature can change phytoplankton ecology (including inter-specific competition, community composition) and have implications for the biogeochemical cycles that these microscopic organisms regulate (Beardall and Raven 2004, Dutkiewicz et al. 2013).

Whilst the implications of increased SST on phytoplankton biogeography has been advanced by examining the effects of high temperatures on species fitness and community composition (Feng et al. 2009, Tatters et al. 2013), it remains unknown how the reorganisation of phytoplankton communities will affect primary productivity and other biogeochemical transformations (Dutkiewicz et al. 2013). To improve these predictions, it is important to parameterise and quantify how key phytoplankton FTs respond to bottom-up controls such as temperature (Finkel et al. 2009). Focusing our attention on the expression of FTs (adopting trait-based approaches; Litchman and Klausmeier, 2008) in key phytoplankton functional groups i.e., taxa that are known to be important contributors to specific elemental fluxes (Le Quere et al. 2005), is fundamentally important for these predictions.

FTs are considered to be physiological/phenotypic characteristics that determine the ecological or biogeochemical role of phytoplankton and are themselves regulated by their environmental surroundings (Litchman and Klausmeier 2008). Some FTs are universal because they apply across all phytoplankton species e.g. cell size, whereas others are unique to particular groups or functional types e.g. silicifying diatoms. By assessing how the expression of FTs change over environmental gradients (e.g. temperature), or, how different phenotypes emerge under different conditions, we can determine how the ecological and biogeochemical niches of phytoplankton are shaped by their surroundings and predict how these processes might change due to climate change.

Diatoms are an example of a biogeochemically significant group due their integral role in the downward export of C (i.e., the delivery of organic C to the deep sea (Smetacek 1985) and regulation of the marine Si cycle (Tréguer and De La Rocha 2013). Frustule silicification, the Si:C (atomic) composition of the diatom cell wall, is a diatom-specific FT that heavily influences penetrability by grazers, BSi production, degree of Si recycling in the surface ocean, increases ballast of vertical C export and the biochemical composition of organic matter transferred to higher trophic levels (Finkel et al. 2009, Raven and Waite 2004, Tréguer and De La Rocha 2013). In other biogeochemically important functional groups, such as the picoautrophs (Le Quere et al. 2005) that contribute up to 50% of the amount of C fixed in marine systems (Partensky et al. 1999), cell size is a particularly important FT. This is because it is the smaller size of picoplankton that facilitates a competitive advantage against larger cells, in terms of nutrient acquisition and utilisation (among others; Raven 1998), but is also a universally important FT because it can be applied across all other phytoplankton types. Cell size governs numerous physiological and ecological processes, such as metabolism, nutrient requirements, light absorption, cellular composition and grazing pressure (Finkel et al. 2009). Therefore, by tracking changes in the expression of universal and functional type-specific FTs across specific environmental gradients, we can better inform predictions in changes of the ecological role of phytoplankton and the transformation of elements (e.g. C and Si) carried out by phytoplankton.

Some regions may be more affected by ocean warming than others (Bopp et al. 2013, Steinacher et al. 2010), for example, south eastern Australia, is a global hot spot for

increases in SST and stratification (Hobday et al. 2006, Ridgway and Hill 2009, Wu et al. 2012). Evidence suggests the strengthening of the EAC is responsible for the long-term increases in temperature (+0.74 °C century^{-1}) observed at Port Hacking PH100; one of the longest sampled coastal time-series stations in the southern hemisphere (Thompson et al. 2009). It is believed that these increased SST are responsible for the observed decline in relative abundance and shifts in the microphytoplankton composition over the most recently recorded decade (1998-2009; Ajani et al. 2014). Yet, it remains unknown what the FT characteristics of these resident phytoplankton communities are, or how these FT may be altered with further warming in this region.

To assess the role of phenotypic plasticity in determining phytoplankton tolerance to ocean change and warming, we exposed a natural, temperate phytoplankton community collected from Port Hacking, NSW to a wide range of temperatures, spanning those encountered on inter-annual timescales and those more representative of oceanic heatwaves. Following an acute (24 h) exposure period, we then examined changes in FTs (magnitude and direction) of important phytoplankton functional groups, specifically diatoms and picoautotrophs, in order to examine the direct and acute effects of temperature on C and Si transformations.

3.2 Methods and Materials

3.2.1 Sample collection and experimental setup

In October 2015, a mixed phytoplankton community was collected aboard the RV *Bombora* from surface waters (5 m depth) at the Port Hacking National Reference Station (PH100; as part of the NSW Integrated Marine Observing System; IMOS), approximately 3 nautical miles southeast of Sydney, Australia (151.2190 °E, - 34.1160 °S; **Figure 3.1**). The initial physicochemical properties of the seawater were characterised by temperature and dissolved nutrients, with the latter estimated following the protocol of Critchley (2012). The resident phytoplankton community was described by the rate of community Cfixation and BSi production, as well as standing stock of chlorophyll (**Table 3.1**).

To represent *in situ* conditions in surface waters (5 m depth), light (200 μmol photons m^{-2} s^{-1}) was provided by an array of LEDs (Schenzen Cidly Group, China) set to a 12 h light: 12 h dark cycle, incident from above and synchronised to the onset of natural dawn and dusk. The incubation irradiance was chosen from a RLC conducted using a FRRf (Soliense Inc., United States of America) on seawater samples and determined to be saturating (but not inhibitory) for photosynthesis. Seawater samples (40 mL) in soda glass test tubes were placed into an aluminum temperature gradient block for a 24 h incubation period. The temperature treatments included 15, 19, 24, 26, 30 and 32 °C; 19 °C was used as the control, representing ambient temperature conditions. Temperature treatments were selected based on annual temperature range recorded for PH100, ~15-24 °C (Thompson et al. 2009) as well as those expected to induce thermal stress (>24 °C) to mimic extreme events (e.g. heatwaves). Volumes at each temperature were then subsampled and analysed to characterise the FT response of the whole phytoplankton community (primary productivity and photophysiology) and the whole diatom community (BSi production). Flow cytometry was then used to two universally important phytoplankton groups (*Synechoccus* spp. and *Prochlorococcus* spp.) in the picoplankton fraction and diatoms in the nanoplankton fraction. Universal (growth rate and cell size) and diatom-specific FTs (frustule silicification) were measured as described below.

3.2.2 Assessment of community functional traits

3.2.2.1 Primary Productivity

To estimate primary productivity across the temperature gradient, C fixation rates were measured using ^{14}C-labelled bicarbonate in small volume incubations as described in (Doblin et al. 2011). Specifically, radiolabeled $NaH^{14}CO_3$ (stock solution 1.85 x 10^7 Bq) was added to 5 mL of seawater in soda glass bottles (1.5 µCi per tube) and incubated in the thermal gradient block for 60–80 min under the growth irradiance. Activity in the samples was determined by removing a 100 µL aliquot from a randomly selected tube from each of six temperatures and placing it into 5 mL of refrigerated 0.1 M NaOH, adding 10 mL scintillation fluid (Ultima Gold^{TM}, Perkin Elmer) and shaking before counting using a liquid scintillation counter (Packard TriCarb 2900 TR). Each temperature contained a dark sample wrapped in aluminum foil to quantify C fixation in the dark and was also incubated for 60-80 min. Following incubation, tube contents were transferred to scintillation jars, acidified with 250 µL 6 M HCl and shaken on an orbital shaker for 12 h to remove inorganic ^{14}C. Scintillation fluid (10 mL Ultima Gold^{TM}; Perkin Elmer) was then added to each sample, vigorously shaken and left for 3 h before counting. Counting time was set to 10 min so that counts were within a 5% counting error.

3.2.2.2 Photophysiology

We applied FRRf to assess the electron transport kinetics of photosystem II (PSII) at each temperature. Samples (2 mL) were harvested following the 24 h incubation period and measurements were made on each sample immediately after being removed from the temperature block at the end of the 12 h dark cycle. The first measurement was performed in the dark (to allow down-regulation of very fast relaxing non-photochemical quenching) and actinic white light at the incubation irradiance intensity (200 µmol photons m^{-2} s^{-1}) was supplied by a white LED for 1 min and measurements performed at 20 s intervals during the actinic light exposure. The last measurement of each set was used in further calculations of photochemical efficiency. A FRRf (Soliense Inc., United States of America) supplied single-turnover excitation flashlets (of 1.1 µs duration) at 450 nm at a rate of 2 µs to achieve full saturation of PSII reaction centers followed by longer intervals of 100 µs to allow relaxation and re-oxidation of Q_A.

Profiles of the fluorescence emission were fitted within the FastPro8 software (v. 1.0.55; Chelsea Technologies) to the Kolber-Prasil-Falkowski (Kolber et al. 1998) model to yield the minimum (F_O or F') and maximum fluorescence (F_M or F_M'), and reoxidation kinetic of Q_A (τ; μs). Values for the photochemical efficiency (Φ_{PSII}; dimensionless) were calculated from these parameters as (F_M-F_O/F_M) or (F_M'-F'/F_M') for light adapted samples. Sample filtrate (after filtration through 0.2 μm Millipore syringe filters) was also measured in the FRRf to account for background fluorescence. The data were visually inspected to ensure no fluorescence induction in the filtrate (indicating an absence of phytoplankton) and the mean F_O and F_M of the filtrate was averaged into a single value to be subtracted from all F_O (or F') and F_M (or F_M') values.

3.2.3 Biogenic silicon production

PDMPO incorporation was used as a proxy of BSi production as described in Leblanc and Hutchins (2005). Briefly, volumes of seawater (120 mL, *n* =3) were added to polycarbonate bottles and incubated in the presence of PDMPO (0.125 μM final concentration) in a laboratory incubator set to 19±0.5 °C for 24 h. In order to assess the effects of temperature on community BSi production, seawater volumes of 40 mL were trialed in the thermal gradient block (0.125 μM; 24 h). Incubations were terminated by filtering samples onto 45 mm diameter, 0.6 μm porosity, polycarbonate filters (Millipore, USA). Filters were washed thoroughly with filtered seawater (0.2 μm, Millipore syringe filters) to remove any residual fluorescent stain and then stored at -20 °C in 15 mL centrifuge tubes until analysis (within 3 months). Community-based PDMPO analysis was carried out per the methods of Leblanc and Hutchins (2005). To convert quantitative PDMPO incorporation to BSi production, we used the recommended linear relationship of BSi: PDMPO = 912.6 × $[Si(OH)_4]$, from McNair et al. (2015).

3.2.4 Diatom-specific frustule silicification

Unlike traditional methods for studying Si biogeochemistry which involve determination of bulk parameters such as BSi stocks (Krause et al. 2011), recent advances in fluorescent tracers have provided the opportunity to assess frustule silicification at the cellular level in natural diatom communities and provide a proxy for BSi production (Leblanc and Hutchins 2005, Shimizu et al. 2001). Only a small number of studies have attempted to track PDMPO incorporation with flow cytometry (Baker et

al. 2016, Durkin et al. 2012) but in doing so have provided measures of cell-specific frustule silicification.

In this study, volumes of seawater (40 mL) were added to soda glass bottles incubated in the presence of the fluorescent label PDMPO (Lysosensor Yellow/Blue DND-160, ThermoFisher Scientific, Australia), along with a control samples that did not contain the stain (to quantify background fluorescence), following the labeling protocol of Leblanc and Hutchins (2005). Briefly, cells were incubated in the presence of the dye (final concentration 0.125 μM) along with a control sample that did not contain PDMPO (to quantify background fluorescence) at experimental conditions for 24 h.

For identification of small diatoms within the nanoplankton community as well as cell-specific frustule silicification/PDMPO incorporation, volumes (2 mL) were subsampled from incubation bottles following 24 h incubation, preserved in glutaraldehyde (1% final concentration), cryopreserved in liquid nitrogen, and stored at -80 °C until analysis (within one month). Volumes (1 mL) of each sample were enumerated flow cytometrically (BD Influx, Becton Dickinson, Brussels, Belgium). Pico- and nano-phytoplankton populations were first discriminated on biplots of phycoerythrin (580/30 nm) and chlorophyll (692/20 nm) fluorescence. Diatoms were then distinguished as PDMPO-positive cells (control samples used to set baseline fluorescence in UV channel) where the relative fluorescence of incorporated PDMPO was normalised to an internal standard of yellow-green fluorescent beads (1 μm, ThermoFisher Scientific, Australia) at UV excitation of 355 nm and blue fluorescence at 469/29 nm.

3.2.5 Cell-specific functional traits of the pico- and nano-phytoplankton community

To discriminate target populations, namely *Synechococcus* spp., *Prochlorococchus* spp. and small (<20 μm) diatoms (PDMPO positive cells) within the pico- and nano-plankton community, and determine cell abundance at T_0 and T_{24} (A_0 and A_{24}, respectively), volumes of 2 mL were subsampled from incubation bottles, preserved in glutaraldehyde (1% final concentration) and flash frozen in liquid nitrogen, and stored at -80 °C until analysis (within one month). Volumes (1 mL) of each sample were enumerated on a flow cytometer (BD Influx, Becton Dickinson, Brussels, Belgium) enriched with known concentrations of 1 μm yellow green beads (Thermofisher Scientific, Australia) to enumerate cell abundances (for growth rate calculations) and

relative cell size (forward scatter; FSC) of each target population (discriminated as described above). Specific growth rates for each phytoplankton group were calculated assuming exponential growth as ($\ln A_0 - \ln A_{24}$)/T where T is incubation time.

3.2.6 Data Analysis

For each FT (primary productivity, photophysiological parameters, growth, PDMPO incorporation, cell size), data were tested for normality and homogeneity of variance before performing statistical analysis. The effect of temperature on the FT response were analysed using one-way repeated-measured analysis of variance (ANOVA) as in (Wilson, 2001) and differences were accepted as significant at $p < 0.05$.

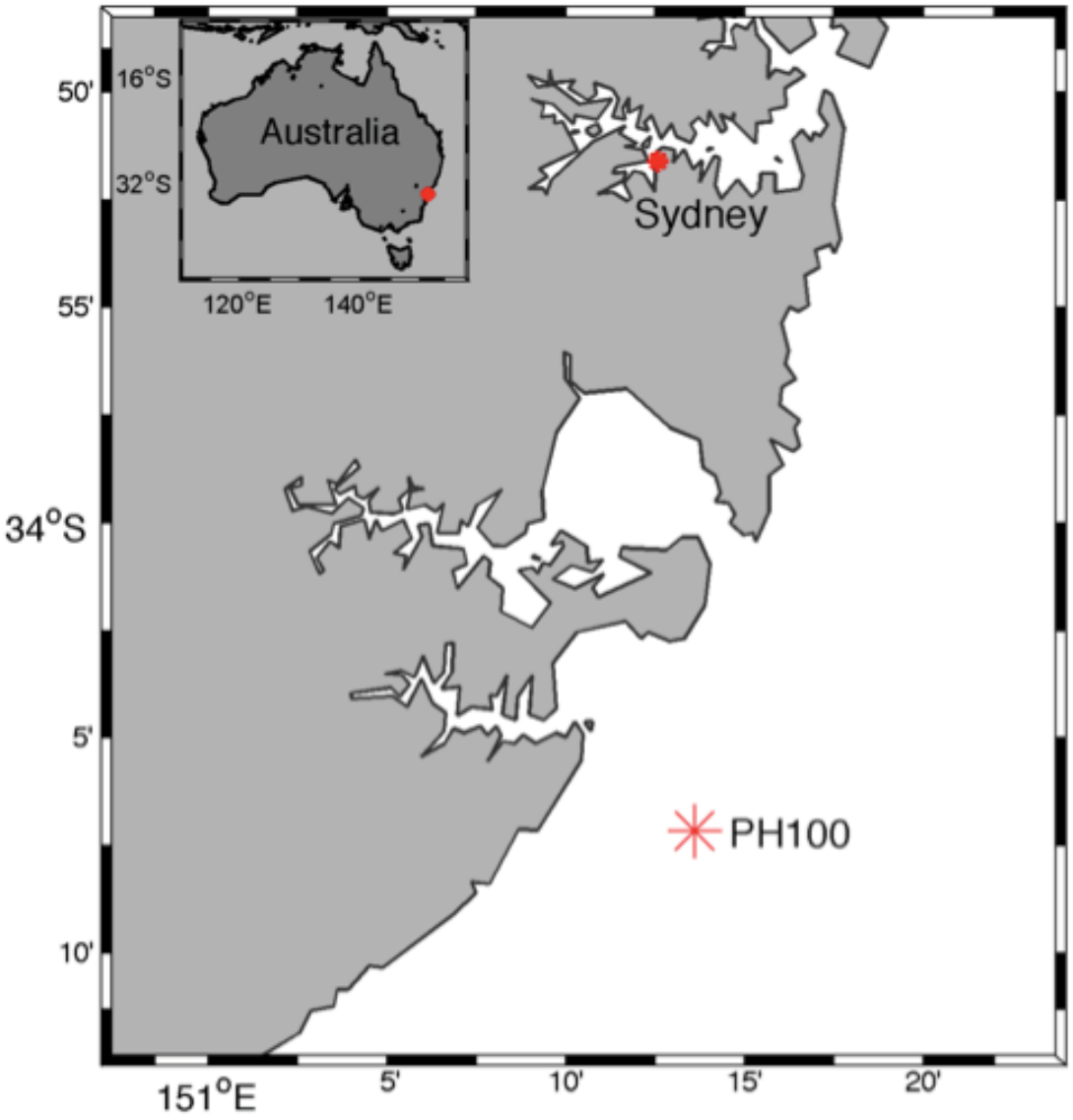

Figure 3.1 Sampling location of source water collected from Port Hacking National Reference Station (PH100) at 151.2190 E, 34.1160 S: approximately 3 nautical miles off the coast of Sydney, NSW, Australia. (Figure credit: V. van Dongen-Vogels)

3.3 Results

3.3.1 Physicochemical and biological characterisation of Port Hacking

Physicochemical characteristics of Port Hacking surface water during October 2015 fell within typical values for this time of year (Thompson et al. 2009) with low concentrations of dissolved phosphate (0.13 μmol L^{-1}), silicate (0.6 μmol L^{-1}), ammonium (0.08 μmol L^{-1}) and nitrate, present in concentrations below instrument detection (≤0.2 μmol L^{-1}) (**Table 3.1**). Biological characterisation of the initial phytoplankton community indicated that picophytoplankton comprised approximately 50% of the total biomass present (Chl *a* m^{-3}; **Table 3.1**). Similarly, size-fractionated net primary production (NPP) incubated under *in situ* conditions indicated that the picophytoplankton dominated whole community production, being responsible for approximately 66% of the total (**Table 3.1**). Community BSi production was estimated to be 1.43±0.2 μmol Si L^{-1} d^{-1} (**Table 3.1**).

Table 3.1 Physicochemical and biological characteristics of seawater collected from surface waters (5 m) of PH100. Where applicable, rates were obtained during daily incubation at *in situ* temperature and light characteristics. Where available, error is the standard deviation from *n*=3 replicates.

Physicochemical characteristic			**units**
Temperature	19		°C
Nitrate	<0.02		μmol L^{-1}
Ammonium	0.08		μmol L^{-1}
Silicate	0.6		μmol L^{-1}
Biological characteristics	**Total Population**	**Picophytoplankton**	
Net Primary Production	±0.69	20.18	mgC m^{-3} d^{-1}
Chlorophyll *a*	0.75	0.39	mgChl *a* m^{-3}
Biogenic silicon production	1.43±0.2	-	μmol Si L^{-1} d^{-1}

3.3.2 Thermally induced changes in functional traits of community

FTs at the community-level (photophysiology and primary productivity) showed differential responses to cooling and warming conditions. The responses of the photosynthetic parameters of the whole phytoplankton community are presented in **Table 3.2**. After exposure to the experimental temperatures, F_V/F_M was similar across all treatments (**Table 3.2**; One-way RM ANOVA; p >0.05), indicating photosynthetic efficiency of PSII was unaffected by temperature or not temperature dependent (Davison 1991, Raven and Geider 1988). In contrast, the proportion of energy directed towards photochemistry was affected by high temperatures, as values of Φ_{PSII} were significantly reduced at 30 and 32 °C in comparison to control temperature (**Table 3.2**; One-way RM ANOVA; p <0.05). Similarly, these high temperature effects were mirrored in values of ETR through PSII (ETR_{PSII}), whereby values of ETR_{PSII} at 30 and 32 °C were significantly reduced by 42 and 70%, respectively (**Table 3.2**; One-way RM ANOVA; p <0.05). Whilst high variability within replicates meant there were no significant differences in non-photochemical quenching (NPQ) between individual treatments, when all treatments were considered together, a strong and significant (R^2 =0.66, p =0.003) decrease with increasing temperature was observed. Reoxidation of $Q_A(\tau)$ was reduced at cold temperatures (15 °C; 1199 μs) and more rapid at high temperatures (32 °C; 200 μs), reflecting a slowing of downstream electron transport at temperatures below the control (-4 °C) and acceleration at temperatures above the control (+13 °C) (**Table 3.2**; One-way RM ANOVA; significant difference between 19 and 15, 32 °C, p <0.05).

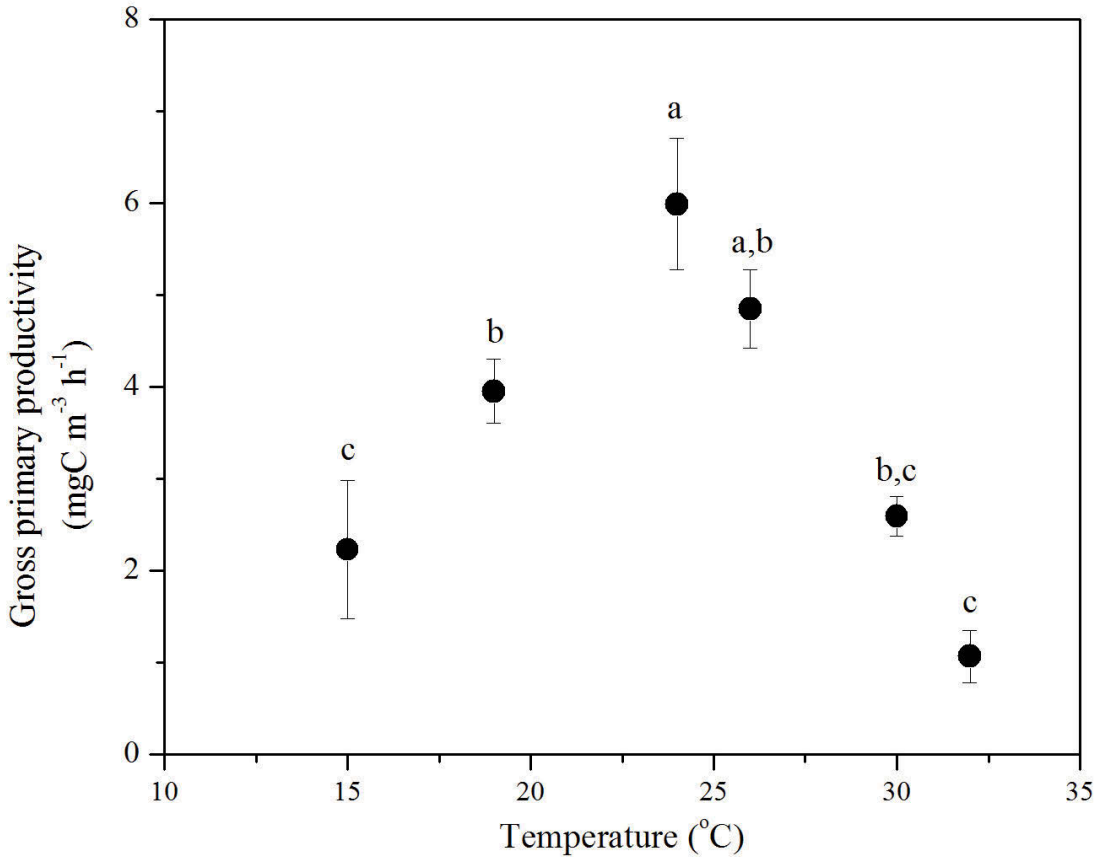

Figure 3.2 Gross primary productivity of surface (5 m depth) phytoplankton community at Port Hacking, NSW (PH100) sampled in October 2015 as a function of temperature. Symbols represent mean and error bars are the standard error of the mean. Letters above symbols indicate statistically significant difference between treatments identified by Tukeys's honest significant difference (HSD) test $p < 0.05$.

Table 3.2 Photosynthetic parameters of the phytoplankton community sampled from surface waters (5 m depth) of Port Hacking, NSW (PH100) and incubated at various temperatures for 24 h at 200 μ mol photons m^{-2} s^{-1}. Shown are F_V/F_M (maximum quantum yield; dimensionless), Φ_{PSII} (photochemical efficiency; dimensionless), ETR_{PSII} (electron transport rate through photosystem II; µmol ē h^{-1}), NPQ (non-photochemical quenching; dimensionless), and τ (reoxidation time of Q_A; µs). Those in bold indicates that there is significant difference (p <0.05) between the assay temperature and ambient control (19 °C). Values given are the means, and values in parentheses are the standard error of the mean of measurements made on triplicate samples.

Temperature	F_V/F_M	p values	Φ_{PSII}	p values	ETR_{PSII}	p values	NPQ	p values	τ	p values
15	0.395 (0.01)	0.995	0.137 (0.01)	0.979	23 (1.6)	0.979	0.304 (0.18)	0.946	1199 (82)	**0.004**
19	0.405 (0.02)	-	0.138 (0.01)	-	24 (0.9)	-	0.181 (0.02)	0.923	859 (68)	-
24	0.437 (0.02)	0.994	0.131 (0.01)	0.784	22 (1.5)	0.784	0.181 (0.06)	0.551	927 (51)	1.000
26	0.421 (0.02)	0.999	0.126 (0.01)	0.596	21 (1.5)	0.597	0.136 (0.03)	2.026	956 (60)	0.641
30	0.338 (0.04)	0.767	0.084 (0.01)	**0.006**	14 (1.2)	**0.007**	0.049 (0.04)	2.030	751 (5)	0.400
32	0.247 (0.08)	0.106	0.038 (0.02)	**<0.001**	7 (2.6)	**<0.001**	0.008 (0.01)	2.420	200 (0)	**<0.001**

The deviations in τ values observed at the coldest and hottest temperatures coincided with the lowest rates of gross primary production (GPP) at 15 and 32 °C, respectively (**Figure 3.2**). At these temperature extremes, GPP was reduced by approximately 40% in comparison to ambient temperatures (**Figure 3.2**; One-way RM ANOVA; significant difference between 19 and 15 °C; p =0.039, and 32 °C; p =0.001). In contrast, greatest GPP occurred at 24 °C (control +5 °C) with rates of 5.98±0.42 mg C m^{-3} h^{-1}, 1.5 times higher than the rate at the control temperature (**Figure 3.2;** One-way RM ANOVA; significant difference between 19 and 24 °C, p =0.014).

3.3.3 Temperature effects on pico- and nano-phytoplankton composition

Initially the phytoplankton community was numerically dominated by *Synechococcus* spp. and *Prochlorococcus* spp. (**Figure 3.3**), with the relative abundance of the picocyanobacteria constituting 46±0.3 and 41±0.6% respectively of the total pico- and nano-plankton (<20 μm) community (One-way ANOVA; no statistical difference at T_0, p =1). Following 24 h incubation at control conditions (19 °C), the abundance of *Synechococcus* spp. and pico-eukaryotes remained within range of the initial concentrations (**Figure 3.3**; One-way ANOVA; no statistical difference between T_0 and T_{24}, p =0.1 and p =1, respectively). However, unlike at T_0, *Synechococcus* spp. were more abundant relative to *Prochlorococcus* spp. and eukaryotic cells in the <20 μm fraction at T_{24}, increasing in relative abundance from 41±0.6 to 61±1% (**Figure 3.3**).

Warming, but not cooling, induced shifts in the composition of the <20 μm phytoplankton community but did not affect populations equally, increasing the relative abundance of some populations but decreasing the abundances of others. At cool temperatures (control –4 °C) of 15 °C, the relative abundances of *Synechococcus* spp., *Prochlorococcus* spp. and eukaryotes (<20 μm) were comparable to control conditions (Two-way RM ANOVA; no statistical difference at T_{24} between 15 and 19 °C, p >0.05 for each population). The *Prochlorococcus* population appeared to be the most affected by warming temperatures, whereby a decrease in abundance was observed at temperatures of 24 °C and above; with a 12±2 to 13±2% reduction at intermediate (24 and 26 °C, respectively) temperatures and a 19±2 and 20±3% reduction at high (30 and 32 °C) temperatures (Two-way RM ANOVA; statistical difference at T_{24} between 19 and 24 °C; p =0.002, 26 °C; p <0.001, 30 and 32 °C; p <0.001). The relative abundance of eukaryotes in the <20 μm fraction (including small diatoms detected using PDMPO)

were only negatively impacted by high temperatures (30 and 32 °C), declining in abundance by 11±2% (Two-way RM ANOVA; statistical difference between 19 °C control and 30, 32 °C treatments, p <0.001). In contrast, the abundance of *Synechococcus* spp. increased with increasing temperatures, coinciding with the decrease in the relative abundance of *Prochlorococcus* spp. and eukaryotes in the <20 µm fraction (including diatoms). At intermediate (24 and 26 °C) temperatures, *Synechococcus* spp. increased by 11±2% (relative to the control) and at high (30 and 32 °C) temperatures, constituted between 80±1 to 90±1% of the total pico- and nanophytoplankton community (Two-way RM ANOVA; statistical difference at T_{24} between 19 and 24 °C; p =0.004, 26 °C; p =0.003, 30 °C; p <0.001, and 32 °C; p <0.001).

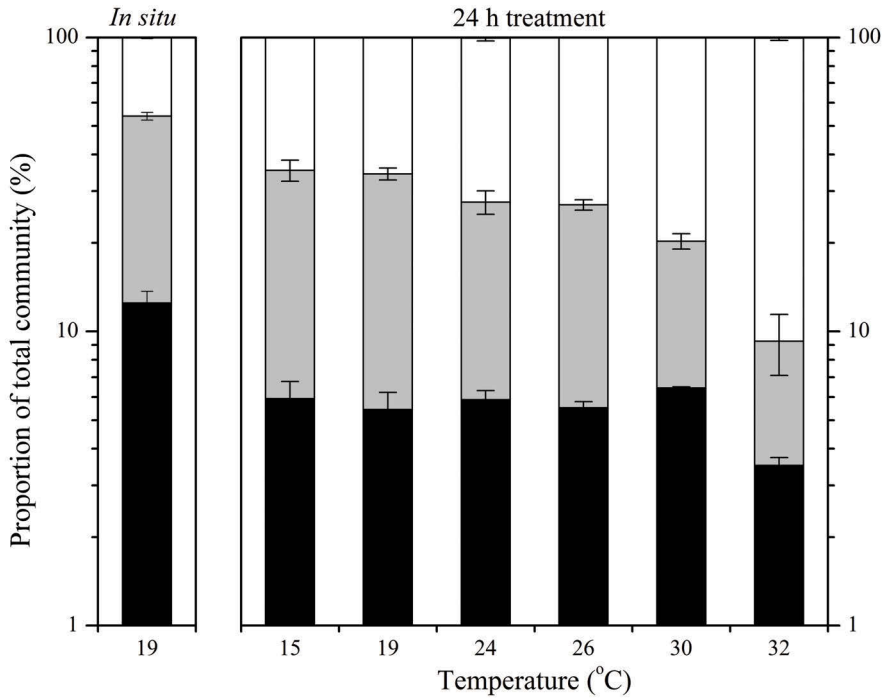

Figure 3.3 Community composition of the initial *in situ* Port Hacking (PH100) phytoplankton in the <20 µm fraction as determined by flow cytometry using cell-specific phycoerythrin fluorescence and forward scatter (FSC) properties: *Synechococcus* spp. (white bars), *Prochlorococcus* spp. (grey bars) and eukaryotes (black bars), as well as the community composition after 24 h at different assay temperatures. Note log scale on y-axis.

3.3.4 Temperature effects on universal functional traits measured in pico- and nano-phytoplankton

Incubation temperature also affected FTs at the population-level, reflecting the results obtained for FTs at the community-level. Whilst the traits measured were universal (i.e. growth rate and cell size), temperature was observed to exhibit population-specific changes in these FTs. For example, in eukaryotes from the <20 μm fraction, growth was comparable over a wide (10 °C) temperature range, with an average growth rate of 1.2±0.3 d^{-1} between 15 and 26 °C (One-way RM ANOVA; no statistical difference between 15, 19, 24 and 26 °C, p >0.3), but there was no growth at high temperatures of 30 °C or above, except for an outlier (0.27 d^{-1}) in the 30 °C treatment (**Figure 3.4a**). Similarly, the average cell size of eukaryotes from the <20 μm fraction remained relatively unaffected by temperature, no change in FSC was observed at intermediate temperatures (between 19 and 26 °C) but was reduced by 5% when incubated at colder temperatures (**Figure 3.4a**; One-way RM ANOVA; statistical difference between 15 and 19 °C, p <0.02).

The thermal niche of *Prochlorococcus* was similar to eukaryotes in the <20 μm fraction, with an average growth rate of 1.7±0.2 d^{-1} between 15 and 26 °C, and no growth observed at 30 or 32 °C **(Figure 3.4b**; One-way RM ANOVA; no statistical difference between 19 and 15, 24, 26 °C). At colder temperatures, however, and unlike small (<20 μm) eukaryote cells, a 25% increase in cell size (FSC) was observed in the *Prochlorococcus* population (One-way RM ANOVA; statistical difference between 15 and 19 °C, p <0.02). In contrast, *Synechococcus* spp. Were observed to have the highest growth rates and greatest thermal limit of the pico- and nano-phytoplankton populations measured. A wide thermal niche for both FTs was observed in *Synechococcus* spp., with growth and cell size being consistent between 15 and 30 °C with an average growth rate of 2.2±0.0 d^{-1}. These *Synechococcus* related FTs were only affected at the hottest temperature measured (32 °C), whereby growth rates were reduced by 33±10% and cell size increased by 22±8% (**Figure 3.4c**; One-way RM ANOVA; statistical difference in growth and cell size between 19 and 32 °C, p =0.01 and p =0.03, respectively).

Together these results show population-specific responses to temperature and different allometric relationships of prokaryotic and eukaryotic cells, with the relative change in cell size being greater for the picocyanobacterial communities. This is because, firstly,

the average cell size of the picoeukaryote and picocyanobacteria communities became smaller and larger, respectively, when exposed to temperatures that are inhibiting for growth (at both cold and hot extremes). Secondly, under inhibiting growth temperatures the average cell size (FSC) of *Prochlorococcus* spp. and *Synechococcus* spp. changed by 26±3 and 21±8%, respectively whereas the size of eukaryote cells from the pico- and nanophytoplankton fraction only shifted by 3±0.1%.

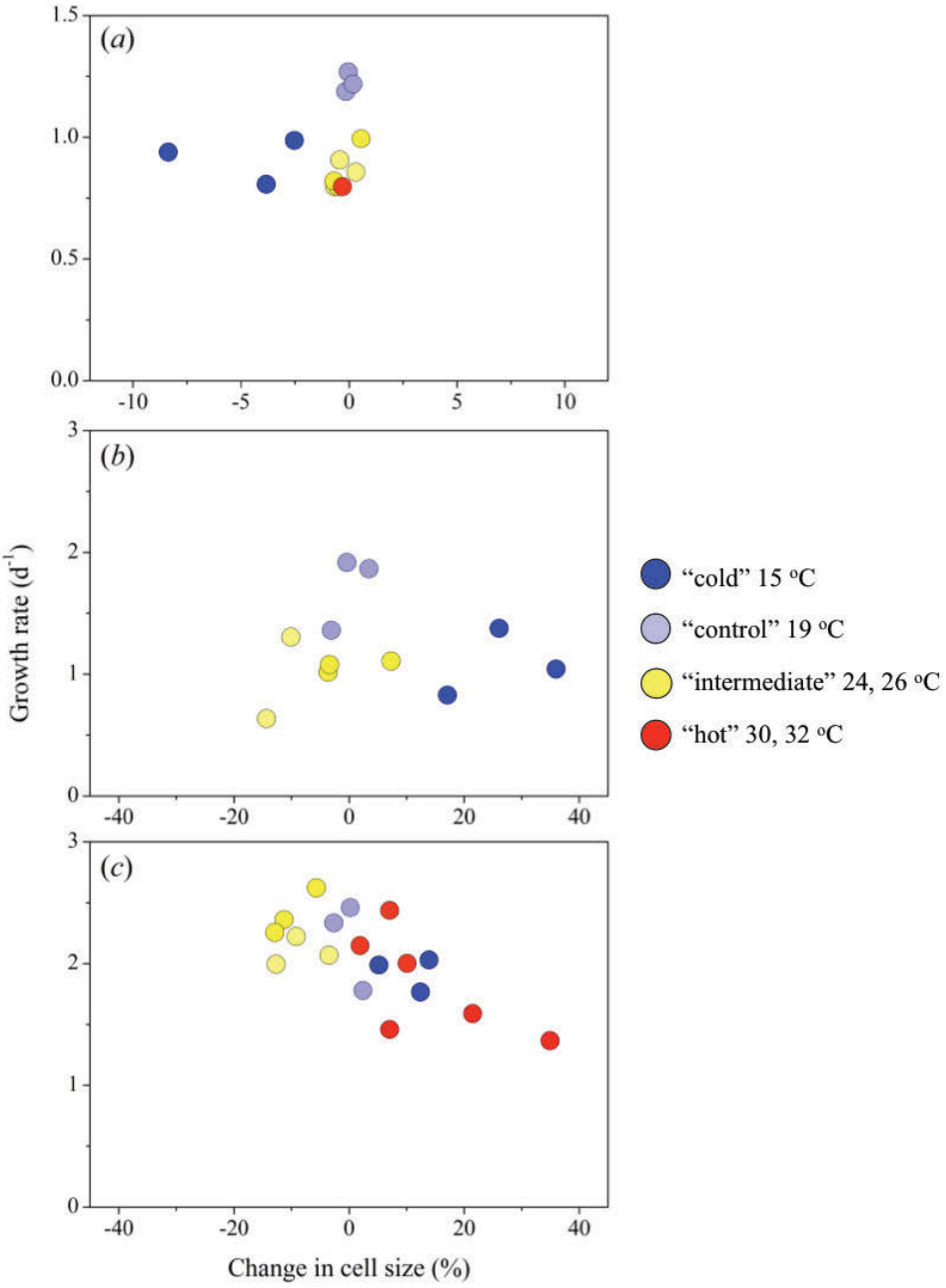

Figure 3.4 Growth rate (d^{-1}) and change in relative cell size (estimated from forward angle light scattering; FSC) from T_0 (%) of the (a) small (<20 µm) eukaryotes, (b) *Prochlorococcus* spp., and (c) *Synechococcus* spp surface (5 m depth) populations at Port Hacking (PH100) after 24 h of exposure to a range of temperatures. Growth rate was calculated as the difference in cell abundance (using counts obtained by flow cytometry) between initial (T_0) and final (T_{24}) for each plankton group. Changes in cell size measurements were calculated as the difference of average bead-normalised FSC between initial (T_0) and final (T_{24}) for each plankton group, obtained via flow cytometry. Each symbol represents an individual replicate with the colour of the symbols reflecting the temperature treatment: 15 °C (cold; dark blue), 19 °C (control; light blue), 24 and 26 °C (intermediate; yellow), and 30 and 32 °C (hot; red). Where symbols are absent, positive growth was not observed.

3.3.5 Temperature effects on diatom specific functional traits

At the community-level, BSi production by small diatoms (<20 µm) increased significantly with decreasing growth, and was reduced at high temperatures that were found to be inhibiting for growth (negative values; **Figure 3.5**). This relationship remained true when all temperatures were considered (i.e., negative growth rates included; R^2 =0.69, p <0.001; **Figure 3.4**) or temperatures inhibiting for growth excluded (R^2 =0.73, p <0.001; 30 and 32 °C). Under temperatures that supported growth (<30 °C), BSi production was equivalent to 754 RFUs L^{-1} d^{-1}.

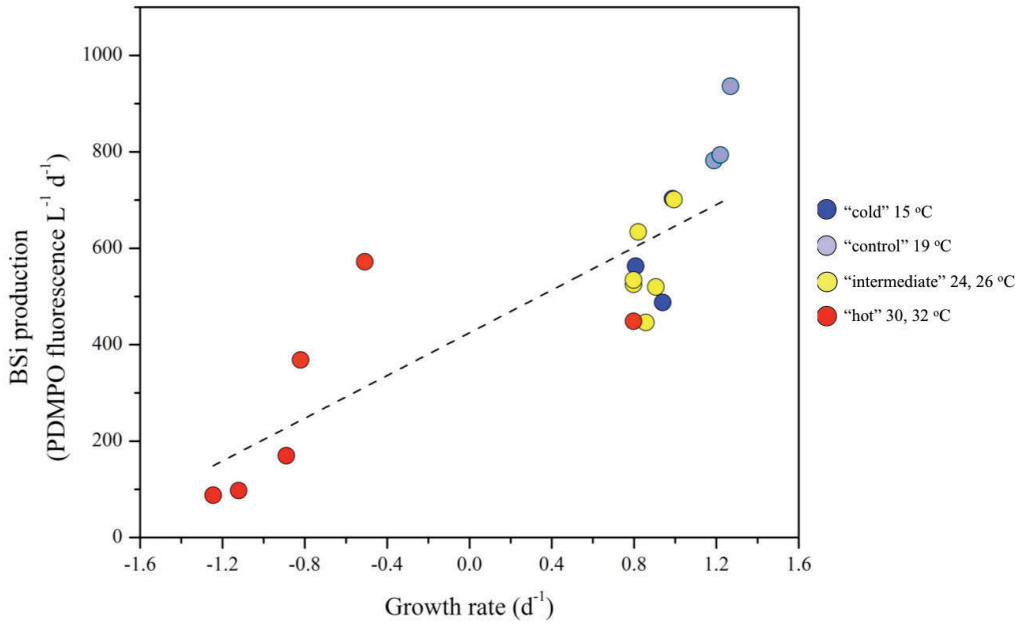

Figure 3.5 Biogenic (BSi) production of small diatoms (<20 µm) from the surface Port Hacking pico- and nano-phytoplankton communities collected in October 2015. BSi production was estimated by multiplying cell-specific bead-normalised PDMPO fluorescence (i.e., the relative amount of silicon deposited) by abundance of PDMPO positive cells (i.e., the number of actively depositing cells). Growth was assumed to be equivalent to division rates of eukaryotes in the <20 μm fraction and was calculated as the difference in cell abundance (using counts obtained by flow cytometry) between initial (T_0) and final (T_{24}). Each symbol represents an individual replicate with the colour of the symbols reflecting the temperature treatment: 15 °C (cold; dark blue), 19 °C (control; light blue), 24 and 26 °C (intermediate; yellow), and 30 and 32 °C (hot; red). Broken line represents the maximum likelihood estimate of linear regression (R^2 = 0.69, p <0.001).

BSi production was still observed in samples exposed to lethal temperatures i.e., temperatures equal to or greater than 30 °C, indicating that Si deposition processes were active in non-dividing cells. Indeed, at the cellular-level, diatoms were fourfold more silicified under high temperatures but not growing (**Figure 3.6**; One-way RM ANOVA; statistical difference in between 30 and 32 °C, and 15, 19, 24 and 26 °C, $p \leq 0.046$). As a

result, at the community level, relative BSi production was reduced by ~85% because a significantly smaller fraction of the diatom community was responsible for Si deposition, amounting to approximately 25 cells L^{-1} at 30 and 32 °C compared to ~175 cells L^{-1} between 15 and 26 °C (**Figure 3.6**; One-way RM ANOVA; statistical difference in between 30 and 32 °C, and 15, 19, 24 and 26 °C, $p \leq 0.002$). In contrast, at temperatures supporting growth (between 15 and 26 °C) the frustule silicification of small diatoms (<20 μm) remained similar (**Figure 3.5**).

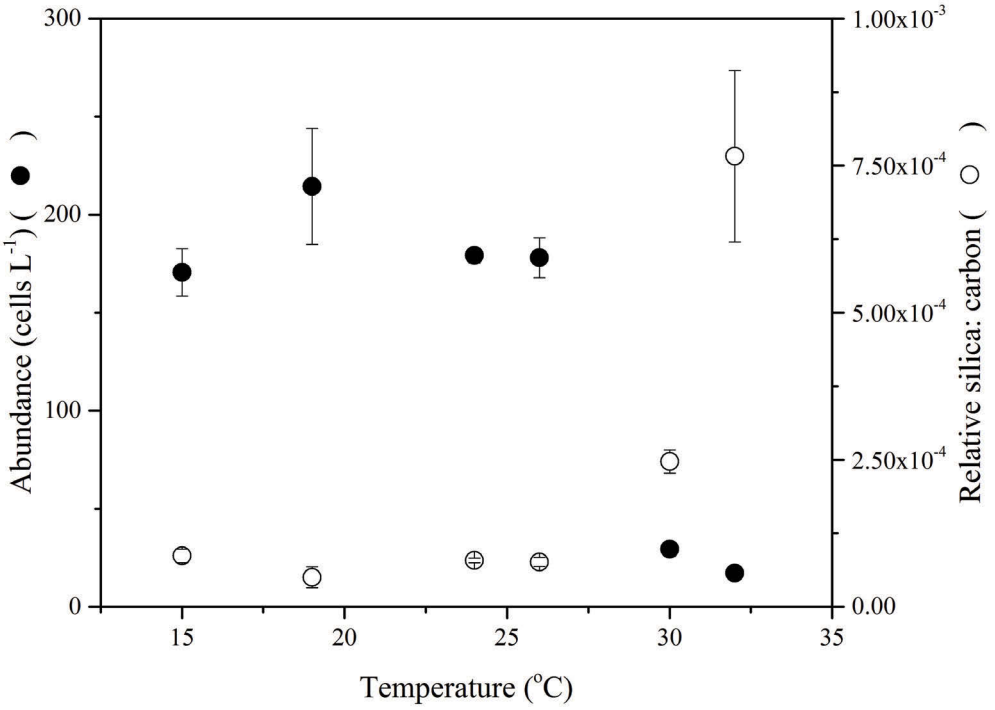

Figure 3.6 Abundance of and cell-specific silicon (Si) deposition by diatoms from the pico- and nano-phytoplankton (<20 μm) fraction of seawater samples sampled from Port Hacking (PH100). Both parameters were obtained using flow cytometry whereby diatoms were first distinguished as PDMPO positive cells and then counted. Si deposition was calculated as cell-specific bead-normalised PDMPO fluorescence. Symbols represent the mean of triplicate samples and the error is the standard error of the mean.

For the diatom community, quantitative assessment of community PDMPO incorporation was only possible for source water because samples along the temperature gradient were below the instrument detection. This was likely due to small volumes (40 mL) of seawater used. However, under *in situ* temperatures of 19 °C where larger incubation volumes (120 mL) were used, we obtained rates of BSi production of 1.43±0.2 μmol Si L^{-1} d^{-1} (**Table 3.1**). Assuming the linear relationship between temperature and BSi production observed for the <20 μm fraction extends to the whole community, we would anticipate rates of BSi production to be approximately 0.99 ±0.4 μmol Si L^{-1} d^{-1} at 15 °C and 0.21 ±0.1 μmol Si L^{-1} d^{-1} at 30 °C.

3.4 Discussion

Examining the direct effects of temperature on key physiological responses of natural phytoplankton provides insight into present-day thermal limits, potential changes under future warming and what implications these shifts have for the ecological and biogeochemical niches that phytoplankton populations occupy (Hofmann and Todgham 2010, Litchman and Klausmeier 2008). In this study, we find a considerable degree of thermal plasticity in a temperate, natural phytoplankton community whereby warming actually enhanced primary productivity – probably as a result of enhanced metabolic activity. Our results coincided with an *in vitro* reorganisation of the underlying community structure over an acute timescale (hours-days), with *Synechococcus* spp. being most tolerant, and *Prochlorococcus* spp. being the most sensitive to short-term warming. These findings are consistent with forecasts of 'winners' and 'losers' under global change (Doney et al. 2012, Dutkiewicz et al. 2013). Cooling rather than warming appeared to have a more significant effect on FTs, notably though, the emergence of 'cool phenotypes' associated with these conditions differed between populations. Overall, our results suggest a high degree of FT plasticity is present in extant phytoplankton at both the community- and population-levels, with wide thermal niches of many FTs including primary productivity, BSi production, photophysiology, growth rate, cell size and frustule silicification.

3.4.1 Thermal responses of community-level functional traits and implications on biogeochemical cycling of carbon and silicon

Tracking changes in community-level FTs such as primary productivity, photophysiology and BSi production over a transient thermal gradient provided insight into how changes in mean SST are likely to affect ocean biogeochemistry in this region. While this study only considered timescales that involve short-term responses (hours-days) of phytoplankton to temperature, it potentially yields some useful insight into whether longer-times of acclimation and adaptive evolution will be important. Our experimental results suggest that the projected long-term increase in mean SST for the region (+2-3 °C; Wu et al. 2012) superimposed over the average temperature for spring (21 °C) and summer (24 °C) at Port Hacking (Thompson et al. 2009) are likely to have undetectable effects on the physiological processes of the resident phytoplankton that regulate C and Si biogeochemical processes.

At the community level, we would expect comparable light harvesting and utilisation because changes in photophysiological parameters and carbon fixation (GPP) under predicted mean temperature conditions of the future were only reduced at temperatures of 30 °C or above (**Figure 3.2**), noting, however, that there may be changes in respiration that influence NPP. Similarly, we would anticipate no significant change in primary productivity by *Synechococcus* spp. and *Prochlorococcus* spp. because C fixation scales with biovolume (Binder et al. 1996, Huete-Ortega et al. 2012) and we observed similar cell sizes over a wide temperature range (between 19 and 26 °C; **Figure 3.3**).

Unlike the physiological processes regulating C transformations, phenotypic traits of diatoms mediating Si cycling in this temperate region are likely to be impacted by warming SST but could only be detected at the community-level (i.e. BSi production) and not at the cell-specific level (i.e., frustule silicification; Baker et al. 2016). It is likely that small changes in growth rate and frustule silicification, whilst undetectable in individual cells (up to 30 °C; **Figure 3.4** and **Figure 3.6**), together culminated in the decrease of BSi production at temperatures above (or below) ambient (**Figure 3.5**). This indicates that non-significant changes in FTs at the cellular-level can have detectable effects on processes at the community-level. Whilst we could not estimate rates of BSi production over a temperature gradient (as intended) because the whole community samples were below the instrument detection limit, these population-specific results nevertheless provide insight into the role temperature plays in diatom physiology and in turn, mediating the marine Si cycle.

The most significant temperature effects on physiological processes that play a role in the biogeochemical cycling of C and Si at the community- and population-level (<20 µm size fraction) occurred at temperatures well above those exposed to on current annual timescales or increases in mean SST anticipated for SE Australia. For example, it is only at temperatures of 30 °C and above where deleterious effects on growth rate (**Figure 3.4**), GPP (**Figure 3.2**) and photophysiology (**Table 3.2**) occur. However, our short-term experiments (24 h exposure) may not provide a complete picture of changes that occur over long-term timescales. For example, locally at Port Hacking, it is hypothesised that decadal changes in abiotic factors, specifically a decline in silicate concentration, has given rise to small and lightly silicified diatom species over the past

two decades (*Thalassiosira* cf. *partheneia*; Ajani et al. 2014). The presence of this species may be indicative of natural selection and species sorting (replacement) that might occur as a response to changing environmental conditions, giving rise to species that are better adapted to warmer, low Si conditions (Litchman et al. 2012). In light of these observations, it is possible that species adapted to warmer temperatures may become more dominant and replace more temperate species, as has been reported at PH100 for other functional groups such as diazotrophs (Ajani et al., 2014). In view of the oceanographic changes occurring in the region, i.e., increased southwards extension of the EAC, potential changes in meso-scale eddy formation and thermal stratification (Hobday et al. 2006), high-temperature diatom phenotypes, like those observed for other taxa (Mackey et al. 2013, Moore et al. 1995), may be delivered to, or become more competitive in this region.

Finally, given the length of the temperature exposure used in this study is relatively short (24 h), it remains unclear whether or not the rates of change reported here may under-/over- estimate the capacity for thermal acclimation of these biological processes (Schulte et al. 2011). For example, in other marine ectotherms such as salmon, the thermal optimum for metabolism can change depending on the prior exposure to temperature (Eliason et al. 2011). Whilst similar studies have not been performed with phytoplankton, it is possible that the temperature effects presented here may only be representative of the spring phytoplankton community, and the phytoplankton would respond differently in summer following seasonal acclimation to warming.

3.4.2 Temperature-specific phenotypes and divergence within and between phytoplankton functional groups

In this study, we find evidence to support the occurrence of temperature-specific phenotypes in natural phytoplankton communities, reflecting findings previously observed in the laboratory on temperate-diatom monocultures (Baker et al. 2016). At temperatures below ambient for spring, we observed the emergence of 'cool phenotypes' that were characterised by smaller cells (compared to ambient temperatures) in the small diatom-containing pico- and nano-eukaryote population (**Figure 3.4a**). However, the magnitude and direction of FT change was not consistent across all populations because 'cool phenotypes' were larger in size than the *Synechococcus* and *Prochlorococcus* populations (**Figure 3.4b, c**). These results

indicate, while cell size itself is a universal FT (Finkel et al. 2009), the magnitude and direction of change for equivalent departures in temperature may not be, suggesting the physiological mechanisms underlying these changes are population-specific. Hence it is important that trait changes be assessed at the taxon-specific level, because ultimately these trait differences may drive interspecific differences in response to stress (Mouillot et al. 2013).

Diversity in thermally-induced physiological responses was also evident within the prokaryotic picophotoautotrophs. Contrary to predictions of Flombaum et al. (2013), we find *Synechococcus* (rather than *Prochlorococcus*) demonstrated a competitive advantage at temperatures above *in situ*. These differences may be due to the fact that niche model estimates are based on observations of current abundance and distributions, and do not take in consideration physiological acclimation strategies, like those presented here. Indeed, *Synechococcus* sp. have been shown to outcompete *Prochlorococcus* sp. under climate change scenarios, when acclimation strategies are taken into account (Fu et al. 2007). The success of *Synechococcus* spp. are likely a combination of decreased abundance of other taxa resulting in reduced competition for resources (e.g. light and nutrients), as well as the possession of characteristics that enable success under warming temperatures, e.g. high growth rates and photosynthesis. For example, laboratory experiments have demonstrated that some ecotypes of *Synechococcus* spp. have a relatively high thermal optimum of approximately 27-28 °C (Mackey et al. 2013, Moore et al. 1995), whereas strains of *Prochlorococcus* show inhibition of growth above 25 °C (Moore et al. 1995). Additionally, it has been demonstrated that the ability of *Synechococcus* spp. to balance growth and photosynthesis over such a wide range of temperatures may be mechanistically supported by dynamic regulation of photosynthetic machinery (and associated proteins), which it turn, facilitate a broad biogeographical distribution (Mackey et al. 2013). These thermal thresholds may explain why warming may differentially stimulate these two marine picocyanobacteria, whereby high temperatures favor the growth of *Synechococcus* spp. (Fu et al. 2007).

3.4.3 Implications and further directions

Through a trait-based approach, we have shown the direct effects of short-term changes in temperature can reorganise phytoplankton composition *in vitro*, alter phytoplankton phenotypes and change rates of phytoplankton mediated biogeochemical processes such as BSi production. In the ocean region examined in this study, increases in average SST (+2 °C) are likely to have small, undetectable effects on the biogeochemical cycles mediated by resident shelf phytoplankton and may not be representative of other temperate regions. However, it is likely that ocean heatwaves (e.g. spring ambient +11 °C, the highest temperature treatment in this study), although rare, will have significant implications on the structure of resident phytoplankton communities and their FTs and hence biogeochemical roles.

Under these ocean heatwave (+11 °C) scenarios, the physiological stress encountered (i.e., decrease in photosynthesis or growth) has implications for C and Si cycling by decreasing rates of NPP and BSi. Furthermore, the ability of *Synechococcus* spp. to acclimate to higher temperatures may preferentially redistribute this group (spatially and at depth) at Port Hacking relative to other taxa such as *Prochlorococcus* spp. and other small picoplankton such as diatoms. However, individual strains of picocyanobacteria may respond quite differently to future warming scenarios due to variability in thermal tolerances between strains (Boyd et al. 2013) and inherent differences in their local acclimation strategies. As a result, the direct temperature effects on picophytoplankton composition and growth are likely region-specific and care should be taken when generalising the responses observed in this temperate system to other regions.

In order to understand the physiological mechanisms behind the emergence of temperature-specific phenotypes, the application of cell-specific fluorescent tracers in conjunction with flow cytometry could be used to target, sort and sequence these populations in order to discriminate between phenotypic acclimation, genetic adaptation and species sorting. To ascertain whether the findings from the time-window (i.e. spring) used in this study are season-specific, future research should consider conducting similar experiments at higher temporal resolution (e.g. monthly) in order to understand whether these direct effects of temperature on biogeochemical processes are dependent on seasonal acclimation of phytoplankton. Finally, replication at other long-

term monitoring stations will help to ascertain whether the findings presented are locally specific or are representative of all Australian waters. The collection of this type of dataset through consecutive years could facilitate the prediction of long-term changes in phytoplankton functional groups, the biogeochemical processes that they mediate and the underlying mechanisms responsible for these changes.

3.5 Acknowledgments

The authors thank the scientific crew, captain and scientists onboard the *RV Bombora* during the IMOS October 2015 Port Hacking, NSW sampling campaign for assistance with sampling and nutrient analysis. We would also like to thank Professor Maria Byrne for access to the thermal gradient blocks.

This research was funded by a student scholarship awarded through the School of Life Sciences and Plant Functional Biology and Climate Change Cluster- (C3), University of Technology Sydney to KB.

3.6 Literature cited

Ajani, P. A., Allen, A. P., Ingleton, T. and Armand, L. (2014) A decadal decline in relative abundance and a shift in microphytoplankton composition at a long‐term coastal station off southeast Australia. *Limnology and Oceanography,* 59(2), pp. 519-531.

Baker, K. G., Robinson, C. M., Radford, D. T., McInnes, A. S., Evenhuis, C. and Doblin, M. A. (2016) Thermal performance curves of functional traits aid understanding of thermally induced changes in diatom-mediated biogeochemical fluxes. *Frontiers in Marine Science,* 3, pp. 44.

Beardall, J. and Raven, J. A. (2004) The potential effects of global climate change on microalgal photosynthesis, growth and ecology. *Phycologia,* 43(1), pp. 26-40.

Binder, B. J., Chrisholm, S. W., Olsen, R. J., Frankel, S. L. and Worden, A. Z. (1996) Dynamics of picophytoplankton, ultraphytoplankton and bacteria in the central equatorial Pacific. . *Deep-Sea Research II,* 43(pp. 907-931).

Bopp, L., Resplandy, L., Orr, J. C., Doney, S. C., Dunne, J. P., Gehlen, M., Halloran, P., Heinze, C., Ilyina, T. and Seferian, R. (2013) Multiple stressors of ocean ecosystems in the 21st century: projections with CMIP5 models.

Boyce, D. G. and Worm, B. (2015) Patterns and ecological implications of historical marine phytoplankton change. *Marine Ecology Progress Series,* 534, pp. 251-272.

Boyd, P. W., Rynearson, T. A., Armstrong, E. A., Fu, F., Hayashi, K., Hu, Z., Hutchins, D. A., Kudela, R. M., Litchman, E., Mulholland, M. R., Passow, U., Strzepek, R. F., Whittaker, K. A., Yu, E. and Thomas, M. K. (2013) Marine Phytoplankton Temperature versus Growth Responses from Polar to Tropical Waters – Outcome of a Scientific Community-Wide Study. *PLoS One,* 8(5), pp. e63091. doi:10.1371/journal.pone.0063091.

Boyd, P. W., Strzepek, R., Fu, F. and Hutchins, D. A. (2010) Environmental control of open-ocean phytoplankton groups: Now and in the future. *Limnology and Oceanography,* 55(3), pp. 1353-1376. doi:10.4319/lo.2010.55.3.1353.

Cubasch, U., Meehl, G. A., Boer, G. J., Stouffer, R. J., Dix, M., Noda, A., Senior, C. A., Raper, S. and Yap, K. S. (2001) *Projections of future climate change. In Climate Change 2001: The Scientific Basis,* New York: Cambridge University Press: 525–582.

Davison, I. R. (1991) Environmental effects on algal photosynthesis: temperature. *Journal of Phycology,* 27(1), pp. 2-8.

Doblin, M. A., Petrou, K. L., Shelly, K., Westwood, K., Van den Enden, R., Wright, S., Griffiths, B. and Ralph, P. J. (2011) Diel variation of chlorophyll-a fluorescence, phytoplankton pigments and productivity in the Sub-Antarctic and Polar Front

Zones south of Tasmania. *Australia Deep Sea Research Part II: Topical Studies in Oceanography,* 58(21), pp. 2189-2199.

Doney, S. C., Ruckelshaus, M., Duffy, J. E., Barry, J. P., Chan, F., English, C. A., Galindo, H. M., Grebmeier, J. M., Hollowed, A. B. and Knowlton, N. (2012) Climate change impacts on marine ecosystems. *Marine Science,* 4. doi:10.1146/annurev-marine-041911-111611.

Durkin, C. A., Marchetti, A., Bender, S. J., Truong, T., Morales, R., Mock, T. and Virginia Armbrust, E. (2012) Frustule-related gene transcription and the influence of diatom community composition on silica precipitation in an iron-limited environment. *Limnology and Oceanography,* 57(6), pp. 1619.

Dutkiewicz, S., Scott, J. R. and Follows, M. J. (2013) Winners and losers: ecological and biogeochemical changes in a warming ocean. *Global Biogeochemical Cycles,* 27(2), pp. 463-477.

Eliason, E. J., Clark, T. D., Hague, M. J., Hanson, L. M., Gallagher, Z. S., Jeffries, K. M., Gale, M. K., Patterson, D. A., Hinch, S. G. and Farrell, A. P. (2011) Differences in thermal tolerance among sockeye salmon populations. *Science*, pp. 109-112.

Eppley, R. W. (1972) Temperature and phytoplankton growth in the sea. *Fisheries Bulletin,* 70(4), pp. 1063-1085.

Falkowski, P. G. (2004) Biogeochemistry of Primary Production in the Sea. in Schlesinger, W. H., (ed.) *Treatise on Geochemistry*: Gulf Professional Publishing. pp. 185–213.

Feng, Y., Hare, C. E., Leblanc, K., Rose, J. M., Zhang, Y., DiTullio, G. R., Lee, P. A., Wilhelm, S. W., Rowe, J. M., Sun, J., Nemcek, N., Gueguen, C., Passow, U., Benner, I., Brown, C. and Hutchins, D. A. (2009) Effects of increased pCO_2 and temperature on the North Atlantic spring bloom. I. The phytoplankton community and biogeochemical response. *Marine Ecology Progress Series,* 388, pp. 13-25. doi:10.3354/meps08133.

Finkel, Z. V., Beardall, J., Flynn, K. J., Quigg, A., Rees, T. A. V. and Raven, J. A. (2009) Phytoplankton in a changing world: cell size and elemental stoichiometry. *Journal of Plankton Research*. doi:fbp098.

Flombaum, P., Gallegos, J. L., Gordillo, R. A., Rincón, J., Zabala, L. L., Jiao, N., Karl, D. M., Li, W. K. W., Lomas, M. W. and Veneziano, D. (2013) Present and future global distributions of the marine Cyanobacteria Prochlorococcus and Synechococcus. *Proceedings of the National Academy of Sciences,* 110(24), pp. 9824-9829.

Fu, F. X., Warner, M. E., Yaohong, Z., Yuanyuan, F. and Hutchins, D. A. (2007) Effects of increased temperature and CO_2 on photosynthesis, growth, and elemental ratios in marine *Synechococcus* and *Prochlorococcus* (cyanobacteria). *Journal of Phycology,* 43, pp. 485-496.

Hobday, A. J., Okey, T. A., Poloczanska, E. S., Kunz, T. J. and Richardson, A. J. (2006) Part C. Literature Review. in *Impacts of climate change on Australian marine life: Report to the Australian Greenhouse Office, Canberra, Australia*,Canberra: CSIRO.

Hofmann, G. E. and Todgham, A. E. (2010) Living in the now: physiological mechanisms to tolerate a rapidly changing environment. *Annual Review of Physiology,* 72, pp. 127-145.

Huete-Ortega, M., Cermeño, P., Calvo-Díaz, A. and Marañón, E. (2012) Isometric size-scaling of metabolic rate and the size abundance distribution of phytoplankton. *Proceedings of the Royal Society of London B: Biological Sciences,* 279(1734), pp. 1815-1823.

Kolber, Z. S., Prášil, O. and Falkowski, P. G. (1998) Measurements of variable chlorophyll fluorescence using fast repetition rate techniques: defining methodology and experimental protocols. *Biochimica et Biophysica Acta (BBA)-Bioenergetics,* 1367(1), pp. 88-106.

Krause, J. W., Nelson, D. M. and Brzezinski, M. A. (2011) Biogenic silica production and the diatom contribution to primary production and nitrate uptake in the eastern equatorial Pacific Ocean. . *Deep Sea Research Part II: Topical Studies in Oceanography,* 58(3), pp. 434-448.

Le Quere, C. L., Harrison, S. P., Colin Prentice, I., Buitenhuis, E. T., Aumont, O., Bopp, L., Claustre, H., Cotrim Da Cunha, L., Geider, R., Giraud, X. and Klaas, C. (2005) Ecosystem dynamics based on plankton functional types for global ocean biogeochemistry models. *Global Change Biology,* 11(11), pp. 2016-2040.

Leblanc, K. and Hutchins, D. A. (2005) New applications of a biogenic silica deposition fluorophore in the study of oceanic diatoms. *Limnology and Oceanography: Methods,* 3, pp. 462-476.

Litchman, E., Edwards, K. F., Klausmeier, C. A. and Thomas, M. K. (2012) Phytoplankton niches, traits and eco-evolutionary responses to global environmental change. *Marine Ecology Progress Series,* 470, pp. 235-248. doi:10.3354/meps09912.

Litchman, E. and Klausmeier, C. A. (2008) Trait-based community ecology of phytoplankton. *Annual Review of Ecology, Evolution, and Systematics,* 39, pp. 615-639.

Mackey, K. R. M., Paytan, A., Caldeira, K., Grossman, A. R., Moran, D., Mcilvin, M. R. and Saito, M. A. (2013) Effect of temperature on photosynthesis and growth in marine *Synechococcus* spp. *Plant Physiology,* 163, pp. 815-829.

Marañón, E., Cermeño, P., Huete-Ortega, M., López-Sandoval, D. C., Mouriño-Carballido, B. and Rodríguez-Ramos, T. (2014) Resource supply overrides temperature as a controlling factor of marine phytoplankton growth. *PLoS One,* 9(6), pp. e99312.

McNair, H. M., Brzezinski, M. A. and Krause, J. W. (2015) Quantifying diatom silicification with the fluorescent dye, PDMPO. *Limnology and Oceanography: Methods,* 13(10), pp. 587-599.

Moore, L. R., Goericke, R. and Chisholm, S. W. (1995) Comparative physiology of *Synechococcus* and *Prochlorococcus*: influence of light and temperature on growth, pigments, fluorescence and absorptive properties. *Marine Ecology Progress Series,* 116, pp. 259-275.

Mouillot, D., Graham, N. A. J., Villéger, S., Mason, N. W. H. and Bellwood, D. R. (2013) A functional approach reveals community responses to disturbances. *Trends in Ecology & Evolution,* 28(3), pp. 167-177.

Partensky, F., Blanchot, J. and Vaulot, D. (1999) Differential distribution and ecology of *Prochlorococcus* and *Synechococcus* in oceanic waters: a review. *Bulletin-Institut oceanographique monaco-numero special*, pp. 457-476.

Raven, J. and Waite, A. (2004) The evolution of silicification in diatoms: inescapable sinking and sinking as escape? *New Phytologist,* 162(1), pp. 45-61.

Raven, J. A. (1998) The twelfth Tansley Lecture. Small is beautiful: the picophytoplankton. *Functional Ecology,* 12(4), pp. 503-513.

Raven, J. A. and Geider, R. J. (1988) Temperature and algal growth. *New Phytologist*, pp. 441-461.

Ridgway, K. and Hill, K. (2009) The East Australian Current. in Poloczanska, E. S., Hobday, A. J. and Richardson, A. J., (eds.) *A Marine Climate Change Impacts and Adaptation Report for Australia 2009*: NCCARF Publication.

Schulte, P. M., Healy, T. M. and Fangue, N. A. (2011) Thermal performance curves, phenotypic plasticity, and the time scales of temperature exposure. *Integrative and Comparative Biology,* 51(5), pp. 691-702. doi:10.1093/icb/icr097.

Shimizu, K., Del Amo, Y., Brzezinski, M. A., Stucky, G. D. and Morse, D. E. (2001) A novel fluorescent silica tracer for biological silicification studies. *Chemistry & Biology,* 8(11), pp. 1051-1060.

Smetacek, V. (1985) Role of sinking in diatom life-history cycles: ecological, evolutionary and geological significance. *Marine Biology,* 84(3), pp. 239-251.

Steinacher, M., Joos, F., Frolicher, T. L., Bopp, L., Cadule, P., Cocco, V., Doney, S. C., Gehlen, M., Lindsay, K. and Moore, J. K. (2010) Projected 21st century decrease in marine productivity: a multi-model analysis. *Biogeosciences,* 7(3). doi:10.5194/bg-7-979-2010.

Tatters, A. O., Roleda, M. Y., Schnetzer, A., Fu, F., Hurd, C. L., Boyd, P. W., Caron, D. A., Lie, A. A. Y., Hoffmann, L. J. and Hutchins, D. A. (2013) Short- and long-term conditioning of a temperate marine diatom community to acidification and warming. *Philosophical Transactions of Royal Society B: Biological Sciences,* 368. doi:10.1098/rstb.2012.0437.

Taucher, J. and Oschlies, A. (2011) Can we predict the direction of marine primary production change under global warming? *Geophysical Research Letters,* 38(2), pp. L02603. doi:10.1029/2010GL045934.

Thomas, M. K., Kremer, C. T., Klausmeier, C. A. and Litchman, E. (2012) A Global Pattern of Thermal Adaptation in Marine Phytoplankton. *Science,* 338(6110), pp. 1085-1088. doi:10.1126/science.1224836.

Thompson, P., Baird, M., Ingleton, T. and Doblin, M. (2009) Long-term changes in temperate Australian coastal waters: implications for phytoplankton. *Marine Ecology Progress Series,* 394, pp. 1-19.

Toseland, A., Daines, S. J., Clark, J. R., Kirkham, A., Strauss, J., Uhlig, C., Lenton, T. M., Valentin, K., Pearson, G. A. and Moulton, V. (2013) The impact of temperature on marine phytoplankton resource allocation and metabolism. *Nature Climate Change,* 3(11), pp. 979-984.

Tréguer, P. J. and De La Rocha, C. L. (2013) The world ocean silica cycle. *Annual Review of Marine Science,* 5, pp. 477-501.

Wu, L., Cai, W., Zhang, L., Nakamura, H., Timmermann, A., Joyce, T., McPhaden, M. J., Alexander, M., Qiu, B. and Visbeck, M. (2012) Enhanced warming over the global subtropical western boundary currents. *Nature Climate Change,* 2(3), pp. 161-166.

CHAPTER 4:
SPATIAL MAPPING OF DIATOM PHENOTYPES REVEALS FUNCTIONAL TRAIT DIVERSITY BETWEEN TWO DISTINCT AUSTRALIAN OCEANIC PROVINCES

K. G. Baker*, C. M. Robinson, A. S. McInnes, L.F. Messer, J. Seymour, and M. A. Doblin

Plant Functional Biology and Climate Change Cluster, University of Technology Sydney, Broadway, Ultimo, New South Wales, 2007, Australia

*** Correspondence:** Kirralee G Baker, Plant Functional Biology and Climate Change Cluster, University of Technology Sydney, Broadway, Ultimo, New South Wales, 2007, Australia
Kirralee.G.Baker@student.uts.edu.au

Keywords: Phytoplankton, PDMPO, Arafura Sea, Timor Sea, Coral Sea, nutrient limitation, silicification

4.1 Introduction

Diatoms (Bacillariophyceae) are one of the most ecologically diverse and functionally important phytoplankton groups. In the marine environment, they are important vehicles for downward C flux because of their relatively large cell sizes, coupled with siliceous cell walls provide ballast to sinking aggregates (Armstrong et al. 2009, Buesseler 1998, Nelson et al. 1995). Indeed, it is estimated that globally, diatoms can account for up to 20-40% of marine C downward export (Jin et al. 2006, Nelson et al. 1995). Furthermore, because of their obligate requirements for Si to construct cell walls, diatoms are the major source of BSi production and other Si fluxes in marine ecosystems (Tréguer and De La Rocha 2013).

Understanding how environmental factors regulate BSi production at the diatom-community level requires insight into processes that occur at the cellular level, because diatom growth and cell wall/frustule synthesis govern the cells final elemental composition (Si:C molar ratio), and in turn, controls the amount of BSi deposited/produced (Hildebrand 2008). These cellular-level activities are regulated by external physical and chemical parameters/factors such as temperature, salinity, light availability, and the concentration of dissolved nutrients, including Si (Claquin et al. 2002, Conley et al. 1989, Durbin 1977, Harrison et al. 1976, Paasche 1975). It is therefore not surprising that diatom silicification (i.e., the Si:C (atomic) composition) is highly variable, between different diatom species (Brzezinski 1985, Durkin et al. 2012) and ocean regions (Baines et al. 2010). Diatom silicification is considered a key FT that is intrinsically linked to the unique role that diatoms play in ocean Si biogeochemical cycling (Baines et al. 2010). This is because the degree of frustule silicification determines the quantity of BSi produced (i.e., thicker cell walls contain more Si on a per cell basis), the amount of Si that is likely to be dissolved and resupplied to future phytoplankton generations, and the elemental composition of organic matter transferred to higher trophic levels (Finkel et al. 2009, Raven and Waite 2004). Therefore, examining patterns in cellular silicification across different spatial scales can provide insight into region variability in diatom-mediated C and Si cycling.

Hotspots in marine biogeochemical cycling of C and Si are known to occur along continental margins (Walsh 1991), however, it is difficult to estimate the contribution of

these regions to global BSi production as they are under sampled, both spatially and temporally (Shipe and Brzezinski 2001). In the Southern Hemisphere, characterisation of standing stocks of BSi and rates of BSi production have so far been restricted to the Southern Ocean (Tréguer and De La Rocha 2013) and BSi dynamics remain unknown for tropical and temperate coastal oceans south of the Equator. Indeed, the coastal waters of tropical, Northern Australia are likely to be an unidentified but significant region for marine biogeochemical cycling of Si and C. Similar to recognised hotspots such as NW Africa that coincide with high diatom species richness (Cermeño et al. 2008, Nelson and Goering 1977, Ragueneau et al. 2000, Robins et al. 1996), the northern shelf of Australia is also known to be highly productive (Condie and Dunn 2006) and characterised by a rich diversity of diatoms (Blondeau-Patissier et al. 2011, Burford et al. 1995, Hallegraeff and Jeffrey 1984, Lourey et al. 2013). Yet, the biogeochemical role of these diatom communities is yet to be proven.

To investigate how the physicochemical and ecological settings of different ocean provinces affect diatom physiology at the single cell level and how this governs diatom-mediated biogeochemical processes, we used the fluorescence tracer, PDMPO to survey the spatial distribution of silicification (a key FT in diatoms) along ocean margins. Our first hypothesis was that spatial mapping of the coastal margins of Northern Australia would show diversity within diatom silicification, due to the distinct biophysical and biochemical settings in this region. For example, the waters of the Arafura-Timor Shelf (ATS) are warm, shallow, and despite little exchange with the adjacent Pacific and Indian Oceans, the ATS is well mixed most of the year due to strong tidal currents and wind-driven circulation (Alongi et al. 2011). In contrast, the Coral Sea (CS) is dominated by oligotrophic surface waters, despite the presence of subsurface nutrients (Brewer et al. 2007). Additionally, given that Australian oceans are generally N-limited (Moore et al. 2013), we tested whether the addition of this nutrient influences patterns in these biogeochemical processes by conducting nitrate addition assays. We then assessed whether the variability in the biogeographical distribution of silicification results from physiological responses to their ambient surroundings or are intrinsic characteristics of the resident community and report the key diatoms responsible for Si processes in these oceanographic provinces.

4.2 Methods and materials

4.2.1 Sample collection

Seawater samples were obtained during a 5000 km transect across the northern coast of Australia, from Broome to Brisbane on board the *RV Southern Surveyor* (SS2013_t03). The voyage was conducted during the austral winter (July-August; **Figure 4.1**) a period corresponding to the middle of the dry season (Alongi et al. 2011). Seawater was collected at dawn from surface waters (5 m depth) and, when discernable (from the down-cast chlorophyll *a* (Chl *a*) fluorescence profile), the sub-surface chlorophyll maximum (Cmax) using a CTD-rosette system equipped with 10 L Niskin bottles.

4.2.2 Physicochemical characterisation of seawater

Vertical profiles of Chl *a* fluorescence, temperature, salinity, oxygen, and photosynthetically active radiation (PAR) were measured at each location using a conductivity-temperature-depth (CTD) sensor (Seabird SBE 911). Dissolved nutrient analysis (nitrate (NO_3^-), phosphate (PO_4^{3-}), ammonium (NH_3^+), silicate (SiO_4^{4-}) was conducted at sea immediately after sample collection. Concentrations of NO_3^-, PO_4^{3-} and SiO_4^{4-} were determined colourmetrically via Flow Injection Analysis (Latchat; detection limit 0.02 μM) whilst NH_3^+ samples were analysed using an AA3HR Segmented Flow nutrient analyser (Seal Analytical; detection limit 0.01 μM).

4.2.3 Biological characterisation of seawater

For pigment analyses, triplicate 2.2 L seawater samples were collected and filtered onto 25 mm Whatman GF/F filters under dim light. Filters were blotted dry, placed into cryotubes, snap-frozen in liquid nitrogen and stored at -80 °C. Post-voyage, pigments were extracted in 3 mL acetone (90%) at 4 °C in the dark for 12 h and then sonicated for 15 min. Samples were recovered using filtration (0.22 μm Millex-GV filter unit, Merck KGaA, Darmstadt, Germany) and a bench vortex. The samples were analysed following the procedure of Van Heukelem and Thomas (2001) using High Performance Liquid Chromatography (HPLC) with an Agilent 1200 series system comprising a 2695XE separations module with column heater and refrigerated autosampler using a C8 column (Zorbax Eclipse XDB-C8, Agilent Technologies) and binary gradient system with an elevated column temperature 55 °C. Following the methods of Vidussi et al. (2001), Hooker et al. (2005) and Uitz et al. (2008), seven diagnostic pigments

were used as biomarkers of specific phytoplankton taxa to assess the contribution of three pigment-based size classes (micro-, nano-, and pico-phytoplankton) to the total phytoplankton biomass. The seven diagnostic pigments used included fucoxanthin (Fuco), peridinin (Peri), alloxanthin (Allo), 19'-butanoyloxyfucoxanthin (19'-BF), 19'-hexanoyloxyfucoxanthin (19'HF), zeaxanthin (Zea), and total chlorophyll *b* (TChl *b*). Microphytoplankton (>20 μm) are associated with Fuco and Peri, nanophytoplankton (2-20 μm) with Allo, 19'BF and 19'HF, and picophytoplankton (<2 μm) with Zea and TChl *b*.

The elemental stoichiometry of particulate organic matter was assessed in order to examine the relative abundance of diatoms as a proportion of the whole phytoplankton community, calculated as a ratio of BSi to C and N. For particulate organic carbon (POC) and nitrogen (PON) measurements, duplicate 2 L seawater samples were collected and filtered on to 25 mm Whatman GF/F filters (precombusted at 450 °C). Post-voyage filters were dried at 60 °C for 48 h. Total POC and PON were then determined using an elemental analyser (Thermo Finnigan MAT Conflo IV) coupled to an isotope ratio mass spectrometer (Thermo Finnigan Delta XP) at the Biogeochemical Stable Isotope Facility, University of Hawaii.

4.2.4 Experimental set-up

To assess whether dissolved NO_3^- was the limiting inorganic nutrient for diatom growth and BSi deposition, nutrient amendment assays were conducted at each site. Experiments were conducted in triplicate and consisted of an unamended seawater control and a NO_3^- addition (supplied as $NaNO_3$) seawater treatment (10 μmol L^{-1}; approximately tenfold greater than *in situ* concentrations). Experiments were conducted with surface and Cmax samples and involved deck-board incubations where *in situ* temperature conditions were maintained by a flow-through surface seawater system. *In situ* irradiance was simulated by screening bottles with shade cloth and appropriate layers of blue filter (061 Mist Blue, Lee Filters, Seattle, United States of America), according to PAR values obtained from vertical CTD casts.

4.2.5 Tracking cell-specific silicification and community-level biogenic silicon production

It has recently become possible to probe patterns in BSi production/silicification at the cellular level, with the use of fluorescent tracers, such as Lysosensor Yellow/Blue DND-160, also known as PDMPO (ThermoFisher Scientific, Australia). In contrast to BSi measurements that quantify the abundance of silicifiers, PDMPO labels actively depositing cells and hence provides a more accurate quantification of diatoms directly contributing to the transformation of DSi to BSi (Shimizu et al. 2001). Additionally, PDMPO coupled with fluorescence microscopy can be used to visualise diatoms actively depositing BSi within natural communities (Leblanc and Hutchins 2005). Furthermore, PDMPO can be used as a proxy for community-level BSi production (Leblanc and Hutchins 2005) and overcomes several changes of traditional analytical techniques, such as measuring net changes in BSi over time or silicic acid uptake using Si isotope tracers that can be restricted by biomass and cost.

In this study, BSi production at the community and cell-specific levels was estimated by incubating natural samples in the presence of PDMPO. Sampled phytoplankton communities were first concentrated five-fold (from 4 L to 800 mL) following the methods of Durkin et al. (2012) via inverse filtration through a polycarbonate filter (0.2 μm, 45 mm, Millipore, Bayswater, Australia) attached to a peristaltic pump under low flow rate (50 RPM). For every 200 mL filtered, the flow was briefly reversed to wash plankton off the filter. The concentrated sample was homogenised, then 150 mL volumes were used to fill triplicate polycarbonate bottles (control and treatments) that were incubated in the presence PDMPO following the labeling protocol of Leblanc and Hutchins (2005). Briefly, cells were incubated for 24 h at ambient temperature and light in the presence of the dye (final concentration 0.125 μmol L^{-1}), along with a control sample that did not contain PDMPO (to quantify background fluorescence).

4.2.5.1 Cell-specific silicification

To accurately measure the degree of silicification in the pico- and nano-phytoplankton size fraction, PDMPO fluorescence was quantified by flow cytometry in order to calculate the relative contribution of these size classes to total new BSi deposition. Incubation volumes (1.5 mL) were preserved (1% glutaraldehyde v/v final concentration), flash frozen in liquid nitrogen and stored at – 80 °C for later analysis

(within 24 months). Post-voyage, samples were enumerated flow cytometrically (BD Influx, Becton Dickinson, Brussels, Belgium) by first identifying phytoplankton populations on biplots of phycoerythrin (580/30 nm) and Chl *a* (692/20 nm) fluorescence. Diatoms were then distinguished as PDMPO-positive cells where the mean relative fluorescence of incorporated PDMPO for each diatom population was quantified against the mean fluorescence of the fluorescent bead population (1 μm, ThermoFisher Scientific, Australia) at UV excitation of 355 nm and blue emission fluorescence at 469/29 nm. In order to make inference about relative differences in cell wall silicification and to make comparisons between cells of different cell volume, the relative fluorescence units (RFU) for each cell were then normalised to forward scatter (FSC, a proxy for cell size; Herzenberg et al. 1976).

In order to link community-level PDMPO incorporation to specific diatom taxa in the nano- and micro-phytoplankton size fractions, the remaining incubation volume (~20 mL) was filtered under low pressure (<10 mm Hg) onto black polycarbonate filters (0.2 μm, 25 mm; Millipore, Bayswater, Australia). The filters were then mounted on glass slides by placing them on a drop of immersion oil and sealing them under a glass cover slip. Prepared slides were then placed in the dark and stored at -20 °C for later analysis via fluorescence microscopy (within 24 months). Post-voyage, PDMPO-labeled cells frozen on filters and mounted on microscope slides were imaged using an upright fluorescence compound microscope (Eclipse N*i*; Nikon, Japan) fitted with a monochrome camera (DS-Qi2; Nikon, Japan). Images were acquired by excitation in the PDMPO channel using a long-pass DAPI filter (Nikon UV-2A filter cube, 330-380 nm excitation and 420 nm emission) and exported in Tagged Image File Format (TIFF). Microscope settings (e.g. objective, gain, exposure time) were kept consistent throughout image acquisition and were collected during a single microscope session to minimise changes in light source. More than 20 photos were captured from each filter at a magnification of 100×. The relative amount of newly deposited Si for each cell was quantified using Image-J software where the background fluorescence for each image was subtracted, positively stained cells were then digitally outlined and the integrated density then recorded (i.e., the product of the size of the region of interest and mean fluorescence). By normalising the fluorescence to the area of interest, differences in cell size between taxa were taken into consideration.

Cells were categorised either by genus or morphological group and PDMPO concentrations were calculated. The mean integrated brightness from each cell type was combined from either ambient (control) or N-enriched samples to determine whether N depletion played a role in the relative silicification of each taxon. To determine the contribution of each cell type towards new BSi production, cell abundance was multiplied by the average PDMPO fluorescence per cell. The number of cells used to calculate the average PDMPO fluorescence per cell is found in **Table 4.2**. Measurements from each site within the ATS and CS regions were combined to determine differences in relative contribution of each taxon to total community BSi production between oceanic provinces.

4.2.5.2 Diatom-community biogenic silicon standing stocks and rates of biogenic silicon production

In order to assess the total abundance of silicifiers and whole-community BSi production during incubations, BSi measurements and PDMPO incorporation (a proxy for BSi production; Leblanc and Hutchins 2005) were performed on PDMPO-stained samples from assay vessels. Sample volumes (130 mL) from assay vessels were filtered under low pressure (<10 mm Hg) onto a polycarbonate filter (0.6 μm, 47 mm; Millipore, Bayswater, Australia). Filters were then rinsed with 0.2 μm filtered seawater to remove any unbound PDMPO and stored at -20 °C until digestion and analysis (within 6 months). Post-voyage, silicifiers were first solubilised by digesting frustules via the hot alkaline digestion method, by adding 4 mL of 0.2 M NaOH to a 15 mL falcon tube that contained the sample filter. Sample tubes were then sealed, wrapped in aluminum foil and immersed in a water bath set to 90 °C for 60 min. Samples were then cooled in an ice bath and neutralised with 1 mL 1 M HCl. The filter in each sample tube was compressed into the tip of the falcon tube with a metal rod and then centrifuged at 2500 RCF for 10 min to clear the digest of cellular debris.

Digest volumes were first analysed for PDMPO incorporation by withdrawing volumes (3 mL) of the supernatant and filtered (0.2 μm membrane; Millipore, Bayswater, Australia) directly into a quartz cuvette where subsequent analysis of PDMPO incorporation was carried out using a scanning UV spectrofluorometer (50 Bio; Cary, Agilent Technologies, USA) equipped with a xenon lamp and set to excite at 375 nm (5

nm slit width). Samples were scanned (600 nm min^{-1}) from 400 to 750 nm (5 nm slit width), with emission values read at 530 nm and compared against a standard curve (R^2 =0.999) made with a 125 μmol L^{-1} PDMPO solution prepared in NaOH-HCl matrix. Paired seawater blanks were processed in the same way in order to correct for background fluorescence. Sample volumes were retained for further processing for BSi analysis.

PDMPO is incorporated in relatively consistent proportions to BSi (mol:mol) in both cultures and in mixed diatom populations (Leblanc and Hutchins 2005), and as a result can be used as a proxy for the amount of new BSi deposited over time in natural phytoplankton communities (Leblanc and Hutchins 2005). To convert quantitative PDMPO incorporation to BSi production, we used the recommended ratio of 2916 mol BSi per mol PDMPO on samples collected from sites where silicic acid concentrations were above 3 μmol L^{-1} and for sites ≤3 μmol L^{-1} silicic acid, the linear relationship: BSi: PDMPO = 912.6 × $[Si(OH)_4]$ as per McNair et al. (2015).

Digest volumes were first analysed for PDMPO incorporation (described above) and then transferred directly to a clean falcon tube for analysis of reactive silicate following methodology of Strickland and Parsons (1968) with modifications according to Nelson et al. (1989) to increase sensitivity. Briefly, each sample (3 mL) was added to a falcon tube containing 4 mL of acidified molybdate solution and allowed to react for 15 min. A 6 mL volume of metol/sulphite reducing reagent was then rapidly added, mixed, and allowed to react for 3 h to complete reduction of the silicomolybdate complex. Absorbance was then measured at 810 nm using a spectrophotometer (Cary Eclipse, Agilent Technologies, United States of America) and compared against a standard curve (R^2 =0.999) made with a 20 μmol L^{-1} silicate stock solution (Na_2SiF_6).

4.2.6 Data analysis

The effect of nitrate addition on standing stocks of BSi, rates of BSi production, and taxon specific abundance and silicification, was examined using a Student's T-test (for paired samples) on pooled samples from each region (ATS and CS examined individually). Tests were performed using Origin Pro software (version b9.2.272; OriginLab Corporation, United States of America) and the assumption of equal or unequal variances were both trialed. Differences were accepted as significant at *p*

<0.05. Similarly, to examine differences between concentrations of particulate matter (POC, PON and BSi) and ratios between these (Si:C, Si:N and C:N), Student's T-tests were performed as outlined above.

To investigate whether the diatom taxa/morphological-type contributing towards whole community BSi production (i.e., the product of species-specific cell abundance and average fluorescence per cell) was significantly different between ocean depth ('surface' and 'Cmax'), region (ATS and CS), and addition of nitrate ('ambient' and 'N-enriched'), we treated each factor separately and used a one-way analysis of similarity (ANOSIM) using Permutational multivariate analysis (PERMANOVA) in Primer (Primer-E, Plymouth, United Kingdom). Ordination by non-metric principal component analysis (PCA) was used to visualise patterns in physicochemical ocean characteristics using standardised environmental data.

We used a Distance-based Linear Modeling (DistLM) procedure in PRIMER to explore the strength of the relationships between taxon-specific BSi contribution and environmental factors that were expected to influence silicification (PAR, temperature, salinity, and total dissolved nutrients; NO_3^-, NH_3^+, PO_4^{3-} and SiO_4^{4-}). Taxon-specific BSi production was log(X+1) transformed and a dissimilarity matrix was calculated using Bray-Curtis distances. Standardised environmental variables were examined for redundancy using a draftsman scatter plot and the correlation matrix to ascertain whether there are variables that were highly correlated with one another. We used the BEST and AIC selection criteria (corrected for small sample size; AICc) in the DistLM. In order to identify the morphological types responsible for community BSi production and their relative contribution, the PRIMER routine "SIMPER" was used. All multivariate tests were performed with unrestricted permutations (999) in the software package PRIMER Version 6.1.12 (Clarke and Gorley 2006).

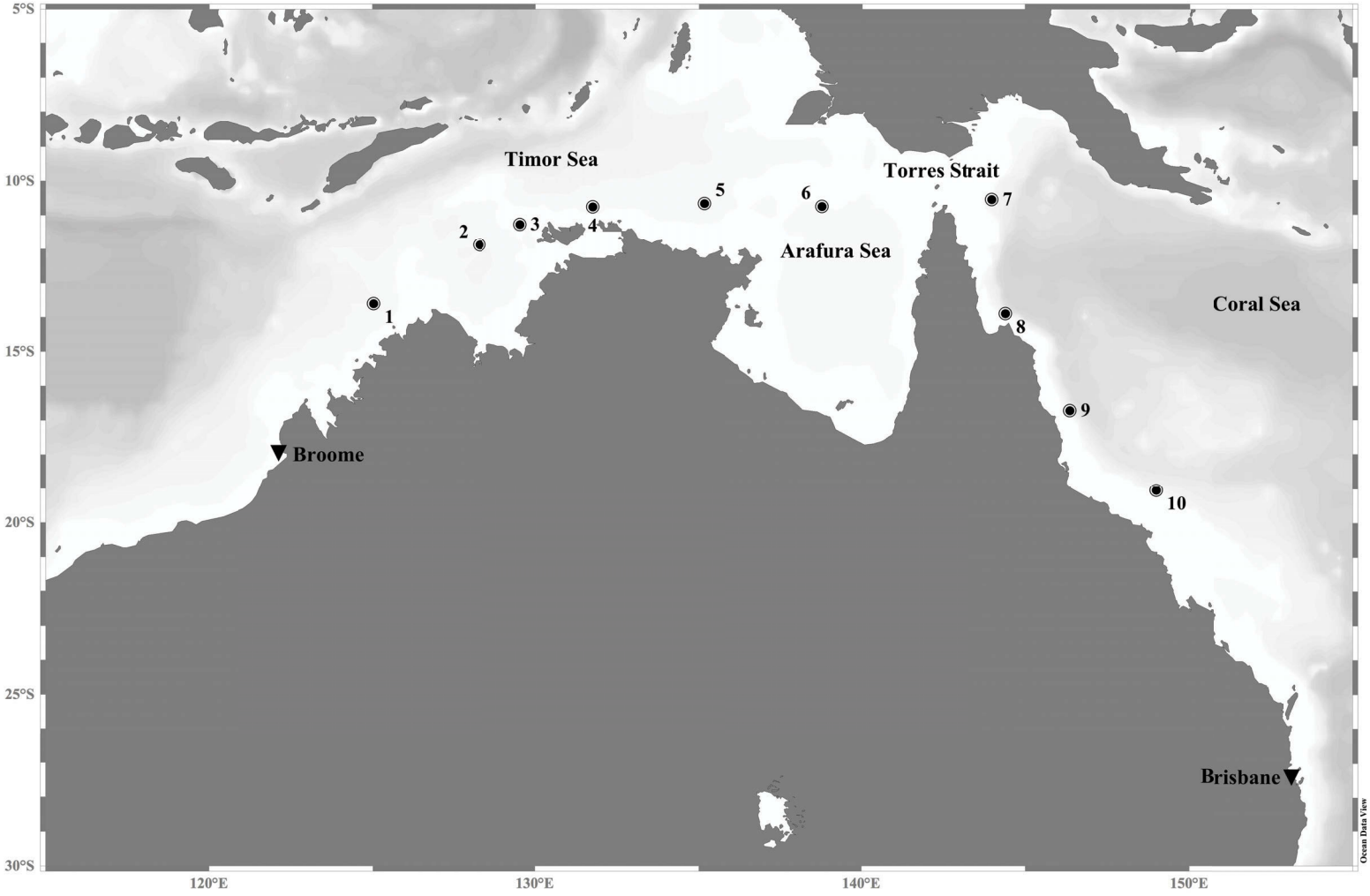

Figure 4.1 Stations (closed circles; numbered 1-10) sampled during a 5000 km transect from Broome to Brisbane aboard the RV *Southern Surveyor* during the Austral winter (July-August; SS2013_t03), including locations referred to in text.

4.3 Results

4.3.1 Physicochemical characterisation of Arafura Timor Shelf and Coral Sea

The physicochemical conditions within the ATS and CS were distinct from one another. Waters from the ATS were warmer, less saline and had higher dissolved nutrients than those from the CS (**Table 4.1**), with conditions in both regions typically within reported ranges for winter in these regions (Condie and Dunn 2006). Average SST in the ATS were 26.6±0.5 °C, compared to 24.5±0.8 °C in CS waters. Dissolved surface ocean concentrations of SiO_4^{4-}, NO_3^- and PO_4^{3-} were approximately 3 to 4 times greater in the ATS than the CS (**Table 4.1**).

The vertical Chl *a* fluorescence depth profiles from stations sampled within the ATS showed relatively uniform fluorescence over depth (**Supplementary Figure 4.1**), indicating a well-mixed water column. As a result, seawater for experimental assays was collected from surface (5 m) waters only. In contrast, within the deeper waters of the CS, Cmax were evident at most stations, whereby the Cmax coincided with higher dissolved SiO_4^{4-} concentrations and lower NO_3^- concentrations than surface waters (**Supplementary Figure 4.1**). A notable exception was Station 10 (CS), where a Chl *a* fluorescence peak was not evident and dissolved SiO_4^{4-} and NO_3^- concentrations were similar between the surface and Cmax.

Table 4.1 Average inorganic silicate (SiO_4^{4-}), nitrate (NO_3^-), and phosphate (PO_4^{3-}) concentrations including elemental ratios for each station sampled in the Arafura-Timor Shelf and Coral Sea. At all stations, seawater samples were taken from surface waters (5 m) and, when discernable the sub-surface chlorophyll maximum (Cmax) as indicated by asterisks. The error term is the standard deviation. Hyphens indicate nutrient concentrations below instrumental detection limit (< 0.02 µmol L^{-1}).

Station number	Co-ordinates	Sample depth (m)	SiO_4^{4-} (µmol L^{-1})	NO_3^- (µmol L^{-1})	PO_4^{3-} (µmol L^{-1})	Si:N (mol:mol)	Si:P (mol:mol)
1	13.6° S, 125.0° E	5	2.96	0.26	0.11	11.38	26.91
2	11.9° S, 128.3° E	5	4.46	0.6	0.23	7.43	19.39
3	11.3° S, 129.5° E	5	5.16	0.1	0.24	51.6	21.5
4	10.8° S, 131.8° E	5	5.7	0.37	0.24	15.4	23.75
5	10.7° S, 135.2° E	5	5.2	-	0.22	260	26.34
6	10.7° S, 138.8° E	5	1.83	-	0.26	183	7.04
Arafura-Timor Shelf average			4.22 ± 1.51	0.22 ± 0.22	0.22 ± 0.05	72 ± 97	20 ± 7
7	10.5° S, 144.0° E	5	0.9	-	0.03	45	30
7	10.5° S, 144.0° E	35 *	1.08	0.12	0.05	9	21.6
8	13.9° S, 144.4° E	5	1.4	-	0.06	70	23.33
8	13.9° S, 144.4° E	80 *	1.6	0.15	0.07	10.66	22.85
9	16.7° S, 146.4° E	5	1.16	-	0.07	58	16.57
9	16.7° S, 146.4° E	70 *	1.57	0.14	0.1	11.24	15.7
10	19.1° S, 149.0° E	5	0.96	0.03	0.09	32	10.66
10	19.1° S, 149.0° E	30	0.95	0.03	0.09	15.8	10.55
Coral Sea average			1.27 ± 0.29	0.07 ± 0.06	0.08 ± 0.02	32 ± 25	16 ± 5

Table 4.2 Average particulate organic carbon (POC), particulate organic nitrogen (PON), and biogenic silica (BSi) of each station sampled in the Arafura-Timor Shelf and Coral Sea. At all stations, seawater samples were taken from surface waters (5 m) and, when discernable the sub-surface chlorophyll maximum (Cmax) as indicated by asterisks. Error term is the standard deviation where applicable.

Station number	Co-ordinates	Sample depth (m)	POC ($\mu mol\ L^{-1}$)	PON ($\mu mol\ L^{-1}$)	BSi ($\mu mol\ L^{-1}$)
1	13.6° S, 125.0° E	5	6.11 ± 0.80	0.58 ± 0.10	2.07 ± 0.69
2	11.9° S, 128.3° E	5	6.20 ± 0.60	0.63 ± 0.28	1.55 ± 0.22
3	11.3° S, 129.5° E	5	-	-	14.60 ± 7.69
4	10.8° S, 131.8° E	5	9.10	0.93	2.98 ± 1.20
5	10.7° S, 135.2° E	5	5.75 ± 0.38	0.63 ± 0.01	1.91± 1.64
6	10.7° S, 138.8° E	5	6.18 ± 0.12	0.71 ± 0.03	7.02 ± 2.35
Arafura-Timor Shelf average			5.96 ± 0.28	0.70 ± 0.14	5.02 ± 5.11
7	10.5° S, 144.0° E	5	4.73 ± 1.12	0.53 ± 0.14	3.63 ± 0.62
7	10.5° S, 144.0° E	35 *	3.64 ± 0.46	0.42 ± 0.00	0.75 ± 0.42
8	13.9° S, 144.4° E	5	3.01± 0.09	0.32 ± 0.28	0.82 ± 0.21
8	13.9° S, 144.4° E	80 *	3.69 ± 1.36	0.30 ± 0.03	0.09 ± 0.16
9	16.7° S, 146.4° E	5	2.46 ± 0.18	0.24 ± 0.00	0.16 ± 0.14
9	16.7° S, 146.4° E	70 *	3.22 ± 0.28	0.31 ± 0.28	0.32 ± 0.16
10	19.1° S, 149.0° E	5	3.46 ± 0.56	0.39 ± 0.53	0.94 ± 0.11
10	19.1° S, 149.0° E	30	3.81 ± 0.02	0.37 ± 0.00	1.15 ± 0.46
Coral Sea average			3.27 ± 0.49	0.32 ± 0.05	0.58 ± 0.45

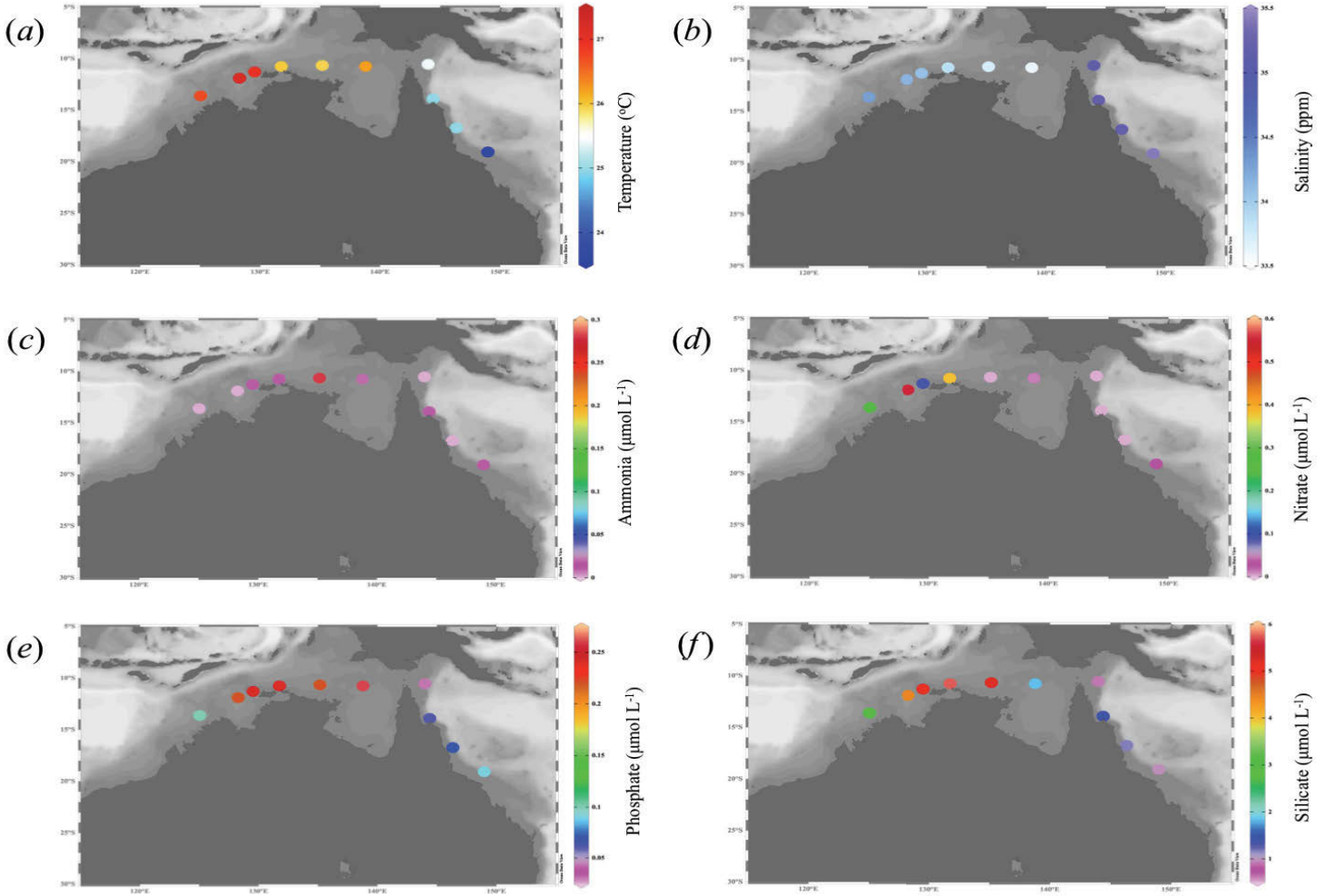

Figure 4.2 Physicochemical characteristics of surface water sampled within the Arafura and Timor shelf regions (ATS) and Coral Sea (CS) oceanographic regions (RV *Southern Surveyor*; July-August; SS2013_t03); (a) temperature, (b) salinity, (c) ammonium, (d) nitrate, (e) phosphate, and (f) silicate.

4.3.2 Biological characterisation of Arafura Timor Shelf and Coral Sea

Pigment analysis revealed that the phytoplankton community sampled from surface waters within the ATS were dominated by microphytoplankton, whereas those sampled from the CS were mainly composed of pico- and nano-phytoplankton (**Figure 4.3a**). A noteworthy exception was Station 7 (CS), where, based on pigment analysis, the phytoplankton composition was more similar to the ATS than other CS stations. At Stations 7, 8 and 9 in the CS where a Cmax was discernable, the phytoplankton composition was similar (Student's t-test; p >0.05*)* in the Cmax to surface waters (**Figure 4.3b**).

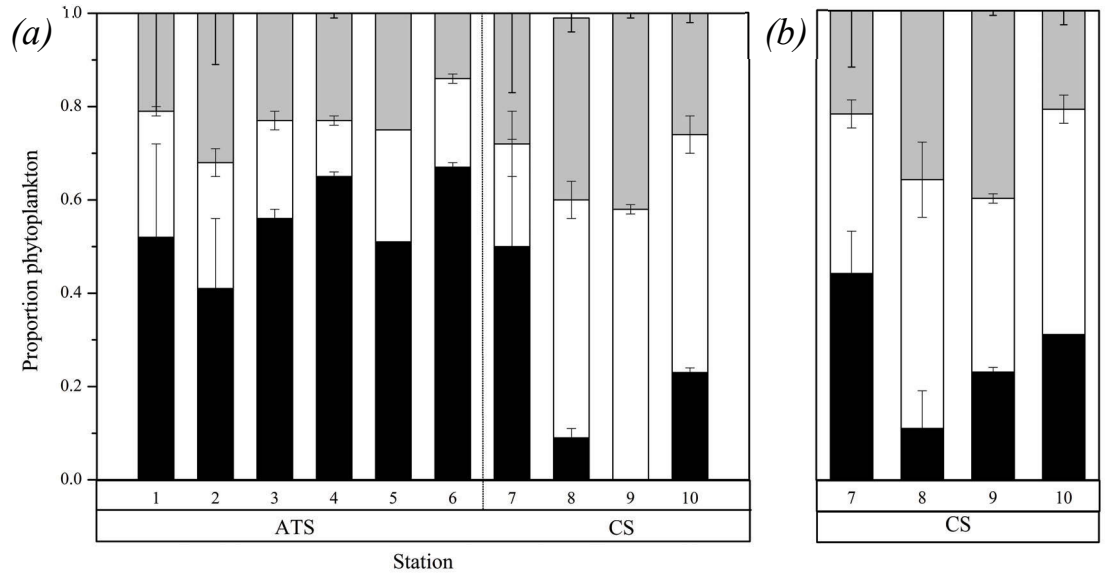

Figure 4.3 Distribution of phytoplankton in three size classes from sampled from (a) surface, and (b) subsurface chlorophyll maximum (Cmax) from the Arafura-Timor Shelf (ATS) and Coral Sea (CS) estimated from pigments algorithms as in Vidussi et al. (2001), Hooker et al. (2005) and Uitz et al. (2008); picophytoplankton <2 µm (grey bars), nanophytoplankton >2 µm and <20 µm (white bars), and microphytoplankton >20 µm (black bars). Station numbers reflect those in **Figure 4.1** and the dashed line represents the transition from the ATS to the CS.

Consistent with a dominance of microphytoplankton (**Figure 4.3**), the concentrations of POC and PON, as well as BSi were greater in the ATS compared to CS region (Student's t-test; p <0.001). Within the ATS, highest concentrations of particulate organic matter were found from surface waters at Stations 2, 3 and 4, with average values of 6.20±0.60 µmol POC L^{-1}, 0.93 µmol PON L^{-1} and 14.60±7.69 µmol BSi L^{-1}, respectively (**Table 4.2**). In contrast, the average POC, PON and BSi concentrations in surface waters of the CS were lower with values of 3.27±0.49 µmol POC L^{-1}, 0.32±0.05

μmol PON L^{-1}, and 0.58±0.4 μmol BSi L^{-1}, respectively. An exception to these trends of lower POC, PON and BSi in the CS occurred at Station 7, where POC and PON concentrations were comparable to the relatively higher values observed in the ATS (**Table 4.2**). Lowest values of organic matter in the CS were observed at Station 9, with values corresponding to 2.46±0.18 μmol POC L^{-1}, 0.24±0.00 μmol PON L^{-1}, and 0.16±0.14 μmol BSi L^{-1} that coincided with the greatest subsurface chlorophyll peak, indicating the majority of biomass was found at the Cmax (**Supplementary Figure 4.1**). Elemental ratios of Si:N and Si:C reflected patterns in absolute concentrations of BSi, with higher Si:C values (Student's t-test; p <0.05) observed in the ATS compared to the CS (**Figure 4.4**). However, the average C:N molar ratio of stations from the ATS were lower (C:N = 8.8) than those from the CS (C:N = 9.9), and were more variable between stations (**Figure 4.4a**). Overall, greater concentrations and lower values of C:N suggest greater pools of fresher organic matter in the ATS.

4.3.3 Nitrate addition assays

In both ocean provinces, samples enriched with NO_3^- showed no change in the standing stocks of BSi after 24 h (Student's t-test; p >0.05; data not shown) or BSi production (Student's t-test; p >0.05; **Figure 4.5**) compared to those that were unamended. These results indicated that NO_3^- addition did not have any affect on diatom growth (BSi stocks) or the amount of BSi produced by diatoms at the community-level.

Similar to findings at the community-level, NO_3^- did not influence diatom abundance or degree of diatom frustule silicification for small cells (i.e., <20 μm, pico and nano-sized PDMPO-positive cells) detected via flow cytometry or larger diatoms (i.e., >20 μm, micro-sized PDMPO-positive cells) detected by fluorescence microscopy (Student's t-test; p >0.05; data not shown). Indicating there were the same number of cells contributing to community BSi production and the relative PDMPO fluorescence between ambient or NO_3^- amended seawater samples was similar. As a result, ambient and N-enriched samples for BSi stocks, production and cell-specific silicification were pooled from the ATS and CS before examining differences between ocean provinces.

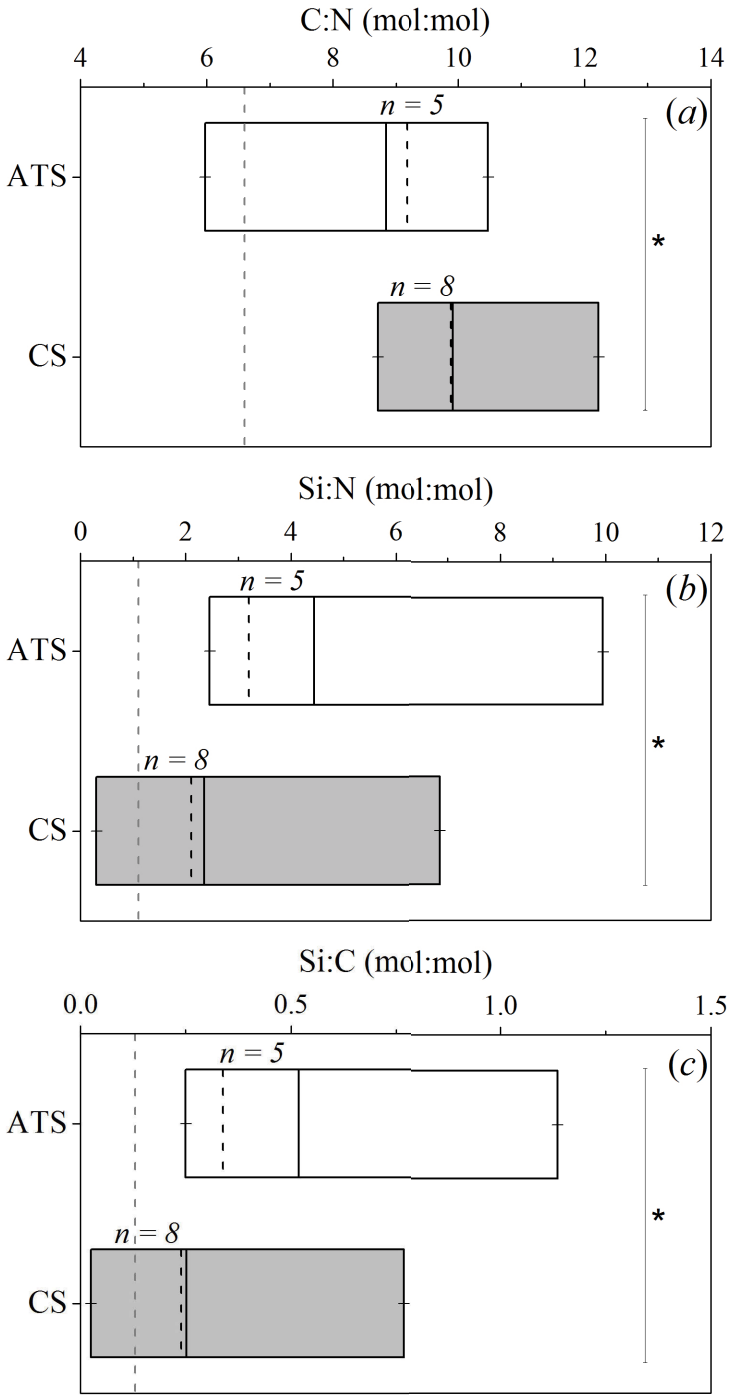

Figure 4.4 Boxplots of the (a) C:N, (b) Si:N, and (c) Si:C molar ratios of particulate organic matter sampled from stations sampled from the Arafura-Timor Shelf (ATS; open boxes) and Coral Sea (CS; grey boxes). The length of the box corresponds to the distance between the 5th and 95th percentiles. The solid line and dashed line inside the box represent the mean and median, respectively. The whiskers extend to the minimum and maximum values of the cluster and "*n*" is the number of values in each cluster. The grey dashed lines represent the typical values of C:N (6.6) reported by Redfield et al. (1963) and typical values of Si:N (1.1) and Si:C (0.13) for nutrient replete diatoms reported by Brzezinski (1985). Asterisks indicate statistically significant differences (p <0.05) of the mean between clusters using Student's t test.

4.3.4 Biogenic silicon production differs between Arafura Timor Shelf and Coral Sea

The study area was characterised by a heterogeneous distribution of BSi production in surface waters (5 m) and at depth (Cmax), differing over two orders of magnitude across the entire dataset (note log axis; **Figure 4.5a**). These results were consistent with highly variable concentrations of BSi within and between ocean provinces (**Table 4.2**). The highest rates of BSi production were found at Station 3 (ATS) with ~5.7±2.3 µmol BSi L^{-1} d^{-1}. In contrast, minimum rates were observed at Station 10 (CS) with values of ~0.1±0.04 µmol BSi L^{-1} d^{-1} and the majority of sampled sites within the CS being below instrument detection limit.

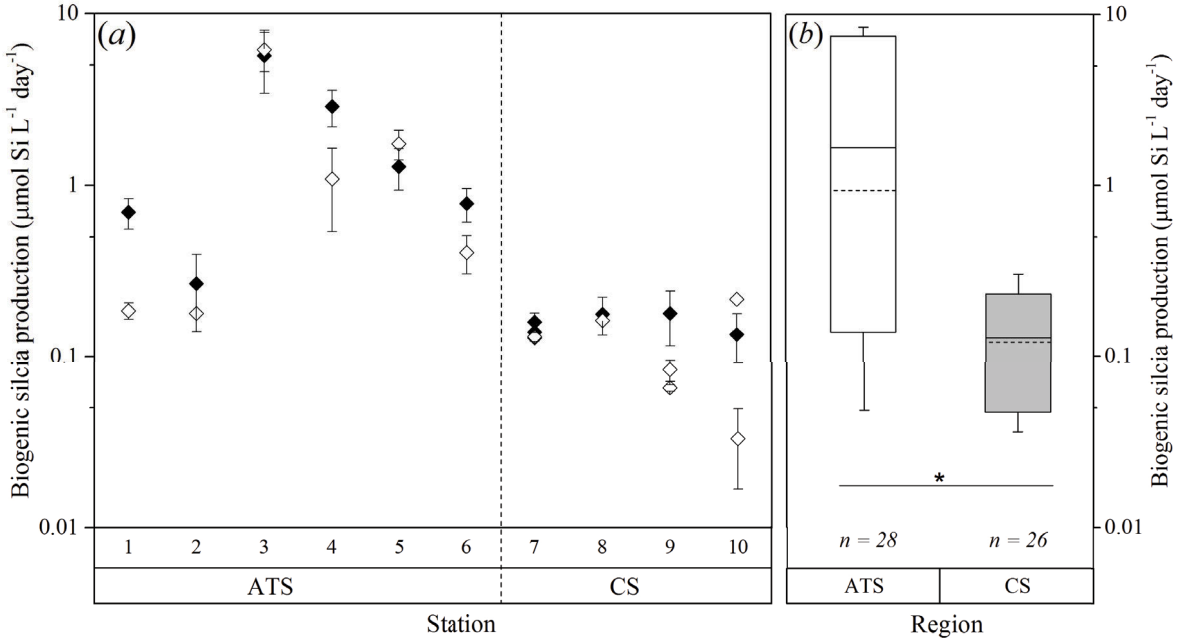

Figure 4.5 (a) Biogenic silica production (BSi; µmol Si L^{-1} d^{-1}) by diatoms at stations sampled within the Arafura and Timor shelf regions (ATS) and Coral Sea (CS), where closed symbols represent unamended seawater control and open symbols represent seawater supplemented with additional nitrate (NO_3^-; 10 µmol L^{-1}) for samples collected from surface waters (5 m) and, when discernable, the sub-surface chlorophyll maximum (Cmax; determined by the down-cast Chl *a* fluorescence profile). The error term is the standard error. Station numbers reflect those in **Figure 4.1** and the dashed line represents the transition from the ATS to the CS. (b) BSi production (µmol Si L^{-1} d^{-1}) by diatoms at stations sampled within the ATS and CS. The length of the box corresponds to the distance between the 5th and 95th percentiles. The solid line and dashed line inside the box represent the mean and median, respectively. The whiskers extend to the minimum and maximum values of the cluster and "*n*" is the number of values in each cluster. Asterisks indicate statistically significant differences (p <0.05) between clusters using Student's t test.

4.3.5 Morphotype-specific differences in silicification between Arafura Timor Shelf and Coral Sea

Silicification of small phytoplankton (i.e., <20 µm, pico and nano-sized cells quantified by flow cytometry), indicated that the relative number of cells contributing to total BSi production was similar between provinces, as there was no significant difference in the abundance of fluorescent cells (Student's t-test; p >0.05) between the ATS and the CS (**Figure 4.6**). However, ocean province did have an affect on the relative degree of frustule silicification as diatoms <20 µm from the ATS displayed greater mean PDMPO fluorescence per relative cell size (RFUs FSC^{-1}) in comparison to the CS (22±0.98 versus 15±0.85 RFUs FSC^{-1}) (Student's t-test; p <0.001; **Figure 4.6**).

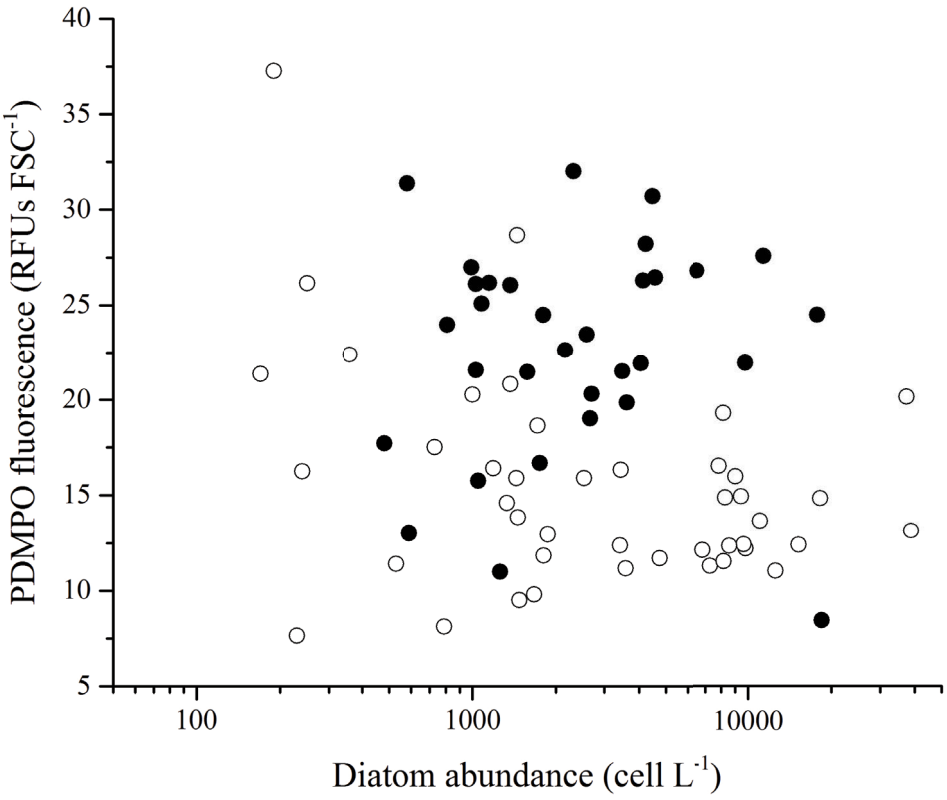

Figure 4.6 Relative fluorescence as a function of diatom abundance (<20 µm sized cells) for positively PDMPO-stained cells quantified by flow cytometry sampled from the Arafura-Timor Shelf (ATS; closed symbols) and Coral Sea (CS; open symbols). Relative fluorescence units (RFUs) were normalised to relative cell size (forward scatter; FSC) in order to determine relative differences in frustule silicification. Note the y-axis is log scale.

Table 4.3 Mean cellular dimensions and relative abundance (%) of diatom morphological types from the Arafura-Timor shelf and Coral Sea regions.

Cell type description	Code	N	Relative abundance %	Length µm	Width µm	Area µm^2	Chain Length	
							Average	Maximum
				Arafura-Timor Shelf				
Small centric	c1	119 (119)	25.98	6.9 ± 0.14	5.93 ± 0.16	32.8 ± 1.44	1.01 ± 0.01	2
Large centric	c2	64 (64)	13.97	23.4 ± 5.57	15.8 ± 1.56	355 ± 93.8	1.03 ± 0.02	2
Chaetoceros sp.	c3	45 (106)	9.83	35.89 ± 5.11	11.45 ± 1.47	287 ± 57.1	3.57 ± 0.38	26
Small pennate	p1	90 (90)	19.65	9.25 ± 0.32	3.40 ± 0.21	23.4 ± 2.11	1.01 ± 0.01	2
Large pennate	p2	123 (123)	26.86	51.86 ± 3.57	6.77 ± 0.90	135 ± 12.4	1.19 ± 0.05	4
Pseudo-nitzschia sp.	p3	1 (6)	0.22	118.2	3.64	116.00	3.67 ± 1.05	8
Thalassionema sp.	p4	12 (61)	2.62	49.2 ± 10.3	14.5 ± 3.72	275 ± 90.8	5.23 ± 0.82	30
Total cells mL^{-1}	270 ± 323							
				Coral Sea				
Small centric	c1	41 (41)	25.2	4.85 ± 0.32	3.95 ± 2.59	16.4 ± 2.12	1.02 ± 0.02	2
Large centric	c2	2 (2)	1.2	25.8 ± 13.5	23.0 ± 15.1	619 ± 546	1.5 ± 0.50	2
Chaetoceros sp.	c3	14 (175)	8.6	2051 ± 1489	18.0 ± 7.15	55.9 ± 14.9	6.57 ± 0.36	22
Small pennate	p1	51 (51)	31.3	8.22 ± 0.47	2.91 ± 90.15	17.7 ± 1.49	1.00 ± 0.00	1
Large pennate	p2	53 (53)	32.5	185 ± 100	7.30 ± 2.21	98.6 ± 27	1.23 ± 0.09	5
Pseudo-nitzschia sp.	p3	0 (8)	0.0	0	0	0	2.75 ± 0.41	5
Thalassionema sp.	p4	2 (10)	1.23	60.0 ± 5.36	36.4 ± 19.4	368 ± 219	2.10 ± 0.28	4
Total cells mL^{-1}	160 ± 94							

Cell type descriptions are provisional taxonomic designations (in italics) or morphological descriptions. ID beginning with the letter "c" are centric diatoms while those beginning with the letter “p” are pennates, and reflect morphotypes in **Figure 4.6**. Averages include cells collected from ambient and nitrogen-enriched conditions in the ATS and CS. N is the number of cells used to calculate means, with values in parentheses being the number used for chain length calculation.

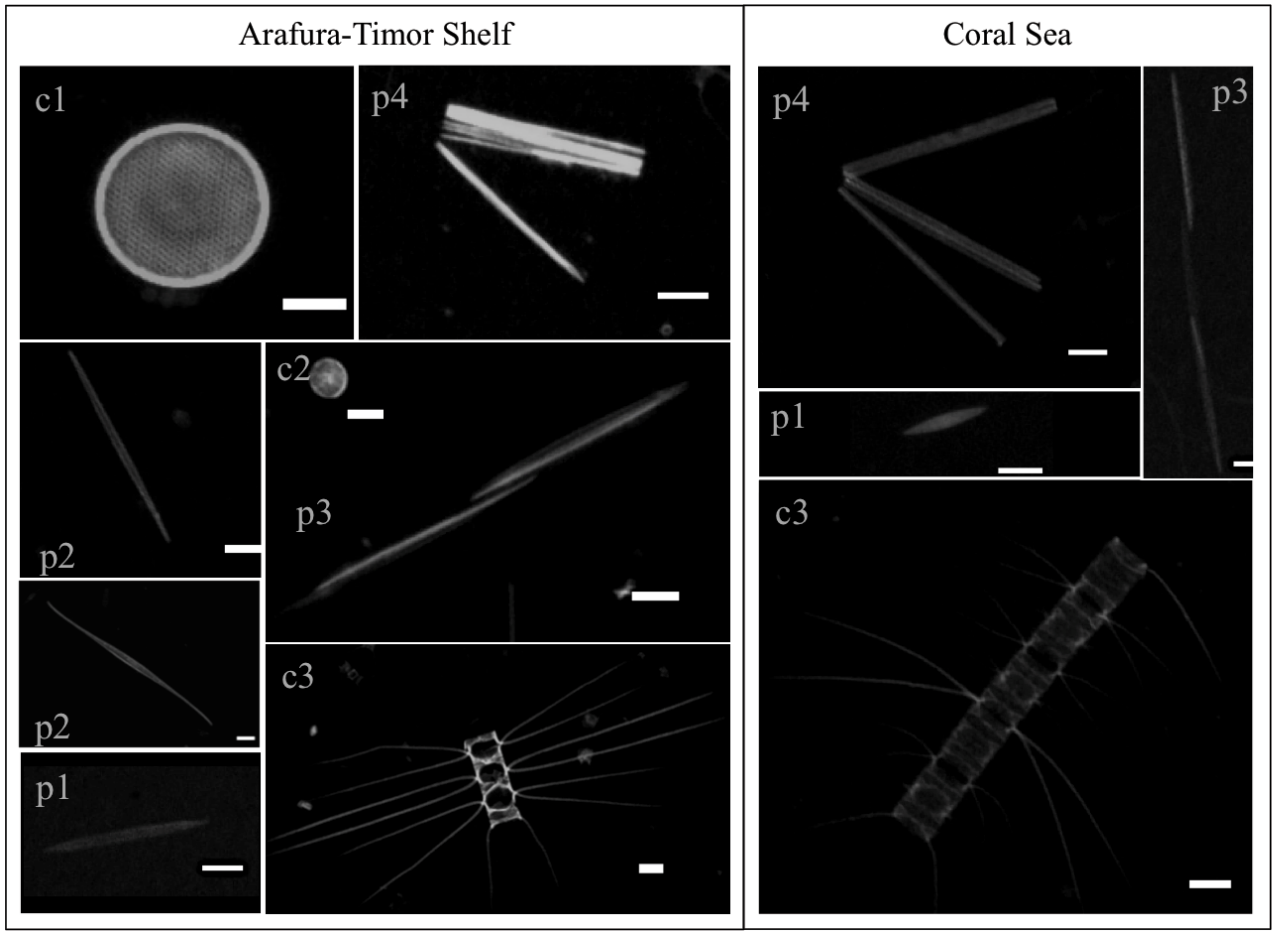

Figure 4.7 Illustrative images of new silicon (BSi) deposition by diatoms incubated with PDMPO for 24 h from stations sampled from the ATS (left) and CS (right) mounted on glass slides and observed under fluorescence microscopy. A DAPI long pass filter was used to visualise PDMPO-stained cells over the entire emission spectrum. Exposure time remained constant for all photos so that pixel intensity is indicative of relative differences in the amount of newly incorporated PDMPO. The scale bar (10 microns) and image brightness is the same for all images to emphasise differences in size and degree of frustule silicification between ocean region and taxa.

In the microphytoplankton size fraction (>20 μm; detected using fluorescence microscopy), diatoms labeled with PDMPO were represented by 7 morphological types consisting of the genera *Chaetoceros* (c3), *Pseudo-nitzschia* (p3), *Thalassionema* (p4) and unidentified large and small centric (c1, c2) and pennate forms (p2, p1) (**Table 4.3; Figure 4.7**). Unlike absolute abundance of Si depositing cells, changes in the degree of silicification were observed at the cellular level, with the relative amount of newly deposited silica per cell for diatoms in Northern Australia varying across two orders of magnitude (**Figure 4.8**). The highest PDMPO fluorescence per cell was found in large centric diatoms (311 140 RFUs $cell^{-1}$) indicating the greatest amount of newly deposited BSi over the 24 h incubation. These highly silicified morphotypes were absent in the CS. At the other end of the spectrum, small, unidentified centric and pennate diatoms were the most weakly silicified taxa, with the lowest PDMPO fluorescence per cell (8 000 and 11 302 RFUs $cell^{-1}$, respectively).

Similar to observations in the pico- and nano- size fractions, differences in the degree of silicification were observed between ocean provinces, whereby diatoms from the ATS appeared to deposit more silica than the CS (**Figure 4.8**). High levels of phenotypic (i.e., within morphotypes) variation meant these differences were significant (Student's t-test) for some morphotypes, namely, *Chaetoceros* spp. (c3; $p < 0.001$), small centric diatoms (c2; $p < 0.001$) and *Pseudo-nitzschia* spp. (p3; $p = 0.03$) which were two, three and four times more silicified in the ATS compared to the CS.

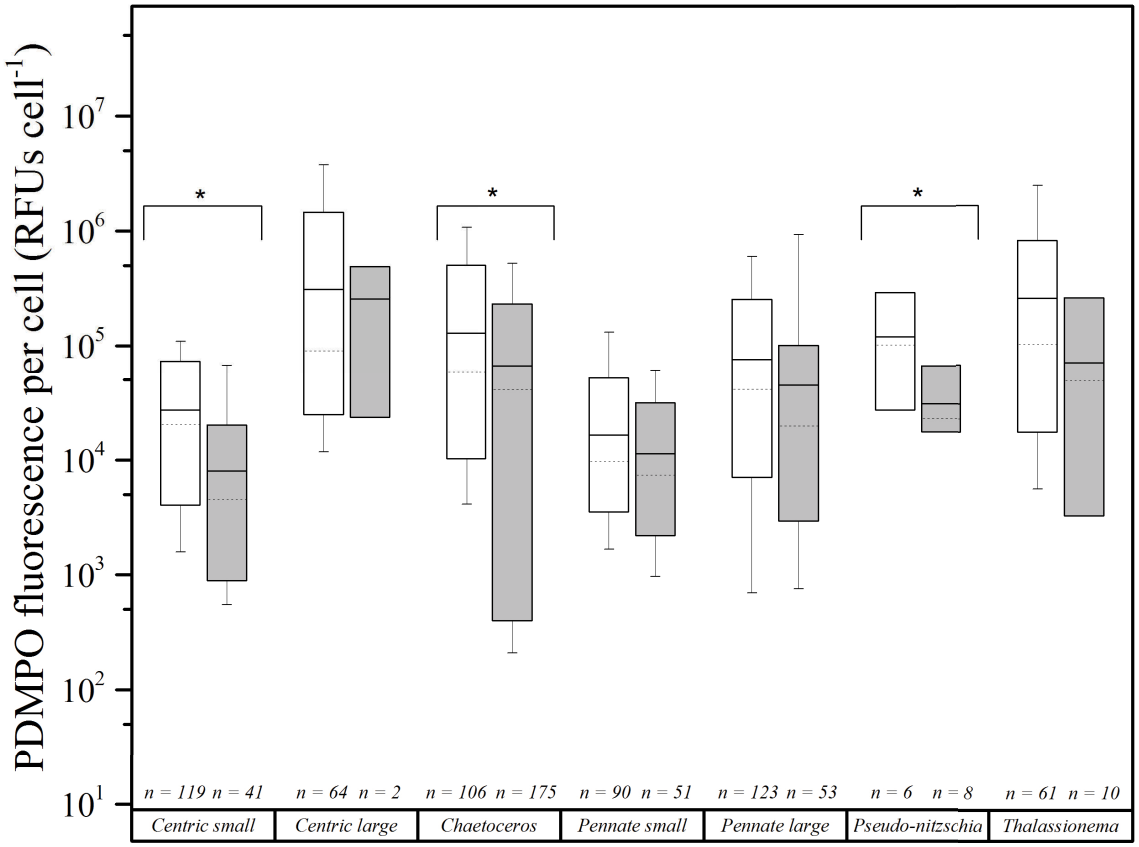

Figure 4.8 Boxplot of integrated fluorescence of individual cells incubated with PDMPO for 24 h from stations sampled from the Arafura Timor Shelf (ATS; open boxes) and Coral Sea (CS; grey boxes) and quantified with fluorescent microscopy. Note that y-axis is a log scale. The length of the box corresponds to the distance between the 5th and 95th percentiles. The solid line and dashed line inside the box represent the mean and median, respectively. The whiskers extend to the minimum and maximum values of the cluster and "*n*" is the number of values in each cluster. Asterisks indicate statistically significant differences (p <0.05) between clusters using Student's t test.

4.3.6 Patterns in morphotype-specific silicification

While there was no significant difference in absolute cell abundance between the oceanic provinces (Student's t-test; p =0.6), differences in diatom-community composition were evident, with changes observed in the underlying relative abundances of specific morphotypes. For example, large centric diatoms were more abundant in the ATS compared to CS, whilst small and large pennate diatoms dominated the CS (Student's t-test; p <0.05; **Table 4.3**). The relative abundance of *Chaetoceros* spp. and *Thalassionema* spp were consistent between provinces, but appeared to differ in their maximum chain-lengths, with the ATS supporting longer chains of these taxa (**Table 4.3**).

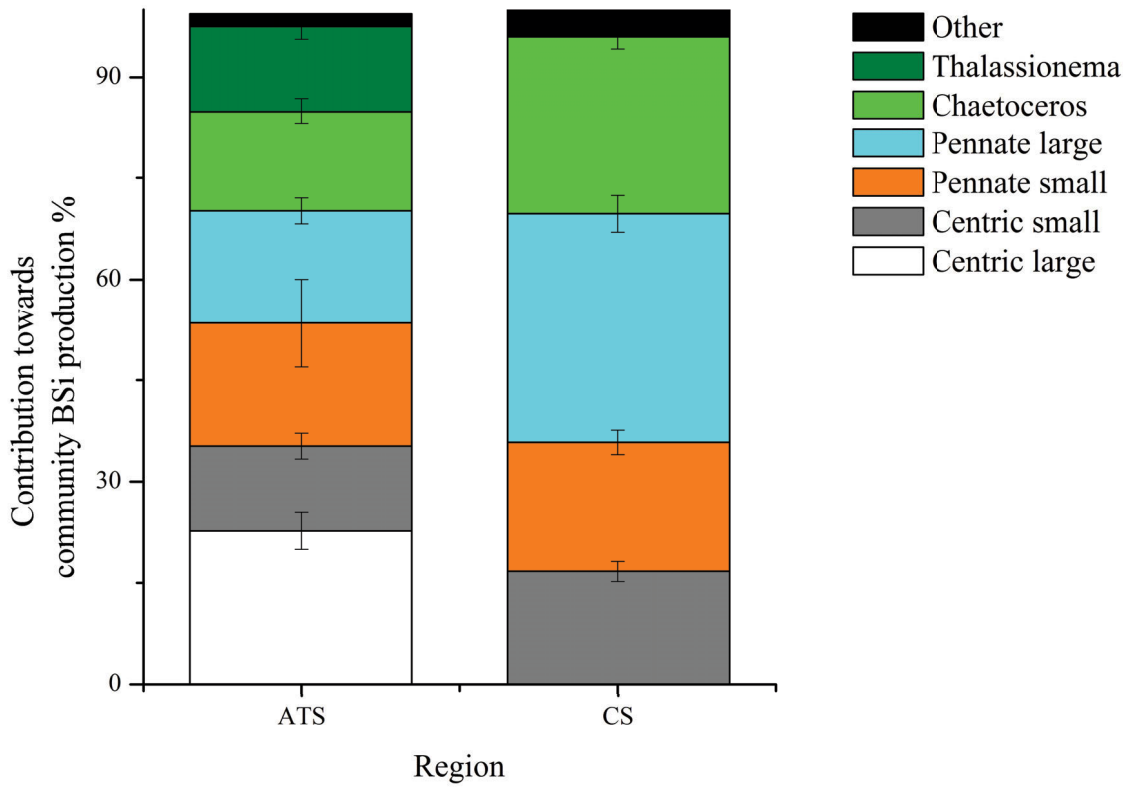

Figure 4.9 The average contribution of each morphological type towards biogenic silica (BSi) production by diatoms sampled from the Arafura Timor Shelf (ATS) and the Coral Sea (CS). The stacked bar graph represents output from similarity percentages (SIMPER) analysis which identified six morphological types that explained >98% of community BSi production (derived from multiplying cell abundance by the average integrated PDMPO fluorescence per cell). The remaining morphological types (e.g. *Pseudo-nitzchia*) contributed <2% and were grouped into 'Other' morphological types. The error terms are standard deviation.

Together, province-specific variations in relative silicification and abundance at the cellular-level underpinned processes occurring at the community-level. Our results reveal that different diatom morphotypes (and their associated characteristics of frustule silicification and abundance) contributed to the divergence in BSi production between the ATS and the CS (ANOSIM, Global R: 0.25, p =0.008). Using SIMPER analysis, we were able to identify that the relative contribution of each morphological type to overall BSi production differed between the ATS and CS (**Figure 4.9**). In the ATS, community BSi production was spread relatively equally across six of the seven morphological types including large centric diatoms (23 ± 3%), small pennates (18 ± 6%), large pennates (17 ± 2%), *Chaetoceros* spp. (15 ± 2%), *Thalassionema* spp. (13 ± 2%), and small centrics (13 ± 2%). In contrast, over half of new BSi production in diatom

communities from the CS was generated solely by large pennates and *Chaetoceros* spp, with weakly silicified small centric and small pennate diatoms (**Figure 4.7**) responsible for the remainder of community production.

The contribution of diatom morphotypes towards community BSi production was not influenced by the addition of NO_3^- (ANOSIM, Global R: 0, p >0.05), but was instead governed by the prevailing physicochemical properties of each ocean province. Differences in community BSi production between the ATS and CS were driven by a combination of environmental factors (**Figure 4.10**). When considered individually, temperature (DistLM marginal tests, p =0.02; 14%), salinity (DistLM marginal tests, p =0.01; 19%), PO_4^{3-} (DistLM marginal tests, p =0.02; 14%), and SiO_4^{4-} (DistLM marginal tests, p =0.01; 18%) were identified as significant explanatory variables. Other environmental factors such as PAR, dissolved NH_3^+ and NO_3^- concentrations were observed to have little effect on trends in community BSi production (p >0.05). When environmental factors were considered collectively using sequential tests to build a multivariate model, BEST analysis revealed salinity and dissolved SiO_4^{4-} concentrations (R^2 =0.29) as the two primary variables explaining differences in community BSi production between the ATS and CS. These results appear to reflect the inherent differences between the two ocean provinces whereby the ATS is less saline and more silicate-rich in comparison to the CS (**Figure 4.2**).

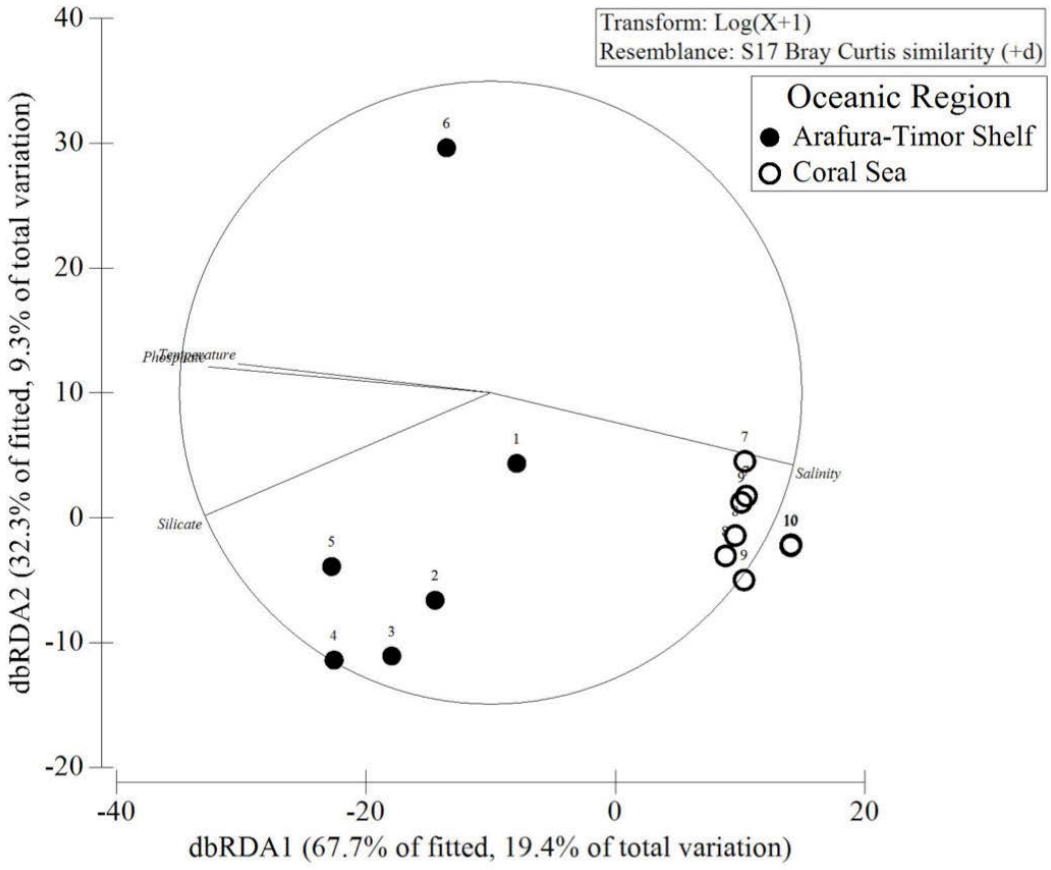

Figure 4.10 Relationship between physicochemical characteristics and new biogenic silica (BSi) production of the diatom community from samples incubated in the presence of PDMPO for 24 h from each oceanic region (Arafura-Timor Shelf and Coral Sea). The plot represents a distance-based redundancy analysis (dbRDA) ordination of new BSi production generated from a Bray-Curtis distance matrix and ocean physicochemical characteristics chosen by the significances of distance linear-based model (DisTLM) marginal tests.

4.4 Discussion

During austral winter, seasonal mixing generates conditions that support an annual peak in phytoplankton biomass and productivity in the ATS (Burford et al. 1995, Condie and Dunn 2006). The physicochemical conditions of the region, in combination with phytoplankton communities dominated by a diverse range of diatom species (Hallegraeff and Jeffrey 1984) likely support high rates of BSi production as has been shown in other ocean regions (Cermeño et al. 2008, Nelson and Goering 1977, Ragueneau et al. 2000, Robins et al. 1996), but until now, has not been empirically tested. Traditionally, standard analytical techniques cannot discriminate between the relative abundance of diatoms to other non-siliceous phytoplankton and the silicification of the diatoms themselves (Baines et al. 2010). Yet, it is important to understand the factors contributing to the Si:C chemical signature of phytoplankton communities because the degree of diatom silicification determines the fate of Si and C within the marine biogeochemical cycle (Baines et al. 2010, Raven and Waite 2004). Using a combination of traditional analytical techniques and fluorescent tracers, we were able to associate community-level processes with those occurring at the individual cellular-level. We find the physicochemical characteristics of two distinct oceanographic provinces in Northern Australia, the Arafura and Timor Shelf and the Coral Sea (Longhurst 2010), drive differential responses in the abundance of key morphological types and their cell-specific silicification, which in turn influence overall community BSi production and capacity for downward C export.

4.4.1 Northern Australia: a medley of biogenic silicon production and carbon export potential

The coastal margin of Northern Australia was characterised by a heterogeneous distribution of BSi standing stock and rates of BSi production. Despite this high variability within regions, distinct differences in BSi production were evident between the two oceanic provinces. In the ATS, a combination of higher nutrient concentrations and water-column mixing supported phytoplankton communities dominated by larger cells (i.e., microphytoplankton size class) with high rates of BSi production. Indeed, the maximum rates of BSi production in surface waters reported here (~5.7 μmol Si L^{-1} d^{-1}) are relatively high compared with other coastal oceans, including the Santa Barbara Basin, a coastal region along the eastern margin of the North Pacific Ocean, <2 μmol Si

L^{-1} d^{-1} (Shipe and Brzezinski 2001) and offshore waters of the Californian Current, <1 μmol Si L^{-1} d^{-1} (Brzezinski et al. 1997). Instead, our observations are more comparable to values recorded downstream of upwelling locations in Monterey Bay, California (>7 μmol Si L^{-1} d^{-1}) – a region noted for the highest recorded rates of marine BSi production in the global ocean (Brzezinski et al., 1997). In stark contrast, in the neighboring oceanic province of the CS, rates of BSi production were more comparable to the open ocean rather than coastal locations, including the eastern equatorial Pacific, ~0.04 μmol Si L^{-1} d^{-1} (Krause et al. 2011), the iron limited central equatorial Pacific, <0.09 μmol Si L^{-1} d^{-1} (Blain et al. 1997), and the Si-limited waters of the western equatorial Pacific, <0.04 μmol Si L^{-1} d^{-1} (Leynaert et al. 2001). These similarities are probably due to the oligotrophic nature of the Coral Sea, with dissolved NO_3^-, PO_4^{3-} and SiO_4^{4-} concentrations comparable to those of the low-nutrient, equatorial Pacific, <2 μmol L^{-1} d^{-1} Si and N (Blain et al. 1997, Leynaert et al. 2001).

On average, BSi production in the ATS was tenfold higher than the CS and coincident with four-fold greater particulate Si:C and Si:N molar ratios than typical values observed for nutrient replete diatoms (Brzezinski 1985). Whilst planktonic elemental ratios in oceanography are traditionally used to inform the relative proportion of diatoms of the total phytoplankton community, in this study, we used a cell-specific fluorescent tracer (i.e., PDMPO) to ascribe regionally-specific Si:C molar ratios and rates of BSi production to greater cellular silicification rather than absolute diatom abundance. Hence we were able to identify the underlying physiological processes that governed the overall community response – an understanding that could not have been achieved without cell-specific techniques.

4.4.2 The role of nitrate limitation in regulating biogenic silicon production

Like the majority of Australia's coastal waters, primary production in the ATS and CS are believed to be N-limited because the inorganic N:P molar ratios in these waters are less than the Redfield ratio (N:P = 16:1; Redfield 1963), suggesting N limits new production (Condie and Dunn 2006). Yet, supplementation with NO_3^- had no observed effect on BSi production, diatom abundance, or silicification at the cellular level. We propose several explanations for these findings.

To our knowledge, no other nutrient amendment experiments have been conducted for this region and as a result, N-limitation has not been directly experimentally tested. Despite nitrate being thought to be the primary limiting nutrient in Australia's coastal surface waters, phosphorus, vitamins and micronutrients (including iron; Fe) may also co-limit marine phytoplankton in this region, because secondary limiting nutrients have not been tested (Moore et al. 2013). Secondly, N-limitation may occur in this region but NO_3^- may not be the limiting chemical form of N. At the time of sampling, rates of N_2-fixation were among some of the highest recorded in the ocean (Messer et al. 2015); meaning whilst concentrations of NO_3^- and NH_4^+ were low, N in the form of dissolved organic N (DON) may have been present in comparably high concentrations. Indeed, phytoplankton communities are known to rely on DON as a source of N when other forms are in low concentrations and, although diatoms are not typically associated with the exploitation of DON, they possess uptake mechanisms which would allow access to these organic sources (Bronk et al. 2007 and references within).

Furthermore, short-term intermittent supplies of NO_3^- may not relieve the physiological 'signs' of N-limitation because resident diatoms within these oceanic-provinces are adapted to N-limitation. For example, even though natural and purposeful Fe fertilization experiments have shown greater Si:C, Si:N, and Si:P ratios in bulk particulate matter under Fe-stress compared to Fe-replete conditions (Franck et al. 2000, Hutchins and Bruland 1998), this is not always the case. For example, observations of diatom Fe-limitation from the field show no differences in cell-specific silicification after Fe addition (Baines et al. 2010, Durkin et al. 2012). Hence, differences in silicification between ocean regions do not appear to be due to short-term physiological responses to ambient conditions. Instead, and aligning with the hypotheses of Baines et

al. (2010), we suggest that the resident diatom communities reflect longer-term prevailing physiological and physico-chemical settings.

4.4.3 Functional trait diversity between Arafura Timor Shelf, Coral Sea and the biogeochemical implications

The degree of frustule silicification affects diatom cell specific gravity and therefore sinking velocity and downward C export, as well as susceptibility of physical dissolution processes and hence Si recycling in upper surface waters. Therefore, by examining patterns of frustule silicification across spatially diverse gradients we can predict the fate of Si and C in their respective settings. In this study, cell-specific fluorescent techniques revealed the same diatom morphotypes from two distinct Australasian ocean regions differ by up to a factor of four in their silicification. Given that diatom abundance (in all size classes) was similar between the ATS and CS, it is likely that the more silicified morphotypes in the ATS, greater amount of BSi on a cellular basis, were responsible for the greater BSi production observed in this province. These findings are supported by independent measures showing higher Si:C of particulate matter from the ATS. Together these results indicate the differences in diatom silicification between the two ocean provinces are more likely a reflection of heavier silicified diatoms from the ATS region, rather than poorly silicified diatoms in the CS.

The differences in diatom morphotypes between the ATS and CS may have important consequences for the marine Si cycle. The less silicified diatoms of the CS may allow for the retention of cells in the photic layer for longer periods, a cellular mechanism which may have evolved to counteract the more rapid rates of sinking prevalent under more stable conditions (Raven and Waite 2004). In contrast, the heavier silicified diatoms from the ATS may be more susceptible to sinking due to their increased cellular density and, as a result, lead to a greater efficiency of diatom downward export (Baines et al. 2010) in comparison to the CS. However, several other processes are known to affect the export of intact diatoms from the surface ocean including grazing, other physiological changes in cell sinking rate (e.g. ratio of vacuole:frustule), aggregation and vertical mixing (Raven and Waite 2004). Some, if not, all of these factors are likely to play a role in determining whether these siliceous particles are sequestered to the sediments in this region.

This study also emphasises the role field surveys play in the appreciation of real-world variability. The range of diatom silicification (Si:C) across Northern Australia spanned several orders of magnitude, comparable to field studies conducted in the northeast subarctic Pacific Ocean (Durkin et al. 2012). Our study contributes to the growing body of research that demonstrates real-world variability can be greater than results observed in manipulative experiments in the laboratory, even when interactions and multiple species are considered. Spatial mapping studies such as ours may provide the key to understanding what drives this functional trait variability, and in turn, what governs regional differences in BSi production across the global ocean.

4.4.4 Implications and future studies

The ATS is a highly productive region, especially during the austral winter (Alongi et al. 2011), and until now the Si-related biogeochemical processes mediated by the diverse diatom flora of this region (Hallegraeff and Jeffrey 1984) were unknown. To the best of the authors knowledge, this study has provided the first characterisation of the diatom morphotypes contributing to the standing stock of BSi and the rate of BSi production in this region, and for any Australian ocean. Our findings reveal that the ATS is not only an important oceanic province for primary production, but also BSi production due to the heavily silicified resident diatom community; meaning diatoms from the ATS play a significant role in the C and Si biological pumps of Northern Australia. Contrary to our hypothesis, N-limitation had no observable effect on BSi production at the community- or cellular-level in the ATS and CS. Instead, similar to other studies, we find that differences in silicification do not appear to be due to short-term physiological responses to ambient conditions such as N concentration, but are due to the long-term prevailing physico-chemical settings characteristic to each ocean province.

This study has furthered our understanding of the role phytoplankton phenotypes have in mediating marine biogeochemical processes by attributing the diversity of cell-specific silicification with BSi surface production. We demonstrate that fluorescent tracers such as PDMPO provide an easy and cost-effective method to explore functional trait diversity in diatoms across spatially and temporally diverse gradients. Future scientific campaigns in this study region should adopt similar approaches to examine temporal variability in Si and C cycling, as frustule silicification among other

biogeochemical processes are known to vary seasonally (Conley et al. 1989, Shimada et al. 2006). Finally, conducting parallel studies that perform PDMPO incubations throughout the entire water column, and in combination with particle interceptor traps, could further understanding of the biophysical processes that control variability of C and Si fate between different oceanic provinces.

4.5 Acknowledgements

The authors thank the scientific crew, captain and scientists onboard the *RV Southern Surveyor* during SS2013_t03 for assistance with sampling and nutrient sample analyses. We also thank Dr. Penelope Ajani for her assistance with diatom identification, and Dr. Daniel Nielsen and Mr. Dale Radford for their assistance with image analysis.

This research was funded by a student scholarship awarded through the School of Life Sciences and Plant Functional Biology and Climate Change Cluster- (C3), University of Technology Sydney.

4.6 Literature cited

Alongi, D. M., Edyvane, K., do Ceu Guterres, M. O., Pranowo, W. S., Wirasantosa, W. S. and Wasson, R. (2011) *Biophysical profile of the Arafura and Timor Seas*. Jakarta, Indonesia: Arafura and Timor Seas Ecosystem Action (ATSEA) Program.

Armstrong, R. A., Peterson, M. L., Lee, C. and Wakeham, S. G. (2009) Settling velocity spectra and the ballast ratio hypothesis. *Deep Sea Research Part II: Topical Studies in Oceanography,* 56(18), pp. 1470-1478. doi:http://dx.doi.org/10.1016/j.dsr2.2008.11.032.

Baines, S. B., Twining, B. S., Brzezinski, M. A., Nelson, D. M. and Fisher, N. S. (2010) Cause and biogeochemical implications of regional differences in silification of marine diatoms. *Global Biogeochemical Cycles,* 24(4). doi:10.1029/2010GB003856.

Blain, S., Leynaert, A., Tréguer, P., Chrétiennot-Dinet, M. J. and Rodier, M. (1997) Biomass, growth rates and limitation of Equatorial Pacific diatoms. . *Deep Sea Research Part I: Oceanographic Research Papers,* 44(7), pp. 1255-1275.

Blondeau-Patissier, D., Dekker, A. G., Schroeder, T. and Brando, V. E. (2011) *Phytoplankton dynamics in shelf waters around Australia*. Canberra, Australia: State of the Environment.

Brewer, D. T., Flynn, A., Skewes, T. D., Pearson, B., Alawo, J. and Young, J. W. (2007) *Ecosystems of the East Marine Planning Region. Report to Department of Environment and Water Resources*. Cleveland, Australia.

Bronk, D. A., See, J. H., Bradley, P. and Killberg, L. (2007) DON as a source of bioavailable nitrogen for phytoplankton. *Biogeosciences,* 4(3), pp. 283-296.

Brzezinski, M. A. (1985) The Si:C ratio of marine diatoms: interspecific variability and the effect of some environmental variables. *Journal of Phycology,* 21(3), pp. 347-357.

Brzezinski, M. A., Phillips, D. R., Chavez, F. P., Friederich, G. E. and Dugdale, R. C. (1997) Silica production in the Monterey, California, upwelling system. *Limnology and Oceanography,* 42, pp. 1694-1705. doi:10.4319/lo.1997.42.8.1694.

Buesseler, K. O. (1998) The decoupling of production and particulate export in the surface ocean. *Global Biogeochemical Cycles,* 12(2), pp. 297-310.

Burford, M. A., Rothlisberg, P. C. and Wang, Y. G. (1995) Spatial and temporal distribution of tropical phytoplankton species and biomass in the Gulf of Carpentaria, Australia. *Marine Ecology Progress Series,* 118, pp. 255-266.

Cermeño, P., Dutkiewicz, S., Harris, R. P., Follows, M., Schofield, O. and Falkowski, P. G. (2008) The role of nutricline depth in regulating the ocean carbon cycle. *Proceedings of the National Academy of Sciences,* 105(51), pp. 20344-20349.

Claquin, P., Martin‐Jézéquel, V., Kromkamp, J. C., Veldhuis, M. J. and Kraay, G. W. (2002) Uncoupling of silicon compared with carbon and nitrogen metabolisms and the role of the cell cycle in continuous cultures of *Thalassiosira pseudonana* (Bacillariophyceae) under light, nitrogen, and phosphorus controls. *Journal of Phycology,* 38(5), pp. 922-930.

Clarke, K. R. and Gorley, R. N. (2006) User manual/tutorial. in,Plymouth, UK: Primer-E Ltd.

Condie, S. A. and Dunn, J. R. (2006) Seasonal characteristics of the surface mixed layer in the Australasian region: implications for primary production regimes and biogeography. *Marine and Freshwater Research,* 57(6), pp. 569-590.

Conley, D. J., Kilham, S. S. and Theriot, E. (1989) Differences in silica content between marine and freshwater diatoms. *Limnology and Oceanography,* 34(1), pp. 205-212.

Durbin, E. G. (1977) Studies on autecology of marine diatom *Thalassiosira nordenskioeldii*. II. Influence of cell-size on growth-rate, and carbon, nitrogen, chlorophyll-a and silica content. *Journal of Phycology,* 13(2), pp. 150-155. doi:10.1111/j.0022-3646.1977.00150.x.

Durkin, C. A., Marchetti, A., Bender, S. J., Truong, T., Morales, R., Mock, T. and Virginia Armbrust, E. (2012) Frustule-related gene transcription and the influence of diatom community composition on silica precipitation in an iron-limited environment. *Limnology and Oceanography,* 57(6), pp. 1619.

Finkel, Z. V., Beardall, J., Flynn, K. J., Quigg, A., Rees, T. A. V. and Raven, J. A. (2009) Phytoplankton in a changing world: cell size and elemental stoichiometry. *Journal of Plankton Research*. doi:fbp098.

Franck, V. M., Brzezinski, M. A., Coale, K. H. and Nelson, a. D. M. (2000) Iron and silicic acid concentrations regulate Si uptake north and south of the Polar Frontal Zone in the Pacific Sector of the Southern Ocean. *Deep Sea Research Part II,* 47(3315-3338). doi:10.1016/S0967-0645(00)00070-9.

Hallegraeff, G. M. and Jeffrey, S. W. (1984) Tropical phytoplankton species and pigments of continental shelf waters of North and North-West Australia. *Marine Ecology Progress Series,* 20, pp. 59-74.

Harrison, P. J., Conway, H. L. and Dugdale, R. C. (1976) Marine diatoms grown in chemostats under silicate or ammonium limitation. I. Cellular chemical composition and steady-state growth kinetics of S*keletonema costatum*. *Marine Biology,* 35(2), pp. 177-186. doi:10.1007/bf00390939.

Herzenberg, L. A., Sweet, R. G. and Herzenberg, L. A. (1976) Fluorescence-activated cell sorting. *Scientific American,* 234(3), pp. 108-117.

Hildebrand, M. (2008) Diatoms, biomineralization processes, and genomics. *Chemical reviews,* 108(11), pp. 4855-4874.

Hooker, S. B., Van Heukelem, L., Thomas, C. S., Claustre, H., Ras, J., Barlow, R., Sessions, H., Schlüter, L., Perl, J. and Trees, C. (2005) The second SeaWiFS HPLC analysis round-robin experiment (SeaHARRE-2). *NASA Tech. Memo,* 212785, pp. 124.

Hutchins, D. A. and Bruland, K. W. (1998) Iron-limited diatom growth and Si: N uptake ratios in a coastal upwelling regime. *Nature,* 393(6685), pp. 561-564.

Jin, X., Gruber, N., Dunne, J. P., Sarmiento, J. L. and Armstrong, R. A. (2006) Diagnosing the contribution of phytoplankton functional groups to the production and export of particulate organic carbon, $CaCO_3$, and opal from global nutrient and alkalinity distributions. *Global Biogeochemical Cycles,* 20, pp. 10.1029/2005GB002532.

Krause, J. W., Nelson, D. M. and Brzezinski, M. A. (2011) Biogenic silica production and the diatom contribution to primary production and nitrate uptake in the eastern equatorial Pacific Ocean. *Deep Sea Research Part II: Topical Studies in Oceanography,* 58(3), pp. 434-448.

Leblanc, K. and Hutchins, D. A. (2005) New applications of a biogenic silica deposition fluorophore in the study of oceanic diatoms. *Limnology and Oceanography: Methods,* 3, pp. 462-476.

Leynaert, A., Tréguer, P., Lancelot, C. and Rodier, M., 2001. (2001) Silicon limitation of biogenic silica production in the Equatorial Pacific. *Deep Sea Research Part I: Oceanographic Research Papers,,* 48(3), pp. 639-660.

Longhurst, A. R. (2010) *Ecological geography of the sea,* 2nd ed.*,* San Diego, California, USA: Academic Press.

Lourey, M. J., Thompson, P. A., McLaughlin, M. J., Bonham, P. and Feng, M. (2013) Primary production and phytoplankton community structure during a winter shelf-scale phytoplankton bloom off Western Australia. *Marine Biology,* 160, pp. 355-369.

McNair, H. M., Brzezinski, M. A. and Krause, J. W. (2015) Quantifying diatom silicification with the fluorescent dye, PDMPO. *Limnology and Oceanography: Methods,* 13(10), pp. 587-599.

Moore, C. M., Mills, M. M., Arrigo, K. R., Berman-Frank, I., Bopp, L., Boyd, P. W., Galbraith, E. D., Geider, R. J., Guieu, C. and Jaccard, S. L. (2013) Processes and patterns of oceanic nutrient limitation. *Nature Geoscience,* 6(9), pp. 701-710.

Nelson, D. M. and Goering, J. J. (1977) Near-surface silica dissolution in the upwelling region off northwest Africa. *Deep Sea Research,* 24(1), pp. 65-73.

Nelson, D. M., Smith Jr, W. O., Muench, R. D., Gordon, L. I., Sullivan, C. W. and Husby, D. M. (1989) Particulate matter and nutrient distributions in the ice-edge

zone of the Weddell Sea: Relationship to hydrography during late summer. *Deep Sea Research Part A. Oceanographic Research Papers,* 36(2), pp. 191-209.

Nelson, D. M., Treguer, P., Brzezinski, M. A., Leynaert, A. and Queguiner, B. (1995) Production and dissolution of biogenic silica in the ocean - revised global estimates, comparison with regional data and relationship to biogenic sedimentation. *Global Biogeochemical Cycles,* 9(3), pp. 359-372. doi:10.1029/95gb01070.

Paasche, E. (1975) Growth of plankton diatom *Thalassiosira nordenskioeldii* Cleve at low silicate concentrations. *Journal of Experimental Marine Biology and Ecology,* 18(2), pp. 173-183. doi:10.1016/0022-0981(75)90072-6.

Ragueneau, O., Tréguer, P., Leynaert, A., Anderson, R. F., Brzezinski, M. A., DeMaster, D. J., Dugdale, R. C., Dymond, J., Fischer, G., François, R., Heinze, C., Maier-Reimer, E., Martin-Jézéquel, V., Nelson, D. M. and Quéguiner, B. (2000) A review of the Si cycle in the modern ocean: recent progress and missing gaps in the application of biogenic opal as a paleoproductivity proxy. *Global and Planetary Change,* 26(4), pp. 317-365. doi:http://dx.doi.org/10.1016/S0921-8181(00)00052-7.

Raven, J. and Waite, A. (2004) The evolution of silicification in diatoms: inescapable sinking and sinking as escape? *New Phytologist,* 162(1), pp. 45-61.

Redfield, A. C. (1963) The influence of organisms on the composition of sea-water. *The sea*, pp. 26-77.

Robins, D. B., Bale, A. J., Moore, G. F., Rees, N. W., Hooker, S. B., Gallienne, C. P., Westbrook, A. G., Marañón, E., Spooner, W. H. and Laney, S. R. (1996) *AMT-1 Cruise Report and Preliminary Results.* NASA Technical Memorandum 104566. NASA Goddard Space Flight Centre, Greenbelt, Maryland, USA.

Shimada, C., Tanaka, Y. and Tanimura, Y. (2006) Seasonal variation in skeletal silicification of *Neodenticula seminae*, a marine planktonic diatom: sediment trap experiments in the NW Pacific Ocean (1997–2001). *Marine Micropaleontology,* 60(2), pp. 130-144.

Shimizu, K., Del Amo, Y., Brzezinski, M. A., Stucky, G. D. and Morse, D. E. (2001) A novel fluorescent silica tracer for biological silicification studies. *Chemistry & biology,* 8(11), pp. 1051-1060.

Shipe, R. F. and Brzezinski, M. A. (2001) A time series study of silica production and flux in an eastern boundary region: Santa Barbara Basin, California. . *Global Biogeochemical Cycles,* 15(2), pp. 517-531.

Strickland, J. D. H. and Parsons, T. R. (1968) *A practical handbook of seawater analysis,* Ottawa, Canada: Fisheries Research Board of Canada.

Tréguer, P. J. and De La Rocha, C. L. (2013) The world ocean silica cycle. *Annual Review of Marine Science,* 5, pp. 477-501.

Uitz, J., Huot, Y., Bruyant, F., Babin, M. and Claustre, H. (2008) Relating phytoplankton photophysiological properties to community structure on large scales. *Limnology and Oceanography,* 53(2), pp. 614–630.

Van Heukelem, L. and Thomas, C. S. (2001) Computer-assisted high-performance liquid chromatography method development with applications to the isolation and analysis of phytoplankton pigments. *Journal of Chromatography A,* 910(1), pp. 31-49.

Vidussi, F., Claustre, H., Manca, B. B., Luchetta, A. and Marty, J. C. (2001) Phytoplankton pigment distribution in relation to upper thermocline circulation in the eastern Mediterranean Sea during winter. *Journal of Geophysical Research: Oceans,* 106(pp. 19939–19956).

Walsh, J. J. (1991) Importance of continental margins in the marine biogeochemical cycling of carbon and nitrogen. *Nature,* 350(6313), pp. 53-55.

4.7 Supplementary Figures

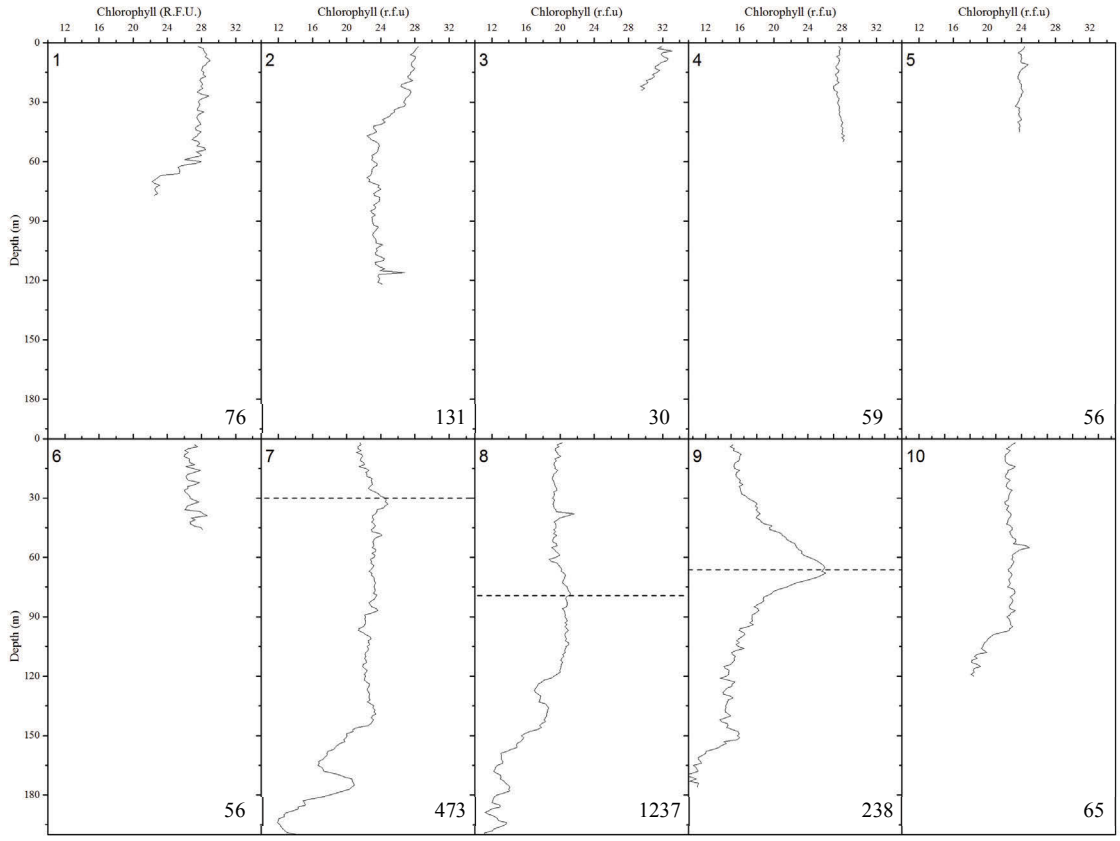

Supplementary Figure 4.1 Vertical down-cast profiles of chlorophyll *a* (solid lines) measured in relative fluorescent units (RFU) from sites sampled within the Arafura Timor Shelf (1-6) and Coral Sea (7-10). Where present, dotted lines indicate sites where a subsurface chlorophyll maximum was discernable and with their location corresponding to the depth water samples were taken. Numbers on plot indicate bottom depth (m) for each station.

CHAPTER 5:
WARMING PROMOTES SPECIALISATION TO SUPRA-OPTIMAL TEMPERATURE IN A TROPICAL DINOFLAGELLATE

K. G. Baker*, D. T. Radford, C. Evenhuis, U. Kuzhiumparambil, P. J. Ralph, M. A. Doblin.

Plant Functional Biology and Climate Change Cluster, University of Technology Sydney, Sydney, New South Wales, Australia.

***Correspondence:** Kirralee G Baker, Plant Functional Biology and Climate Change Cluster, University of Technology Sydney, Broadway, Ultimo, New South Wales, 2007, Australia
Kirralee.G.Baker@student.uts.edu.au

Key words: adaptation, phytoplankton, functional traits, thermal performance curves, microbe, thermal optimum, niche width, cell size

5.1 Introduction

Of all abiotic factors that regulate life on Earth, temperature has a fundamental importance because of it's universal effects on biological rate processes that control nearly all physiological functions (Johnston and Bennett 1996). Understanding how organisms adapt to temperature has long intrigued both physiologists and evolutionary biologists (Angilletta 2009). More recently this interest has gathered momentum in the context of global change, particularly in ectothermic organisms, due to their basic physiological functions (e.g. growth, reproduction) being governed by the ambient environmental temperature (Huey and Kingsolver 1989).

In the face of contemporary changes to thermal regimes, organisms have two choices: relocate to a more hospitable region or stay put and cope (Hofmann and Todgham 2010). Many adult organisms are sessile, and only have the latter option, which involves genetic and non-genetic components of physiological adjustment, depending on whether the temperature change is within an individuals' life-span or persists over multiple life-spans (Clarke 1996). Differentiating between these two timescales is complicated for organisms such as microbes that often encounter natural variations in temperature on time-scales that are equivalent to their short generational times (i.e., hours-days). In extreme cases, diel fluctuations in sea surface temperatures SST can exceed 5 °C (Kawai and Wada 2007).

Phytoplankton are a diverse group of photosynthetic marine microbes that are distributed throughout the upper ocean and play a unique role in the functioning of marine ecosystems. They underpin the marine food web and their metabolic activity mediates the biogeochemical cycles of many elements (Falkowski et al. 1998). Due to their planktonic nature, physical processes of advection and mixing determine their thermal exposure history (Lévy et al. 2014) and ultimately their survival depends on their ability to acclimate (physiologically adjust) to environmental conditions. Short-term (hours-weeks) temperature acclimation is well documented for phytoplankton exposed to temperature changes equivalent to individual life-spans (Davison 1991), but their ability to cope with temperature changes that persist for many generations

(between generational exposure; months to years) is now receiving more attention (Huertas et al. 2011, Schluter et al. 2014).

The temperature window in which an organism can survive and reproduce dictates the thermal niche width of an individual, that dynamically changes over time through physiological and biochemical processes that enable cellular adjustment/acclimation (Angilletta Jr 2013). Theory predicts prolonged exposure (over multiple generations) to a certain environment provides cellular cues for permanent changes that enhance performance for this environment, a theory that has become known as *The Beneficial Acclimation Hypothesis* (Huey and Berrigan 1996). Long-term (weeks-years) experiments and reciprocal transplant assays have served as a valuable tool for testing this hypothesis, particularly in microbes. In experiments with the bacterium, *Escherichia coli*, adaptation (over tens-hundreds of generations) to high temperatures sometimes enhances fitness under these new conditions, but not always (Bennett and Lenski 1997). Whilst vast differences exist between phytoplankton and bacteria, such *in vitro* evolution experiments provide an appropriate framework for assessing the effects of phenotypic acclimation on microbial performance, but until recently had not been considered in the context of phytoplankton and climate change (Reusch and Boyd 2013).

Most reciprocal transplant assays have been directed towards understanding the long-term (weeks-years) effects of ocean acidification (for a review see Collins et al. 2014), whereas other variables such as temperature have received less attention. An experimental population from the genus *Symbiodinium* (the coral symbiotic dinoflagellate) adapted to warmer temperatures (60 generation exposure to ambient +8 °C) was able to grow and reproduce at these hotter, whereas non-adapted individuals could not (Huertas et al. 2011). Others have examined the adaptability of important functional traits (Schluter et al. 2014), the underlying elements of a phenotype that dictate fitness and ecological function (Litchman and Klausmeier 2008), but it remains unknown what costs are associated with this high temperature adaptation.

Acclimation, irrespective of whether it is beneficial or not, imposes energetic costs to the individual that are often expressed as trade-offs between FTs, which ultimately affect fitness because energy must be expended to tune an individual's physiology to match the altered environment (Angilletta Jr 2013). The associated costs of high-

temperature adaptation in phytoplankton are largely unknown but have been observed for other microbes such as bacteria. For example, an increase in fitness at high temperatures comes at a cost to performance at cold temperatures (Bennett and Lenski 2007). Trade-offs can be visualised through TPCs that describe the relationship between an organism's traits (e.g. fitness) and their immediate thermal environment. Understanding these trade-offs in phytoplankton have significant implications for the functioning of marine ecosystems because many FTs are directly or indirectly related to ecological and biogeochemical processes (Falkowski et al. 1998, Litchman and Klausmeier 2008).

To further understand the ecological and biogeochemical implications of adaptation to supra-optimal temperatures in phytoplankton, we assessed the benefits and costs of adaptation (approximately 500 generations) to supra-optimal temperature (ambient +5 °C) on the performance of a free-living, tropical, benthic dinoflagellate, *Amphidinium massartii*. We first evaluated whether high-temperature (HT) adaptation and HT acclimation produces similar phenotypes and assessed if this HT-adaptation was reversible by conducting a reciprocal transplant assay. Secondly, to understand the physiological constraints of HT-adaptation, we obtained TPCs for multiple traits (fitness, photosynthesis and net flux of dissolved nutrients) in both adapted and non-adapted populations.

5.2 Methods and Materials

5.2.1 Establishment of high-temperature adapted strain and culture conditions

The tropical benthic dinoflagellate, *Amphidinium massartii* CS-259 was obtained from the Australian National Algae Culture Collection (CSIRO, Hobart, Australia), founded from a single cell isolated from Kurrimine Beach, Queensland, Australia. Members of *Amphidinium* are considered 'model dinoflagellates' for both genetic and ecological studies due to their: relatively small genome size and genetic transformability for use in DNA manipulation studies (LaJeunesse et al. 2005, Lohuis and Miller 1998), abundance and wide distribution in benthic systems (Lee et al. 2003), and rapid reproductive rates that make them easy to culture.

A. massartii was maintained in semi-continuous batch cultures in cell culture flasks (BD Biosciences, California, Unites States of America) in seawater medium (0.2 μm filtered coastal seawater obtained from the Port Hacking National Reference Station, PH100, New South Wales, Australia) with modified f/2 enrichment lacking silicic acid (Guillard and Ryther (1962); 8.82 x 10^{-4} M $NaNO_3$; 3.62 x 10^{-5} M, NaH_2PO_4 H_2O, trace metal solution and vitamin solution. Cultures were maintained at tropical conditions of 25±0.5 °C (control temperature; CT) and an irradiance of 100 μmol photons m^{-2} s^{-1} on a 12 h:12 h light:dark cycle. A HT-adapted population (HT-population) was established by transferring the parent culture from the CT through a series of increasing temperatures (+2 °C steps) until a sub-lethal temperature (30 °C) was reached (Hou 2011). This HT-population was maintained at 30±0.5 °C whilst the non-adapted, parent culture (CT-population) was maintained at of 25±0.5 °C for more than three years (~500 generations) before experimentation commenced.

5.2.2 Experimental set up and sampling:

5.2.2.1 Reciprocal transplant assay to estimate costs of acclimation and adaptation

To provide insight into the environmental effects and potential costs of adaptation, a full reciprocal transplant assay was performed using an inoculum from the CT- and HT-populations. Triplicate cultures (250 mL; BD Biosciences, California, United States of America) of each population were assayed at two temperatures (25 and 30 ˚C) under

100 µmol photons m^{-2} s^{-1} (12 h: 12 h, light: dark cycle). A phenotypic characterisation of the CT- and HT- populations was undertaken by measuring a variety of traits, as described below. To evaluate the effects of HT acclimation, the mean trait values of the CT-population at 30±0.5 ˚C were compared to those at 25±0.5 ˚C. To determine whether the duration of high-temperature exposure had differential costs or benefits associated with HT acclimation vs.adaptation; the mean trait values of CT-population at 30±0.5 ˚C were compared with the HT-population at 30±0.5 ˚C. Finally, to ascertain whether the phenotype of HT-adaptation remained fixed or was reversible, values of the HT-population at 25±0.5 ˚C were compared to the HT-population at 30±0.5 ˚C and CT-population at 25±0.5 ˚C, respectively. For each trait, data were tested for normality and homogeneity of variance before performing statistical analysis. One-way ANOVA was used to determine whether there were significant differences between treatments with subsequent Tukey's honestly significant differences (HSD) post-hoc comparisons. Differences were accepted as significant at $p < 0.05$.

5.2.2.2 Thermal performance curves to examine fitness trade-offs

To acquire TPCs of fitness and other FTs (photophysiology, carbon assimilation, nitrate and phosphate uptake; described below) for the *A. massartii* CT- and HT- populations, cultures (40 mL) were grown in triplicate glass vessels for at least five generations over a temperature gradient spanning 17 to 40 ˚C. This temperature range was selected as to capture the minimum and maximum temperatures for growth (*CTmin* and *CTmax*, respectively) in order to constrain estimates of these parameters in later analysis (discussed below). A temperature gradient was established using a thermal gradient block: an aluminium block (30 × 15 × 150 cm) bored to accommodate glass vials (~40 mL) (for experimental set-up see **Supplementary Figure 2.1**). Circulation immersion heater chillers (Julabo GmbH, Germany) at opposite ends maintained the temperature differential (±0.25 ˚C per gradient position), monitored using a calibrated thermocouple (Comark, United Kingdom) over the course of the experiment. Light (cool white) was supplied (100 µmol photons m^{-2} s^{-1}) by an array of LEDs (Schenzen Cidly Group, China) set to a 12 h:12 h light:dark cycle. This irradiance was consistent with previous light conditions of inoculum cultures and was verified with a microspherical quantum sensor (Walz, Germany). Samples were harvested daily to measure, growth, cell viability, photosynthetic health and dissolved inorganic nutrient stocks. Each replicate

was monitored independently (using daily cell count measurements) in order to target exponential phase, where samples for gross primary productivity (GPP) were harvested and net uptake rates of inorganic nutrients were calculated.

5.2.3 Characterisation of phenotype: trait analysis

5.2.3.1 Growth and viability

Phenotype fitness was assessed across the thermal gradient (17 to 40 ˚C) using methods previously described in Baker et al. (2016) with small modifications. Briefly, samples of 500 µL were harvested from each temperature treatment and incubated in the presence of a nucleic acid stain (SYTOX green, Molecular Probes, Leden, Nederland; final concentration 0.5 µM) in order to discriminate between dead and living cells. This discrimination is based on cell membrane integrity, whereby the stain is impervious to live cells but permeates dead cells, resulting in positively stained dead cells and negatively stained live cells. Counts were performed daily using a flow cytometer (Accuri, Becton Dickinson, Brussels, Belgium). A minimum of 1000 particles were counted and population statistics were calculated using gates that were consistent across the experiment, acquired with the same instrument settings. Growth rate estimates were then made using abundance of viable cells. For the temperature at which growth ceased in each treatment, a lethal exposure time (i.e. the time at which 50% of the population was viable; Lex_{50}) was calculated for each population. Mortality data in both treatments were first adjusted for the observed mortality at the T_{opt} and the data were then fitted with an exposure-response function for computation of Lex_{50} using Origin Pro software (Origin Corporation Inc., 2015).

5.2.3.2 Cell size

Cells were harvested in exponential growth phase when volumes of 2 mL were sampled and stored in glutaraldehyde (final concentration 1% v/v) until later analysis. Small changes in cell size may have resulted from this fixation procedure, and as a result, we compared relative differences. Samples were loaded into a Sedgewick-Rafter counting chamber (Graticules Limited, England) and images captured via microscopy (×20; bright field; Nikon Eclipse Ti, Nikon, Japan). Image processing was automated via an image processing script written for Image-J software as described in Suggett et al. (2015). Cell volume was estimated from cell diameter and assuming cells were

ellipsoidal (Hillebrand et al. 1999). A minimum of 1500 cells was measured and the cell volume was determined as the median of the cell population.

5.2.3.3 Fatty acid composition analysis

Given the fatty acid (FA) composition of membranes has been shown to confer thermal sensitivity or tolerance in dinoflagellates (Tchernov et al. 2004), we examined the effect of temperature on saturated and unsaturated FA composition of adapted and non-adapted populations. Samples of 150 mL were harvested at late-exponential early-stationary phase and centrifuged at 5000 *g* for 10 min at 20 ˚C. The supernatant was discarded and the cell pellets were stored frozen at –20 ˚C until analysis (within 6 months).

Fatty-acid methyl ester (FAME) analysis was performed as per previously reported methods of Folch et al. (1957) and Carreau and Dubacq (1978). Lyophilised biomass in the tube was combined with a 3 mL mixture of chloroform and methanol 2:1 [*v/v*] and vortexed for 3 min to allow lipids in algal cells to be extracted, the tube was then centrifuged at 2000 *g* for 15 min. Supernatant was collected and the residue re-extracted twice with 2 mL of the above solvent mixture. Supernatants were pooled and evaporated to dryness under a stream of nitrogen. The resulting crude lipid mass was saponified in the presence of 1 mL 1% NaOH for 15 min at 55 ˚C. Samples were allowed to cool, an internal standard was then added (10 µL; nonadecanoic acid [1 mg/mL], Sigma Aldrich, NSW, Australia), followed by transesterification in the presence of 2 mL 5% methanolic HCl solution for 15 min at 55 ˚C. To aid phase separation, 1 mL MilliQ was added, followed by 1 mL hexane. The reaction mixture was allowed to settle and the top, fatty acid enriched, non-polar phase was collected and transferred to a gas chromatography (GC) sample vial. Liquid-liquid extraction with hexane was repeated and the pooled hexane layer was evaporated to dryness under nitrogen.

The resultant residue was reconstituted in 100 µL hexane and analysed by GC-MS (gas chromatography- mass spectrometry; Agilent 7890 series GC coupled to an Agilent quadrupole MS(5975N)) on a HP-5MS fused capillary column (5%-phenyl-methylpolysiloxan, 30 m long, 0.25 mm i.d., film thickness 0.25 µm, Agilent Technologies). Splitless mode of injection (5 µL volume) was used with a purge time of

1 min. Injection volume was 5 µL. The injector temperature was held at 280 °C. Initial column temperature was 50 °C (held for 2 min) and increased at a rate of 4 °C min^{-1} to 220 °C and then increased to 300 °C at a rate of 60 °C min^{-1} (held for 3 min). Data was analysed using Agilent GC Chemstation software where peaks were identified by matching the retention time and mass spectra of high purity FA (99.9%) standards (Sigma Aldrich, NSW, Australia).

5.2.3.4 Chlorophyll *a* analysis

Samples (2 mL) harvested in late-exponential early-stationary phase were centrifuged at 5000 *g* for 5 min at 20 ˚C. The supernatant was discarded and cell pellets stored frozen at -80 °C until analysis (carried out within 3 months). Chlorophyll *a* extraction and analysis were performed as previously described in Baker et al. (2016). Briefly, 3 mL volume of extraction reagent (90% acetone: 100% dimethyl sulfoxide; 3:2 v/v) was added to cell pellets, vortexed and incubated for 15 min in the dark at 4 °C (Shoaf and Lium 1976). Chlorophyll *a* was determined using a calibrated fluorometer (TD-700, Turner Designs, USA) using the non-acidification method of Welschmeyer (1994).

5.2.3.5 Photophysiology

For the reciprocal transplant assay (whereby the CT- and HT- populations were introduced into the thermal environment of the other), steady-state RLC curves were conducted on all replicate samples in exponential phase. Here, dark-adapted (15 min) samples were measured in a Water-PAM (Walz, Effeltrich, Germany) that supplied red light (650 nm) at increasing intensities of 0, 1, 11, 21, 36, 56, 81, 111 and 146 µmol photons m^{-2} s^{-1}. Light steps of 4-min duration were used with a saturating pulse every 30 s. The average of the last three measurements at each light step used to calculate effective quantum yield (Φ_{PSII}) relative electron transport rates (rETR) using the following equations:

$$\Phi_{PSII} = \frac{(F_{M'} - F')}{F_{M'}} \qquad \textbf{(Equation 5.1)}$$

where, F' and F_M' is the minimum fluorescence emission and the maximum fluorescence signal respectively, both in light-adapted state.

$$rETR = PAR \times \Phi_{PSII} \times 0.85 \qquad \textbf{(Equation 5.2)}$$

where, *PAR* is photosynthetically active radiation.

Once complete, a Photosynthesis-Irradiance curve was modelled by fitting rETR rates to a Jassby-Platt model (Jassby and Platt 1976) to derive the light utilisation efficiency (α) and light saturation irradiance (E_k) according to the equations in Ralph and Gademann (2005).

To allow for the simultaneous analysis of multiple samples across a thermal gradient, a photosynthetic assessment of *A. massartii* was performed using an imaging-PAM (Walz, Effeltrich, Germany). Here, 300 µL samples were dark-adapted for 15 min, exposed to a saturation pulse (>2000 µmol photons m^{-2} s^{-1}, 800 milliseconds; 450 nm) to determine maximum fluorescence yield (F_M). Samples were then light adapted to their growth irradiance (100 µmol photons m^{-2} s^{-1}) for 15 min, then exposed to another saturation pulse to determine effective quantum yield (**Equation 5.1**). Using values from both saturation pulses non-photochemical quenching (NPQ) was calculated using the following equation from Baker (2008).

$$\text{NPQ} = \frac{F_M}{F_{M'}} - 1 \qquad \textbf{(Equation 5.3)}$$

5.2.3.6 Net flux of dissolved nutrients

Estimates of net cellular uptake of N and P (added to cultures as $NaNO_3$, NaH_2PO_4 H_2O) were determined by methods previously described in Baker et al. (2016). Subsamples of 1 mL were taken daily and centrifuged at 5000 *g* for 5 min at 20 ˚C. Supernatant volumes of 500 µL were removed and stored frozen at -20 °C until colorimetric analysis was conducted (within 3 months). Net flux was calculated as the difference between nutrient concentrations at the start and end of the experiment. Each nutrient concentration was normalised to cell abundance to account for differences in growth.

Briefly, NO_3^- contents were determined indirectly via the vanadium chloride (VCl_3) reduction reaction as described in Schnetger and Lehners (2014). Specifically, NO_2^- concentrations were determined by adding 30 µL of Griess reagent (0.2% N-1-naphthylethylenediamine dihydrochloride (NEDD) solution and 2% sulfanilamide solution, 1:1 [v/v]) to 300 µL of sample or standard, mixed thoroughly and incubated

for 45 ˚C for 30 min. Total NO_x (NO_3^- + NO_2^{2-}), was determined by adding 150 µL of reduction reagent (VCl_3 0.05M prepared in 1.02N HCl and Griess reagent 5:1, [v/v]) to 180 µL of sample or standard, mixed thoroughly and incubated for 45 ˚C for 60 min. Absorbance was then read using a spectrophotometer at a wavelength of 540 nm across independent samples and the average of four replicate reads was used. The NO_3^- values were linear between 1 and 100 µM and the detection limit was 0.15 µM.

Inorganic P (PO_4^{3-}) was determined by the sensitive detection method of Hoenig et al. (1989). The detection reagent was prepared by combining ammonium molybdate (2.6g/ 100mL) with 2.5N HCl, 1:1 [v/v] immediately before analysis. From this solution, 180 µL was then added to 70 µL sample (previously diluted 1:10 with MilliQ) or standard and analysed within 5 min. Absorbance was then read using a spectrophotometer at a wavelength of 620 nm and the average of four replicate reads was used. Inorganic phosphorus values were linear between 1 and 15 µM and the detection limit was 0.95 µM. Where necessary, samples were diluted in order to obtain concentrations within the linear detection range of each colorimetric method.

5.2.4 Data analysis

Trait responses to changes in temperature are characterised by TPCs described by three thermal properties: maximum trait value, optimum temperature for trait and thermal niche width (the temperature range over which the trait value is positive, i.e., between the CT_{min}; critical minimum temperature and CT_{max}; critical maximum temperature). We estimated these thermal properties for each trait by fitting a thermal tolerance function to the data (Thomas, 2012) using the following equation:

$$f(T) = ae^{bT}\left[1 - \left(\frac{T - T_{av}}{(CT_{max} - CT_{min})/2}\right)^2\right] \qquad \textbf{(Equation 5.4)}$$

where $T_{av} = (CT_{max} + CT_{min})/2$.

The shape of the TPC is controlled by three important temperature traits, CT_{min} and CT_{max} (which determine the thermal niche width), a and b (coeffecients of the 'Eppley' curve; Eppley 1972), an exponential relationship thought to provide the constraint on community-level phytoplankton growth as a function of temperature, and T_{av} which determines the location of the maximum quadratic portion of this function. When fitting

curves to data for individual traits, it was found that estimates of CT_{min} produced unrealistic results and therefore it was necessary to constrain b and CT_{min} to positive values.

The point estimates for values of the thermal properties listed above were calculated as in Baker et al. (2016) using MLE (assuming normally distributed errors) and the CI were calculated by parametric bootstrapping. To determine whether differences in thermal properties (i.e., maximum trait value, optimum temperature for trait and thermal niche width) for each trait were statistically significant between the CT- and HT-populations, we calculated the 95% CI for the difference between the two population means for each trait. We considered these differences to be significant at alpha =0.05, if the 95% CI did not contain the null hypothesis (i.e. the mean difference was zero).

5.3 Results

5.3.1 Costs, benefits and reversibility of high temperature adaptation

Costs of HT acclimation were not evident across all FTs, as the value of some traits increased/decreased in the CT-population at 30 °C in comparison to 25 °C, whilst others did not **(Figure 5.1)**. Furthermore, a comparison of FT within the same population under HT acclimation (5 generations of exposure) and adaptation (~500 generations of exposure) revealed no observable change in fitness and little difference in the remaining FTs i.e., the phenotype of CT-population was similar to HT-population at 30 °C.

Overall fitness of *A. massartii* was unaffected by HT acclimation because growth rates of the CT-population were comparable between 25 and 30 °C (p >0.05; open bars, **Figure 5.1a**). Similarly, cellular traits such as FA unsaturation index (**Figure 5.1c**), cellular chlorophyll *a* content (**Figure 5.1d**) and saturation irradiance (**Figure 5.1f**) did not change following short-term (5 generations) exposure to high temperature. In contrast, in the CT-population, increases in cell volume were observed (p =0.027; **Figure 5.1b**), as well as greater rates of maximum electron transport (p =0.030; **Figure 5.1e**) at 30 °C compared to 25 °C. Consequently, these observations indicate that HT acclimation results in a phenotype with comparable fitness to that expressed under ambient temperatures. However cells were larger and despite the same chlorophyll *a* content, were capable of transferring more energy to downstream photosynthetic processes (i.e. had greater ETR_{max}) indicative of greater photosynthetic capacity.

This high temperature phenotype was similar between HT acclimation and adaptation, with one significant difference: the unsaturation index of FA, was greater in the CT population than the HT-population at 30 °C (p=0.022; **Figure 5.1c**). These results indicate that HT acclimated and adapted phenotypes can only be distinguished by one of the six traits measured in this study: the biochemical composition of FA.

Reversibility of HT adaptation was not consistent across all measured FTs. Some traits remained fixed and did not revert during a short re-acclimation period (5 generations) to the CT including growth rate (**Figure 5.1a**), FA unsaturation index (**Figure 5.1c**), and ETR_{max} (**Figure 5.1e**). However, the reduced pigmentation of cells at high temperatures was dynamically altered to levels expressed by the CT-population (**Figure 5.1d**). The remaining FTs changed in response to control temperatures but did not have the same

values as the CT population. For example, cell volume in the HT-population decreased by 60 % when grown at 25 °C compared to 30 °C, but still remained 50 % smaller than the CT-population (p <0.001; **Figure 5.1b**). Likewise, E_k of the HT-population decreased six-fold when grown at 30 °C compared to 25 °C (p <0.001; **Figure 5.1f**). Consequently, some traits of the phenotype remained fixed e.g. FA composition, whilst others were dynamic but did not necessarily reflect values of the CT-population e.g. smaller cell size. Therefore, reversibility of FT in the HT-population appears to be trait-specific.

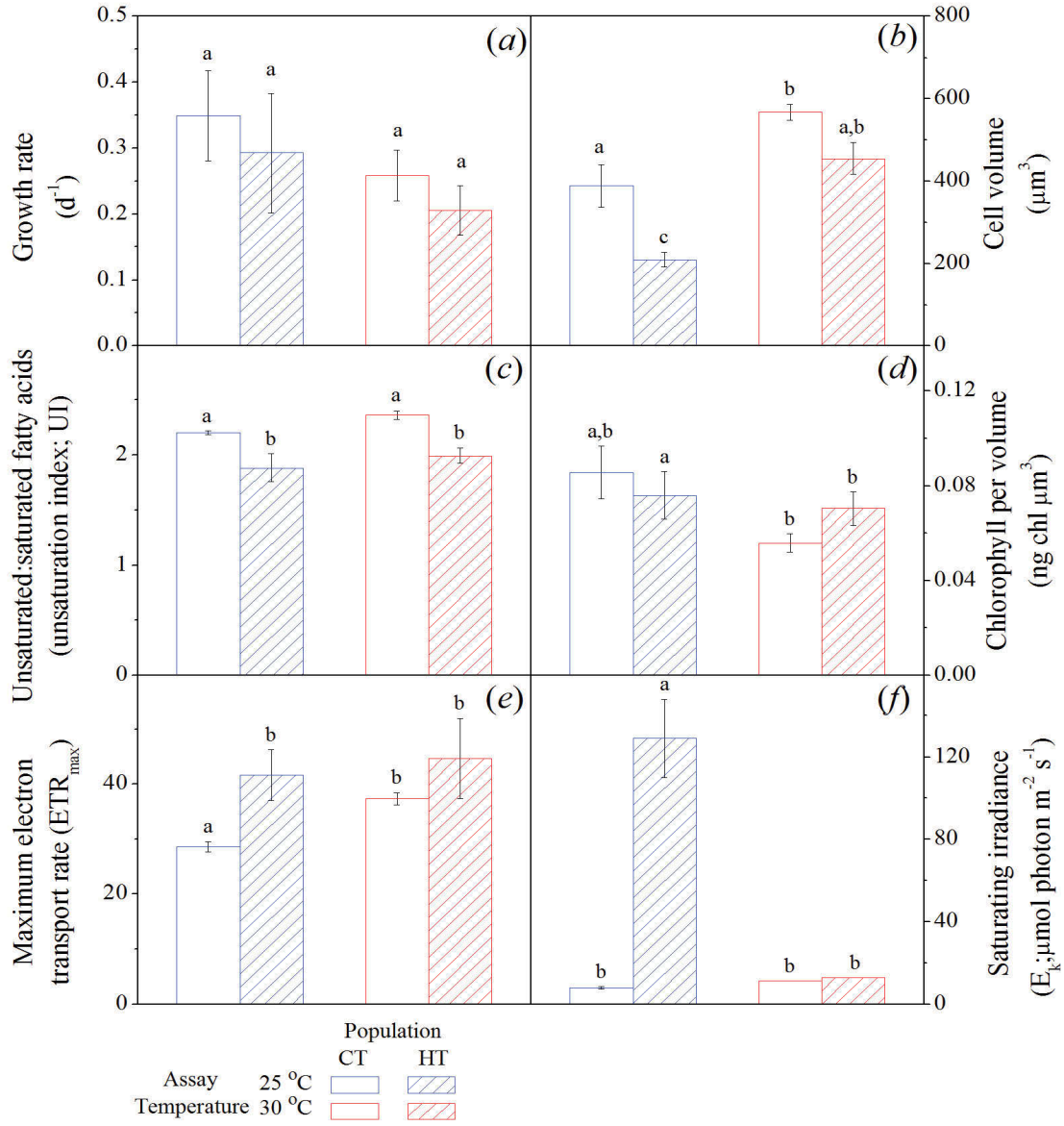

Figure 5.1 Physiological characterisation of the tropical dinoflagellate *Amphidinium massartii* following three years (~500 generations) of exposure to control (CT) or +5 °C (HT) conditions (25 °C versus 30 °C). Mean trait values (± standard error of the mean, n = 3) of control-temperature (CT)-population and high-temperature (HT)-populations (open versus hatched bars, respectively) when assayed at control (25 °C) and high (30 °C) temperatures (blue versus red bars, respectively) of (a) growth, (b) cell volume, (c) unsaturation index (unsaturated:saturated fatty acids), (d) chlorophyll *a* content per cell volume, (e) maximum electron transport rate, and (f) saturating irradiance. Letters above bars represent Tukey's honestly significant difference (HSD) between groups (p <0.05).

5.3.2 Trade-offs and evolution of the thermal performance curve following HT adaptation

TPCs of the tropical, benthic dinoflagellate, *A. massartii* demonstrated a significant amount of thermal plasticity, with growth rates >0.25 d^{-1} over a large temperature range (**Figure 5.2**). In the CT-population, the MLE of the T_{opt} for growth was 23.9 °C (95% CI, 21.6 to 25.9). However, long-term exposure to HT (~500 generations; 30 °C) significantly altered these thermal characteristics, with the directional changes for each trait summarised in **Table 5.1**.

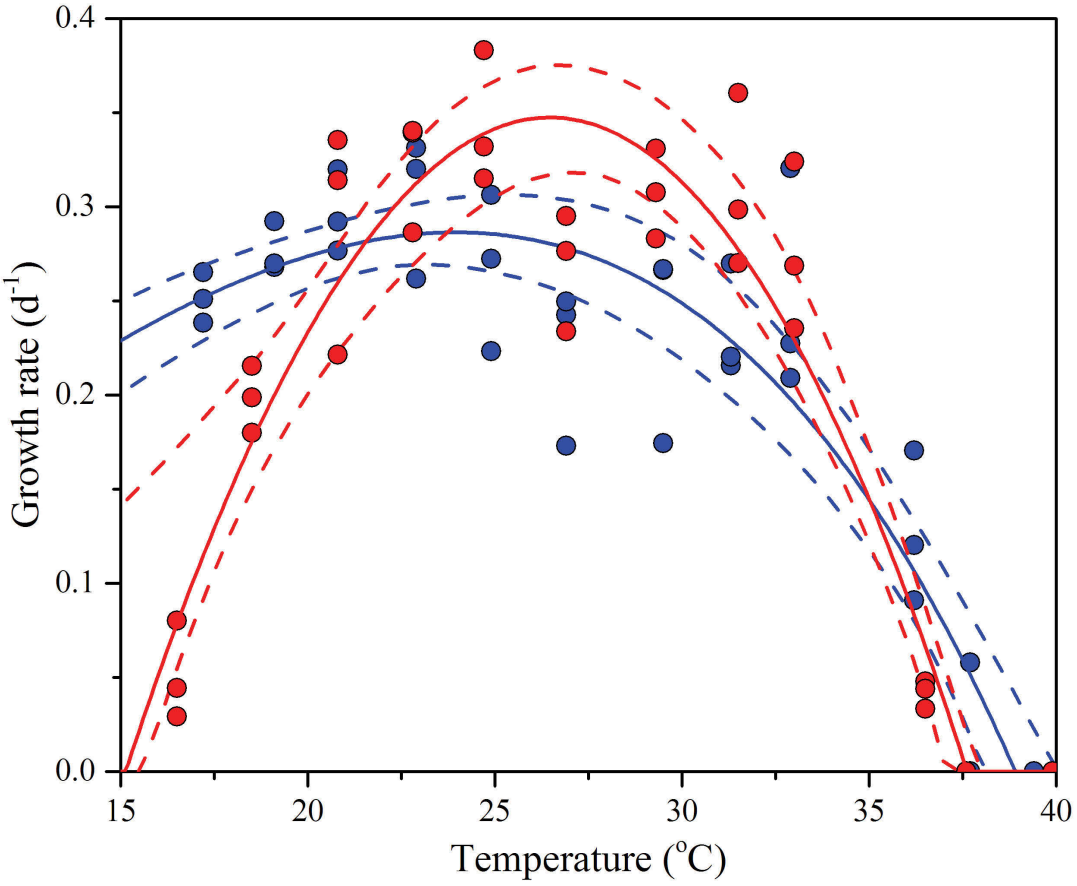

Figure 5.2 Thermal performance curves (TPC) of fitness in the dinoflagellate *A. massartii* depicting growth rate as a function of temperature in the control-temperature (CT)-population (blue symbols; n = 36, MSE = 0.0022) and high-temperature (HT)-population (red symbols; n = 36, MSE = 0.0017). Each symbol represents a distinct biological replicate. Solid lines represent maximum likelihood estimates (MLE) and broken lines correspond to the 95% confidence intervals (CI) of the bell-shaped function (Equation 5.4), of the CT and HT-populations (blue and red lines, respectively).

Table 5.1 A summary of the statistically significant directional changes in thermal characteristics of traits measured in *A. massartii* following long-term high-temperature exposure (~500 generations at 30 °C).

Trait	T_{opt}	V_{max}	*Niche*	CT_{min}	CT_{max}
Growth	↑	↑	↓	↑	↓
Carbon fixation	=	↑	=	=	=
N uptake	↑	↑	=	=	=
P uptake	=	↑	=	=	↓
Photochemistry (ϕ_{PSII})	=	↓	↓	↑	=
Photoprotection (NPQ)	↓	↑	=	=	=

Shown are T_{opt} (thermal optimum), V_{max} (maximum trait value attained), *Niche* (thermal niche width), CT_{min} (critical minimum temperature), CT_{max} (critical maximum temperature). Arrows depict the directional change in trait value of HT-population relative to CT-population, = means no detectable change.

The HT-population attained higher maximum growth rates (0.35 d^{-1}) at a warmer T_{opt} of 26.6 °C (95% CI, 26.0 to 28.2), in comparison to the CT-population (0.29 d^{-1}; ~23.9 °C)– corresponding to a 20% enhancement in fitness at temperatures almost 3 °C warmer (**Table 5.2a**; **Figure 5.2**). However, this increased fitness in the HT-population at warmer temperatures, was associated with a 40% contraction of the thermal niche (95% CI, 53 to 17) and a warmer CT_{min} (+14.6 °C; 95% CI, 5.1 to 15.5); effectively increasing the thermal sensitivity of the HT-population to colder temperatures (**Table 5.2a**; **Figure 5.2**). Although, growth ceased for both the CT- and HT- populations at temperatures ≥38 °C, the HT-population displayed enhanced resistance to these lethal temperatures with longer lethal exposure times (**Figure 5.3**). Results indicate that the Lex_{50} for the HT-population was ~80 h longer than the CT-population at 40 °C, with a Lex_{50} of 160 h (R^2 =0.90), compared to 24 h in the CT-population (R^2 =0.86; **Figure 5.3a**). In contrast to the CT-population, where 50% of cells exposed to 38 °C were not viable within 80 h (R^2 =0.96), no lethal exposure time for the HT-population could be calculated and was estimated to be longer than 200 h (**Figure 5.3b**).

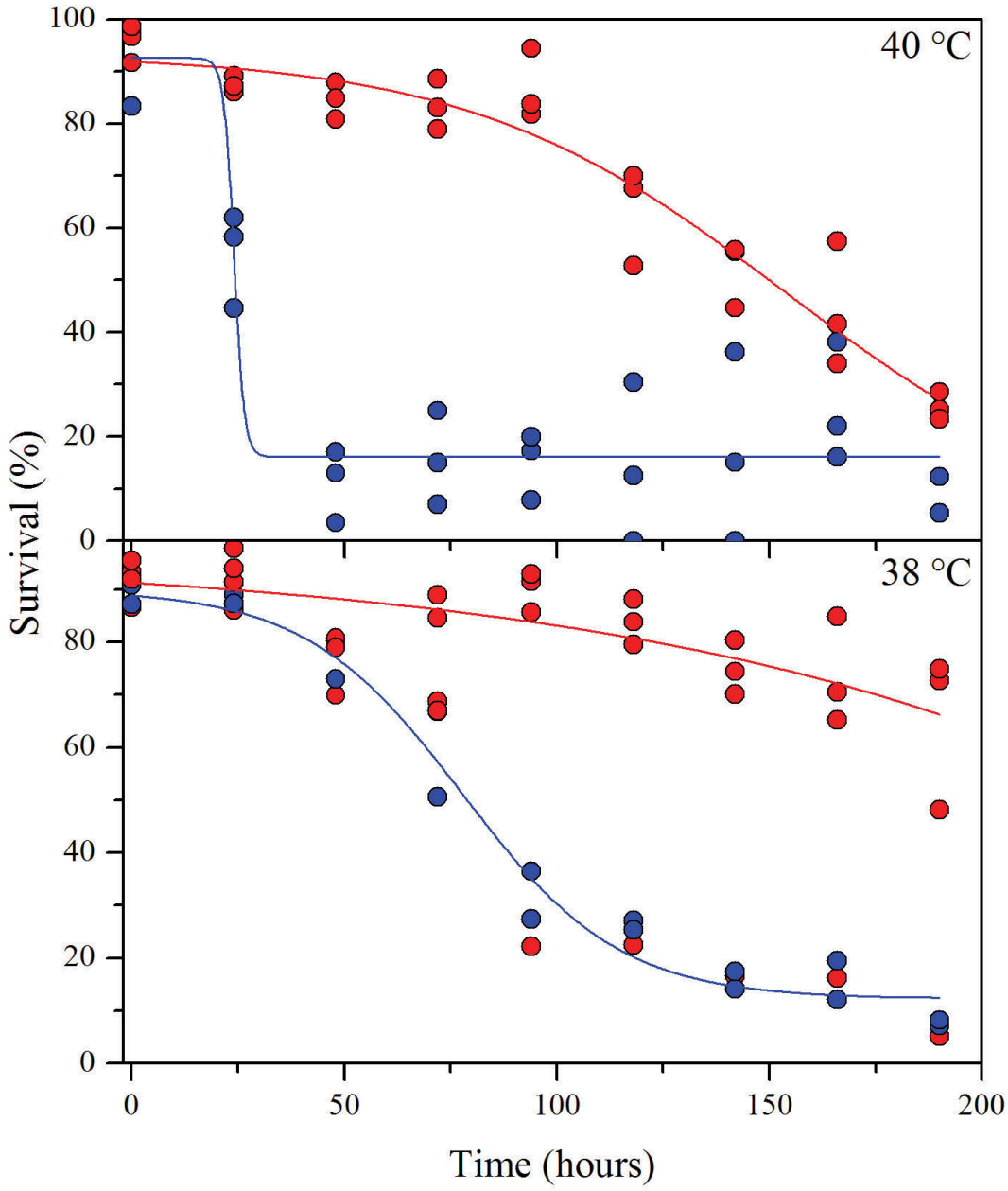

Figure 5.3 Exposure-response curves in the dinoflagellate *A. massartii* representing the percentage of viable cells (negative for SYTOX green nucleic acid stain) as a function of time (hours) of control-temperature (CT)-population (blue symbols; n = 12) and high-temperature (HT)-populations (red symbols; n = 12) assayed at the two highest temperatures (a) 40 ^{o}C and (b) 38 ^{o}C where growth was not observed. Each symbol represents a distinct biological replicate. Solid lines represent maximum likelihood estimates (MLE) of the exposure-response function of the CT- and HT-populations (blue and red lines, respectively).

Table 5.2a Estimated thermal performance curve (TPC) parameters and associated uncertainty for control-temperature (CT)- and high-temperature (HT)-populations calculated from parametric bootstrapping for growth rate and gross primary productivity fitted using Equation 5.4; thermal optimum T_{opt}, trait value at thermal optimum V_{max}, critical maximum temperature CT_{max}, critical minimum temperature CT_{min} and thermal niche width. The mean squared error (MSE) approximation provides a measure of uncertainty of the fitted function, whereas the 95 % confidence intervals (CI) provide a measure of uncertainty on the derived parameters. The shift in TPC associated with HT adaptation (ΔHT) was calculated as the difference in derived parameters between the CT and HT population. These differences were considered to be significant at alpha = 0.05, if the 95% CI did not contain 0 (i.e. the null hypothesis rejected) and are indicated as bold text.

		Growth rate (d^{-1})			Gross primary productivity (ng C $cell^{-1}$ h^{-1})		
		CT	HT	ΔHT	CT	HT	ΔHT
T_{opt}	MLE	23.94	26.61	**2.83**	28.47	29.67	0.81
	95% CI	[21.60 , 25.95]	[25.99 , 28.26]	[0.56 , 5.55]	[25.73 , 42.71]	[27.32 , 31.70]	[-7.57 , 4.62]
V_{max}	MLE	0.29	0.35	**0.06**	1.08	1.904	**0.796**
	95% CI	[0.27 , 0.31]	[0.32 , 0.38]	[0.027 , 0.093]	[0.86 , 2.27]	[1.58 , 2.19]	[0.14 ,1.37]
CT_{max}	MLE	38.9	37.43	**-1.48**	36.57	36.66	0.1
	95% CI	[38.08 , 40.04]	[37.04 , 37.93]	[-2.69 , -0.48]	[34.76 , 44.87]	[36.50 , 37.68]	[-2.21 , 2.17]
CT_{min}	MLE	0.019	14.94	**14.57**	15.45	16.83	1.98
	95% CI	[0.00 , 5.79]	[6.38 , 15.59]	[5.06 , 15.55]	[0.018 , 36.32]	[5.60 , 18.29]	[-19.02 , 17.62]
Niche width	MLE	38.58	22.58	**-15.88**	22.06	19.97	-2.56
	95% CI	[33.24 , 39.89]	[21.68 , 30.75]	[-17.71 , -6.72]	[11.20 , 36.68]	[18.27 , 30.92]	[-17.29 , 10.99]
MSE		0.002	0.002		0.13	0.13	

Table 5.2b Estimated thermal performance curve (TPC) parameters and associated uncertainty for control-temperature (CT)- and high-temperature (HT)-populations calculated from parametric bootstrapping for non-photochemical quenching (NPQ) and effective quantum yield (ϕ_{PSII}) fitted using **Equation 5.4**; thermal optimum T_{opt}, trait value at thermal optimum V_{max}, critical maximum temperature CT_{max}, critical minimum temperature CT_{min} and thermal niche width. The mean squared error (MSE) approximation provides a measure of uncertainty of the fitted function, whereas the 95 % confidence intervals (CI) provide a measure of uncertainty on the derived parameters. The shift in TPC associated with HT adaptation (ΔHT) was calculated as the difference in derived parameters between the CT and HT population. These differences were considered to be significant at alpha = 0.05, if the 95% CI did not contain 0 (i.e. the null hypothesis rejected) and are indicated as bold text.

		Effective quantum yield (ϕ_{PSII}; a.u.)			Non-photochemical quenching (NPQ; a.u.)		
		CT	HT	ΔHT	CT	HT	ΔHT
T_{opt}	MLE	28.40	27.57	-0.84	28.26	26.75	**-1.45**
	95% CI	[27.65 , 29.19]	[26.18 , 29.53]	[-2.50 , 1.28]	[27.29 , 28.93]	[25.89 , 27.70]	[-0.17 , -2.62]
V_{max}	MLE	0.40	0.13	**-0.27**	0.49	0.59	**0.096**
	95% CI	[0.39 , 0.42]	[0.11 , 0.15]	[-0.30 , -0.25]	[0.47 , 0.51]	[0.57 , 0.61]	[0.13 , 0.07]
CT_{max}	MLE	38.11	37.67	-0.56	38.13	37.76	-0.56
	95% CI	[37.74 , 39.46]	[32.40 , 38.47]	[-5.9 , 0.43]	[37.70 , 39.93]	[36.64 , 38.96]	[0.84 , -2.28]
CT_{min}	MLE	0.009	13.78	**13.39**	0.07	0.011	-0.037
	95% CI	[0.00 , 5.43]	[1.49 , 17.89]	[0.78 , 17.61]	[0.00 , 7.78]	[0.00 , 1.67]	[1.24 , -7.63]
Niche width	MLE	38.01	23.65	**-14.18**	37.84	37.68	-0.079
	95% CI	[32.94 , 39.36]	[15.42 , 34.94]	[-22.43 , -2.43]	[31.17 , 38.80]	[35.84 , 38.87]	[6.49 , -2.25]
MSE		0.001	0.001		0.004	0.003	

Table 5.2c Estimated thermal performance curve (TPC) parameters and associated uncertainty for control-temperature (CT)- and high-temperature (HT)-populations calculated from parametric bootstrapping for nitrate (NO_x) and phosphate (PO_4) uptake fitted using **Equation 5.4**; thermal optimum T_{opt}, trait value at thermal optimum V_{max}, critical maximum temperature CT_{max}, critical minimum temperature CT_{min} and thermal niche width. The mean squared error (MSE) approximation provides a measure of uncertainty of the fitted function, whereas the 95 % confidence intervals (CI) provide a measure of uncertainty on the derived parameters. The shift in TPC associated with HT adaptation (ΔHT) was calculated as the difference in derived parameters between the CT and HT population. These differences were considered to be significant at alpha = 0.05, if the 95% CI did not contain 0 (i.e. the null hypothesis rejected) and are indicated as bold text.

		NO_X uptake (ng $cell^{-1}$ h^{-1})			Phosphate uptake (ng $cell^{-1}$ h^{-1})		
		CT	HT	ΔHT	CT	HT	ΔHT
T_{opt}	MLE	25.60	27.24	**1.63**	26.00	27.38	1.36
	95% CI	[24.46 , 26.64]	[25.97 , 28.10]	[0.03 , 3.08]	[24.98 , 26.94]	[26.19 , 28.19]	[-0.10 , 2.70]
V_{max}	MLE	0.065	0.093	**0.028**	0.003	0.005	**0.002**
	95% CI	[0.06 , 0.07]	[0.09 , 0.10]	[0.02 , 0.03]	[0.003 , 0.003]	[0.005 , 0.005]	[0.001 , 0.002]
CT_{max}	MLE	38.51	37.84	-0.79	38.59	37.03	**-1.54**
	95% CI	[37.97 , 39.70]	[36.88 , 38.66]	[-2.23 , 0.37]	[38.01 , 39.61]	[36.64 , 37.93]	[-2.72 , -0.36]
CT_{min}	MLE	0.04	0.62	0.23	0.02	0.07	0.02
	95% CI	[0.00 , 6.49]	[0.00 , 10.37]	[-4.82 , 9.60]	[0.00 , 3.40]	[0.00 , 9.10]	[-2.93 , 9.00]
Niche width	MLE	38.281	36.90	-1.43	38.45	36.76	-1.83
	95% CI	[32.31 , 39.56]	[27.91 , 38.31]	[-10.09 , 3.71]	[35.17 , 39.55]	[28.2 , 37.8]	[-10.34 , 1.29]
MSE		2.16	1.96		-0.005	0.005	

The maximum values (V_{max}) of ϕ_{PSII} were reduced by ~70% (95% CI, 72 to 64) in the HT-population and occurred over a smaller operational range of temperatures (**Table 5.2b**; **Figure 5.4a**). These results were evidenced by the lower V_{max} values for ϕ_{PSII} (0.13; 95% CI, 0.11 to 0.15) and a smaller niche width (-14.2 °C; 95% CI, -22.4 to -2.4 °C). Similar to our observations for growth, an increase in the CT_{min} (rather than a decrease in the CT_{max}) appeared responsible for this niche contraction, increasing by 13.4 °C (95% CI, 0.8 to 17.6 °C; **Table 5.2b**). Additionally, photoprotective mechanisms were altered following HT adaptation, with values of NPQ reaching higher maximum values (0.586; 95% CI, 0.567 to 0.608) in the HT-population, in comparison to 0.490 (95% CI, 0.471 to 0.514) the CT-population (**Table 5.2b**; **Figure 5.4b**). These differences were equivalent to an increase in NPQ of approximately 15%. Furthermore, there was greater regulated energy dissipation (NPQ) at colder temperatures in the HT-population, with a significantly cooler T_{opt}, -1.5 °C (95% CI, -0.17 to -2.60 °C) in comparison to the CT-population. Together these results suggest an up regulation of NPQ at colder temperatures in the HT-population; typically indicative of the absorption of light energy in excess of light utilisation and may be a result of the slowing of downstream processes such as C fixation.

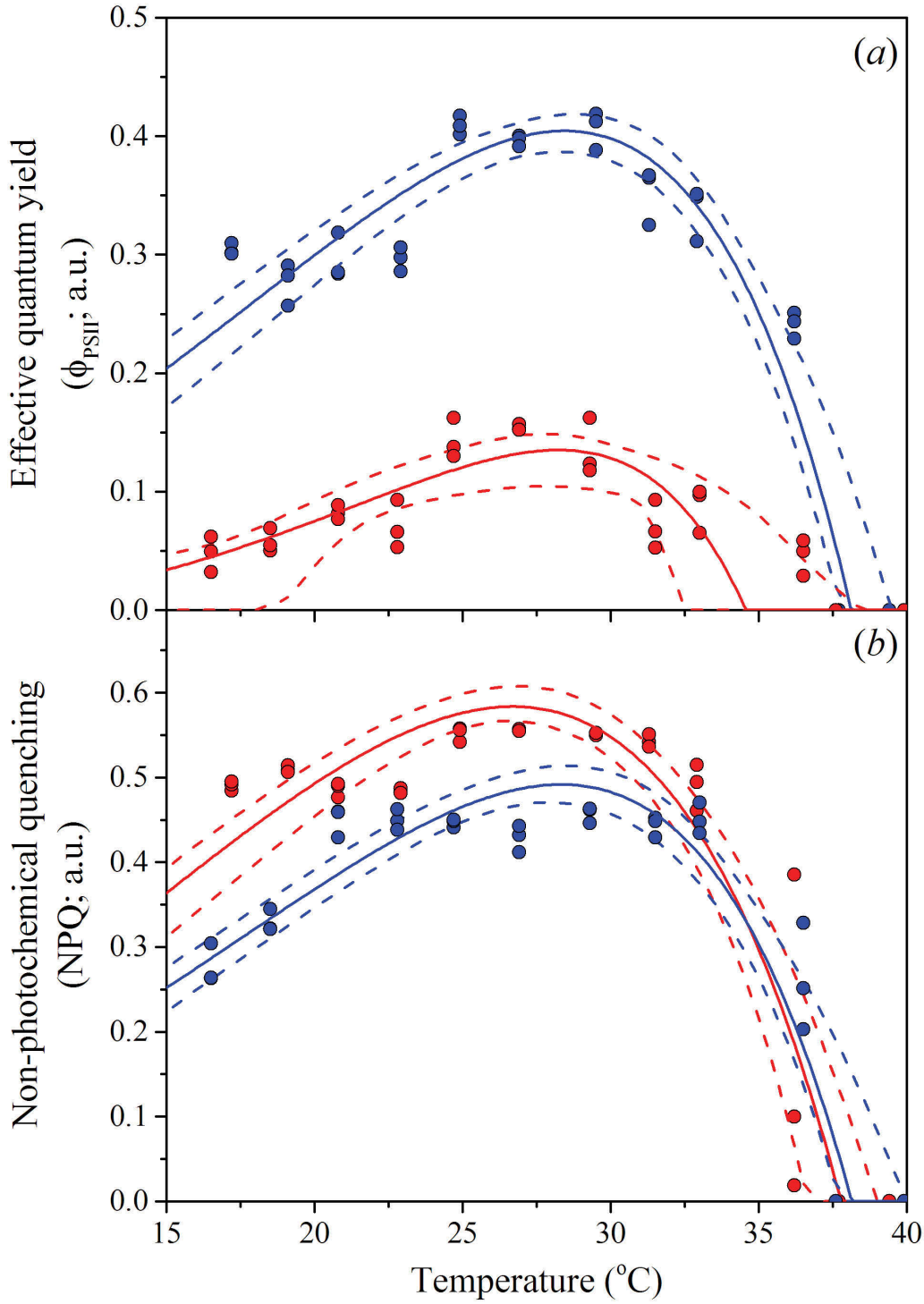

Figure 5.4 Thermal performance curves (TPC) of photophysiological parameters in the dinoflagellate *A. massartii* portraying (a) effective quantum yield (Φ_{PSII}), and (b) non-photochemical quenching (NPQ) in the control-temperature (CT)-population (blue symbols; n = 36, MSE = 0.0012) and high-temperature (HT)-population (red symbols; n = 36, MSE = 0.0010). Each symbols represents a distinct biological replicate. Solid lines represent maximum likelihood estimates (MLE) and broken lines correspond to the 95% confidence intervals (CI) of the bell-shaped function (Equation 5.4), of the CT and HT-populations (blue and red lines, respectively).

Indeed, C fixation was reduced at cold temperatures in the HT-population, with complete cessation at 18 °C, and although low (0.5 ng C cell h^{-1}), primary productivity was still measureable in the CT-population at this temperature (**Figure 5.5**). Low resolution of treatments at colder temperatures in conjunction with poor fits (MSE = 0.129) resulted in non-detectable differences in CT_{max}, CT_{min} and hence niche width between the two populations. However, a significant difference in maximum C fixation was evident, with the HT-population fixing almost 0.8 ng C cell h^{-1} more than the CT-population (**Figure 5.2b**). Similarly, maximum rates of N and P uptake were also greater in the HT-population with values of 0.0648 ng N cell h^{-1} (95% CI, 0.0627 to 0.0676 ng N cell h^{-1}) and 0.0031 ng P cell h^{-1} (95% CI, 0.0029 to 0.0032 ng P cell h^{-1}) – almost 1.5 times rates of uptake in the CT-population (**Figure 5.2c**; **Figure 5.6**). However, enhanced uptake rates of C, N and P in the HT-population were proportional, with no significant difference in C:N, or C:P molar ratios between the two populations (**Table 5.3**). These results suggest an increase in the absolute requirement of nutrients with HT adaptation, but no significant alteration in elemental stoichiometry of particulate matter.

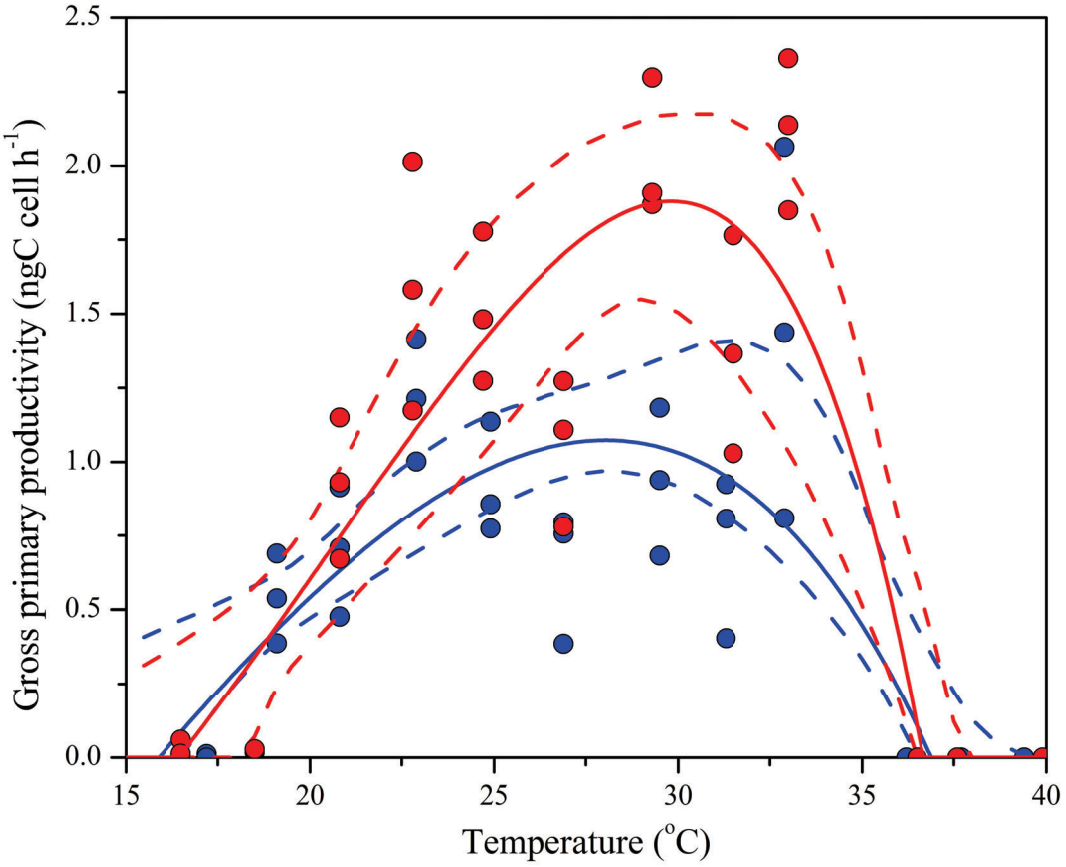

Figure 5.5 Thermal performance curves (TPC) of gross primary productivity (GPP) in the dinoflagellate *A. massartii* as a function of temperature in the control-temperature (CT)-population (blue symbols; n = 36, MSE = 0.1235) and high-temperature (HT)-population (red symbols; n = 36, MSE = 0.1296). Each symbols represents a distinct biological replicate. Solid lines represent maximum likelihood estimates (MLE) and broken lines correspond to the 95% confidence intervals (CI) of the bell-shaped function (**Equation 5.4**), of the CT and HT-populations (blue and red lines, respectively).

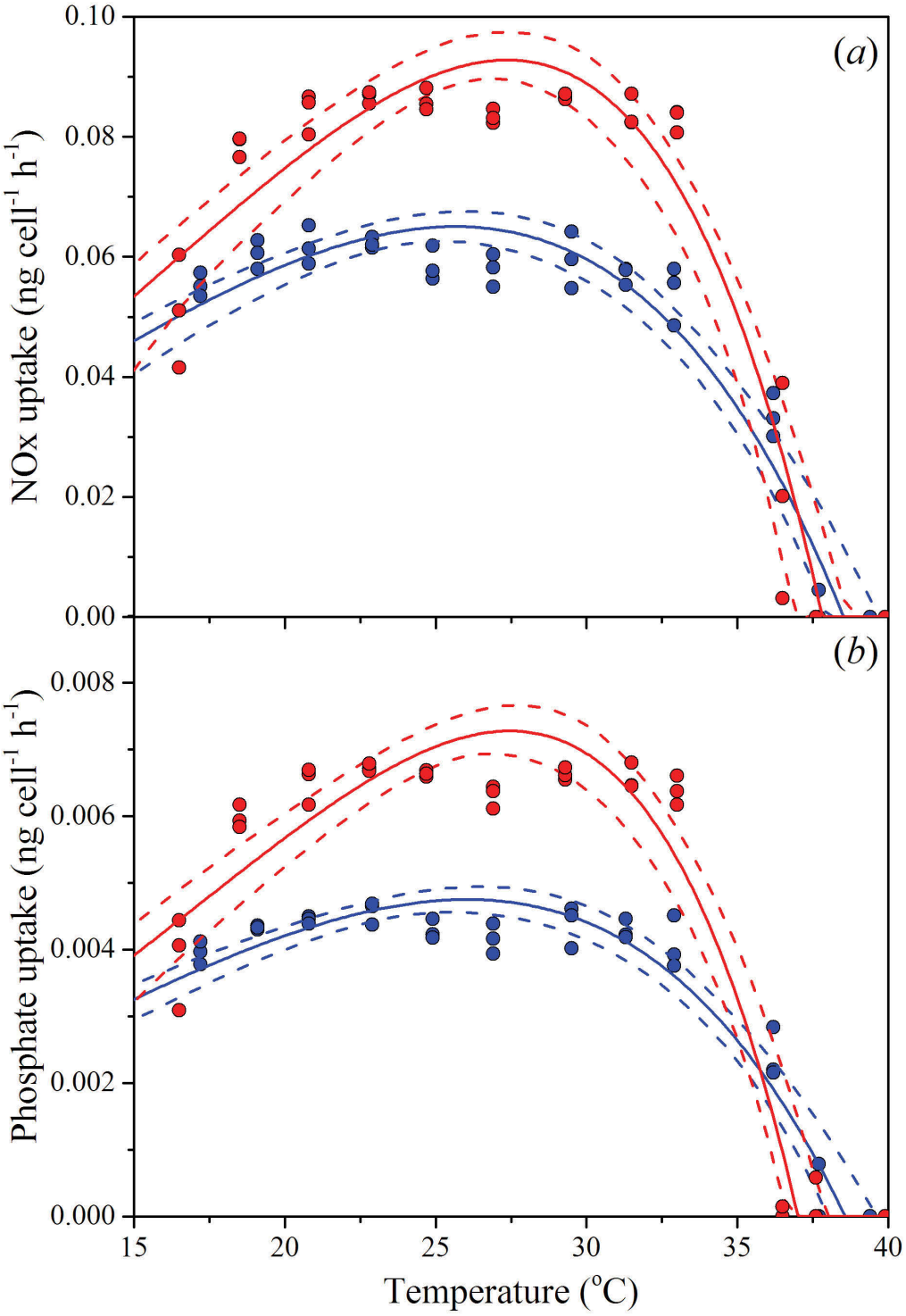

Figure 5.6 Thermal performance curves (TPC) of nutrient uptake (net flux of dissolved nutrients) in the dinoflagellate *A. massartii* depicting (a) NOx (nitrate and nitrite), and (b) phosphate uptake in the control-temperature (CT)-population (blue symbols; n = 36, MSE = NOx; 2.1618, PO_4;-0.0053) and high-temperature (HT)-population (red symbols; n = 36, MSE = NOx; 1.9561, PO_4;0.0046). Each symbol represents a distinct biological replicate. Solid lines represent maximum likelihood estimates (MLE) and broken lines correspond to the 95% confidence intervals (CI) of the bell-shaped function (**Equation 5.4**), of the CT and HT-populations (blue and red lines, respectively).

Table 5.3 Estimated maximum carbon to nitrogen (C:N) and carbon to phosphorus (C:P) molar ratios in organic matter and associated uncertainty for CT and HT populations calculated using maximum trait value at thermal optimum (V_{max}) estimates from parametric bootstrapping for carbon (GPP), nitrogen (NO_x) and phosphorus (PO_4^{3-}) uptake. A change in molar ratios associated with HT adaptation (ΔHT) was calculated as the difference in derived parameters between the CT and HT population. These differences were considered to be significant at alpha = 0.05, if the 95% CI did not contain 0 (i.e. the null hypothesis rejected) and are indicated as bold text.

		CT	HT	Δ
C:N	MLE	16.69	20.43	**28.13**
	95% CI	[13.70, 33.49]	[17.60 , 22.46]	[5.69 , 41.48]
C:P	MLE	349.94	402.31	**484.48**
	95% CI	[288.14 , 701.42]	[348.74 , 437.83]	[97.13 , 713.84]

5.4 Discussion

This study has revealed the likely emergence of warm-specialists following adaptation to supra-optimal temperatures (≈2 °C below CT_{max}) and sheds new light on the physiological costs and benefits associated with HT adaptation in phytoplankton. Reciprocal transplant assays revealed similar phenotypes of dinoflagellates exposed to short (i.e., weeks) or long (i.e., years) -term exposure to HT, with the majority of traits comparable between adapted and non-adapted populations. However, whether or not these traits remain fixed or are reversed when re-exposed to CT appeared to be trait-specific. The physiological constraints (costs and benefits) associated with HT-adaptation could only be examined by comparing TPCs between the CT- and HT-temperature populations. Long-term warming caused a reduction in thermal niche width but an increase in maximum growth rate, increased tolerance to short-term periods of extreme heat at a cost of cold sensitivity, and finally, greater maximum rates of C assimilation but higher nutrient demand.

5.4.1 High-temperature phenotype comprised of fixed and dynamic traits

The overall phenotype of the HT-population was a combination of both fixed and reversible traits as evidenced by comparisons between the CT- and HT-populations at the CT (25 °C; 5 generations). The biochemical composition of FA remained similar in the HT-population when re-exposed to 25 °C for several generations (**Figure 5.1c**), whereas other cellular characteristics were dynamic (e.g. chlorophyll *a* content; **Figure 5.1d**). These results demonstrate the time-scale of thermal exposure is important, especially when conducting multi-trait assessments, because some cellular changes may take longer to adjust than others, for example, weeks compared to hours or days.

Some traits in the HT-phenotype showed the same directional change as the CT-population when exposed to warmer temperatures but did not express the same values as the CT-population. For example, cell size remained almost half the volume of cells from the CT population (**Figure 5.1b**) and may help to explain why other traits expressed by the HT-population at HT were retained at control temperatures. Because smaller cells divide more quickly (Banse 1976, Raven 1998), this trait is likely to have resulted in similar fitness in the HT-population to the CT-population at both 25 and 30 °C (**Figure 5.1a**). Similarly, being smaller may enable the HT-population to retain

higher values of ETR_{max} (**Figure 5.1e**). This is because smaller cells have lowered pigment-packaging effects and as a result can meet energy requirements of downstream reactions at lower incident irradiances (Raven 1998) i.e., the HT-population can achieve higher ETR_{max} at the same light and temperature conditions as the larger cells of the CT-population. However, other parameters related to light acquisition (e.g. E_k) were not stable, increasing six-fold when exposed to CT (**Figure 5.1f**). These findings suggest a significant increase in the photon flux density required for the HT population to achieve the same ETR_{max} and meet energy demands of downstream processes, such as C fixation, at the CT. Indeed, in a future ocean, an increase in shoaling may help to facilitate this increased requirement of higher irradiance by providing an increase in the average irradiance of phototrophs in the upper ocean (Doney et al. 2012).

5.4.2 High-temperature phenotype remains indistinguishable from the control-temperature phenotype under intermediate temperatures

When exposed to temperatures previously encountered i.e., 25 and 30 °C, the HT phenotype could only be distinguished from the CT phenotype using a multi-trait analysis. Almost all measured traits had comparable values between the two populations during HT exposure, including fitness (i.e., growth rates; **Figure 5.1a**) and cell size (**Figure 5.1b**); traits that have previously been shown to be altered by HT adaptation in other phytoplankton types (coccolithophores; Schluter et al. 2014). Instead, differences between the dinoflagellate populations could only be detected on a biochemical basis, whereby adjustments in lipid composition were evident in the HT-population (i.e., increase in saturated FAs; **Figure 5.1c**). This result is consistent with those of HT tolerant higher plants (Upchurch 2008). Indeed, increased saturation of thylakoid membranes has been shown to help thermal stability of PSII in photosynthetic organisms (Tchernov et al. 2004). It is suggested this HT tolerance comes from stabilisation of lipid membranes (i.e. increase in saturated FAs) and reduces the susceptibility of damage by reactive oxygen species (Lesser 2006).

Changes in the FA composition of cells appeared to explain the different shapes of the TPC in the HT versus CT population. The alteration in biochemical composition appeared to benefit the HT-population under supra-optimal temperatures (i.e., short-lived extreme temperatures; **Figure 5.3**), but because this trait remains fixed when exposed to alternative conditions (e.g. ambient temperature; **Figure 5.1c**), their more

stable membranes appear to increase cellular susceptibility to cold temperature stress (**Figure 5.2**) (Sato et al. 1996) – representing clear physiological constraints in the HT-phenotype.

5.4.3 Costs and benefits associated with high-temperature phenotype

Enhanced overall fitness over a narrower range of temperatures and warmer thermal optimum (i.e., increase in growth, V_{max}, T_{opt} and contraction in niche width, **Table 5.2a**; **Figure 5.2**) suggests that HT-adaptation results in the emergence of high-temperature specialisation (Angilletta Jr et al. 2003). An increase of the T_{opt} is consistent with previous studies examining the evolution of the TPC following high temperature adaptation (bacteriophages,Knies et al. 2006, coccolithophores, Listmann et al. 2016). However, unlike Listmann et al. (2016) we do not find evidence of an increase in the $CT_{max,}$ for growth, but instead find the contrary, i.e., a decrease in the CT_{max} (**Table 5.2a**). Differences in isolation location may explain these differences, as low latitude (tropical) species (this study) typically have optimal temperatures closer to upper thermal limits (Chen 2015, Thomas et al. 2012); meaning the CT_{max} may be restricted from upwards shifts unlike high latitude species.

Benefits of high-temperature specialisation in this tropical, benthic dinoflagellate included increased tolerance to high temperature extremes (≥ 38 °C), evidenced by a lengthening of the lethal exposure time in comparison to the CT-population (**Figure 5.3**). These findings suggest that HT-adaptation benefits individuals through passive tolerance; enabling their persistence (rather than reproduction) during short-lived hostile periods (Pörtner 2002). However, an increase in cold sensitivity (i.e. warmer CT_{min}; **Table 5.2a**) is clear evidence of a generalist versus specialist trade-off (Angilletta Jr et al. 2003). These findings are significant as they suggest supra-optimal temperature adaptation may equip phytoplankton populations with advantageous life strategies to cope with extreme warming events, such as those predicted to increase in frequency with climate change (Meehl and Tebaldi 2004). In this particular benthic dinoflagellate, HT tolerance may increase its fitness in shallow water habitats during summer, but these populations are potentially at increased risk of seasonal cold temperature excursions.

For HT cells, being 50% smaller has additional benefits such as facilitating more effective acquisition of inorganic nutrients (C, N, P; Raven 1998 and references within) leading to higher V_{max} values of C fixation, N and P uptake in the HT-phenotype (**Figure 5.5**, **Figure 6.6** and **Supplementary Table 5.1)** and being used to support higher maximum growth rates (**Table 5.2**). Whilst these traits would be advantageous under oligotrophic conditions, smaller cells would be less competitive in nutrient-rich or variable nutrient environments due to reduced nutrient storage capacity (Marañón et al. 2013, Verdy et al. 2009). Given the important ecological role that benthic phytoplankton have in storing nutrients at the sediment-water interface (Dudley et al. 2001), this reduction in nutrient storage may make nutrients more available to the pelagic phytoplankton community and increase incidence of eutrophication in the above water column. Furthermore, despite lowered packaging effects satisfying downstream demands for electrons (e.g. C fixation), smaller cells are more susceptible to photoinhibition (Raven 1998) evidenced by the 70% reduction of Φ_{PSII} in the HT-population (**Figure 5.4a**). Although, smaller cells have been shown to rapidly repair PSII following damage (Key et al. 2010) elevated temperatures can slow this process (Takahashi and Murata 2008), resulting in net photoinhibition. The light sensitive nature of PSII in the HT-population is also reflected by increased NPQ at temperatures below the T_{opt} (i.e. ~26 °C; **Figure 5.4b**)– further evidence of the costs of high-temperature specialisation.

ation. Indeed, cold temperature exposure can mimic photoacclimation to high-light, acting as a signal for acclimation involving physiological, biochemical and molecular adjustments of the photosynthetic apparatus (Maxwell et al. 1995, Maxwell et al. 1994). Indeed, greatest values of NPQ in the HT-population (i.e. V_{max}; **Table 5.2**) coincide with temperatures at which C fixation and growth begin to decline towards the CT_{min} (~26 °C; **Figure 5.2** and **Figure 5.5**). As a result, the perception of excess light energy by the HT-population and preferential dissipation as heat, means at colder temperatures, fewer electrons may be directed to downstream processes and may create sink-limitations, e.g. in the Calvin Cycle. This may help explain why C fixation and growth become inhibited due to a reduction in available reductants (i.e. ATP and NADPH).

5.4.4 Implications and further research

In this study, a multi-trait analysis provided a phenotypic characterisation of a HT-adapted phytoplankton population, and in conjunction with TPCs furthered our understanding of the associated physiological constraints to warming. The emergence of a population specialised for higher temperatures but increased sensitivity to colder temperatures, has significant implications for niche evolution of phytoplankton adapted to warmer oceans. Firstly, thermal specialists can achieve greater maximum growth rates but over a narrower range of temperatures. In environments with increased thermal stratification this is potentially a competitive strategy, but is likely to be less competitive in fluctuating thermal environments e.g. extreme events. Secondly, smaller cells may facilitate more efficient nutrient acquisition and utilisation but trade-off maximum storage capacity, making HT phenotypes more competitive under oligotrophic conditions and less competitive under nutrient-rich environments. Finally, smaller cells can meet energy requirements at lower irradiances but are more susceptible to photoinhibition compared to larger cells in similar light environments. Together, these traits associated with thermal specialisation also make them specialised for low-light, low-nutrient environments and less competitive under fluctuating, nutrient-rich environments. As a result, it is possible benthic dinoflagellates may vertically migrate deeper into sediments where temperatures are more buffered from fluctuations in the above water column, light incidence is lower, and hence environmental conditions are more favourable. As a result, it is possible future warm oceans will create ideal conditions for HT-adapted dinoflagellates dominating under thermally-stratified environments. Contrary to previous findings in a temperate species of coccolithophore, we do not observe an increase in the CT_{max} with long-term warming but instead report an increase in the CT_{min} for a tropical dinoflagellate. Future studies should examine whether these disparities are related to functional-group or latitudinal differences between the two species. Finally, the future ocean represents a complex, multifaceted environment where alterations in the mean and variance of numerous environmental factors are changing concurrently. As a result, it remains unknown how the TPCs of existing genotypes will change when faced with multiple selection regimes, whether these adaptive mechanisms will facilitate the persistence of current species or whether they will be replaced by other species/strains better suited to these novel conditions.

5.5 Acknowledgements

The authors would like to thank Professor David Hutchins, Associate Professor David Suggett, Dr. Allison McInnes, Dr. Olivier Laczka, Dr. Milán Szabó, and Miss Charlotte Robinson for their insightful discussions, Professor Maria Byrne for access to the thermal gradient blocks and Miss Lisa Hou for the initial establishment of cultures used in this study.

This research was funded by a student scholarship awarded through the School of Life Sciences and Plant Functional Biology and Climate Change Cluster- (C3), University of Technology Sydney.

5.6 Literature cited

Angilletta Jr, M. J. (2013) Biochemical and Physiological Adaptations. in *The Princeton Guide to Evolution*. pp. 282.

Angilletta Jr, M. J., Wilson, R. S., Navas, C. A. and James, R. S. (2003) Tradeoffs and the evolution of thermal reaction norms. *Trends in Ecology & Evolution,* 18(5), pp. 234-240.

Angilletta, M. J. (2009) *Thermal adaptation: a theoretical and empirical synthesis,* Oxford University Press.

Baker, K. G., Robinson, C. M., Radford, D. T., McInnes, A. S., Evenhuis, C. and Doblin, M. A. (2016) Thermal performance curves of functional traits aid understanding of thermally induced changes in diatom-mediated biogeochemical fluxes. *Frontiers in Marine Science,* 3, pp. 44. doi:10.3389/fmars.2016.00044.

Baker, N. R. (2008) Chlorophyll fluorescence: a probe of photosynthesis *in vivo*. *Annual review of plant biology,* 59 pp. 89-113.

Banse, K. (1976) Rates of growth, respiration and photosynthesis of unicellular algae as related to cell size– a review. *Journal of Phycology,* 12(2), pp. 135-140.

Bennett, A. F. and Lenski, R. E. (1997) Evolutionary adaptation to temperature. VI. Phenotypic acclimation and its evolution in *Escherichia coli*. *Evolution,* 1, pp. 36-44.

Bennett, A. F. and Lenski, R. E. (2007) An experimental test of evolutionary trade-offs during temperature adaptation. *Proceedings of the National Academy of Sciences,,* 104((suppl 1)), pp. 8649-8654.

Carreau, J. P. and Dubacq, J. P. (1978) Adaptation of a macro-scale method to the micro-scale for fatty acid methyl transesterification of biological lipid extracts. *Journal of Chromatography A,* 151(3), pp. 384-390.

Chen, B. (2015) Patterns of thermal limits of phytoplankton. *Journal of Plankton Research*. doi:fbv009.

Clarke, A. (1996) The influence of climate change on the distribution and evolution of organisms. in Johnston, I. A. and Bennett, A. F., (eds.) *Animals and Temperature: Phenotypic and Evolutionary Adaptation*,Cambridge, UK: Cambridge University Press. pp. 377-407.

Collins, S., Rost, B. and Rynearson, T. A. (2014) Evolutionary potential of marine phytoplankton under ocean acidification. *Evolutionary Applications,* 7(1), pp. 140-155. doi:10.1111/eva.12120.

Davison, I. R. (1991) Environmental effects on algal photosynthesis: temperature. *Journal of Phycology,* 27(1), pp. 2-8.

Doney, S. C., Ruckelshaus, M., Duffy, J. E., Barry, J. P., Chan, F., English, C. A., Galindo, H. M., Grebmeier, J. M., Hollowed, A. B. and Knowlton, N. (2012) Climate change impacts on marine ecosystems. *Marine Science,* 4. doi:10.1146/annurev-marine-041911-111611.

Dudley, B. J., Gahnström, A. M. E. and Walker, D. I. (2001) The role of benthic vegetation as a sink for elevated inputs of ammonium and nitrate in a mesotrophic estuary. *Marine Ecology Progress Series,* 219, pp. 99-107.

Eppley, R. W. (1972) Temperature and phytoplankton growth in the sea. *Fisheries Bulletin,* 70(4), pp. 1063-1085.

Falkowski, P. G., Barber, R. T. and Smetacek, V. (1998) Biogeochemical controls and feedbacks on ocean primary production. *Science,* 281(5374), pp. 200-206.

Folch, J., Lees, M. and Sloane-Stanley, G. H. (1957) A simple method for the isolation and purification of total lipids from animal tissues. *Journal of biological chemistry,* 226(1), pp. 497-509.

Guillard, R. R. and Ryther, J. H. (1962) Studies of marine planktonic diatoms. I. *Cyclothella nana* Hustedt and *Detonula confervacea* Gran. *Canadian journal of microbiology,* 8(2), pp. 229-239.

Hillebrand, H., Dürselen, C. D., Kirschtel, D., Pollingher, U. and Zohary, T. (1999) Biovolume calculation for pelagic and benthic microalgae. *Journal of Phycology,* 35(2), pp. 403-424.

Hoenig, M., Lee, R. J. and Ferguson, D. C. (1989) A microtiter plate assay for inorganic phosphate. *Journal of biochemical and biophysical methods,* 19(2), pp. 249-251.

Hofmann, G. E. and Todgham, A. E. (2010) Living in the now: physiological mechanisms to tolerate a rapidly changing environment. *Annual Review of Physiology,* 72, pp. 127-145.

Hou, L. (2011) *Variability in the thermal response of the microalga Amphidinium massartii*. Unpublished Honours, University of Technology Sydney.

Huertas, I. E., Rouco, M., López-Rodas, V. and Costas, E. (2011) Warming will affect phytoplankton differently: evidence through a mechanistic approach. *Proceedings of the Royal Society B: Biological Sciences,* 278(1724), pp. 3534-3543.

Huey, R. B. and Berrigan, D. (1996) Testing evolutionary hypotheses of acclimation. in Johnston, I. A. and Bennett, A. F., (eds.) *Animals and temperature: Phenotypic and evolutionary adaptation*,Cambrige, UK: Cambridge University Press. pp. 205-237.

Huey, R. B. and Kingsolver, J. G. (1989) Evolution of thermal sensitivity of ectotherm performance. *Trends in Ecology & Evolution,* 4(5), pp. 131-135.

Johnston, I. A. and Bennett, A. F. (1996) *Animals and Temperature: Phenotypic and Evolutionary Adaptation, Society for Experimental Biology seminar series,* Cambridge, UK: Cambridge University Press.

Kawai, Y. and Wada, A. (2007) Diurnal sea surface temperature variation and its impact on the atmosphere and ocean: A review. *Journal of oceanography,* 63(5), pp. 721-744.

Key, T., McCarthy, A., Campbell, D. A., Six, C., Roy, S. and Finkel, Z. V. (2010) Cell size trade‐offs govern light exploitation strategies in marine phytoplankton. *Environmental microbiology,* 12(1), pp. 95-104.

Knies, J. L., Izem, R., Supler, K. L., Kingsolver, J. G. and Burch, C. L. (2006) The genetic basis of thermal reaction norm evolution in lab and natural phage populations. *PLoS biology,* 4(7), pp. 10.1371/journal.pbio.0040201. doi:e201.

LaJeunesse, T. C., Lambert, G., Andersen, R. A., Coffroth, M. A. and Galbraith, D. W. (2005) *Symbiodinium* (Pyrrhophyta) genome sizes (DNA content) are the smallest among dinoflagellates. *Journal of Phycology,* 41(4), pp. 880-886.

Lee, J. J., Olea, R., Cevasco, M., Pochon, X., Correia, M., Shpigel, M. and Pawlowski, J. (2003) A marine dinoflagellate, *Amphidinium eilatiensis* n. sp., from the benthos of a mariculture sedimentation pond in Eilat, Israel. *Journal of Eukaryotic Microbiology,* 50(6), pp. 439-448.

Lesser, M. P. (2006) Oxidative stress in marine environments: biochemistry and physiological ecology. *Annual Review of Physiology,* 68, pp. 253-278.

Lévy, M., Jahn, O., Dutkiewicz, S. and Follows, M. J. (2014) Phytoplankton diversity and community structure affected by oceanic dispersal and mesoscale turbulence. *Limnology and Oceanography: Fluids and Environments,* 4(1), pp. 67-84.

Listmann, L., LeRoch, M., Schlüter, L., Thomas, M. K. and Reusch, T. B. H. (2016) Swift thermal reaction norm evolution in a key marine phytoplankton species. *Evolutionary Applications*. doi:10.1111/eva.12362.

Litchman, E. and Klausmeier, C. A. (2008) Trait-based community ecology of phytoplankton. *Annual Review of Ecology, Evolution, and Systematics,* 39, pp. 615-639.

Lohuis, M. R. and Miller, D. J. (1998) Genetic transformation of dinoflagellates (*Amphidinium* and *Symbiodinium*): expression of GUS in microalgae using heterologous promoter constructs. *The Plant Journal,* 13(3), pp. 427-435.

Marañón, E., Cermeño, P., López‐Sandoval, D. C., Rodríguez‐Ramos, T., Sobrino, C., Huete‐Ortega, M., Blanco, J. M. and Rodríguez, J. (2013) Unimodal size scaling of phytoplankton growth and the size dependence of nutrient uptake and use. *Ecology letters,* 16(3), pp. 371-379.

Maxwell, D. P., Falk, S. and Huner, N. P. A. (1995) Photosystem II excitation pressure and development of resistance to photoinhibition. I. Light harvesting complex II abundance and zeaxanthin content in *Chlorella vulgaris*. *Plant Physiology,* 107, pp. 687-694.

Maxwell, D. P., Falk, S., Trick, C. G. and Huner, N. P. A. (1994) Growth at low temperature mimics high-light acclimation in *Chlorella vulgaris*. *Plant Physiology,* 105, pp. 535-543.

Meehl, G. A. and Tebaldi, C. (2004) More intense, more frequent, and longer lasting heat waves in the 21st century. *Science,* 305(5686), pp. 994-997.

Pörtner, H. O. (2002) Climate variations and the physiological basis of temperature dependent biogeography: systemic to molecular hierarchy of thermal tolerance in animals. *Comparative Biochemistry and Physiology Part A: Molecular & Integrative Physiology,* 132(4), pp. 739-761.

Ralph, P. J. and Gademann, R. (2005) Rapid light curves: a powerful tool to assess photosynthetic activity. *Aquatic botany,* 82(3), pp. 222-237.

Raven, J. A. (1998) The twelfth Tansley Lecture. Small is beautiful: the picophytoplankton. *Functional Ecology,* 12(4), pp. 503-513.

Reusch, T. B. and Boyd, P. W. (2013) Experimental evolution meets marine phytoplankton. *Evolution,* 67(7), pp. 1849-59. doi:10.1111/evo.12035.

Sato, N., Sonoike, K., Kawaguchi, A. and Tsuzuki, M. (1996) *Contribution of lowered unsaturation levels of chloroplast lipids to high temperature tolerance of photosynthesis in Chlamydomonas reinhardtii*. *Journal of Photochemistry and Photobiology B: Biology,* 36(3), pp. 333-337.

Schluter, L., Lohbeck, K. T., Gutowska, M. A., Groger, J. P., Riebesell, U. and Reusch, T. B. H. (2014) Adaptation of a globally important coccolithophore to ocean warming and acidification. *Nature Climate Change,* 4(11), pp. 1024-1030. doi:10.1038/nclimate2379.

Schnetger, B. and Lehners, C. (2014) Determination of nitrate plus nitrite in small volume marine water samples using vanadium (III) chloride as a reduction agent. *Marine Chemistry,* 160, pp. 91-98.

Shoaf, W. T. and Lium, B. W. (1976) Improved extraction of chlorophyll a and b from algae using dimethyl sulfoxide. *Limnology and Oceanography,* 21(6), pp. 926-928.

Suggett, D. J., Goyen, S., Evenhuis, C., Szabó, M., Pettay, D. T., Warner, M. E. and Ralph, P. J. (2015) Functional diversity of photobiological traits within the genus Symbiodinium appears to be governed by the interaction of cell size with cladal designation. *New Phytologist,* 208(2), pp. 370-381.

Takahashi, S. and Murata, N. (2008) How do environmental stresses accelerate photoinhibition? *Trends in plant science,* 13(4), pp. 178-182.

Tchernov, D., Gorbunov, M. Y., de Vargas, C., Narayan Yadav, S., Milligan, A. J., Häggblom, M. and Falkowski, P. G. (2004) Membrane lipids of symbiotic algae are diagnostic of sensitivity to thermal bleaching in corals. *Proceedings of the National Academy of Sciences of the United States of America,* 101(37), pp. 13531-13535. doi:10.1073/pnas.0402907101.

Thomas, M. K., Kremer, C. T., Klausmeier, C. A. and Litchman, E. (2012) A Global Pattern of Thermal Adaptation in Marine Phytoplankton. *Science,* 338(6110), pp. 1085-1088. doi:10.1126/science.1224836.

Upchurch, R. G. (2008) Fatty acid unsaturation, mobilization, and regulation in the response of plants to stress. *Biotechnology letters,* 30(6), pp. 967-977.

Verdy, A., Follows, M. and Flierl, G. (2009) Optimal phytoplankton cell size in an allometric model. *Marine Ecological Progress Series,* 379, pp. 1-12.

Welschmeyer, N. A. (1994) Fluorometric analysis of chlorophyll *a* in the presence of chlorophyll *b* and pheopigments. *Limnology and Oceanography,* 39(8), pp. 1985-1992.

5.7 Supplementary Tables

Supplementary Table 5.1 Net flux of nitrate (NO_3^-) and phosphate (PO_4^{3-}) in CT- and HT-populations of *A. massartii* at 25 and 30 °C estimated using cell size data from reciprocal transplant assay and nutrient data from thermal performance curve (TPC) experiments.

A. massartii population	Assay temperature	NO_3^- uptake	PO_4^{3-} uptake
	(°C)	(ng μ m^3 h^{-1})	(ng μ m^3 h^{-1})
CT	25	1.0×10^{-4}	1.0×10^{-5}
	30	7.0×10^{-5}	7.0×10^{-6}
HT	25	4.0×10^{-4}	3.0×10^{-4}
	30	1.6×10^{-4}	1.6×10^{-4}

CHAPTER 6:
GENERAL DISCUSSION

The healthy functioning of our marine ecosystems is not only dependent on the abundance and productivity of phytoplankton but also the composition of these communities, as it is this community structure that influences food webs and biogeochemical cycling. Examining how bottom-up environmental processes regulate phenotypic distributions of phytoplankton can further our understanding of ecological and biogeochemical niches and help to determine the likelihood of these changing under ocean climate change. In this thesis, I have addressed some of the existing gaps in knowledge of the direct implications of warming on phytoplankton. In particular, I present data that contributes towards a better understanding of how the overall phenotype and underlying FTs are linked to the ocean cycling of C, Si and N and how these processes are affected by temperature. A combination of field and laboratory studies delivers new information on environmental processes that control FT expression, in particular temperature, and how acclimation and adaptation at the cellular level influence the overall phenotype. The key findings and implications for these insights are discussed in the following sections and future research directions that transpire from the thesis are presented.

6.1 The role of functional trait diversity in regulating biogeochemical cycling

While species diversity at the community-level provides resilience to ecosystem disturbance, FT diversity at the cellular level (i.e., phenotypic plasticity) allows species to persist in unfavorable conditions; effectively expanding extant niches. Examining FT diversity over spatially diverse gradients provides insight into the range of natural FT variability, how clusters of environmental characteristics select for different phenotypes, and the primary controlling factors of FT expression. This information can be used to map the spatial distributions of phenotypes and, when superimposed over the biogeographical provinces of Longhurst (2010), provides an opportunity to link phytoplankton phenotypes with their biogeochemical functions.

The FT spatial mapping approach was adopted in **Chapter 3** to survey an important diatom-related FT over two distinct and ecologically important biogeographical provinces of Northern Australia. The study showed that the Arafura-Timor Shelf and Coral Sea fostered diatom communities that were clearly different from one another, in terms of both structure and function. The well-mixed and more silicic-acid-rich waters

of the Arafura-Timor Shelf supported communities dominated by more heavily silicified taxa and centric species, whereas the more stable and oligotrophic Coral Sea favored less silicified and pennate species. The phenotype therefore played a significant role in the determining the overall community structure and silicification, and in turn could be shown to control differences in organic matter composition (POC:BSi), BSi production and the capacity for the downward export of C between the two ocean provinces. By linking silicification, a FT that is entwined with the role diatoms play in C and Si cycling, this study demonstrated the informative power that FT mapping can provide in enhancing our understanding of how different clusters of environmental properties influence phytoplankton phenotypes, and in turn, control differences in biogeochemical fluxes between different oceans.

6.2 Environmental 'filtering' on functional traits

Spatial mapping of silicification not only revealed the diversity of the diatom flora present and the variability in Si and C fluxes, but also offered a snapshot view of how the biogeochemical role of diatoms may be altered by ocean climate change (**Chapter 4**). By studying the emergent phenotypes and their associated biogeochemical processes in marine environments that are similar to those forecasted for future ocean regions, this thesis offered predictions of how current marine cycling in other regions may be affected under future climate change. The warm, oligotrophic and Si poor conditions of the Coral Sea selected for diatoms with less silicified frustules and morphologies adapted for low-silicate regimes (e.g. pennates; Finkel and Kotrc 2010). These findings suggest that diatom phenotypes with less silicified frustules are better suited for these conditions, and are likely to emerge in future oceans that are becoming increasingly warmer and more Si-poor (e.g. SE Australia; Thompson et al. 2009).

Diatom populations that currently inhabit ocean-warming hotspots, such as SE Australia show significant thermal tolerance and FT plasticity when exposed to short-term (hours) perturbations in temperature (**Chapter 3**) and therefore may possess the diversity required when faced with the longer-term decadal changes that are predicted. When diatoms were exposed to temperatures 10 °C higher than current *in situ* temperatures, no significant alterations in biogeochemically-related FTs were detected, including frustule silicification, which has previously been shown to decrease by ~5.7±1.5 % $°C^{-1}$ in *T.*

pseudonana cultures (Baker et al. 2016). Differences between these patterns in FTs may be related to higher-order processes, such as species sorting (i.e. selection by local environmental conditions), that are unavailable for a single species but are clearly important in maintaining the overall fitness of phytoplankton communities in response to environmental change (Litchman et al. 2012). In the case of species sorting, species with compatible FTs may replace redundant species with non-functional FTs (Cornwell and Ackerly 2009). This reshuffling is likely to occur within a phytoplankton community over a thermal gradient because species that are morphologically identical could have a different T_{opt}. As a result, at each temperature, the fittest diatom species could replace the previous 'unfit' diatom species and still possess the same FT value as the previous species (**Figure 6.1**).

In this way, temperature indirectly selects for a 'fit' frustule silicification value, due to its relationship with growth (Baker et al. 2016). These changes in community structure may help to explain conflicting reports on the effect of temperature on frustule silicification between laboratory (Baker et al. 2016) and field (**Chapter 4**) studies, as this reshuffling would be undetectable using flow cytometry methods alone. As a result, it is suggested that species-sorting may be the leading mechanism for community resilience to environmental change and hence investigating species traits in the context of other adaptive mechanisms (e.g. natural selection) is required, in order to determine how ecological and biogeochemical niches may be altered by future climate change (Litchman et al. 2012).

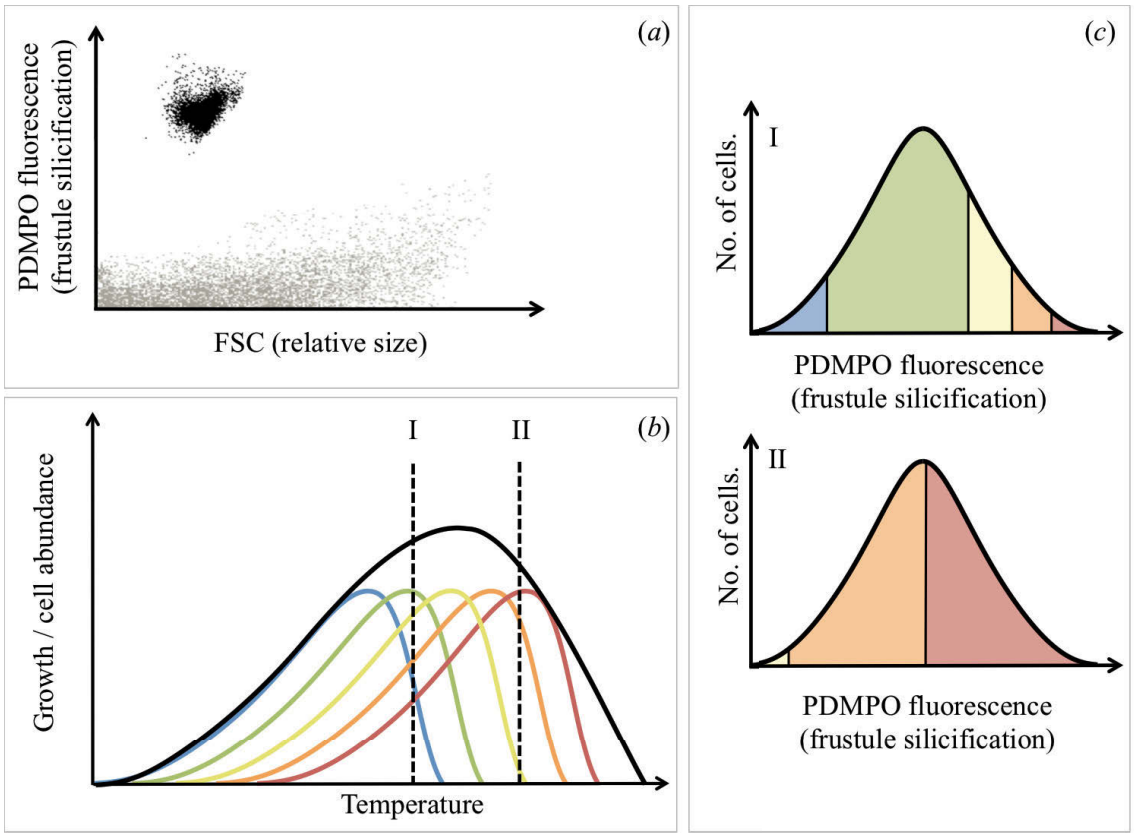

Figure 6.1 Natural selection on functional trait (FT) expression via species sorting; a proposed hypothesis arising from data presented in this thesis (a) A combination of flow cytometry and fluorescent stain, PDMPO (ex. 355; em. 488) is used to target a diatom community (black symbols) within a natural picophytoplankton community. Mean PDMPO fluorescence of the diatom community as a measure of the degree of frustule silicification. (b) A thermal performance curve is constructed using cell abundance of diatom community (black line) consisting of multiple species (different colours) differing in their thermal characteristics e.g. thermal optima. For each temperature, a different species will be more numerically dominant. (c) Population statistics of the FT (e.g. frustule silicification) are reported for the diatom community (black line). The FT value (e.g. median PDMPO fluorescence) observed at each temperature is weighted by species abundance and therefore reflects the FT trait value of the most dominant species due to their numerical dominance. As a result, the median FT value of the community remains consistent across a large temperature range due to the shuffling of species that occurs at each temperature and therefore reflects the locally 'optimal' trait value.

6.3 The effects of thermal acclimation and adaptation on marine biogeochemical cycling

To predict biogeographical shifts and displacements, previous studies have quantified TPCs for growth in many phytoplankton species (Boyd et al. 2013). Yet, until now, the accompanying implications for the biogeochemical processes they mediate were largely unknown, because the physiological costs, benefits and trade-offs associated with thermal acclimation and adaptation remain relatively unexplored. By adopting trait-based approaches in **Chapter 2** and **Chapter 5,** this thesis quantified TPCs for multiple FTs in two key phytoplankton functional types in order to provide a more comprehensive understanding of how thermal acclimation and adaptation affects current and future marine biogeochemical cycling.

A unique TPC may be expressed by individual FTs, varying in terms of their shape and thermal characteristics (Baker et al. 2016). Prior to this thesis, the TPCs and derived thermal properties (T_{opt}, thermal niche width, CT_{min}, CT_{max}) for many phytoplankton FTs had not been described and were hypothesised to scale with the growth response. Yet this thesis demonstrates many underlying FTs, such as net uptake of N, P and Si, operated at greater capacity over a broader range of temperatures than growth in model species from two different functional types; diatoms and dinoflagellates (**Chapter 2 and 5**). These findings suggest acquisition and utilisation of nutrients continues at similar rates despite reduced requirement for growth and implies other processes, such as maintenance and repair, are consuming these resources. The implications being that when phytoplankton are exposed to temperatures outside their optimal window for growth, elements such as C, N, P and Si are still being used but not being converted into new biomass. Consequently, these elements are not transferred to higher trophic levels, and instead are more likely to be recycled in upper surface waters. As a result, this thesis predicts increased nutrient recycling by phytoplankton with warming (or cooling) outside the thermal window for growth, demonstrating that the direct effects of temperature can alter the fate of elements such as N, P and Si in the marine environment.

Trade-offs between underlying FTs of the phenotype can affect the ecological and/or biogeochemical role of phytoplankton (Baker et al. 2016). Inverse correlations (i.e., trade-offs) between expressions of traits resulted in distinct phenotypes along a temperature gradient. For example, small, thick diatoms were characteristic of cold temperatures, whilst large, thin cells were evident at warmer temperatures (**Chapter 2**). Whilst a mechanistic understanding behind this trade-off has yet to be elucidated, it may result from an allocation trade-off (Angilletta Jr et al. 2003). In this case, a fixed quantity of Si is available to the diatom for frustule synthesis and a hypothetical difference in Si allocation between valve and girdle band formation could create distinctly different phenotypes at either end of the temperature gradient; building thicker valves at cold temperatures but more girdle bands at high temperatures, resulting in the formation of distinctly different phenotypes (**Figure 6.2**).

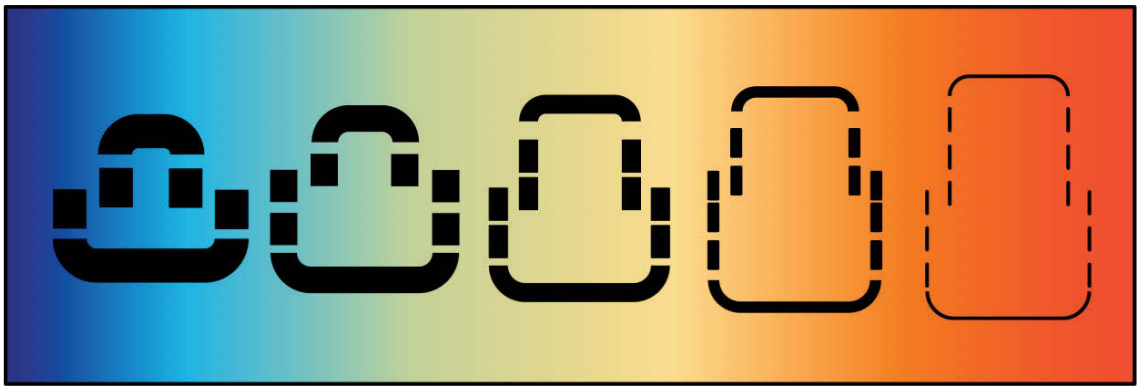

Figure 6.2 Hypothetical allocation tradeoff arising from findings presented in this thesis. An allocation tradeoff arises along a temperature gradient, between silicic acid distributed towards girdle band or valve synthesis. For each cell, the extreme upper and lower parts are valves, and the series of dashes on the sides represent girdle bands. At cold temperatures (cold colours), silicic acid is distributed towards valve synthesis resulting in small cells with thicker valves. At warm temperatures (warm colours), silicic acid is distributed towards girdle band synthesis resulting in larger cells with thinner valves.

The phenotypic plasticity observed over temperature gradients (**Chapter 2** and **5**) creates divergent ecological and biogeochemical roles of diatoms under different environmental conditions, similar to what has been shown in different ocean regions (Baines et al. 2010). For example, at supra-optimal temperatures where diatom frustules are thinner, increased vulnerability to grazers and bacterial/viral attack (Raven and Waite 2004), and greater dissolution rates (Baines et al. 2010, Kamatani 1982) leads to more Si being recycled within the water column (Nelson et al. 1995). In contrast, at cold temperatures where diatom frustules are thicker, greater cellular density and resistance to grazers (Raven and Waite 2004), will likely increase the downward export of Si and C. Indeed cell-specific silicification has been shown to substantially influence sinking rates of diatoms, increasing by a factor of 2-3 times in more heavily silicified diatoms from colder waters in comparison to less silicified diatoms from warmer waters (Antarctica versus Equatorial Pacific; Baines et al. 2010). It is, therefore, apparent that the biogeochemical and ecological niche of the cold-diatom phenotype has the capacity to accelerate the biological carbon pump by enhancing downward export of C. In comparison, the warm diatom phenotype plays a more significant role in the trophic transfer of C and the generation of silicic acid for use by future generations of upper ocean diatoms and other silicifiers. Understanding how these niches change along environmental gradients can help us to predict whether these roles may be altered by future environmental change: are thinner diatoms likely to be favorably selected by future warmer and less Si-rich oceans, like the phenotypes currently found in the Coral Sea (**Chapter 4**).

6.4 The emergence of new phenotypes from extant species

Predictions of future ocean functioning must also consider evolutionary processes that occur over hundreds of generations. In **Chapter 5,** I expanded upon the only other study of its kind (Schluter et al. 2014) by examining the FTs of a dinoflagellate population maintained at high temperature (ambient + 5 °C) for >500 cell divisions. Firstly, this long-term study demonstrated the capacity for extant species to alter thermal characteristics (e.g. their thermal optimum and niche width) in order to better suit their new environment. Secondly, in quantifying a number of traits over an unprecedented

range of temperatures, I provided new insights on the physiological constraints of adaptation to ocean warming.

Importantly, the costs associated with high-temperature adaptation were not detectable by comparing performance at control and high-temperatures alone (i.e., reciprocal transplant assay). Instead, it was only when each population was exposed to an extended range of environmental conditions (i.e., through TPCs) where variations in fitness were observed and associated physiological constraints could be identified. Adaptation to warming generated the emergence of a warm-specialist with higher maximum growth rates and warmer thermal optimum and specialisation for these traits resulted in: (i) smaller cells, (ii) increased tolerance to short-term periods of extreme heat at a cost of cold sensitivity, and (iii) higher maximum rates of C, N and P acquisition. It is these other characteristics of the warm-specialist phenotype that may result in low fitness in other low-nutrient or high-light environments. For example, when nutrients are in poor supply, growth rates facilitated by enhanced C, N, and P uptake are likely to be reduced, and are likely to be further constrained by their reduction in cell size, as smaller cells have reduced intracellular storage capacity (Marañón et al. 2013). Similarly, long-term (years; 500 generations) high-temperature adapted cells have increased light sensitivity and are better suited to low-light environments. As a result, it is possible the physiological mechanisms underlying specialisation to increased SST will only be viable in high-nutrient, low-light environments, and consequently, may alter ecological niche occupancies of extant species.

6.5 Perspectives for further research

This thesis has provided new information on FT responses to warming, the associated biogeochemical consequences and observations of how these traits change across environmental gradients. A number of questions have arisen from these findings and should be addressed in future research.

In this thesis, the thermal responses of various FTs were measured at a single time point, following a relatively short (weeks; 5 generations) acclimation period (Baker et al. 2016), or after a long (years; 500 generations) adaptation period (**Chapter 5**) but with no interim measurements. As a result, it remains unclear how these responses adjust (~hours), acclimate (~days-weeks) and adapt (~years) as a function of time, and if so, at what rate. Indeed the cardinal temperatures (*Topt*, CT_{min} and CT_{max}) and the overall shape of the TPC is likely to change with the duration of exposure (Schulte et al. 2011), but until recently this has not been demonstrated in phytoplankton (Chapter 5;Listmann et al. 2016, Padfield et al. 2016). In order to understand the rate at which phytoplankton respond to changes in temperature, future work should investigate the rate of thermal evolution in FTs. Priority should be given to measuring a single trait, namely cell size, in a few model species. The choice of this FT is two-fold. Firstly, many allometric relationships have been demonstrated for phytoplankton and can be predicted using measures of cell volume (see Finkel et al. 2009 and references within). Secondly, measures of cell size permit the use of high throughput techniques (e.g. automated microscopy imaging in conjunction with automated image analysis), providing the statistical power to identify detectable changes in the biological response over relatively small temperature increments (e.g. 2 °C). Indeed, this is important in the design of TPC experiments because increasing the number of species or FTs measured, should not be at the expense of the number of temperatures assayed- as these determine the accuracy in estimates of the key parameters of interest (e.g. T_{opt}, CT_{min}, and CT_{max}).

Despite the logistical constraint discussed above, collecting TPCs of multiple traits over a number of time points during acclimation should yield further insight into what FTs are more physiologically constrained or can adapt more readily than others, and whether these extant species will be able to adapt in time or be displaced by other better-suited species. Moreover, in **Chapter 5**, the capacity for adaptation in a major phytoplankton

type was demonstrated, and the benefits, costs and reversibility of this adaptation were explored. To my knowledge, few thermally-adapted taxa exist in culture collections; a calcifying cocolithophore (Emiliana huxleyi, Listmann et al. 2016, Schluter et al. 2014), two dinoflagellates (*Amphidinium massartii,* **Chapter 5**; *Symbiodinium sp.,* M. V. Oppen pers. comm.), a diatom (K. Schmidt pers. comm.) and a green alga (*Chlorella vulgaris*, Padfield et al. 2016). Other previously high-temperature adapted species investigated in Huertas et al. (2011) have since died (A. Flores-Moya pers. comm.). These insights highlight two aspects that should be carefully considered in future research. Firstly, to improve the generality of the documented trait responses, further research should be conducted with other biogeochemically or ecologically significant taxa, such as nitrogen fixers. Secondly, these organisms are invaluable tools for understanding evolution and should be deposited in to (inter)national culture collections so that they are available as a resources for further studies.

In **Chapter 2** and **5**, TPCs for a number of FTs and their sensitivities to temperature were presented, but the list is by no means exhaustive. It is possible that measurements used to characterise processes such as nutrient acquisition, i.e., the net flux of dissolved inorganic nutrients, are not representative of the effects of temperature on all underlying processes of nutrient acquisition. For example, the growth affinity of nitrate, which is a combination of maximum growth rate and the half saturation constant, is influenced by temperature (Reay et al. 1999). Yet, results from this thesis show nitrate uptake to be relatively unaffected by temperature, except at extremes (**Chapter 5**). Further research should be conducted to characterise the underlying physiological processes that shape these TPCs.

Another important consideration for future work is that the TPCs presented in this thesis were characterised under constant temperature, optimal light and nutrient replete conditions, and as such, will not accurately represent the physiological limits to phenotypic plasticity in the natural environment. Other bottom-up processes such as light and nutrient availability have been shown to alter characteristics of TPCs such as the height, width and thermal optimum (Edwards et al. 2016, Sandnes et al. 2005). Furthermore, TPCs differ in organisms exposed to stable or fluctuating environments (Gilchrist 1995). Observing how TPCs are altered by interacting factors e.g. CO_2 and temperature, will allow for better predictions of how ecological niche occupancy is

likely to change in the future. In conjunction, other ecological processes such as species sorting can occur in natural communities and may influence the TPCs collected from field samples (**Chapter 3**; **Figure 6.1)** To examine the influence of non-genetic and genetic contributions of species towards community-level TPCs of natural phytoplankton communities, flow cytometry coupled with sorting and sequencing could be used to; (i) target a subpopulation of the pico/nano-phytoplankton fraction, (ii) sort the targeted cells, and (iii) use molecular techniques to sequence and quantify the relative abundance of target cells present. Experimental designs such as these would be a valuable test of the hypothesised patterns and mechanisms presented in **Figure 6.1**.

Field studies presented in this thesis were conducted in one season, i.e., in austral spring 2015 (**Chapter 3**) and austral winter 2013 (**Chapter 4**), and as a result, may not be representative of the resident phytoplankton population in other seasons. Indeed, different morphotypes of diatom species are known to appear during winter compared to summer (Shimada et al. 2006) and as a result, the heavily silicified species in the Arafura-Timor Shelf may only be representative of the winter diatom community. Similarly, shifts in the diatom community may change interannually particularly before and after spring bloom events or during particular climate phenomena (e.g., El Nino). Hence, the TPC collected at Port Hacking, NSW in October 2015 may be representative of a post-bloom community (Hallegraeff 1981) with different thermal characteristics to a community collected at a different time. Future research should consider conducting similar sampling strategies but in higher resolution (e.g. seasonally, or monthly) to determine whether findings presented in this thesis are season-specific or can be temporally generalised to their respective water masses.

Finally, the development of UV-laser flow cytometry for use with the fluorescent tracer PDMPO (**Chapter 2, 3** and **4**) has provided a stepping-stone to advance knowledge in a number of areas of research. This thesis provided insight into the relationship between environmental gradients and the degree of silicification using relative changes in PDMPO fluorescence. However, in order to quantify rates of transformation of DSi into BSi using flow cytometry, further studies should work towards the advancements of this technique to be used as a proxy for quantities of Si (μmol Si $cell^{-1}$), as has been done in conjunction with fluorescence microscopy (McNair et al. 2015). In order to progress the use of flow cytometry to trace biogeochemical cycling, parallel samples quantified by flow cytometry and fluorescence microscopy could be used to generate a calibration curve relating PDMPO fluorescence to moles of Si deposited. However, it is likely calibration curves would need to be conducted for number of species in culture before generalisations could be made about mixed diatom communities. Secondly, the further development of fluorescent tracers that label other important biogeochemical cycles (e.g. N) mediated by other phytoplankton functional types (e.g. N_2-fixers) would enable multiple elemental cycles to be traced across spatially diverse gradients simultaneously, and provide a more holistic approach of the healthy functioning of the phytoplankton community as a whole. Applying these types of techniques can be used to further understand how the relationship between the composition of phytoplankton communities and the processes that they mediate are driven by changes in environmental conditions. This will provide invaluable insight into the health of future ocean ecosystem function.

6.6 Literature cited

Angilletta Jr, M. J., Wilson, R. S., Navas, C. A. and James, R. S. (2003) Tradeoffs and the evolution of thermal reaction norms. *Trends in Ecology & Evolution,* 18(5), pp. 234-240.

Baines, S. B., Twining, B. S., Brzezinski, M. A., Nelson, D. M. and Fisher, N. S. (2010) Cause and biogeochemical implications of regional differences in silification of marine diatoms. *Global Biogeochemical Cycles,* 24(4). doi:10.1029/2010GB003856.

Baker, K. G., Robinson, C. M., Radford, D. T., McInnes, A. S., Evenhuis, C. and Doblin, M. A. (2016) Thermal performance curves of functional traits aid understanding of thermally induced changes in diatom-mediated biogeochemical fluxes. *Frontiers in Marine Science,* 3, pp. 44. doi:10.3389/fmars.2016.00044.

Boyd, P. W., Rynearson, T. A., Armstrong, E. A., Fu, F., Hayashi, K., Hu, Z., Hutchins, D. A., Kudela, R. M., Litchman, E., Mulholland, M. R., Passow, U., Strzepek, R. F., Whittaker, K. A., Yu, E. and Thomas, M. K. (2013) Marine Phytoplankton Temperature versus Growth Responses from Polar to Tropical Waters – Outcome of a Scientific Community-Wide Study. *PLoS One,* 8(5), pp. e63091. doi:10.1371/journal.pone.0063091.

Cornwell, W. K. and Ackerly, D. D. (2009) Community assembly and shifts in plant trait distributions across an environmental gradient in coastal California. *Ecological Monographs,* 79(1), pp. 109-126.

Edwards, K. F., Thomas, M. K., Klausmeier, C. A. and Litchman, E. (2016) Phytoplankton growth and the interaction of light and temperature: A synthesis at the species and community level. *Limnology and Oceanography*. doi:10.1002/lno.10282.

Finkel, Z. V., Beardall, J., Flynn, K. J., Quigg, A., Rees, T. A. V. and Raven, J. A. (2009) Phytoplankton in a changing world: cell size and elemental stoichiometry. *Journal of Plankton Research*. doi:fbp098.

Finkel, Z. V. and Kotrc, B. (2010) Silica Use Through Time: Macroevolutionary Change in the Morphology of the Diatom Frustule. *Geomicrobiology Journal,* 27(6-7), pp. 596-608. doi:10.1080/01490451003702941.

Gilchrist, G. W. (1995) Specialists and generalists in changing environments. I. Fitness landscapes of thermal sensitivity. *American Naturalist,* 146(2), pp. 252-270.

Hallegraeff, G. M. (1981) Seasonal study of phytoplankton pigments and species at a coastal station off Sydney: importance of diatoms and the nanoplankton. *Marine Biology,* 61(2-3), pp. 107-118.

Huertas, I. E., Rouco, M., López-Rodas, V. and Costas, E. (2011) Warming will affect phytoplankton differently: evidence through a mechanistic approach.

Proceedings of the Royal Society B: Biological Sciences, 278(1724), pp. 3534-3543.

Kamatani, A. (1982) Dissolution rates of silica from diatoms decomposing at various temperatures. *Marine Biology,* 68(1), pp. 91-96. doi:10.1007/BF00393146.

Listmann, L., LeRoch, M., Schlüter, L., Thomas, M. K. and Reusch, T. B. H. (2016) Swift thermal reaction norm evolution in a key marine phytoplankton species. *Evolutionary Applications*. doi:10.1111/eva.12362.

Litchman, E., Edwards, K. F., Klausmeier, C. A. and Thomas, M. K. (2012) Phytoplankton niches, traits and eco-evolutionary responses to global environmental change. *Marine Ecology Progress Series,* 470, pp. 235-248. doi:10.3354/meps09912.

Marañón, E., Cermeño, P., López‐Sandoval, D. C., Rodríguez‐Ramos, T., Sobrino, C., Huete‐Ortega, M., Blanco, J. M. and Rodríguez, J. (2013) Unimodal size scaling of phytoplankton growth and the size dependence of nutrient uptake and use. *Ecology letters,* 16(3), pp. 371-379.

McNair, H. M., Brzezinski, M. A. and Krause, J. W. (2015) Quantifying diatom silicification with the fluorescent dye, PDMPO. *Limnology and Oceanography: Methods,* 13(10), pp. 587-599.

Nelson, D. M., Treguer, P., Brzezinski, M. A., Leynaert, A. and Queguiner, B. (1995) Production and dissolution of biogenic silica in the ocean - revised global estimates, comparison with regional data and relationship to biogenic sedimentation. *Global Biogeochemical Cycles,* 9(3), pp. 359-372. doi:10.1029/95gb01070.

Padfield, D., Yvon‐Durocher, G., Buckling, A., Jennings, S. and Yvon‐Durocher, G. (2016) Rapid evolution of metabolic traits explains thermal adaptation in phytoplankton. *Ecology letters,* 19(2), pp. 133-142.

Raven, J. and Waite, A. (2004) The evolution of silicification in diatoms: inescapable sinking and sinking as escape? *New Phytologist,* 162(1), pp. 45-61.

Reay, D. S., Nedwell, D. B., Priddle, J. and Ellis-Evans, J. C. (1999) Temperature dependence of inorganic nitrogen uptake: reduced affinity for nitrate at suboptimal temperatures in both algae and bacteria. *Applied and environmental microbiology,* 65(6), pp. 2577-2584.

Sandnes, J. M., Källqvist, T., Wenner, D. and Gislerød, H. R. (2005) Combined influence of light and temperature on growth rates of *Nannochloropsis oceanica*: linking cellular responses to large-scale biomass production. *Journal of applied phycology,* 17(6), pp. 515-525.

Schluter, L., Lohbeck, K. T., Gutowska, M. A., Groger, J. P., Riebesell, U. and Reusch, T. B. H. (2014) Adaptation of a globally important coccolithophore to ocean

warming and acidification. *Nature Climate Change,* 4(11), pp. 1024-1030. doi:10.1038/nclimate2379.

Schulte, P. M., Healy, T. M. and Fangue, N. A. (2011) Thermal performance curves, phenotypic plasticity, and the time scales of temperature exposure. *Integrative and Comparative Biology,* 51(5), pp. 691-702. doi:10.1093/icb/icr097.

Shimada, C., Tanaka, Y. and Tanimura, Y. (2006) Seasonal variation in skeletal silicification of *Neodenticula seminae*, a marine planktonic diatom: sediment trap experiments in the NW Pacific Ocean (1997–2001). *Marine Micropaleontology,* 60(2), pp. 130-144.

Thompson, P., Baird, M., Ingleton, T. and Doblin, M. (2009) Long-term changes in temperate Australian coastal waters: implications for phytoplankton. *Marine Ecology Progress Series,* 394, pp. 1-19.